Nutrient sorption potential of treated and untreated hydrochars and biochars derived from various waste feedstocks

By

Chibi Asabe Takaya

Submitted in accordance with the requirements for the degree of

Doctor of Philosophy

The University of Leeds

Centre for Integrated Energy Research

September 2016

The candidate confirms that the work submitted is her own, except where work which has formed part of jointly-authored publications has been included. The contribution of the candidate and the other authors to this work has been explicitly indicated below. The candidate confirms that appropriate credit has been given within the thesis where reference has been made to the work of others. Further details of the jointly-authored publications and the contributions of the candidate and the other authors to the work are listed below.

Chapter 5 is based on one publication:

Takaya C.A., Fletcher, L.A., Singh, S., Anyikude, K.U., Ross, A.B. 2016. Phosphate and ammonium sorption capacity of biochar and hydrochar from different wastes. Chemosphere, 145, 518-527.

As the project was part of a larger research project, Fertiplus, some experimental procedures excluding data interpretation were done by other researchers: Dr. Surjit Singh did experimental work involving TPO, most Py-GC-MS and surface area/porosity analysis, ultimate and proximate analysis of untreated chars; Dr. Kelechi Anyikude performed char solvent extractions. The candidate performed all of the analysis, write up, and all experiments involving ion exchange and nutrient sorption. Dr. Fletcher contributed with comments and guidance. Dr. Ross contributed with comments, guidance and proof reading.

Chapter 6 is based on one publication:

Takaya C.A., Fletcher, L.A., Singh, S., Okwuosa, U.C., Ross, A.B. 2016. Recovery of phosphate with chemically modified biochars. Journal of Environmental Chemical Engineering. 4(1), 1156-1165.

The candidate performed all of the analysis, write up, char modification, surface area analysis and some sorption experiments. Dr. Singh performed the proximate, ultimate and metal analyses. Ms. Okwuosa performed some sorption experiments during her MSc project. Dr. Fletcher contributed with comments and guidance. Dr. Ross contributed with comments, guidance and proof reading.

Acknowledgments

I would like to thank a number of individuals without whose support this thesis would not have been possible:

I am very grateful to The Petroleum Technology Development Fund (PTDF) Nigeria for granting me the funding to do this research. Thank you also to the FERTIPLUS Consortium for providing me with great research collaboration opportunities.

My sincere gratitude to my supervisor Dr. Andrew Ross for his generous guidance, mentorship, and confidence in me throughout my PhD. I am also grateful to my supervisor Dr. Louise Fletcher for her guidance and support during my PhD.

It has been a real pleasure working alongside my University of Leeds research team: I would like to thank Dr. Surjit Singh for his assistance with experimental work and his exceptional patience and dedication while helping me develop various analytical skills. Thanks also to Dr. Patrick Biller, Antonio, Kelechi, Ugo, Thomas, Kiran, James, Aidan, Hattie, Dorian, Christian, Uju, Iram, Callum, Sepo, Alex. Thank you to the researchers at CSIC-CEBAS Spain for their time, support and advice: Dr. Miguel Ángel Sánchez-Monedero, Dr. Asunción Roig, Dr. Maria Luz Cayuela, Dr. Inés Lopez-Cano, Dr. María Sánchez-Garcia, visiting post-doctoral researcher Dr. Gustavo Curaqueo and Dr. Claudio Mondini (Italy).

I am grateful to the technical staff at the School of Chemical and Process Engineering and School of Civil Engineering for their tireless support: Mr. Simon Lloyd, Dr. Adrian Cunliffe, Ms. Karine Alves Thorne, Dr. David Elliot and Ms. Sheena Bennet. Thank you to my colleagues Amal, Yee Sing, Faith, Kisandra, Zainab, Francis, Pessu, Seun, Buland, Femi, Lifita, Efosa, Ganiyu, Peace, Abubakar, Bala, Farooq, Onyebuchi and many others for your friendship and scholarly advice.

Thank you Paul, Kasang, Vicky, Helen, Shiktira, Ute, Chito, Yuwa, Tina, Yemisi, Dami, Roberta, Grace, Ibrahim, Barka, Ordondo for your understanding and patience.

Thank you to my family: Baba, Mama, Wikaya, Valli, Tammi, and Aiyatu. In spite of the distance, your invaluable support at all times kept me going. Thank you Mr. Henry Ugege for all your encouragement, Mr. Adejo and Mr. Ohikhuare for being ever supportive.

Table of Contents

List of Publications

Takaya C.A., Fletcher, L.A., Singh, S., Anyikude, K.U., Ross, A.B. 2016. Phosphate and ammonium sorption capacity of biochar and hydrochar from different wastes. Chemosphere, 145, 518-527.

Takaya C.A., Fletcher, L.A., Singh, S., Okwuosa, U.C., Ross, A.B. 2016. Recovery of phosphate with chemically modified biochars. Journal of Environmental Chemical Engineering. 4(1), 1156-1165.

List of Tables

List of Figures

Abbreviations

AAS	Atomic Absorption Spectroscopy
AD	Anaerobic Digestion
ATR-FTIR	Attenuated Total Reflectance-Fourier Transform Infrared (spectroscopy)
BET	Brunauer-Emmett-Teller
CEC	Cation Exchange Capacity
CHNS	Carbon Hydrogen Nitrogen Sulphur
DAF	Dry, Ash-Free
DB	Dry Basis
EBC	European Biochar Certificate
EXC	Extractable Carbon
FA	Fulvic Acid
GH	Greenhouse waste
GHG	Greenhouse Gas
GW	Greenwaste
HA	Humic Acid
HTC	Hydrothermal Carbonization
IBI	International Biochar Initiative
IC	Ion Chromatography
MW	Municipal Waste
NMR	Nuclear Magnetic Resonance
OAK (Comm.)	Commercial Oak wood biochar (*Proininso*)
OW	Oak wood
PK	Presscake
PM	Pig Manure
Py-GC-MS	Pyrolysis Gas Chromatography Mass Spectrometry
SEM / EDS	Scanning Electron Microscopy / Energy Dispersive x-ray Spectroscopy
TOC	Total Organic Carbon
TPO	Temperature-Programmed Oxidation

Abstract

Biochars have traditionally been associated with soil amendment but are also useful in a number of sectors as they show potential to be cost-effective, multi-functional products particularly if they are produced from waste biomass. Current research is geared towards enhancing char agronomic value via physical, chemical and/or biological means although further studies are still required to gain a better understanding of the parameters which can be optimized to produce chars with specific functionality.

This research set out to evaluate the potential for hydrochars and biochars derived from herbaceous and treated municipal waste to be used for nitrogen and phosphorus recovery from simulated wastewater, in addition to ammonia gas emission reduction during co-composting. This study also focused on providing more insight on some of the factors influencing hydrochar and biochar performance in nutrient-rich environments and investigating the potential for modifying char characteristics for enhanced nutrient recovery. Consequently, analysis of the physicochemical properties of hydrochars and biochars produced from paprika waste from a greenhouse, the treated organic fraction of municipal waste, greenwaste and pig manure has been performed. Comparisons are also made with relatively low-contaminant hydrochars and biochars derived from bark-free holm oak wood. Processing parameters include hydrothermal carbonization at 250°C for 60 min, slow pyrolysis at 400–700°C and gasification at 600–750°C over 30–60 min residence times.

As oak and paprika waste chars possess carbon contents >50%, these have been categorised as Class 1 biochars in accordance with the international biochar initiative product specifications, while hydrochars and slow pyrolysis biochars derived from municipal waste, presscake, and greenwaste are ranked as Class 2–3 chars. in spite of differences in biomass inorganic content, the various feedstocks decompose into chars in a similar manner. Char morphological properties are observed to be more dependent on processing temperature and reactor system than to feedstock property, based on the substantial differences in surface area of holm oak biochars produced using three different reactor types. However, from batch sorption tests with synthetic wastewater, char surface area and porosity are of less importance than char oxygen and inorganic mineral contents in terms of ammonium and phosphate sorption, respectively. Overall however, all chars

demonstrate similarly low capacities for ammonium and phosphate sorption (up to 14.6% and 7%, respectively). Conversely, in terms of ammonia removal, two of the hydrochars selected for further study are shown to possess higher ammonia emission reduction capacities relative to their biochar counterparts in 17-day laboratory co-composting trials. These differences are likely attributable to the acidic functional groups present in the hydrochars. While both oak and greenhouse waste hydrochars demonstrated higher levels of inorganic nitrogen (ammonium and nitrate) mineralization relative to their biochar counterparts, mineralization and carbon dioxide evolution was more prominent in the latter hydrochar. These findings are in agreement with previous studies in the literature, which have shown that hydrochars possess more mineralizable carbon and nitrogen species than biochars.

Following from an understanding of the respective effects of char acid oxygen groups and inorganic content on char ammonium and phosphate sorption capacities, attempts have been made to enhance these properties via mild chemical activation of biomass or char samples. results show that modest increases in both ammonium and ammonia sorption capacity of the chars can be achieved following acid treatment, while phosphate sorption can be enhanced from low levels (2.1–3.6%) to relatively high levels (66.4–70.3%) by impregnation with magnesium. various treatments will understandably produce different effects on the different hydrochars. this is evident in the case of greenhouse waste, which experiences a considerable increase in ammonia sorption capacity following potassium hydroxide treatment of greenhouse waste 250°C hydrochar and 400°C biochar, from 3.3% to 44.1% in the latter char while the effect is less pronounced following sulphuric acid treatment. overall, findings from this study suggest that it is possible to enhance waste-derived char capacity for ammonia / ammonium and phosphate recovery by treatment of chars or char precursors (raw feedstock) via mild chemical activation processes.

CHAPTER 1

1.0 Nomenclature

Chars obtained from the thermochemical treatment of organic matter (biomass) can generally be categorised as black carbon as this term is used to describe all charred matter with high carbon contents (Lehmann and Joseph 2009). Black carbon intended for use in soil or carbon capture and storage is often referred to as 'biochar' or 'agrichar' to differentiate from charcoal designed for energy generation and other purposes (EBC 2012; Kambo and Dutta 2015). Biochars or agrichars are further differentiated based on thermochemical processing route into 'pyrochars' or 'hydrochars' when produced via slow pyrolysis or hydrothermal treatment in sub-critical water respectively. However, as the International Biochar Initiative (IBI) refers to the solid product obtained from pyrolysis as biochar, this nomenclature is also adopted in this study while 'hydrochar' is reserved for the solid product obtained from Hydrothermal Carbonization. For brevity, 'char' will be used to refer to both biochar and hydrochar in some cases.

1.1 Hydrochar and biochar production

Hydrochars and biochars are heterogeneous structures comprised of carbonized organic matter, inorganic matter, sorbed volatiles and functional groups of nitrogen, sulphur and oxygen (Atkinson et al. 2010; Knicker 2007; Novak et al. 2009; Spokas et al. 2012), and are becoming increasingly attractive in a number of sectors as they show potential as relatively cost-effective, multi-functional products (**Table 1.1**). Char properties are largely dependent on processing conditions and feedstocks (Downie et al. 2009; Zhao et al. 2013a), and an essential step preceding their large-scale deployment involves understanding the effects of such parameters on char properties and functionality. Thermochemical processes used for char production include Hydrothermal Carbonization (HTC), various sub-classes of pyrolysis (slow, intermediate, fast, flash or microwave pyrolysis) and gasification. In each of these processes, variations in processing parameters such as temperature, pressure, heating rate, and residence time result in solid (char), aqueous, and gaseous products in different proportions as summarised in **Figure 1.1**.

Table 1.1 Some potential hydrochar and biochar applications

Sector	Applications	Potential limitations	References
Agronomy	Chars reduce soil acidity, adsorb toxic compounds, enhance soil structure, water and ion retention due to char physico-chemical properties.	Some of the properties chars are recommended for result in negative soil responses, as highlighted in **Section 1.2.2**.	Granatstein et al. (2009); Lehmann et al. (2006); Liang et al. (2006); Sarkhot et al. (2011); Spokas et al. (2012); Xu et al. (2013)
Wastewater treatment	• Adsorption of pathogenic viruses (RV and HAdV) and E.coli using hydrochar derived from sewage sludge and maize residue respectively due to surface functional groups.	Loss of hydrophobic sites or heterogeneous surface charge on hydrochar could result in reduction in virus removal capacity.	Chung et al. (2015)
	• Sorption of various organic species: Polycyclic Aromatic Hydrocarbons (PAHs) removal efficiencies of chars comparable to bitumen-derived activated carbon in some cases; sorption of phenols such as dyes, pharmaceutical active compounds (e.g., ibuprofen) and Endocrine Disrupting Chemicals (EDCs).	The lower surface areas of chars relative to activated carbon make uptake of freely dissolved PAH lower in the former. Char performance also varies with feedstock material and processing temperature.	Oleszczuk et al. (2012); Libra et al. (2011); Mohan et al. (2014); Mondal et al. (2016); Sun et al. (2011); Tan et al. (2015)
	• Reduction in bioavailability of heavy metals from contaminated soils, aquatic sediments and other contaminated sites possibly due to biochar microporosity, pH and complexation with N species.	Lack of policies supporting biochar use for reducing contaminant bioavailability due to biochars' inability to remove all traces of contaminants (no cure-all promise). Long-term effectiveness also a concern, as heavy metal immobilization by biochar may be reversed by soil acidification.	Ghosh et al. (2011); Houben et al. (2013); Mohan et al. (2014); Tan et al. (2015); Titirici and Antonietti (2010); Yang and Jiang (2014)
	• Nutrient recovery using various biochars owing to their surface functional groups and surface areas: NH_4^+, NH_3 and PO_4^{3-} removal due char O, S and Mg contents resp.; $ZnCl_2$-activated biochar compared favourably with commercial activated carbon for humic acid uptake due to surface area.	Chars often require some form of modification to enhance their nutrient uptake capacity.	Gokce et al. (2009); Ismadji et al. (2016); Petit et al. (2010); Tian et al. (2016); Yao et al. (2011)

Table 1.1 Some potential hydrochar and biochar applications

Sector	Applications	Potential limitations	References
Climate control (carbon sequestration)	• Stabilization of soil organic carbon after application of high temperature (recalcitrant carbon) biochar in some soils may be possible 2.3 years after application. • N-doped hydrochars may also possess greater oxidation stability, and potential for (pyrrolic) N enriched activated biochar to improve CO_2 uptake.	C sequestration potential of biochars may vary with soil type and vegetation. For instance, stabilization of organic carbon from both biochar and soil occurred possibly via organo-mineral complex formation within mineral soil.	Chen et al. (2015); Ghosh et al. (2011); Singh and Cowie (2014); Titirici and Antonietti (2010)
Energy generation	• Direct Carbon Fuel Cells (DCFCs) & Microbial Fuel Cells (MFCs) using wood-based biochar and glucose-based hydrochar. Char oxygen surface groups influence electrochemical reactivity.	Contamination may arise from char volatile matter and ash.	Ahn et al. (2013); Ganesh and Jambeck (2013); Titirici and Antonietti (2010)
	• Low-cost, reusable catalysts for esterification of free fatty acids during biodiesel production using activated wood-based biochar.	Char performance lower than that of activated carbon (70% versus 97% resp.) and requires more regeneration cycles between uses than activated carbon.	Kastner et al. (2012)
	• Catalyst or catalyst support for tar cracking/reduction during pilot-scale biomass gasification, comparable to traditional coal-based catalyst owing to biochar's disordered carbon structure. Mineral content, pore size, surface area may also play important roles in tar reduction.	In some cases, biochars require higher temperatures for catalytic reforming or removal of tar (toluene) than commercial catalysts.	El-Rub et al. (2008); Mani et al. (2013); Zhang et al. (2013)
Other industrial functions	• Calcined hydrochar as anode in Li ion batteries.	Capacity may be lower than that of silicon.	Titirici and Antonietti (2010)
	• Electrodes for capacitive deionization (CDI) using activated wood-based biochar likely due to mesoporous structure.	Removal efficiency for some metals (e.g. Zn^{2+}) may decline after a limited number of uses regardless of regeneration.	Dehkhoda et al. (2016)
	• Catalyst for hydrogenation reactions, e.g., phenol to cyclohexanone due to hydrochar hydrophilicity.		Reza et al. (2013); Titirici and Antonietti (2010)

Product characteristics also vary; for instance, solid products obtained from torrefaction possess enhanced fuel characteristics relative to the original biomass such as energy density and grindability due to low temperature (250–300°C) treatment (Tan et al. 2015) but such low temperature treatment is insufficient to fully convert biomass to char for soil amendment or carbon sequestration. As such, torrefaction is often considered as a useful pre-treatment process for biofuel industries and thus not classified as biochar (Mohan et al. 2014). Reactors frequently optimized for biochar production include auger, vertical tubular, fixed and fluidized beds and extensive studies on thermochemical processes and their associated technologies have been outlined elsewhere (Bridgwater and Bridge 1991; Mohan et al. 2014; Shen et al. 2013; White et al. 2011). In this study, more emphasis is placed on the proposed mechanisms governing HTC and slow (conventional) pyrolysis and the respective effects of such processes on hydrochar and biochar physico-chemical properties.

1.1.1 Slow pyrolysis

Pyrolysis refers to the thermal decomposition of biomass into useful end products in the absence of air, often at temperatures below 1000°C (Bahng et al. 2009). As the pyrolysis process yields several products such as chars, oils, gases and chemicals such as methanol and acetic acid, it is sometimes described as the dry distillation of wood (Libra et al. 2011). Such products are formed during biomass thermal treatment due to dehydration, decarboxylation and other degradation reactions like chain scission, depolymerisation, or splitting of weakly bonded side groups within the biomass structure (Silverio et al. 2008). Consequently, water, condensable volatiles (tars or oils) and non-condensable volatiles (C_1–C_2 hydrocarbon fractions, CO, CO_2, H_2) are released during char formation (Diebold 1994; Duku et al. 2011; McGinnes 1976; Schimmelpfennig and Glaser 2012; White et al. 2011). Compared to fast pyrolysis and gasification, slow pyrolysis favours the formation of chars (**Figure 1.1**) and potential reaction pathways for char formation from lignocellulosic biomass have been the subject of extensive research for decades, with amendments to established pyrolysis kinetics detailed in studies like Burnham et al. (2015).

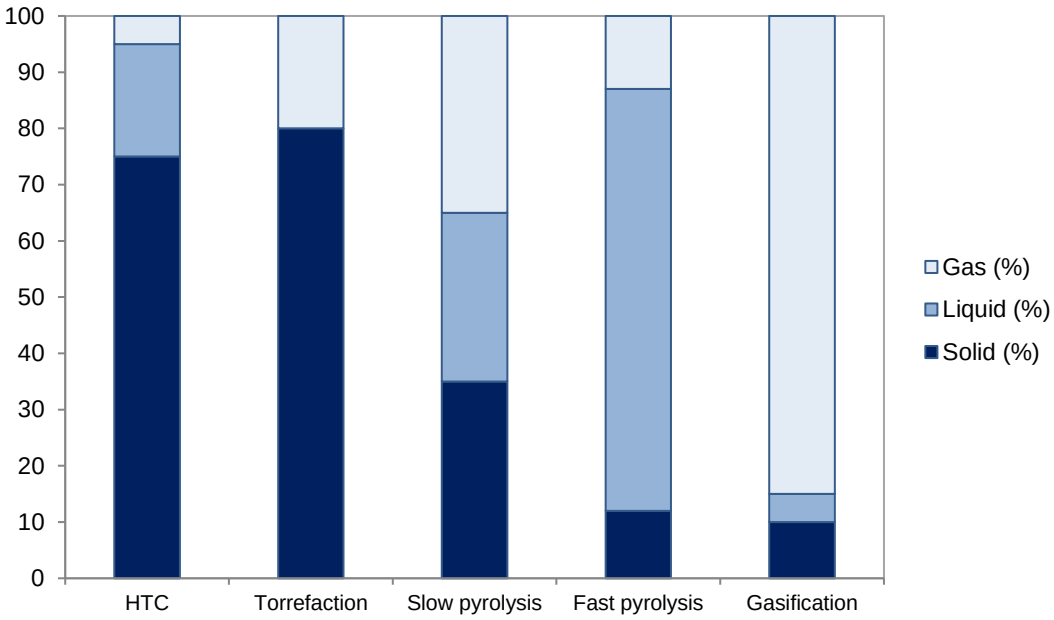

Figure 1.1 General distribution of products obtained from various thermochemical processes. Adapted from IEA Bioenergy (2007), Jahirul et al. (2012) and Libra et al. (2011).

Reaction pathways are often modelled for cellulose as this is the major component of lignocellulosic biomass (Diebold 1994; Duku et al. 2011; Lin et al. 2009; White et al. 2011; Wooten et al. 2004). Cellulose is comprised of D-glucopyranose units linked by β-(1,4)-glycosidic bonds (White et al. 2011). Many pathways suggest the degradation of cellulose into an intermediate reactive polymer often considered to be 'active cellulose' or anhydro-cellulose, which degrades into anhydrosugars such as levoglucosan ($C_6H_{10}O_5$) from 300°C and subsequently into volatile compounds, or to char following dehydration, isomerization, retro-aldol condensation, and re-polymerization reactions (Burnham et al. 2015; Diebold 1994; Lin et al. 2009; Rutherford et al. 2008; Saiz-Jimenez 1994; Shafizadeh 1982; Shen et al. 2013). Wooten et al. (2004) proposed a slightly different reaction route for char formation from pure cellulose at low temperatures (<350°C). The proposed mechanism involves the formation of a carbohydrate termed 'final carbohydrate' which differs from 'intermediate carbohydrate' (active cellulose) in that the former is produced from the volatiles released during cellulose depolymerization. Slow pyrolysis appears to favour active cellulose formation (Wooten et al. 2004) and its degradation is considered to be an endothermic reaction with activation energy of about 200 KJ mol^{-1} (Burnham et al. 2015; Lin et al. 2009; Wooten et al. 2004), the rate of which may not be first order as initially thought (Burnham et al. 2015).

The thermal degradation of hemicellulose, a hetero-polysaccharide characterised by pentose or hexose units linked by β-(1,4)-glycosidic bonds (Scheller and Ulvskov 2010; Yang et al. 2007), also contributes to char formation via its degradation into organic acids such as acetic acid, which catalyse the depolymerization of other polysaccharides (Nuopponen et al. 2005). Lignin is a complex biopolymer which depolymerizes into phenolic compounds, aromatic hydrocarbons, *para*-coumaryl, coniferyl, syringyl alcohols (Harvey et al. 2012a; Saiz-Jimenez 1994), char and non-condensable gases (Yang et al. 2007) depending on biomass nature.

Ultimately, biomass pyrolysis process is more complex as other components of lignocellulosic biomass may indirectly contribute to char formation (**Figure 1.2**) (Brownsort 2009; Shen et al. 2013; White et al. 2011). For instance, biomass extractives and certain inorganic elements favour the formation of low molecular weight species (formic acid, acetic acid) over levoglucosan in some cases (Guo et al. 2010; Patwardhan et al. 2010). Certain cations also alter lignin product distribution patterns; Kleen and Gellerstedt (1994) found that the presence of sodium altered the relative abundance of phenols and catechols.

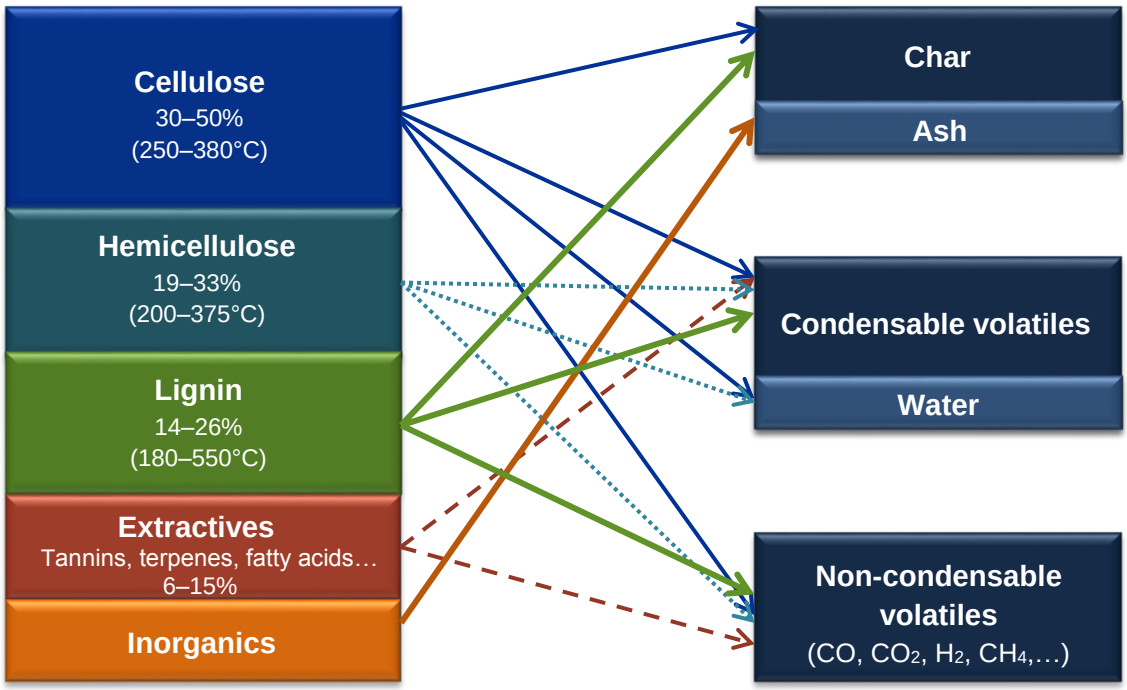

Figure 1.2 General illustration of the conversion of lignocellulosic biomass components into solid, liquid and gas phases during pyrolysis, with typical decomposition temperatures of the main components in parentheses. Adapted from Brownsort (2009), Crombie and Mašek (2014), Reza et al. (2013) and White et al. (2011).

1.1.2 Hydrothermal Carbonisation (HTC)

Hydrothermal Carbonisation (HTC), also referred to as wet torrefaction or hydrous/wet pyrolysis (Libra et al. 2011; Lynam et al. 2011; Reza et al. 2014) involves the dehydration of complex polymeric biomass structures into simpler units in subcritical water. HTC is often conducted at temperatures between 180–260°C with or without catalysts (Lynam et al. 2011; Ramke et al. 2009). Reactor pressure is autogenous and rise to about 4.2 MPa, although much higher pressures of >25 MPa have been reported (Benavente et al. 2015; Wiedner et al. 2013a) possibly due to the high biomass loading ratios employed.

Similar to slow pyrolysis, HTC involves degradation reactions but at lower reaction temperatures, beginning with hydrolysis of cellulose, hemicellulose, and lignin into oligosaccharides and phenols, soon followed by dehydration, decarboxylation, aromatization, and re-condensation reactions (Cao et al. 2013; Heilmann et al. 2011; Hoekman et al. 2011; Reza et al. 2014; Stemman et al. 2013; Sun et al. 2011) as shown in **Figure 1.3**. Dehydration of carbohydrates such as pentose and hexose sugars into furfural and hydroxymethyl furfural (HMF), respectively, followed by polymerization of HMF to polyfurans and dehydration results in char formation and other low molecular weight species (Nuopponen et al. 2004; Stemman et al. 2013; Titirici and Antonietti 2010). The high reaction pressures observed during HTC at relatively low processing temperatures likely result from the exponential relationship between temperature and the vapour pressure of water as expressed by the Clausius-Clapeyron equation (Equation 1.1):

$$P = A\, e^{\left(-\Delta H_v / RT\right)} \quad (1.1)$$

where P is vapour pressure (atm), T is absolute temperature (K), ΔH_v is the enthalpy of vaporization, R is a gas constant (8.314 J K^{-1} mol^{-1}), and A is an experimental constant (MIT 2008).

Distilled water is a frequently used solvent in HTC as its purity enables a clearer evaluation of biomass transformations occurring although recent studies also incorporate salts or acids to enhance the rate of dehydration reactions (Ramke et al. 2009). At temperatures of 227–327°C, water serve as an acid or base catalyst since its ionic product is highest at this temperature range. Studies also show that at this temperature range, the dielectric constant of water is lowest thus causing it to act

non-polar (Lynam et al. 2011), although faster cellulose degradation occurs at super-critical conditions (>374°C, 25 MPa) as demonstrated by Sasaki et al. (2000). Typical HTC residence times range from minutes to several hours (Lynam et al. 2011; Yan et al. 2014) although it has been suggested that most products are formed during the first few minutes of the HTC process (Lynam et al. 2011) while most decarboxylation reactions occur during hold time (Hoekman et al. 2011).

As with other thermochemical processes, the product streams from HTC exist in solid, aqueous and gaseous phases (**Figure 1.1**). The solid products, hydrochars, are often recovered from the aqueous phase by filtration (Heilmann et al. 2011) or mechanical dewatering. Hydrochars generally possess higher O/C and H/C ratios compared to biochars (Libra et al. 2011; Smith et al. 2016) possibly because oxygen loss during HTC occurs through decarboxylation reactions (Knežević et al. 2010).

Hydrochars are in contact with process water during HTC, thus the amount of extractives present in hydrochars are sometimes relatively higher than the original biomass on a weight/weight basis, since sugars and acids are deposited within char pores (Reza et al. 2013). As cellulose and hemicellulose are increasingly degraded, the aqueous or condensable volatile phase is often comprised of acids (acetic, formic and lactic acids) and sugars (glucose, 5-HMF) (Reza et al. 2013), amounts of which are dependent on the carbonization temperature and feedstock characteristics. Hoekman et al. (2011) observed that most sugars are present in the aqueous phase at low carbonization temperatures (<225°C). This also holds true for organic acids, which increase until about 255°C when total acid content decreases, leaving mainly acetic and lactic acids (Hoekman et al. 2011), and as the aqueous phase is rich in organics, it possesses a high Total Organic Carbon (TOC) content (Ramke et al. 2009). The gaseous or non-condensable volatile phase is predominantly comprised of carbon dioxide (70–90%), carbon monoxide, hydrogen, and 1–10% low molecular weight hydrocarbons (methane, ethane, propene) (Benavente et al. 2015; Ramke et al. 2009).

As HTC is capable of processing high moisture content biomass, conservation of the thermal energy that would otherwise be required to dry the bio-feedstock is considered to be one of the key advantages of the process, although energy requirements for drying the recovered chars must be factored in as has been researched by Benavente et al. (2015). However, in terms of commercial HTC operations, some form of recycled process water is necessary from a sustainability perspective.

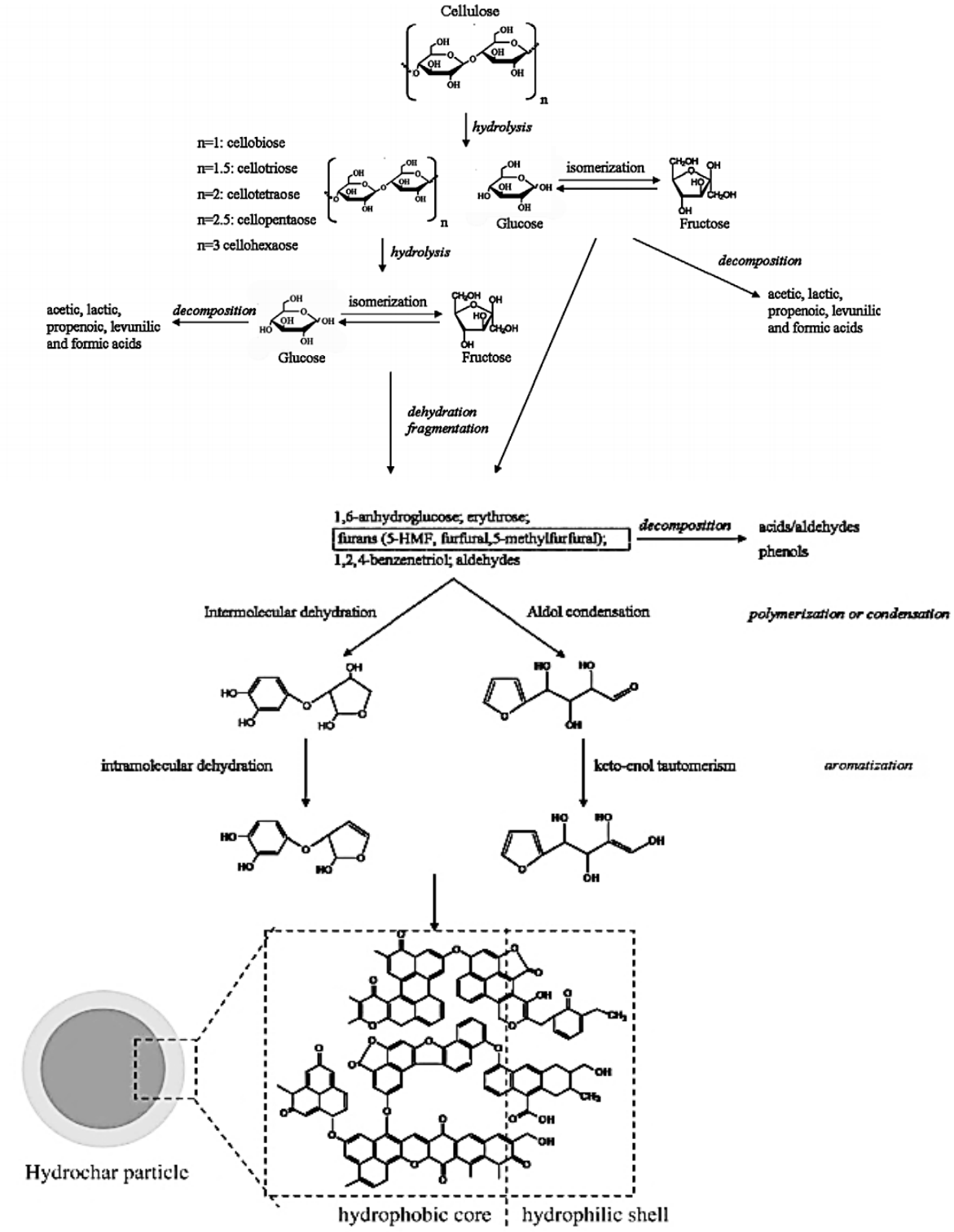

Figure 1.3 A proposed mechanism for the conversion of cellulose to hydrochar (Sevilla and Fuertes 2009).

1.2 Hydrochar and biochar agronomic effects

1.2.1 Positive responses

Plants are thought to require 17 nutrients in the right balance to function adequately, and while carbon (C), hydrogen (H) and oxygen (O) are obtained during photosynthesis, macronutrients (N, P, K, Ca, Mg, S) and micronutrients (Cu, Zn, Mn, B, Mo, Fe, Cl and Ni) are obtained from soil (Miller and Oldham 2014). In combination with soil microorganisms and nutrients, it has been suggested that the application of biochar to soil may result in soils that are comparable to the fertile Amazonian Terra Preta soils, based on the fact that Terra Preta soils are comprised of black (pyrogenic) carbon, microorganisms (fungi and bacteria), soil organic matter, and nutrients from plant matter and excrement (Glaser and Birk 2012). Black carbon is also thought to contribute to nutrient availability in these soils owing to its nutrient retention capacity and supply of inorganic elements (Glaser et al. 2002; Spokas et al. 2012a). However, the positive effects in soils with biochar application as outlined in **Table 1.1** have mostly been observed in mostly tropical regions or highly weathered oxisols because such soils experience high rainfall and nutrient leaching and therefore derive only temporary nutrient benefits from the application of organic matter or vegetative burning (Atkinson et al. 2010; Galinato et al. 2010; Glaser et al. 2002). In addition to a supply of nutrients and increasing soil nutrient retention capacity (Jindo et al. 2012a; Glaser et al. 2002; Lehmann et al. 2006), chars improve soil structure by serving as bulking agents (Dias et al. 2010; Jindo et al. 2012b) and supplying decomposable carbon for microbes depending on char production temperature (Hunt et al. 2010). A number of studies have also shown that chars are capable of minimising nitrogen losses through the uptake of total ammoniacal nitrogen (Hunt et al. 2010; Steiner et al. 2010).

In addition to soil enhancement, biochars show potential for longer-term carbon sequestration compared to untreated bio-feedstocks (**Figure 1.4**) owing to their more recalcitrant aromatic carbon structures (Atkinson et al. 2010; Glaser et al. 2002; Sparkes and Stoutjesdijk 2011; Yao et al. 2011; Zhao et al. 2013b) although the timeframe for which chars remain stable in soils is uncertain given the different climatic conditions (Atkinson et al. 2010), biochar properties (Chan et al. 2007) and soil types. There are some reports of biochars increasing CO_2 emissions in soils however (Sarkhot et al. 2011), and based on analyses of molar O/C ratios, Spokas et al. (2012) suggested that carbon sequestration potential in black carbon decreases as surface oxygen group concentration increases.

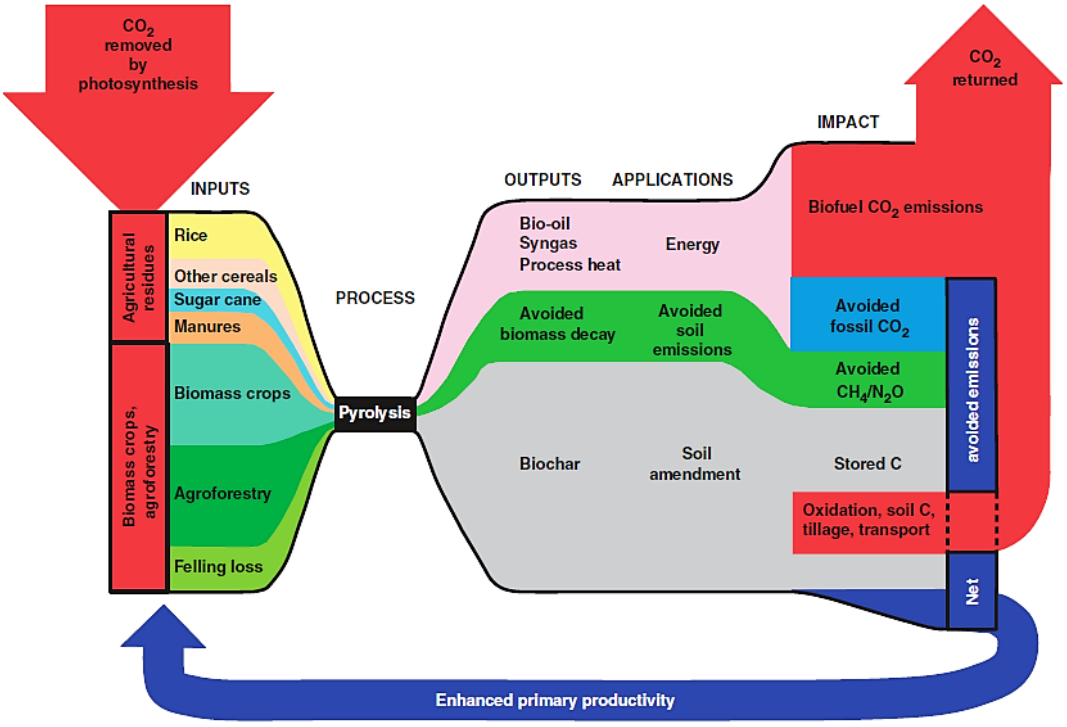

Figure 1.4 A sustainable-biochar model (Woolf et al. 2010).

1.2.2 Negative responses

While several studies highlight positive soil and biomass responses following biochar and hydrochar application, negative effects have also been observed (Chan and Xu 2009; Galinato et al. 2011; Glaser et al. 2002; Lehmann et al. 2006; Schmidt 2011) For instance, because biochars possess high cation exchange and adsorption capacities, they initially render nutrients and water unavailable to plants in some cases (Schmidt 2011). Other studies have observed micronutrient deficiencies arising from the soil pH increase following biochar application (Chan and Xu 2009; Glaser et al. 2002), and phenolic compounds in black carbon stimulate microbial activity resulting in N immobilization (Deenik et al. 2010). Adverse effects are also observed due to the presence of volatile matter in chars, described as the labile fraction of black carbon (Deenik et al. 2011), sometimes present as resins and tars on the surfaces of freshly produced chars (Hunt et al. 2010). Deenik et al. (2011) and McClellan et al. (2007) suggested that high char volatile matter was partly responsible for short term negative effects on plant yield, based on pot trials with tropical soils amended with low and high volatile matter corncob charcoal showing higher biomass yields in the former case. Consequently,

production processes resulting in biochars with minimal volatile matter may be preferable (Hunt et al. 2010). Similarly, hydrochars could also benefit from longer processing times and to some extent temperatures to reduce their toxic (furane) content (Lu et al. 2013).

1.3 Char modification

As some studies have shown that chars with hydrophilic surfaces improve soil nutrient retention and aggregation (Borchard et al. 2012), there is growing interest in modifying char properties to enhance their effectiveness in soils and to improve specific physical and chemical properties such that smaller quantities of designer or bespoke chars are required for soil amendment (Novak et al. 2009; Silber et al. 2010). Furthermore, Nguyen et al. (2012) observed that most agricultural by-products considered as adsorbents require some form of modification to perform efficiently. Char modification is broadly categorised under physical, chemical or biological activation, where physical modification involves high temperature gas-phase treatment of biochars with steam, air or carbon dioxide; chemical modification, which involves the incorporation of chemical species onto chars via thermal or electro-modification (Jung et al. 2015; Krishnan and Haridas 2008); biological modification, which includes co-composting, lactic acid fermentation and urine-treatment. Chemical activation is often considered to be more cost-effective and less time-consuming, but various processing temperatures, activating agents and loading ratios understandably result in chars with different properties even when similar chemical activation agents are used. **Figure 1.5** outlines some proposed mechanisms through which species uptake occurs on the surfaces of chemically modified biochars, adapted from Rajapaksha et al. (2016).

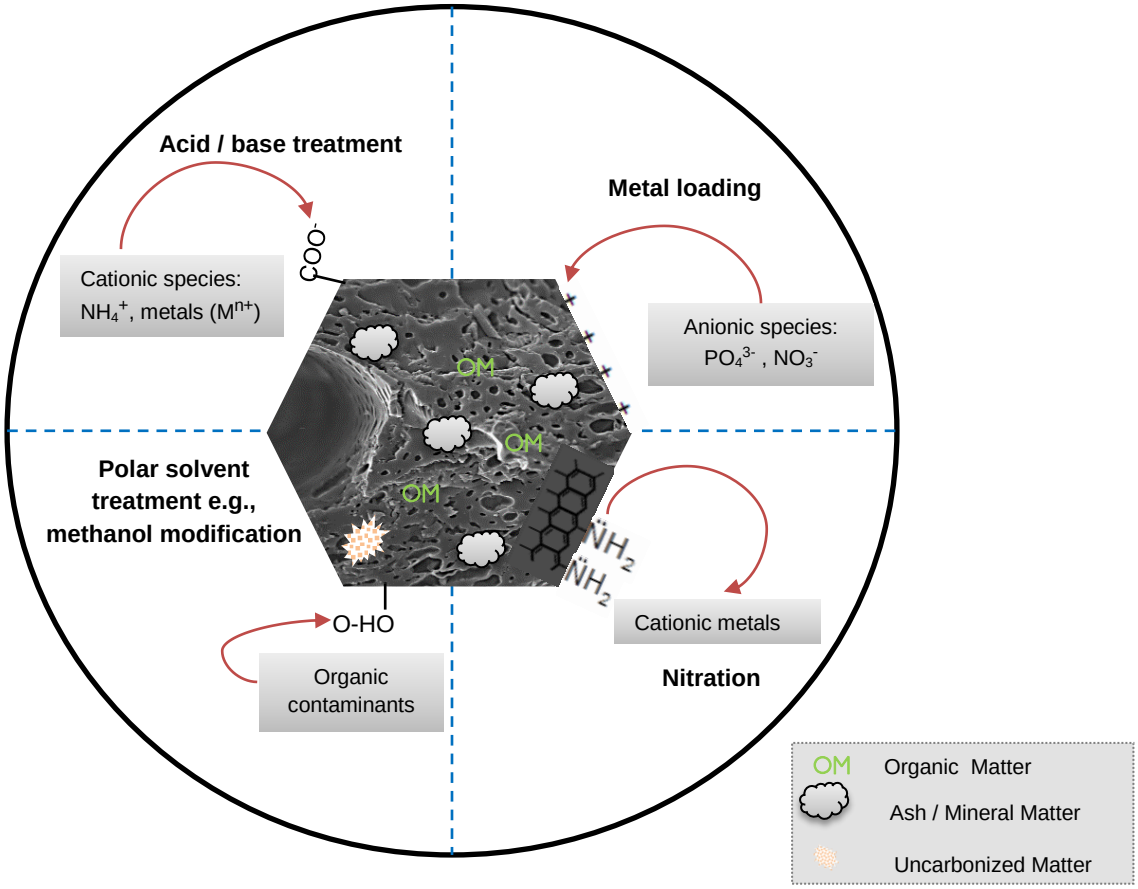

Figure 1.5 Some proposed surface interactions between species after char chemical treatment, adapted from Rajapaksha et al. (2016).

1.4 Research aim and objectives

Further studies are required to gain a better understanding of the parameters that can be optimized to produce chars with specific functionality. This study is therefore focused on examining the influence of key feedstock and processing parameters on char nutrient sorption capacity with a view towards enhancing char nutrient sorption potential via mild chemical activation processes. Such findings are important from environmental and economic perspectives due to current challenges associated with wastewater quality and char commercial competitiveness, respectively. Consequently, the main objectives of this study are as follows:

Objective 1: To evaluate the physicochemical properties and nutrient sorption capacities of hydrochars and biochars derived from various organic waste feed-stocks (pepper waste from a greenhouse, the treated organic fractions of municipal waste, greenwaste, and pig manure) in comparison to relatively low-contaminant commercial and non-commercial oak biochars. Consequently, an evaluation of the ammonium/ammonia and phosphate sorption capacities of unmodified chars from pure solutions in batch sorption tests and proposing possible sorption mechanisms. Furthermore, the effect of coexisting ions on char ammonium/ammonia and phosphate sorption capacities using batch sorption tests were assessed.

Objective 2: To produce chars with enhanced ammonia/ammonium and phosphate sorption capacities via:

i) Development of modified chars using mild activation methods based on well-known carbon activation methods, via char post-treatment and biomass pre-treatment.
ii) Comparison of key physicochemical properties between treated and untreated chars.
iii) Analysis of the reaction mechanisms involved with ammonia/ammonium and phosphate sorption capacities of modified chars in single and multiple ion systems.

Objective 3: To evaluate char degradation rates via short-term laboratory incubation tests which quantify carbon dioxide and nitrogen dynamics (NH_3, NH_4-N and NO_3-N) between chars within a high pH soil, in addition to small-scale co-composting trials with a selection of hydrochars and biochars to investigate their potential for reducing NH_3 emissions.

1.5 Organisation of Chapters

Chapter 1 established the purpose and importance of this study and provided an outline of the thesis' structure.

Chapter 2 provides a summary of previous research on hydrochar and biochar properties, functions, as well as the measured and potential effects these have on nutrient recovery in soils, compost and aqueous solutions. As previous literature

places emphasis on char surface functional groups and elemental content, these are explored in this study, with particular focus on their impact on char nutrient uptake and retention.

Chapter 3 outlines the main methods used throughout this study for investigating hydrochar and biochar physicochemical properties including elemental and organic matter contents, surface morphology and cation exchange capacity. Methods for evaluating char interactions in soil and nutrient-rich environments are also outlined, specifically inorganic nitrogen and phosphate dynamics via batch sorption tests in addition to small-scale co-composting and soil incubation tests. Methods involved in hydrochar and biochar chemical treatment are also highlighted.

Chapter 4 evaluates the influence of biomass feedstock properties and processing conditions on char functionality using a number of char characterization techniques, to determine the factors that serve as predictors of chars' ability to minimize nutrient losses from wastewater and composting systems.

Chapter 5 evaluates the ammonium/ammonia and phosphate removal efficiencies of various chars and adsorption models are used to determine possible sorption mechanisms. Furthermore, char interactions with compost and with a high pH soil are evaluated in terms of inorganic nitrogen mineralisation and carbon dioxide evolution using small-scale incubation tests.

Chapter 6 assesses the effect of some frequently recommended biochar modification methods on hydrochar and biochar ammonium/ammonia and phosphate sorption capacities.

Chapter 7 summarises the results from previous chapters, and these results are used to highlight potential benefits and challenges involving hydrochar and biochar use for sustainable agriculture. Recommendations for future work are also proposed, and references are provided at the end of the thesis.

CHAPTER 2

Literature Review

2.0 Introduction

Hydrochars and biochars show potential for application across a number of sectors and are produced from increasingly diverse feedstocks. This chapter therefore takes advantage of the wide variety of chars that have been generated by previous researchers to establish connections between some key char properties and biomass feedstock type, and the influence of processing conditions and pre- and/or post-treatment on such properties. This is useful for developing a clearer understanding of often inter-related factors and may guide decisions on the most effective thermal processing conditions required for producing biochars and hydrochars with specific functions.

2.1 Hydrochar and biochar properties

The International Biochar Initiative (IBI) and European Biochar Certificate (EBC) require that chars produced from various bio-feedstocks must meet certain quality criteria as outlined in **Tables 2.1**–**2.2**. Central to these criteria are organic carbon content requirements which must be >50% of dry mass or otherwise be termed as "pyrolysis ash"; stable, aromatic black carbon contents must represent 10–40% of overall biochar carbon content. Furthermore, nutrients must be bioavailable, while maximum thresholds for heavy metals and Polycyclic Aromatic Hydrocarbons (PAH) in basic and premium quality biochars must not be exceeded (IBI 2015). Both EBC and IBI make little reference to hydrochar quality criteria however.

2.2.1 Carbon structure

Aromaticity or extent of carbonization generally increases with heat treatment, and the extent of carbonization has frequently been predicted using elemental ratios (Spokas 2010). H/C_{org} atomic ratios are used as indicators of biochar aromaticity, with characteristic black carbon H/C_{org} atomic ratios being $\leq$0.2 and even lower for graphite (Schimmelpfennig and Glaser 2012; Xiao et al. 2016). Hydrochars and biochars however tend to have higher ratios depending on the biomass and production temperature used; typically $\leq$ 0.6 in the latter category at elevated temperatures (Schimmelpfennig and Glaser 2012; Xiao et al. 2016).

Furthermore, quantitative predictions on char aromatic clusters, char sorption capacities for aromatic pollutants, and production temperature have been made based on dry, ash-free H/C_{org} atomic ratios by Xiao et al. (2016). While some studies have stated that H/C_{org} atomic ratios ≥ 0.7 result from uncondensed aromatics (Schimmelpfennig and Glaser 2012; Wiedner et al. 2013a), Cao et al. (2013) suggested that elemental analysis (H/C atomic ratio) solely does not provide sufficient information on char ring condensation. O/C atomic ratios are also indicative of biochar aromaticity, being between 0.2–0.4 for charcoal, <0.2 for soot (Schimmelpfennig and Glaser 2012), and should preferably be ≤ 0.4 for char (EBC 2012; Wiedner et al. 2013a).

Table 2.1 IBI and EBC requirements for biochar

Parameter	IBI	EBC
C content	Class 1: ≥ 60% (db)	Biochar: ≥ 50% (db)
	Class 2: 30–60% (db)	Bio Carbon Mineral (BCM): < 50%
	Class 3: 10–30% (db)	
Surface Area	Must be declared.	>150 $m^2\ g^{-1}$
Molar O/C ratio	n.a	Maximum of 0.4
Molar H/C_{org} ratio	Maximum of 0.7	Maximum of 0.7
Electrical Conductivity	Declared, as dS m^{-1}	Declared, as µS cm^{-1}
pH	Must be declared	Handling data for pH >10
Bulk Density	Not required	Must be declared
Macronutrients (NPK)	IBI and EBC: Should be expressed as % total mass (db)	
Total Ash	IBI and EBC: Must be declared, as % total mass (db)	
Volatile Matter	IBI and EBC: Must be declared, as % total mass (db)	
Water Content	IBI and EBC: Must be declared, as % total mass (db)	

db: dry basis; n.a: unavailable data.

Table 2.2 Standard limits for contaminants present in biochar

Class	g t^{-1}							mg kg^{-1}		ng kg^{-1}
	Pb	Cd	Cu	Ni	Hg	Zn	Cr	PAH	PCB	Dioxins/ Furans
Basic	<150	<1.5	<100	<50	<1	<400	<90	<12	<0.2	<20
Premium	<120	<1.0	<100	<30	<1	<400	<80	<4	<0.2	<20

2.2.2 Surface area and porosity

Temperature understandably influences char porosity and surface area development since pore development occurs due to loss of water molecules during dehydroxylation and volatilization of condensed volatiles such as tars thus freeing pores ((Bagreev et al. 2001; Chan and Xu 2009; Downie et al. 2009). Consequently, both hydrochar and biochar surface areas increase with temperature but only up to a certain point. This is due to the deformation that occurs as ash melting points are reached at elevated pyrolysis temperatures in biochars (Downie et al. 2009). In hydrochars, this decrease in surface area is observed at much lower temperatures possibly because of the exponential increase in vapour pressure with carbonization temperature. The presence of sorbed volatile matter on hydrochars does not appear to affect hydrochar surface areas a great deal (Annex Table A1). For instance, hydrochars washed with water or acetone to reduce their volatile matter contents possessed comparable surface areas to unwashed hydrochars' in Fang et al. (2015) and Kalderis et al. (2014).

Pressure and heating rate also play important roles in pore development as these influence the mass transfer of volatiles (Downie et al. 2009). For instance, when pine sawdust was pyrolysed at low heating rates and atmospheric pressures, Cetin et al. (2004) observed micro-pore formation in the resulting biochars while high heating rates and pressure (up to 2 MPa) led to the formation of biochars with smooth surfaces and spherical macro-pores due total melting of the char particle. This was also observed in hardwood feedstocks like eucalyptus and to an extent, high volatile matter feedstocks like sugarcane bagasse (Cetin et al. 2004). It therefore follows that chars with specific pore-sizes are obtained by varying the process parameters outlined above. Feedstock properties also influence char surface area however; plant-based biochars tend to be higher than animal-based

biochars, and lignin-containing feed-stocks could likely result in hydrochars with greater porosity development compared to cellulosic feed-stocks (Cao et al. 2013). Cao and Harris (2010) further suggested that feedstock properties may influence char specific surface areas to a greater extent than production process as feedstocks with higher C_{org} contents provide more opportunities for porosity development.

The influence of char surface area and porosity in soil management has been widely researched. Soil microbial activity, water cycling and sorption of organic species are affected by surface area (Cao and Harris 2010; Downie et al. 2009; Moreno-Castilla 2004) and it is suggested that chars with high surface areas improve soil nutrient retention since more sites for cation adsorption are available (Liang et al. 2006). A combination of micro-, meso- and macro-pores have been observed in biochars, described as pores with internal diameters <2 nm, 2–50 nm, and >50 nm respectively (Downie et al. 2009; Klobes et al. 2006; Lowell et al. 2004). Each of these pores perform certain functions in soil: micro-pores enhance gas-solid adsorption, and are therefore useful for adsorbing gases and solvents; meso-pores facilitate liquid-solid adsorption and hence useful for soil water retention (Downie et al. 2009). Glaser et al. (2002) suggested that nutrients like NO_3-N and base cations like K which are easily leached from soils at high and low soil pH conditions, respectively retained if soil water is trapped in meso-pores; macro-pores provide a habitat for many soil organisms and also enhance soil aeration and hydrology (Downie et al. 2009; Duku et al. 2011).

According to McLaughlin (2010), it is reasonable to assume that since biochar adsorption sites become obstructed or coated with foreign matter with time, biochar adsorption capacity is at its peak when freshly produced. Similarly, oxidation over time result in blockage of pores by O and H groups (Pradhan and Sandle 1999). On the other hand, considerable amounts of condensed volatiles may also block pores of some freshly produced chars at lower temperatures (< 450°C) (Downie et al. 2009). Chun et al (2004) demonstrated that wheat residue biochars with high surface areas and low oxygen contents may be better suited for sorption of low concentration non-polar neutral organic compounds like benzene. This is likely because oxygen groups attract water molecules and the latter impede access of organic species to carbon pores. In some cases however, char surface area and porosity may be of lesser importance for nutrient cycling compared to the surface functional groups present on both hydrochars and biochars (Spokas et al. 2011; Bargmann et al. 2014): Sun et al. (2011) observed that 250°C poultry litter

hydrochar (O/C = 0.4) had superior capacity for non-polar species (17α-ethinyl estradiol, bisphenol A) sorption compared to 400°C poultry litter biochar (O/C = 0.2), while sorption of phenanthrene was comparable in both chars. Conversely, some studies have suggested that since higher temperature chars tend to have higher NO_3^- removal efficiencies this may result from higher specific surface areas (Hale et al. 2013). More studies are required to confirm this however, since production temperature influences not only surface area but surface functionality and as such, a reduction in the number of acidic or negatively charged functional groups with temperature might result in similar improvements to NO_3^- removal efficiency.

2.2.3 Surface functional groups

As black carbon surfaces possess diverse heteroatoms or acidic, basic, hydrophilic and hydrophobic functional groups (Amonette and Joseph 2009; Brennan et al. 2001; Knicker 2007), they exhibit heterogeneous surface chemical characteristics owing to differences in the electronegativities of oxygen, nitrogen, phosphorus and sulphur with respect to that of carbon (Brennan et al. 2001). Oxygen-based surface functional groups are considered to be the most important surface functional groups on black carbon (Boehm 1994; Moreno-Castilla 2004; Puri and Bansal 1964); heterocyclic oxygen surface sites are thought to be responsible for anion exchange capacity (Lawrinenko and Laird 2015), CEC, and other char properties. Previous studies have attributed surface acidic properties in black carbon to high oxygen contents although Rutherford et al. (2008) however cautioned against using char oxygen content as a measure of acid functional groups due to observed differences in behaviour of both parameters with processing time.

The high oxygen content of biomass-derived black carbon results from the high oxygen content of biomass (30–40%, db) which is second only to carbon content (30–60%, db) (Jenkins et al. 1998), owing to the nature of its lignocellulose components (**Figure 2.1**)**.** Following thermochemical treatment, oxygen functional groups as shown in **Figure 2.2** exist on black carbon surfaces as acidic and/or basic oxides bound to carbon layer edges. Phenolic, lactone and other acidic oxygen groups are responsible for the acidic properties of black carbon and cation exchange properties (Boehm 1994; Puri and Bansal 1964) whereas black carbon with low oxygen contents possess basic surface properties and therefore exhibit anion exchange properties (Boehm 1994). K, Mg, Na, P and Ca present in feedstocks are the main components of ash (Wu et al. 2012), and these cations also

serve as catalysts for the formation of oxygen-containing functional groups like pyranones at low temperatures (Mészáros et al. 2007; Song and Guo 2012).

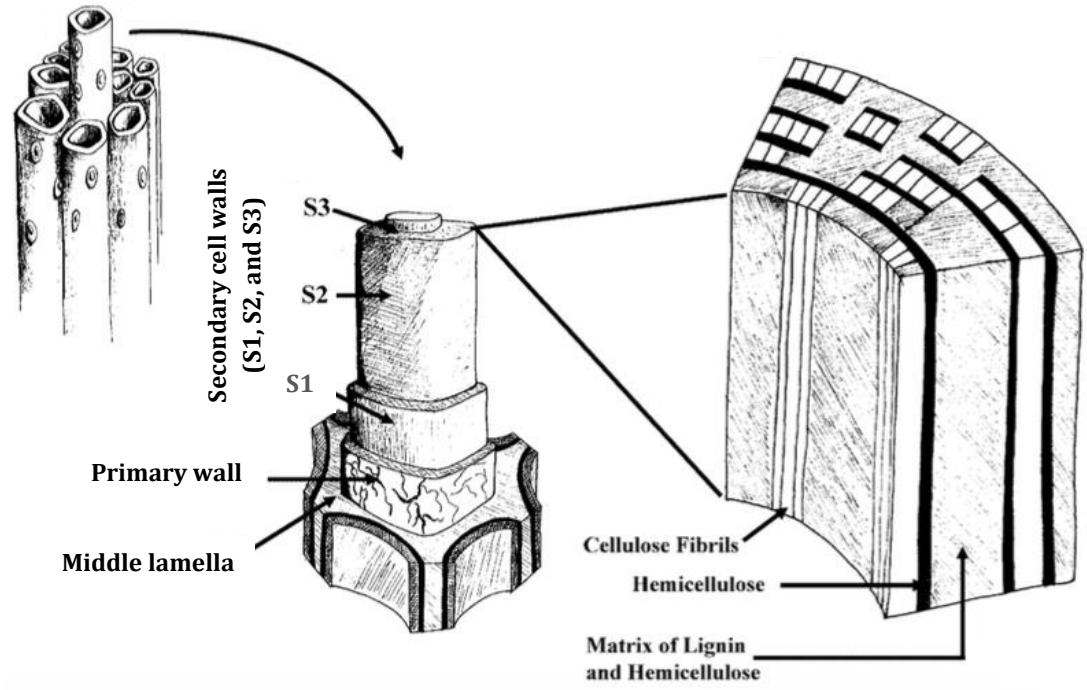

Figure 2.1 The structure of lignocellulosic biomass as illustrated by Perez et al. (2002), with minor adjustments.

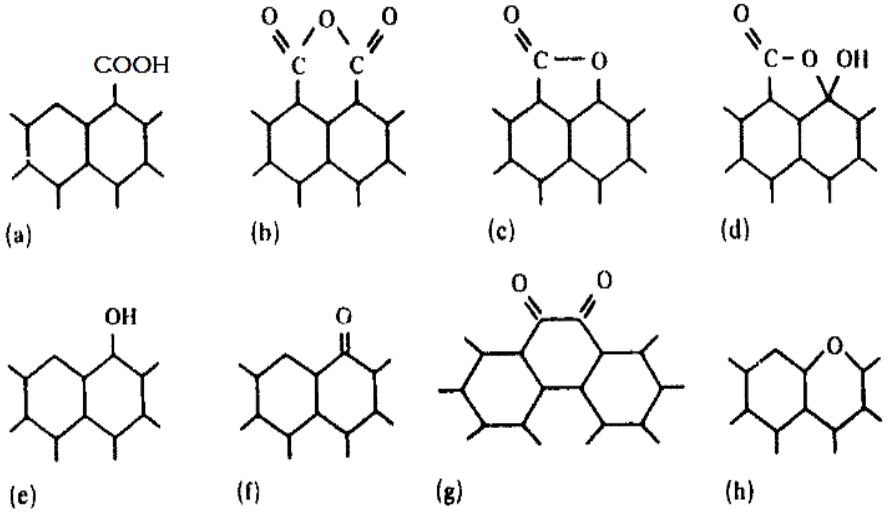

Figure 2.2 Nature of oxygen groups present in black carbon: (a) carboxyl groups; (b) carboxylic anhydrides; (c) lactone groups; (d) lactols; (e) hydroxyl groups with phenolic characteristics; (f) carbonyl groups; (g) quinone; (h) ether- or xathene-type oxygen groups (Boehm 1994).

2.2.4 Nutrient content and availability

The mechanisms through which chars adsorb nutrients and thus enhance soil productivity are not fully understood due to variations in climate and soil. Furthermore, as char properties are a function of the nature of feedstocks used and biomass processing conditions (Collison et al. 2009; Wang et al. 2015a; Zhao et al. 2013), these variations further contribute to the challenges involved with quantifying their effect on nutrient cycling. Moreover, biochars influence nutrient cycling via biological, physical, and chemical processes in the short- and long-term (Laird et al. 2010a; Biederman and Harpole 2013). In the short-term, labile fractions of biochar and hydrochar may introduce bioavailable phosphorus and potassium to soils (Biederman and Harpole 2013; Laird et al. 2010b; Uzoma et al. 2011) as well as retain nutrient-rich soil water within their pores, while long-term biochar effects involve creating favourable habitats for soil fungi such as mycorrhizae which influence nutrient cycling (Yamato et al. 2006). Biochar alkalinity results from the presence of various organic and inorganic compounds with varying degrees of solubility (Fidel et al. 2017), potentially contributing to soil alkalinity. High soil pH levels increase phosphorus availability, since in acidic conditions (pH <4), phosphorus is otherwise bound as insoluble iron and aluminium phosphates (Biederman and Harpole 2013; Uzoma et al. 2011; Xu et al. 2014).

In an attempt to identify char contributions to nutrient cycling in soils, this two-part section highlights the key factors influencing char nutrient bioavailability, after which a summary of char effects on soil nutrient cycling are outlined.

2.2.4.1 Intrinsic hydrochar and biochar nutrient contents

Biochars are comprised of labile and recalcitrant portions, both of which contain organic and inorganic components (McLaughlin 2010) such that they are comprised of complex aromatic-aliphatic organic compounds. Biochars also possess mineral compounds present as ash (Downie et al. 2009) and heavy metals depending on feedstock and thermal processing, as summarised in **Figure 2.3**. For instance, K is present in the organic matrix of biomass in the form of alkali-carboxylic groups, complex ions or as dissolved salts (Miles et al. 1995). When heated, K decomposes into various forms of low-melting point oxides, hydroxides, chlorides, and sulphates, some of which are reactive owing to their solubility in water or ion exchange ability (Miles et al. 1995). Hydrochars are equally heterogeneous (Cao et al. 2013) but compared to biochars, lower concentrations of inorganic elements (oxides of K, Ca,

Mg, P, Fe) are observed as a result of acid solvation reactions during hydrothermal carbonization (Kambo and Dutta 2015).

Quantification of char nutrient content is a necessary step towards gaining a better understanding of their effect on nutrient recovery (DeLuca et al. 2009). Following biochar application in soil, an increase in P, K, Ca, Mg, Mo, N and Cu solubility has been observed (Atkinson et al. 2010; DeLuca et al. 2009) yet large quantities of biochar would however need to be added to soils to provide the desired amounts required for plants (Ippolito et al. 2015). Furthermore, although nutrients are present in chars, their bioavailability or soil-extractable fractions, as measured at pH 7 with water or salt-based extractants (Ippolito et al. 2015) may be low (Atkinson et al. 2010; Cao and Harris 2010; Gaskin et al. 2008). For instance, Cao and Harris (2010) and Zhao et al. (2013b) found that while concentrations of P, Ca and Mg increased with pyrolysis temperature, water-extractable concentrations decreased substantially following pyrolysis owing to the formation of stable compounds. Gaskin et al. (2008) similarly found that weak acid (Mehlich I) extractable nutrients decreased with increasing pyrolysis temperature. Cao and Harris (2010) observed that P bioavailability decreased at about 500°C due to the formation of stable calcium phosphate. The decrease in water soluble P was also consistent with the formation of whitlockite at elevated temperatures (Cao and Harris 2010). Biochar K has however been found to be highly bioavailable, attributable to the formation of soluble sylvite (Fidel et al. 2017; Zhao et al. 2013b). Similarly, N bioavailability (in form of NO_2-N, NO_3-N and NH_4-N) often decreases as pyrolysis temperature increases, likely due to both conversion to more stable heterocyclic N forms and to gaseous N losses which begin from 200°C (Cao and Harris 2010; Gaskin et al. 2008; Tian et al. 2016; Quayyum et al. 2012).

In terms of nutrient retention capacity, processing temperature is also influential (Chan and Xu 2009; Bargmann et al. 2014; Ippolito et al. 2015) since surface area and functionality, both of which are suggested to influence biochar ion exchange capacities (Xu et al. 2013), are temperature-dependent (Chan and Xu 2009; Sparkes and Stoutjesdijk 2011). Liang et al. (2006) for instance noted that high O/C ratios could be responsible for nutrient adsorption since K/C ratios were at least 0.18 higher at black carbon surfaces than at char interiors.

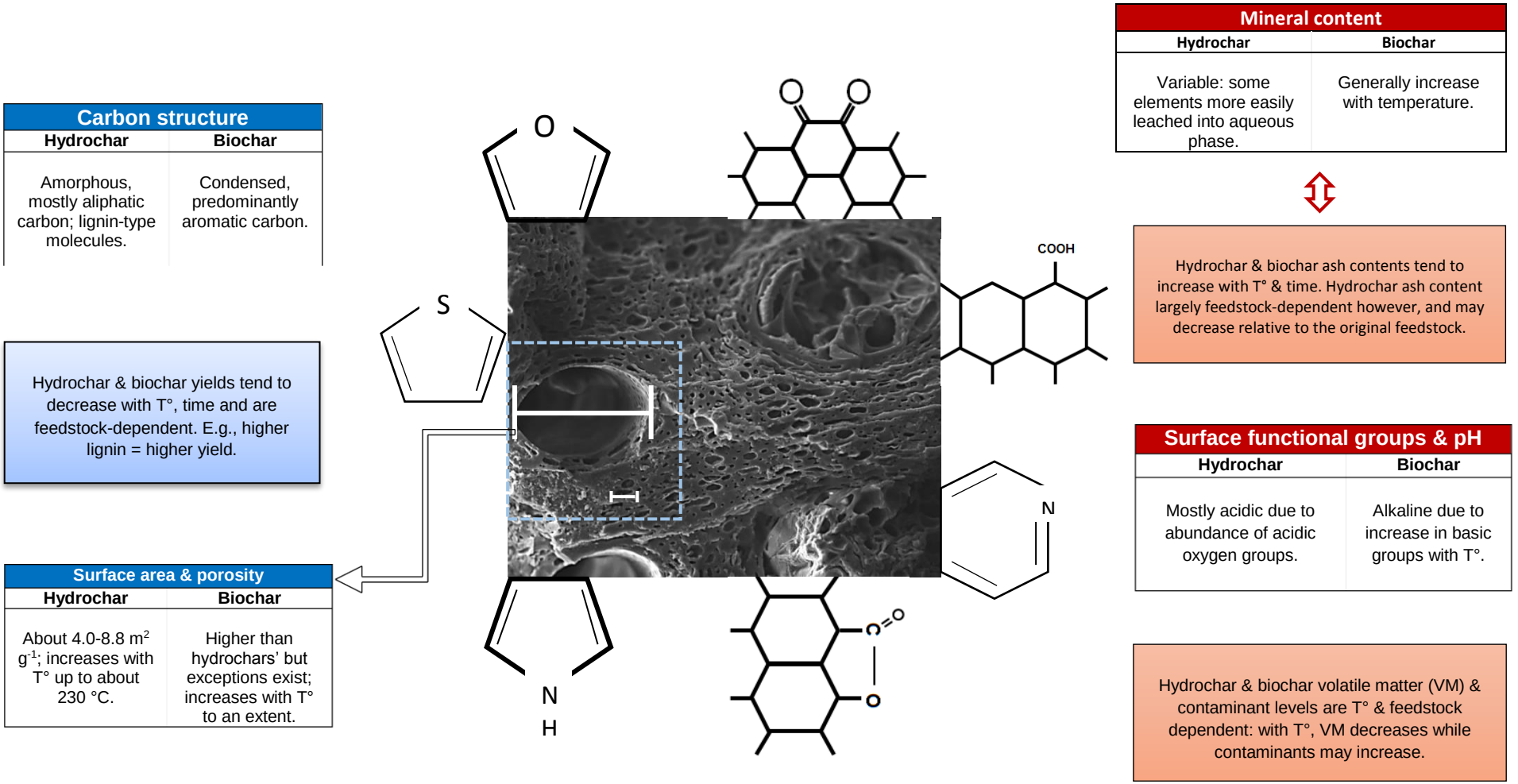

Figure 2.3 Generalized summary of the influence of processing conditions and feedstock properties on char physico-chemical characteristics (T° = temperature). Collated from: Benavente et al. (2015); Cao and Harris (2010); Chun et al. (2004); Danso-Boateng et al. (2015); Eibisch et al. (2015); Fang et al. (2015); Gronwald et al. (2015); Hoekman et al. (2011); Kalderis et al. (2014); Parshetti et al. (2014); Reza et al. (2013); Smith et al. (2016); Sun et al. (2011); Wiedner et al. (2013a); Zhao et al. (2013b). Further details are provided in Annex Table A1.

The length of time with which chars maintain effective nutrient retention capacities in soil is currently uncertain however, although Gronwald et al. (2015) reported that within a relatively short period (7 months), biochar and hydrochar nutrient retention capacities diminished and suggested that this was possibly due to blockage of nutrient binding sites by soil matter (microbes, organic matter and/or minerals).

2.2.4.2 Biochar and hydrochar effects on soil nutrient cycling

Chars may have favourable effects on biomass not necessarily because of their nutrient content but because they increase fertilizer-use efficiency by minimising nutrient leaching or by enhancing soil physical structure (Chan and Xu (2009). Biochars may influence soil nutrient content indirectly by improving soil water holding capacity since nutrients are present in soil water, and by creating favourable conditions for certain soil microbes. Variations in soil pH have cascading effects on soil organisms like bacteria, fungi, and earthworms. As such, multiple soil processes such as soil mixing, channel formation, C and N mineralisation are altered by slight changes in soil pH (Fidel et al. 2017; McCormack et al. 2013). Furthermore, several studies have also linked improvements in soil nutrient availability to pH effects. For instance, from a series of experiments designed to identify mechanisms through which biochars enhanced nutrient availability in soil, Xu et al. (2013) suggested that an increase in pH was responsible for the increase in P solubility. Tryon (1948) proposed that ash content in charcoal is mostly responsible for soil buffer capacity based on observations of an increase in soil buffer capacity when high ash content charcoals were applied to sandy soil, but an opposite effect when low ash content charcoal was incorporated. As such, it is unclear whether hydrochars will therefore reduce the solubility of some nutrients given their acidic nature, or if the more readily-soluble nutrients in hydrochars compensate for any adverse effects resulting from low soil pH. Similar to biochars however, hydrochars produced under different processing conditions and feedstocks understandably have varying effects on important soil microbes, plants and earthworms (Bargmann et al. 2014; Reza et al. 2014; Rillig et al. 2010). For instance, while yeast-based hydrochars were shown to have no major effect on microbial biomass, glucose-based hydrochars had a negative effect (Reza et al. 2014). Rillig et al. (2010) noted, however, that even the hydrochar source material had a negative effect on plants.

In terms of soil nitrogen dynamics, char effects in soil vary: no marked effect on nitrification has been observed following biochar addition in spite of increased

organic matter mineralisation (Dempster et al. 2012; Schulz and Glaser 2012); other studies have reported increases in soil nitrification and mechanisms have been proposed for this increase, as outlined by Prommer et al. (2014), including increases in nitrifying bacteria activity as such pH-sensitive organisms thrive at higher pH conditions (Dempster et al. 2012); conversely, that hydrochar and biochar addition have decreased nitrous oxide emissions (Kammann et al. 2012), NO_3-N concentrations (Bargmann et al. 2014) and organic nitrogen transformation (Prommer et al. 2014). With regard to why nitrification decreases with biochar addition, Kammann et al. (2012) and Schulz and Glaser (2012) suggested that N-immobilization occurred. This is possible since biochar C/N ratios can be about 67 on average (Chan and Xu 2009), and C/N ratios >25–30 result in inorganic nitrogen immobilization, yet Chan and Xu (2009) suggested that as biochar carbon is recalcitrant, nitrogen immobilisation could be minimal. In cases where biochars have improved NH_3-N and NH_4-N retention, a number of biotic and abiotic mechanisms have been suggested, such as electrostatic interactions with oxygenated or organic ligand functional groups (Ippolito et al. 2015; Wang et al. 2015b), interactions with S-functional groups, conversion of NH_3-N to NH_4-N at low pH, as well as physisorption reactions (Ippolito et al. 2015). Chars also influence denitrification by participating in reversible electron donor or acceptor interactions and increasing certain bacterial populations (Tian et al. 2016).

2.2.5 Cation Exchange Capacity (CEC)

CEC is a measure of the capacity to which a material's negatively charged sites are neutralised by exchangeable cations (Mukherjee et al. 2011) and is expressed in milliequivalents (mEq) per 100 g of soil (Rhoades 1982) or more recently as centimoles of charge per kilogram ($cmol_c\ kg^{-1}$), both of which are equivalent units (Sumner and Miller 1996). While neutralization occurs at negatively-charged sites by interactions with cations, a small portion of negatively-charged sites are also responsible for repelling anions. To reflect the small contribution of anionic species, CEC is considered to represent an abundance of cationic charge over anionic charge (Sumner and Miller 1996).

Statistical analysis of some biochar properties by Morales et al. (2015) suggested that CEC is independent of biochar elemental contents, which is in agreement with earlier findings of Kirchmann and Witter (1992) which suggested that inorganic content possessed a marginal effect on the CEC of relatively high organic content feedstocks such as manure. Other studies have however implied that higher ash

contents could result in higher char CEC values (Gaskin et al. 2008; Zhao et al. 2013b). The consensus however is that chars created at low temperatures would be better suited for soil since several studies including Lehmann (2007) and Sparkes and Stoutjesdijk (2011) have observed a decrease in CEC with increasing pyrolysis temperature, corresponding to a loss of functional groups like carboxylic acids. Carboxylic acids are formed from the thermal degradation of lignocellulose via thermal oxidation of phenols and alcohols from lignin, or cycloreversion, transglycosylation, or Ei-elimination of cellulose (Harvey et al. 2012a). Black carbon CEC is also thought to increase due to the gradual production of carboxylic groups at the ends of charcoal's aromatic backbone (Glaser et al. 2002). Other studies have also inferred that oxidised organic matter on black carbon surfaces lead to the formation of net negatively charged oxygenated functional groups like carboxyl and hydroxyl groups, fulvic acids, humic acids and other humic substances thus increasing soil CEC (Boehm 1994; Kirchmann and Witter 1992; Lehmann, 2007; Petrov et al. 1992; Song and Guo 2012).

Studies have shown that black carbon increases soil CEC per unit surface area; Liang et al. (2006) observed that: Amazonian anthrosols which contained black carbon possessed a higher CEC and suggested that CEC per unit soil carbon increased due to an increase in surface area thus creating more adsorption sites for cations, or because soil organic matter was oxidized to a greater extent due to its higher charge density. This was based on observations that while O/C ratios were generally low, microprobe elemental analysis of one of the soil samples showed that O/C ratios were higher at the surface of black carbon than at the centre of the black carbon structure, indicative of surface oxidation, adsorption of organic matter from plants/microbial metabolites or both. As biochar properties change in the environment, aged biochar CEC may become higher than freshly made biochar CEC Lehmann (2007).

CEC analysis is dependent on parameters like pH, concentration and ionic strength of saturating solution (index cation), nature of washing solution and temperature; variations in these parameters understandably yields different CEC results (Papanicolaou and Overstreet 1969; Rhoades 1982; Sumner and Miller 1996). Skinner et al. (2001) also demonstrated this based on CEC determination of humified organic matter, kaolinite and vermiculite. Each method yielded different values while the general trend remained the same as shown in **Figure 2.4**. As a result, selection of CEC method tends to be dependent on the purpose for which the analysis is required (Ross and Ketterings 1995; Sumner and Miller 1996). Generally,

four main methods for determining soil CEC were outlined by Rhoades (1982): *the summation method*, where CEC is determined as the amount of exchangeable cations present in the leachate obtained after a saturating salt solution displaces exchangeable soil cations; *direct displacement*, with three steps involving: (i) displacement of exchangeable cations with an index cation, (ii) desorption of index cation by another cation, and (iii) subsequent determination of the displaced index cation, as done by Harada and Inoko (1975) and Keeney and Bremner (1969); *displacement after washing*, which differs from the direct displacement method because an intermediate step is included, involving washing excess index cation from sample with a solvent prior to desorption with other cations; *radioactive tracer method*, which involves labelling saturated salt solutions with radioactive isotopes of the saturating cation (Rhoades 1982). Ammonium salts are frequently used saturating solutions, either as index or displacement cation (Gaskin et al. 2007; Méndez et al. 2013; Song and Guo 2012; Wu et al. 2012; Yuan et al. 2011) although concentrations vary.

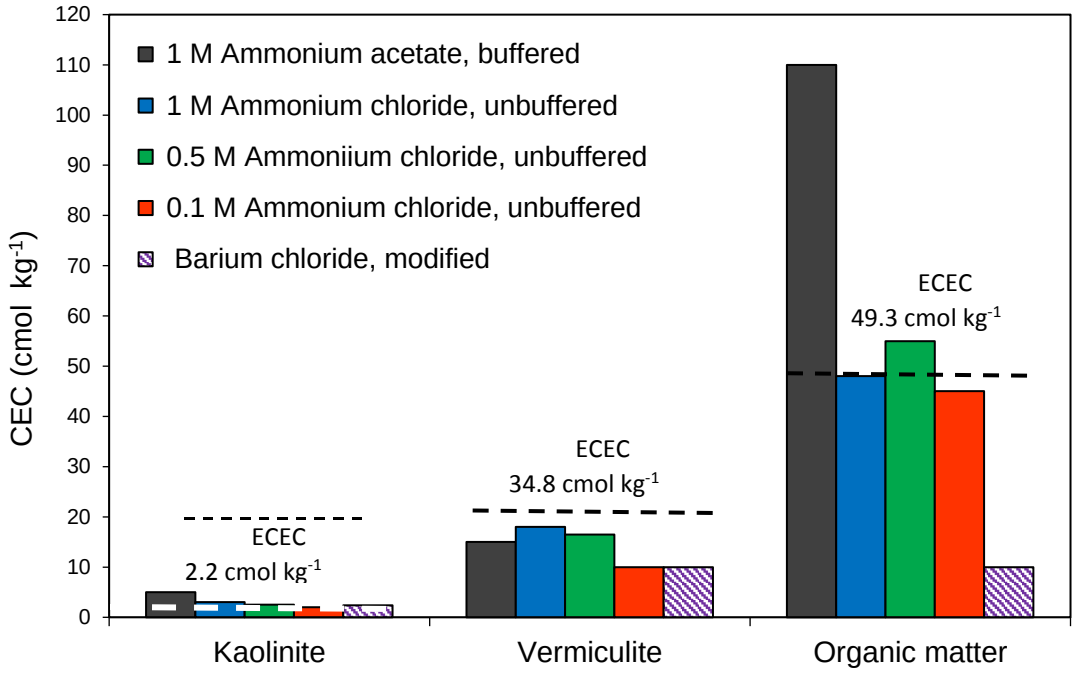

Figure 2.4 Approximate CEC values obtained from column CEC experiments by Skinner et al. (2001), adapted to highlight variations in CEC with method and sample type. Dashed lines represent effective/established CEC values (ECEC) determined from summation of K, Na, Mg, Ca and Al ions.

Errors can arise during any of the CEC analysis steps:

1. At the saturation stage, cations from the saturating solution might not be as strong as cations already present, such as aluminium and its hydroxyl

cations. Furthermore, dissociation of compounds like calcium carbonate and silicate during saturation cause these cations to compete for exchange sites (Rhoades 1982; Sumner and Miller 1996).

2. The washing stage typically involves rinsing off the excess index cation with water, alcohol, or acetone; errors may arise due sample losses during decantation, in addition to loss of some index cation via hydrolysis (Rhoades 1982), although Harada and Inoko (1975) did not find this to be the case; removal of some organic matter when washing with alcohol. In some samples, errors arise due to dissociation of calcium carbonate, resulting in adsorption of calcium ions onto the sample.
3. At the displacement stage, errors arise when nonexchangeable cations are displaced; this occurs in arid soils when displacing solutions containing calcium or magnesium or ammonium acetate are used. Calcareous soils and soils containing minerals like zeolites, magnesium and iron (mafic), feldspars are also susceptible to this problem (Rhoades 1982). By implication, this may suggest that chars rich in soluble Ca may pose similar challenges.

2.3 Potential for nutrient recovery with hydrochars and biochars

While traditional activated carbon is the standard adsorbent used in wastewater treatment and gas adsorption, it is considered expensive for agricultural purposes so alternative waste-derived feed-stocks have been evaluated (Kastner et al. 2009) ranging from agricultural by-products to industrial waste materials (Pollard et al. 1992). As chars are produced from a wide range of waste biomass feedstocks, they show potential as cost–effective, environmentally sustainable products for integrated waste management. As this study focused on the potential for minimizing nutrient losses arising from agricultural and industrial activities, this section highlights hydrochar and biochar interactions in nutrient-rich environments like composts and wastewater and outlines some of the proposed mechanisms governing such interactions.

2.3.1 Co-composting with hydrochars and biochars

Composting has been used for stabilising organic waste with the aid of microbes at aerobic conditions (Dias et al. 2010). The resulting product has a low moisture content, odour and pathogen population compared to raw bio-waste, making it suitable for land application (Kelleher et al. 2002; Kithome et al. 1999). During

composting however, nitrogen losses occur due to ammonia volatilisation (Kelleher et al. 2002), ranging from 17–63% in high nitrogen-content wastes (Kithome et al. 1999). This is because nitrogen in such wastes is present as uric acid and urea (Kelleher et al. 2002; Kithome et al. 1999; Nahm 2003; Schmidt 2012) and when pH, temperature and moisture conditions are suitable for microbes, these compounds are enzymatically hydrolysed into ammonia and carbon dioxide rapidly (Kithome et al. 1999; Nahm 2003; Steiner et al. 2010). Ammonia exist in gaseous or ionic state, both of which cause environmental problems when present in excess. High concentrations of free ammonia inhibit anaerobic microbes while NH_4^+ raise soil acidity (Kelleher et al. 2002; Schmidt 2012). Additionally, microbes nitrify ammonium ions into nitrates which are easily leached to groundwater (Kelleher et al. 2002; Nahm, 2003).

A number of attempts have therefore been made to minimise the hydrolysis of uric acid to ammonia with the aid of organic chemicals like formaldehyde (Kithome et al. 1999), stabilising urea by lactic acid fermentation (Schmidt 2012), or reducing ammonia volatilisation using inert adsorbents like clinoptilolite zeolites and montmorillonite clay, carbon-rich organic wastes or inorganic chemicals (Kastner et al. 2009; Long et al. 2008; Park and Jin 2006; Steiner et al. 2010). Some of these amendments affect compost properties adversely however. For instance, the addition of organic chemicals affects nitrification and results in poultry litter unfit for composting (Kithome et al. 1999). Similarly, while matter with high C/N ratios minimise ammonia volatilization, this is achieved at the expense of decomposition speed (Steiner et al. 2010). Furthermore, materials rich in soluble organic carbon lead to anaerobic conditions due to the release of CO_2.

Kithome et al. (1999) found that zeolites applied on manure surfaces adsorbed ammonia more effectively meanwhile clays increased ammonia volatilization. Other adsorbents considered for ammonia adsorption include activated carbon (Kastner et al. 2009; Long et al. 2008; Park and Jin 2006; Steiner et al. 2010) and black carbon possessing good pore surface area, pore structure and surface functional groups (Kastner et al. 2009; Steiner et al. 2010). While earlier studies suggested that activated carbon surfaces were not sufficiently polar (Park and Jin 2006; Rodríguez-Reinoso 1998), more recent studies have shown that their above-mentioned properties make activated carbons effective ammonia adsorbents (Kastner et al. 2009; Steiner et al. 2010). As aforementioned, activated carbon may be expensive for agricultural purposes (Kastner et al. 2009) since substantial modifications are typically required for carbon activation. Consequently, low-cost black carbon

adsorbents such as biochar and hydrochar produced from organic waste have been considered for minimizing ammonia emissions.

The synergistic nature of co-composting with chars has been widely reported. Chars benefit from the sorption of dissolved organic matter during composting (Borchard et al. 2012) and may show potential for the sorption of humic-like acids, particularly chars rich in Ca^{2+} and Mg^{2+} based on adsorption studies by Daifullah et al. (2004). Concurrently, organic matter blended with chars benefit from reduced odour, and improvements in bulk structure and supply of nutrients for microbes have been (Bargmann et al. 2014; Dias et al. 2010; Hunt et al. 2010; Reza et al. 2014). The lattermost may be especially true for hydrochars as they possess less recalcitrant carbon than biochars (Busch and Glaser 2015). Steiner et al. (2010) found that chars minimised ammonia volatilisation and hydrogen sulphide emissions substantially. Dias et al. (2010) also reported reductions in ammonia volatilization in biochar-amended composts. The final products obtained from char co-composting possessed balanced nutrient contents (Dias et al. 2010), and Vandecasteele et al. (2016) showed that NH_4-N sorption was higher in biochar-amended compost material compared to un-amended compost material after 14 days of composting.

To obtain maximum soil NH_4-N retention benefits from biochar-compost mixtures, some studies have recommended incorporating biochars at the start of composting, as biochar surface oxidation by microbes improves biochar CEC and oxygen content (Borchard et al. 2012; Dias et al. 2010; Schulz and Glaser 2012). In terms of mixing proportions, some studies recommend mixing equal parts of biochar and compost to produce the best co-composting results (Busch and Glaser 2015; Schulz and Glaser 2012), although lower biochar and char ratios have been used (Busch and Glaser 2015).

2.3.1.1 Composting stages

Four composting stages were outlined by Bernal et al. (1998): an initial stage where no biological degradation has occurred; thermophilic stage where degradation occurs and temperatures rise to >40°C; a stage marking the end of biological activity and a consequent decrease in temperature; a maturation phase resulting in a stabilized, humic-like product (compost). During composting, CO_2 evolution and/or O_2 sorption is measured, as these serve as indicators of steady soil and microbial respiration, the latter described as soil basal respiration resulting from organic matter mineralization (Creamer et al. 2014).

Although the composting process does not produce humus, adequate composting practices begin the process of humification (Epstein 1997), thus higher amounts of humic-like substances are indicative of higher compost quality (Dias et al. 2010). Biochars have been found to increase the humic acid content of organic matter during composting, and Dias et al. (2010) suggested that this might have been due to the addition of water soluble carbon (carbohydrates) from the biochars, but from earlier studies by Sánchez-Monedero et al. (1999) no correlation was observed between water-soluble carbohydrates and % humic acid or humification index in most cases. In other words, this increase in humic acid content during biochar co-composting may not have been due to the synthesis of humic-like substances from water-soluble carbohydrates. However, as a relatively low temperature biochar (450°C) was used in Dias et al. (2010), it may be possible that the additional supply of water soluble carbon served as a food source for microbes thus indirectly facilitating carbon further lignin degradation. This may have resulted in the production of phenols, which Sánchez-Monedero et al. (1999) found to be correlated to the humification process.

2.3.1.2 Ammonia and black carbon interaction

Previous studies have suggested that ammonia adsorption by black carbon is influenced by acidic functional groups such as carboxyl, lactone, phenol and acid anhydride groups (Corre et al. 2013; Kastner et al. 2009; Park and Jin 2006; Taghizadeh-Toosi et al. 2012a) more substantially than surface area and micro-pore volume (Corre et al. 2013). Oxygen functional groups also influence the stability of nitrogen groups (Pietrzak et al. 2007). Mechanisms for NH_3 sorptioninvolve interactions at Brønsted and/or Lewis acid sites. In the former case, protonation of NH_3 occur as NH_3 dissociates in water, or via acid-base neutralization reactions with carbonyl and phenolic OH^- groups present on adsorbents to form NH_4^+ complexes (Corre et al. 2013; Le Leuch and Bandosz 2007; Long et al. 2008; Petit and Bandosz 2009; Steiner et al. 2010; Taghizadeh-Toosi et al. 2012a). These findings suggest that hydrochars are likely to possess greater ability for NH_3-N / NH_4-N sorption compared to biochars given their higher proportion of acidic functional groups. On the other hand, since some studies have reported that high adsorbent surface areas and pore volumes improve NH_3-N / NH_4-N removal efficiencies (Ismadji et al. 2016; Petit and Bandosz 2009), the higher surface areas of biochars might compensate for their lower acidic functionalities. Chen et al. (2010) noted that the addition of bamboo pyrolysis products (char and vinegar) significantly reduced Total Kjeldahl Nitrogen (TKN) losses from pig manure compost. It is also known that

pH plays an important role in ammonia volatilisation, leading to ammonia losses at pH values > 7 (Steiner et al. 2010). For instance, Kithome et al. (1999) found that when poultry manure was amended with two types of zeolites, ammonia volatilisation was lower from the compost amended with lower pH zeolite (pH 7.9) compared to the zeolite (pH 9.1). Kastner et al. (2009) explored the possibility of producing chars from agricultural residues that were comparable to activated carbon but cheaper, and found that chars produced at low pyrolysis temperatures (400–500 °C) could adsorb ammonia provided they possessed acid functional groups. Taghizadeh-Toosi et al. (2012a) also found that biochars with lower pH values and higher surface acidity retained more nitrogen. This is possibly because $CO\text{-}NH_4^+$ complexes are formed when ammonia reacts with the acid part of carbonyl and phenolic hydroxyl groups on carbon surfaces (Long et al. 2008). At ambient temperatures, ammonium salt and amide formation occurs when ammonia reacts with surface carbonyl groups (Spokas et al. 2011).

With regard to the relationship between ammonia adsorption on carbonaceous materials, Corre et al. (2013) suggested that since ammonia is a basic compound, adsorbents benefit from having acidic surface functional groups like carboxylic acids, as well as small pores and electrical conductivity. Park and Jin (2005) similarly found that even though ozone treatment reduced char specific surface area, micro-pore volume and total pore volume over time, ammonia removal efficiency improved due to the incorporation of strong and weak oxygenated acid functional groups like ether and carbonyl onto the carbon material. Subedi et al. (2015) similarly found that surface area and porosity did not influence ammonia sorption. It is therefore important to ensure that biochar production processes improve biochar acidity (Taghizadeh-Toosi et al. 2012a). Subedi et al. (2015) however observed that in hydrochar-amended soils, more ammonia was volatilized relative to biochar-amended soils and un-amended soils possibly due to hydrochar hydrophobicity's effect on slurry infiltration into soil as well as soil NH_4-N sorption.

2.3.2 Wastewater sorption processes

Various wastewaters can contain high concentrations of ammonium and phosphates as shown in **Table 2.3**, excessive quantities of which contribute to eutrophication. Some existing chemical and biological technologies for ammonium and phosphate removal and recovery have been outlined in Kney and Zhao (2004), Molinuevo et al. (2009), and Morse et al. (2008).

Table 2.3 Ammonium and phosphate concentrations in some effluents

S/N	Effluent source	Phosphate (mg L^{-1})	Ammonium (mg L^{-1})	Reference(s)
AS-RECEIVED WASTEWATER				
Agricultural wastewater				
1	Beef liquid manure slurry	1700†	3560†‡	Barker et al. (2001)
2	Swine wastewater	34–654§	90–3030	Barker et al. (2001); Capdevielle et al. (2013); Fernando et al. (2005); Suzuki et al. (2006); Ye et al. (2010)
3	Anaerobic Digestion (AD) swine wastewater supernatant	22.2–161	380–706	Huang et al. (2011); Song et al. (2011); Szogi and Vanotti (2009)
4	Hydrothermally treated pig manure	560–8510¶	10600–62000¶	Ekpo et al. (2016)
5	Vegetable (potato) processing	14–115	61–426	Carballa et al. (2009)
6	Poultry (layer) liquid manure slurry	2800†	5730†‡	Barker et al. (2001)
Industrial wastewater				
7	Wet process phosphoric acid	46–15,700	1150	Battistoni et al. (2006); Grzmil and Wronkowski (2006)
8	TFT-LCD manufacturing	188	n.a	Lu and Liu (2010)
9	Semi-conductor manufacturing	265	213	Warmadewanthi and Liu (2009)
10	Phosphorus plant	2000	85‡	Bott et al. (2003)
11	*Various:* Paper mill, textile, tannery, winery and olive mill	0.6–182¶	1.1–532¶	Cai et al. (2013)
Municipal wastewater				
12	Characteristic residential	6–12¶	26–75¶	USEPA (2002)
POST-TREATED WASTEWATER				
1	Pig manure effluent from post-digested, partially oxidised Upflow Anaerobic Sludge Blanket (UASB) reactor	n.a	670 (82% removal)	Molinuevo et al. (2009)
2	Treated municipal effluent wastewater	9	n.a	Kney and Zhao (2004)

†Calculated from mean of values presented; ‡as mg L^{-1} TKN and NO_3^--N; §data presented as 654(±232); ¶As mg L^{-1} total phosphorus or total nitrogen; n.a: unavailable data.

As the central theme of this study involved investigating possible interactions between nutrients and chars, the subsequent section expatiates on the main sorption principles used in this study.

2.3.2.1 Factors influencing char sorption capacity

Adsorption involves the transfer of “adsorptive” or “adsorbate” to a solid phase “adsorbent” (Giles et al. 1974; Limousin et al. 2007; Sparkes 2003), wherein adsorptive refers to the species that has potential to be adsorbed from solution and adsorbate refers to the substance accumulated at the interface or solid surface of an adsorbent. Adsorption differs from absorption because the former process tends to be a surface phenomenon in which phase changes or chemical reactions do not necessarily occur between adsorbent and adsorbate (Mantell 1987). However, because chemical reactions like surface precipitation or polymerization occur along with adsorption, the term “sorption” is thought to be preferable (Mantell 1987; Sparks 2003). It has been assumed that sorption can occur in 3 steps: movement of solute from bulk fluid to adsorbent surface via a thin liquid film layer surrounding the adsorbent; movement of solute from adsorbent pores to adsorption sites (intra-particle diffusion); adsorption of solute at adsorption sites (Sun et al. 2015).

Factors influencing adsorption include adsorbent porosity which has a direct relationship with effective diffusivity, which in turn influences the rate of solute (e.g. nutrient) sorption to and from adsorbents. Adsorbents are considered suitable if minimal quantities are required and if sorption occurs over brief residence times (Do 1998). Adsorbents are therefore often required to have high surface areas or micropore volumes and good pore networks; for instance, mesopores may serve as conduits to micropores (Do 1998; Marsh and Rodríguez-Reinoso 2006). Adsorbent molecular size, solubility and quantity also influence adsorption effectiveness (Kizito et al. 2015; Dias et al. 2007). Other factors include initial adsorptive/solution concentration, competition for adsorbent sites by solutes, time (kinetically controlled reactions) and affinity for the adsorbate, and to an extent temperature influence adsorption/desorption isotherm characteristics (Foo and Hameed 2010; Ng et al. 2002; Kizito et al. 2015; Limousin et al. 2007; Wang et al. 2011). With regard to the effect of initial solution/adsorptive concentration (C_o), studies have observed that as C_o increases, the quantity of adsorbate deposited on the adsorbent material (q_e) increases. Conversely, adsorbent removal efficiency decreases due to a reduction in available sorption sites (Wang et al. 2011).

Sorption tests are performed in open-flow systems (e.g. column tests) or closed systems (e.g. batch tests) and Limousin et al. (2007) expanded on the merits and demerits of both systems and proffered possible measures for reducing some of the associated systems' shortcomings. Tian et al. (2016) and Yao (2013) however observed that both systems appeared to be comparable. In laboratories, batch sorption tests are the frequently used methods due to their low time and cost requirements (EPA 1999). While the nature of the sorption system may not affect the quantity of solute adsorbed to the same extent as does adsorbent to adsorbate ratio (Limousin et al. 2007), the use of adsorption systems and ratios that are representative of real-case scenarios are preferable (Fernando et al. 2005; Limousin et al. 2007). An additional factor to consider involves the use of simple (pure) versus complex component systems. Do (1998) and EPA (1999) suggested that more information about adsorption equilibria are obtained from pure component systems as fewer species are involved and the system is well defined. However, small but significant factors such as the presence of organics and some metal oxides affect quantities of solute adsorbed.

2.3.2.2 Adsorption isotherms

Following batch or column sorption tests, quantitative information on adsorbent sorption capacity must be obtained. This is made possible by correct interpretation of sorption isotherms and equations, the former which are curves that provide useful measureable information on the distribution of adsorbate between the liquid and solid phases at equilibrium and constant temperature (Ayoob and Gupta 2008; Foo and Hameed 2010; Limousin et al. 2007; Ng et al. 2002). The sorption isotherm model classification system proposed by Giles et al. (1974) is comprised of 4 main isotherm classes as shown in **Figure 2.5**, of which Limousin et al. (2007) and Sparkes (2003) expatiated:

1. The sigmoidal S isotherm occurs because at low adsorptive concentrations, the slope increases but only until available adsorption sites become occupied. This suggests that at low adsorptive concentrations, the adsorbent has low affinity for the adsorptive while the reverse is observed at higher concentrations. Such behaviour is observed in surfactants and non-polar organic compound-clay systems.

2. In the concave L isotherm, the slope continues to increase from low adsorptive concentrations until available adsorption sites on the adsorbent become filled. Since the slope decreases as adsorptive concentration increases, adsorbent affinity for adsorptive may be greater at low adsorptive concentrations.

3. The H isotherm is a different version of the L isotherm, with high affinity between the adsorbent and adsorptive suggestive of strong interactions such as inner-sphere complexes, in which the adsorptive is bound to adsorbent surface functional group(s) without a water molecule present between them.

4. In the linear C isotherm, solute concentration in adsorbent remains the same regardless of adsorptive concentration provided adsorbent saturation is yet to be attained. This isotherm class suggests partitioned distribution of adsorptive between the interfacial and bulk solution phases. Partitioning mechanisms are also suggested for situations where there is no competition between adsorptives, or when temperature has a minor effect on sorption, or when reversible sorption occurs.

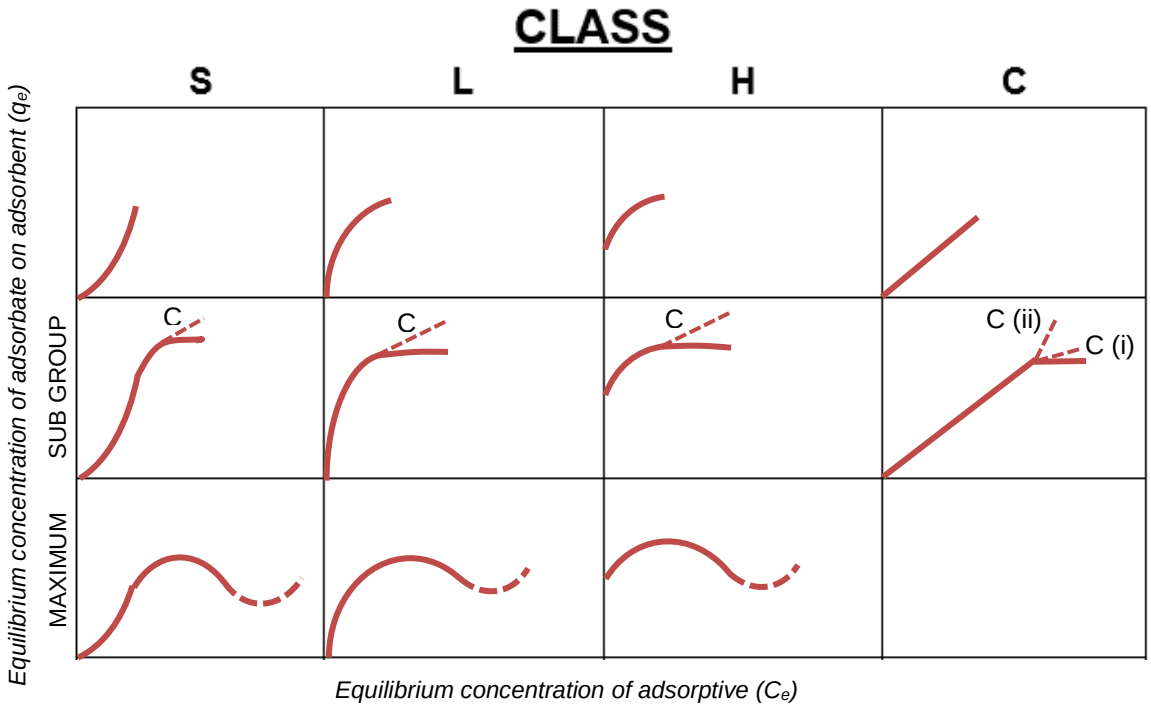

Figure 2.5 The sorption isotherm classification system adapted from Giles et al. (1974).

As outlined in Inyang and Dickenson (2015), adsorption of polar and non-polar organic compounds is dependent on the nature of the char and on the species, and occurs by: pore diffusion or filling, which may occur in biochars with low volatile matter or at low organic pollutant initial concentrations (C_o); sorption onto organic matter, as suggested for biochars with high volatile matter contents or at high organic pollutant C_o; adsorption of hydrophobic organic compounds by partitioning on biochar sites; adsorption of ionic organic compounds by electrostatic interaction; adsorption of planar aromatic compounds on low-temperature biochars via π-electron donor-acceptor interactions; hydrogen bonding between biochars and polar electronegative organic compounds. Similar mechanisms have been proposed for inorganic species sorption in Schlegel et al. (1999) and Limousin et al. (2007).

To gain a better understanding of the mechanisms involving hydrochar and biochar nutrient sorption and release, equilibrium and kinetic adsorption models are required. Choosing appropriate models is a decisive step towards obtaining accurate predictions of adsorption behaviour (Foo and Hameed 2010; Limousin et al. 2007; Mane et al. 2007). As no one model is currently capable of being applied to all adsorption systems, various models are compared to obtain the best fit using linear and/or nonlinear regression analyses (Ayoob and Gupta 2008; Prasad and Srivastava 2009), compared by their number of degrees of freedom (Maurya and Mittal 2006). Key equilibrium and kinetic models are outlined subsequently.

2.3.2.3 Equilibrium adsorption isotherm models

Isotherm model development involves potential theory, a thermodynamic approach and a kinetic approach, and adsorption equilibrium is attained when the rates of adsorption and desorption are equal (Foo and Hameed 2010; Limousin et al. 2007; Malek and Farooq 1996). Annex Table A2 summarises some of the frequently kinetic models used in the literature. Equation 2.1 provides a general description of the relationship between adsorbate-adsorbent systems in equilibrium and whose physico-chemical properties are constant (Limousin et al. 2007):

$$Q = f[C] \qquad (2.1)$$

where Q = amount of solute on adsorbent (mol kg^{-1} or kg kg^{-1}); C = concentration of solute remaining in adsorbate solution (mol L^{-1} or kg L^{-1}).

Equation 2.1 describes Henry's Law and is applicable at only low concentrations (Maurya and Mittal 2006). Q is determined as the difference between the initial solute concentration in solution and the final equilibrium concentration (Limousin et al. 2007). The relationship between Q and the initial and final solution concentrations was proposed in the late 19th Century (Limousin et al. 2007) and is given in Equation (2.2):

$$Q = \left(C_o - C_e\right) \frac{V}{m} \qquad (2.2)$$

where C_O and C_e = initial and equilibrium solution concentrations respectively (mol L^{-1} or kg L^{-1}); V = volume of solution (L); m = adsorbent mass (g).

However, sorption occurs by surface reactions, precipitation and co-precipitation reactions as aforementioned, none of which Equation (2.2) describe (Limousin et al. 2007. Consequently, several liquid-solid equilibrium and kinetic adsorption models exist, some of which are presented in Annex Table A2. Generally, the most popular equilibrium isotherm models used are the Langmuir, Freundlich and Redlich-Peterson models (Foo and Hameed 2010; Ho 2004). The Langmuir and Freundlich adsorption models are used to evaluate possible adsorption mechanisms and adsorption affinities (Angin et al. 2013; Sakadevan and Bavor 1998). The Langmuir model suggests mono and multilayer adsorption (Saleh et al. 2012), while adsorbents with heterogeneous surfaces are better described by the Freundlich model (Angin et al. 2013; Sakadevan and Bavor 1998).

There are challenges associated with obtaining accurate models however, such as mathematical complexity. Malek and Farooq (1996) noted that the number of independent parameters in an isotherm model is directly related to model accuracy in nonlinear systems but at the expense of its mathematical simplicity and consequently, versatility. Nonlinear isotherm models are required to have at least 3 independent parameters. Limousin et al. (2007) however advised on starting from the simplest model and then moving onto more complex models when required. Another challenge lies in the linearisation process: in linear regression, coefficients of determination (R^2) values closer to 1 are preferable (Ayoob and Gupta 2008). Unfortunately, a linearised model deemed best fit by linear analysis sometimes be

inaccurate from a nonlinear analysis point of view, as observed by Ayoob and Gupta (2008) in their comparison of R^2 and sum of normalised error (SNE) X^2 functions. This is because the transformation of a nonlinear equation result in differing outcomes due to a distortion of experimental error distributions (Ayoob and Gupta 2008; Ho 2004; Kumar and Sivanesan 2006a) since a Gaussian distribution of scatter points with equal errors are assumed (Kumar and Sivanesan 2006a). Consequently, rather than relying solely on the coefficient of determination (*R2*) values obtained from linear plots, comparisons of both linear and nonlinear regression parameters are considered preferable (Ayoob and Gupta 2008). The absolute error function (X^2) values are compared by Chi-square analysis (Equation 2.3), which compares all isotherms on the same ordinate and abscissa (Ho, 2004); smaller X^2 values imply that experimental and model data are similar (Ayoob and Gupta 2008).

$$X^2 = \sum \frac{\left(q_{exp}-q_{cal}\right)^2}{q_{cal}} \qquad (2.3)$$

where q_{exp} = amount of adsorbed solute in adsorbent obtained from experimental data ; q_{cal} = amount of adsorbed solute in adsorbent obtained from model (Ayoob and Gupta 2008; Ho 2004).

Other error functions are used for nonlinear regression analysis (Mane et al. 2007), and some spectroscopic and microscopic methods can also be used to verify model assumptions (Limousin et al. 2007).

2.3.2.3.1 Langmuir adsorption model

A number of assumptions govern this model: identical adsorption sites, each of which adsorb one molecule from the adsorbate (i.e., monolayer adsorption) and these adsorbed molecules are capable of remaining sterically independent each other (i.e., intermolecular forces are negligible) and possess equal affinity for the adsorbate (Foo and Hameed 2010; Limousin et al. 2007; Malek and Farooq 1996). In this model, an ideal surface is assumed, being one that has periodic energy fluctuations (Do 1998). Furthermore, the thermal energy of an adsorbate molecule is smaller than the magnitude of these energy fluctuations, such that the troughs of

equal depth serve as adsorbent sites (Do 1998), as illustrated in **Figure 2.6**. Identical trough depths imply that upon adsorption, the same heat is released, keeping adsorption energy constant thereby making the surface homogeneous (Do 1998). When adsorbate molecules possess far smaller diameters compared to the distance between the troughs, molecules are adsorbed at localised sites, each adsorbate molecule occupying a single site (Do 1998).

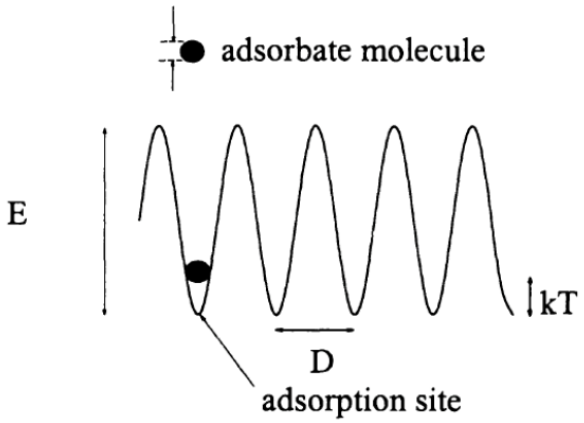

Figure 2.6 Energy fluctuations on an ideal surface (Do 1998; Moradi 2011).

In this empirical model, 3 independent parameters are used: amount of solute adsorbed onto adsorbent, adsorption equilibrium constant, and heat of adsorption (Malek and Farooq 1996). Equation 2.4 is derived from the fact that solute concentration is proportional to the ratio of the number of active sites occupied to the number of sites available. Limousin et al. (2007) put it as:

$$L = \frac{[\text{surface complex}]}{[\text{solute}][\text{free site}]} = \frac{Q}{C(Q_{max} - Q)} \qquad (2.4)$$

where Q refers to the concentration of adsorbed solute on adsorbent and (Q_{max} – Q) represents the concentration of the unoccupied adsorbent site.

In terms of initial adsorbate concentration and equilibrium conditions,

$$q_e = \frac{Q_o b C_e}{1+bC_e} \qquad (2.5)$$

where q_e = amount of adsorbed solute in adsorbent at equilibrium (mg g^{-1}); Q_o = maximum monolayer coverage capacity (mg g^{-1}); b = Langmuir

isotherm constant (L mg^{-1}); C_e = equilibrium concentration (mg L^{-1}) (Foo and Hameed 2010).

Sun et al. (2015) noted that useful predictions can be made from the equilibrium constants q_e and b; as b is the ratio of the adsorption rate coefficient to desorption rate coefficient, it describes the rate of sorption of solutes like nutrients while q_e understandably determines how much solute can be adsorbed. Equation (2.5) can be linearised in up to 4 ways (Prasad and Srivastava 2009), with Equation (2.6) being one of the most popular (Kumar and Sivanesan 2006a; Prasad and Srivastava 2009): The Langmuir isotherm model may not be applicable in systems with high adsorbate concentrations due to increasing intermolecular forces however (Malek and Farook 1996). Another equation was therefore proposed to account for species competition which is not ion exchange-based (Limousin et al. 2007), Equation A2.6 in the Annex Table A2.

$$\frac{C_e}{q_e} = \frac{1}{bQ_o} + \frac{C_e}{Q_o} \quad \text{or} \quad \frac{C_e}{q_e} = \frac{1}{k_a q_m} + \frac{C_e}{q_m} \qquad (2.6)$$

A useful measure of sorption known as the distribution or partition coefficient (K_d) is determined at equilibrium as the ratio of mass adsorbed on a unit mass of adsorbent to the adsorbate remaining in solution (EPA 1999) based on Equation (2.6). K_d values can be determined after laboratory, field or modelling sorption tests conducted in batch or column (flow-through) methods for various forms of adsorption processes such as chemisorption, physisorption, precipitation or complex formation (EPA 1999).

$$K_d = \frac{q_e}{C_e} \qquad (2.7)$$

where K_d = distribution coefficient (L g^{-1}); q_e = quantity adsorbed at equilibrium (mg g^{-1}), C_e = equilibrium concentration (mg L^{-1}).

2.3.2.3.2 Freundlich adsorption model

This model may be comparable to the Langmuir model at moderate adsorbate concentrations but not at low or very high concentrations (Ayoob and Gupta 2008).

As seen in Annex Table A2, various forms of the empirical Freundlich model exist, which can account for competing species and are therefore useful for modelling cation and anion adsorption in soils and organic compounds on activated organic carbon (Limousin et al. 2007). The non-linearised model equation is given as:

$$q_e = K_F C_e^{1/n} \qquad (2.8)$$

where K_F = Freundlich constant ($mg^{1-(1/n)}\ L^{1/n}\ g^{-1}$), n = adsorption intensity.

The Freundlich model constant *n* provides information about the nature of adsorbent as well as the favourability of adsorption process: it can be an indicator of adsorbent heterogeneity, wherein the greater the value of n, the more heterogeneous the adsorbent (Ismadji et al. 2016). Favourable adsorption occurs within $1 < n < 10$, where $n < 1$ is considered unfavourable (Parshetti et al. 2014). Furthermore, greater nonlinearity is observed as *n* increases; as *n* = 10, the isotherm becomes 'rectangular' or irreversible (Do 1998). The Freundlich isotherm model has been adapted for adsorbents with heterogeneous surfaces, non-uniform adsorption energies and affinities for the adsorbate (Ayoob and Gupta 2008; Foo and Hameed 2010; Mane et al. 2007; Yao 2013). Consequently, sorption of organics onto activated carbon is often described by the Freundlich isotherm (Do 1998) as is gas sorption onto heterogeneous surfaces even though Henry's Law not quite obeyed at low pressure (Do 1998). Variations of this model have been presented in Annex Table A2.

2.3.2.3.3 Other adsorption models

While the Langmuir and Freundlich isotherms are the most frequently used adsorption equilibrium isotherms (Ayoob and Gupta 2008; Maurya and Mittal 2006), they may not be suitable for predicting ion adsorption, and they also have fairly restrictive model parameters (Ayoob and Gupta 2008). Other adsorption isotherm models incorporate both Langmuir and Freundlich isotherm models, such as the Langmuir-Freundlich, Sips and Redlich-Peterson isotherm models (Foo and Hameed 2010; Prasad and Srivastava 2009) which are applicable in heterogeneous systems (Foo and Hameed 2010; Ye et al. 2015).

As observed from the collation of adsorption models used by previous researchers, Foo and Hameed (2010) noted that forms of the Langmuir, Freundlich and Redlich-Peterson isotherm models have been relied on for investigating the adsorption characteristics of activated carbon, zeolite, agricultural waste (rice husk, wood sawdust, sugarcane dust) and clay materials. This is likely due to the models' mathematical simplicity and versatility (Malek and Farooq 1996). As this research was focused on agricultural waste, the former two isotherm models were also used.

2.4 Improving char functionality

As hydrochars and biochars can be produced from a range of organic waste feedstocks, they show potential as low-cost adsorbents for various species including NH_4-N and PO_4-P (Laird et al. 2010; Wang et al. 2015a; Yao 2013; Zeng et al. 2013; Zheng et al. 2010) thereby complementing fertilizer use (Zheng et al. 2010). There is also interest in modifying char properties such that bespoke or even smaller quantities of biochars are required for soil amendment (Eberhardt et al. 2006; Novak et al. 2009; Silber et al. 2010; Wang et al. 2015a). Char modification can be broadly categorised under physical, chemical or biological activation which will be discussed in this section, but as this study was focused on chemical activation methods, more emphasis is placed on chemical modification.

Compared to physical activation, it has been suggested that chemical activation can be cheaper, less time-consuming and may provide more opportunities for char porosity development (Krishnan and Haridas 2008; Lillo-Ródenas et al. 2003; Marsh and Rodríguez-Reinoso 2006; Sricharoenchaikul et al. 2008). Moreover, in physical activation, porosity development is achieved at the expense of carbon yield in some cases (Viswanathan et al. 2009). Chemical agents within the carbon feedstock might improve microporosity by interfering with the reduction in volume which is known to occur as processing temperature increases, and by leaving behind new pores when such agents are washed off (Marsh and Rodríguez-Reinoso 2006). Chemical activation agents include transition metal salts, potassium and sodium hydroxides (Chen et al. 2011; Marsh and Rodríguez-Reinoso 2006; Park et al. 2015). Other studies have focused on increasing acidic surface functional groups via oxidation or acid treatment (Kastner et al. 2009; Moreno-Castilla et al. 2000; Sricharoenchaikul et al. 2008; Xue et al. 2012), since earlier mentioned studies have shown that acidic and basic surface oxides are responsible for black carbon cation and anion exchange properties respectively (Boehm 1994).

2.4.1 Physical treatment

Physical activation is capable of increasing surface area, pore development and CEC without generating hazardous by-products or potential safety risks as is the case during some chemical activation processes (Arriagada et al. 1994; Borchard et al. 2012; Nakajima et al. 2009; Zhang et al. 2004). Heating chars in the presence of air, steam, carbon dioxide or ozone has been shown to increase char surface area (Kastner et al. 2009; Sricharoenchaikul et al. 2008; Zhang et al. 2004). Petrov et al. (1992) found that the oxidation of anthracite with air at 416 °C increased acidic oxygenated groups with a consequent decrease in anthracite pH. Furthermore, Kastner et al. (2009) found that ozone increased the adsorption capacity of chars, and that since this was achieved at room temperature, ozone treatment could perhaps be better alternative to steam activation. However, this conclusion assumes that ozone generation is cheaper than steam generation. Steam activation is sometimes performed at the highest treatment temperature that was used to create the chars (Bimer et al. 1997). Such activation removes low-volatile tars within biochars, based on evidence of decreased H and O contents (Borchard et al. 2012). Borchard et al. (2012) also found that available NO_3-N and P decreased substantially possibly due to the release of N-containing volatiles and conversion of labile nitrogen to heterocyclic nitrogen. Slow pyrolysis of various lignocellulosic bio-feedstocks in the presence of steam also yield acidic biochars due to the activation of carboxylic groups (Amonette 2009). Arriagada et al. (1994) however found that that steam activation of a lignocellulosic char reduced highly acidic functional groups like carboxylic groups in favour of weaker acidic functional groups. The application of physically activated biochar to soil resulted reduced NO_3-N and P leaching compared to non-activated biochars in Borchard et al. (2012).

2.4.2 Chemical treatment

As earlier mentioned, chemical activation of chars can be conducted at lower temperatures and shorter treatment times than physical activation (Sricharoenchaikul et al. 2008), with the possibility of microwave heat treatment to minimize treatment time even further (Ahmed 2016). Marsh and Rodríguez-Reinoso (2006) recommended controlled chemical activation processes over physical activation processes, stating that the former offers more opportunities for porosity development in carbon-based materials since adjustments to physical activation parameters do not alter carbon microporosity greatly. Two forms of chemical activation have been adapted for hydrochar and biochar modification; chemical treatments followed by high temperature heat treatment or calcination, and chemical

treatments without further high heat treatment (surface activation). Surface activation improves char surface chemistry and in some cases surface areas (Sricharoenchaikul et al. 2008) but based on previous studies, further heat treatment may be required to obtain surface area and porosity development comparable to traditional activated carbon. Lim et al. (2010) outlined temperatures frequently employed for chemical activation which ranged from 500–700 °C and in particular, studies like Hao et al. (2014) and Islam et al. (2015) respectively pyrolyzed beer waste and factory-rejected tea hydrochars with H_3PO_4 and NaOH between 600–800 °C to enhance their methylene blue sorption capacities.

For both chemical treatment types, biomass or chars benefit from being immersed in the desired activating agent solution for a sufficient period of time as this ensures that as water causes swelling of the material, the reagent gains better access into orifices; after appropriate thermal treatment and washing, the resulting char possesses greater porosity resulting from freed spaces created from removal of the reagent (Daifullah et al. 2004; Marsh and Rodríguez-Reinoso 2006). Other chemical oxidation methods include electrochemical activation which improve carbon sorption capacity for heavy metals like Cu and Pb (Harry et al. 2006).

2.4.2.1 Acid treatment

Acid treatment often results in an increase in oxygen functional groups although biochar morphologies tend to be unaffected (Budarin et al. 2007). The surface functionality of carbonaceous materials are modified by wet oxidation using various acids, notably HNO_3, H_2SO_4, H_3PO_4 and H_2O_2. A comparison of the effects of both steam and chemical activation of chars by Moreno Castilla et al. (2000) showed that HNO_3 increased the amount of carboxyl, lactone and phenol groups compared to $(NH_4)_2S_2O_8$ and H_2O_2, with $(NH_4)_2S_2O_8$ having the least effect on oxygen groups. Compared to untreated hydrochars, Xue et al. (2012) observed that simple activation steps like soaking hydrochars in 10% H_2O_2 for 2 h at room temperature increased the chars' carboxyl surface functional groups and also improved their capacity to sorb lead from water.

Liang et al. (2010) used a one-step copolymerisation HTC process at 180°C to produce carbonaceous matter with enhanced surface acidity and oxygen content using sulphonic groups from hydroxyethylsulphonic acid. Zhang et al. (2012) similarly found that treating bamboo with various chemical agents including sulphuric acid and oleum considerably increased biomass surface functionality and

catalytic ability. Such acid-treated carbon materials also showed potential for reuse: modified carbon retained its acidity after being boiling in water for over 15 h in Liang et al. (2010) and after repeated use as a catalyst during esterification in Nakajima et al. (2009) and Toda et al. (2005). Such treated chars therefore show potential for regeneration although high temperatures may be required for regeneration in some cases as observed in Tseng and Wey (2004).

Dehydrogenation reactions with H_3PO_4 can result in the development of cross-links which strengthen the carbon matrix (Rajapaksha et al. 2016; Sricharoenchaikul et al. 2008). Lin et al. (2012) found that activating biochars with H_3PO_4 encouraged the formation of nanopores by roughening biochar surfaces and also found that the addition of H_3PO_4 increased water extractable organic carbon (WEOC), which is beneficial since WEOC content is an important substrate for microbes (Jandl and Sollins 1997; Taylor 2010). Liang et al. (2012) suggested that H_3PO_4 treatment increased WEOC possibly due to the dissociation of labile carbon and weakly bonded compounds.

Nitrogen enrichment of carbonaceous matter is done via an ammoxidation process at low temperatures, which simultaneously oxidises and enriches carbon matter with nitrogenous compounds like amides, amines, imides and imines thereby modifying its acid-base properties (Jureswicz et al. 2004; Pietrzak 2009). Bimer et al. (1997) observed that the carboxyl group content of the carbonaceous materials played a role in the quantity of nitrogen incorporated and Jureswicz et al. (2004) further observed that the position that nitrogen heteroatoms located on carbon matter influenced the electrochemical properties of the carbon matter. With regard to activation procedure, studies have shown that the sequence of treatment is important (Jureswicz et al. 2004; Pietrzak et al. 2007; Pietrzak 2009). In Jureswicz et al. (2004), in-situ ammoxidised demineralised coal which was steam activated at 800 °C had a higher surface area than its carbonised, ammoxidised and steam activated counterpart. Pietrzak (2009) compared the morphological properties and nitrogen content of demineralised coal samples that were ammoxidised before and after carbonisation (in-situ and post-treatment, respectively) and found that post-treated samples had higher nitrogen contents and experienced additional chemical and morphological changes. Other studies show that in-situ treatment of bio-feedstocks is suitable for ammoxidation of carbonaceous materials like lignites (Burg et al. 2002; Starck et al. 2006).

2.4.2.2 Base treatment

Activation of carbon materials with alkali hydroxides is one of the most frequently used processes. Surface areas comparable to that of graphene can be obtained following KOH and NaOH treatment in some cases (Azargohar and Dalai 2008; Gu and Wang 2012; Sricharoenchaikul et al. 2008). Sricharoenchaikul et al. (2008) found that when nut samples pyrolysed at 800 °C were activated with KOH at 80 °C for 24 h, char surface areas were at least 300 m^2 g^{-1} higher than untreated chars, which they attributed to a separation of char crystalline lamellae by potassium metal at a certain temperature, after which washing of the potassium salts left meso-pores in the chars. Materials with high inorganic contents may experience less micropore development during KOH treatment compared to low inorganic content materials. This is the observed differences in pore development experienced by as-received and demineralised/acid-washed coal in Ehrburger et al. (1986). The authors suggested that KOH or K_2CO_3 reacted with inorganic matter, thereby decreasing potential gasification sites.

Sricharoenchaikul et al. (2008) compared chemical activation of chars with chemical agents at 60 °C for 24 h and physical activation with CO_2, and found that KOH produced chars with the highest surface area. While activation at lower temperatures produce the best porosity development in chars (<450 °C and <500 °C for H_3PO_4 and $ZnCl_2$ activation respectively), KOH treatment benefits from much higher activation temperatures (>700°C) (Marsh and Rodríguez-Reinoso 2006). Furthermore, size of the activating agent may influence the kinetics of reaction; For instance, Sricharoenchaikul et al. (2008) suggested that because KOH was smaller in size than H_3PO_4, it diffused through the carbon pores faster, hence the higher surface areas and porosity observed with KOH surface activation. KOH treatment may also enhance char agronomic potential, as it has been found to increase WEOC possibly because of an increase in the rate of phenolic/humic dissolution (Lin et al. 2012). Activation of carbonaceous materials with KOH prior to other treatments like ammoxidation has also been shown to increase char nitrogen content (Pietrzak et al. 2007) and CEC (Nguyen et al. 2014).

2.4.2.3 Metal incorporation

Carbonaceous matter can also be activated using metal carbonates (X_2CO_3) where X represents metals like sodium or potassium, as done by Urabe et al. (2008) who found that addition of such chemicals to bread yeast grains prior to pyrolysis improved the gas adsorption capacity of the resulting chars. Similarly, the

incorporation of transition metals enhance carbon materials' adsorption capacities for various species (Cam et al. 2010; Gaur et al. 2008): iron impregnated porous black carbon structures could be a cost-effective means of removing arsenic (Chen et al. 2007); the addition of ferric oxide (Fe_2O_3) or magnetite (Fe_3O_4 or $FeO{\cdot}Fe_2O_3$) can increase phosphate adsorption capacity in some biochars (Chen et al. 2011; Yao et al. 2011). Some transition metals perform better than others, as studies by Gaur et al. (2008) showed that activated carbons impregnated with Cu and Ni metals adsorbed and removed SO_2 more effectively than Co and Cr metal-impregnated activated carbons. However, reagents such as $ZnCl_2$ may not be suitable for chemical activation due to environmental concerns (Azargohar 2009; Gu and Wang 2012; Lim et al. 2010); while $ZnCl_2$-activated chars can possess superior surface areas compared to chars activated with KOH (Ioannidou and Zabaniotou 2007) and H_3PO_4 (Williams and Reed 2004), excessive quantities of Zn can be detrimental to plants (Rout and Das 2009) therefore Zn-treated chars are likely to be less suitable for soil amendment purposes. Similar arguments can be made against Na-treated chars and other metal-loaded chars, since excessive amounts of such cations are detrimental to plants (Jeffery et al. 2013; Pardo and Quintero 2002).

2.4.3 Biological treatment

Based on short-term soil incubation tests, Sarkhot et al. (2011) found that biochars enriched with dairy manure effluent possessed higher nitrogen contents which could potentially be used as a slow-release fertilizer and Wiedner et al. (2015) observed an increase in char oxygen functionality after co-composting. Schmidt (2011) also considered the nutrient enrichment of biochars with manure in combination with lactic acid bacteria. On-going research is also aimed at activating biochars with compost at char loading ratios starting from 10% biochar with frequent mixing (Schmidt 2011) to enhance their surface properties, as discussed in **Section 2.3.1** Co-composting with hydrochars and biochars.

2.5 Sustainability of char production and deployment

As farmers and companies become increasingly interested in producing biochars at small and large scale, it is important to generate good quality chars, or minimise risks associated with toxin introduction (Sparkes and Stoutjesdijk 2011). Life cycle assessments of biochars and their production systems are useful tools that are used to ensure that GHG emissions are not inadvertently increased (Gwenzi et al. 2015;

Roberts et al. 2010). When produced from feedstocks that are not in competition with livestock or human needs, biochars show potential to minimise carbon dioxide emissions (Woolf et al. 2010). Roberts et al. (2010) determined the energy, economic and GHG emission balances and found that when biochars were applied to soils, GHG emissions were significantly lower than when they were used to generate energy in some cases. The variability in soil and crop responses to char application has led to some unease about the application of as-received chars, and while research is geared towards enhancing char agronomic value via physical, chemical and/or biological means, such treatments are likely to increase char costs. Yet the increase in char cost may be offset by the benefits gained from its potential multi-functionality (**Table 1.1**).

In terms of socio-economic potential, biochar production presents opportunities at both small and large scale and depends on country contexts; at the small scale level, cook-stoves are used to supply energy for cooking after which the by-product (biochar) are applied to soil (Whitman and Lehmann 2009; Woolf et al. 2010), top-lit upscale updraft gasifiers (Kisiki et al. 2015) and other technologies as outlined in Gwenzi et al. (2015). Biochars could also be instrumental in assisting developing countries to meet their Clean Development Mechanism (CDM) targets via carbon sequestration (Whitman and Lehmann 2009), provided the chars possess recalcitrant forms of carbon. Granatstein et al. (2009) noted that biochar production may best undertaken close to feedstock sources as this minimises transportation costs, and for large-scale biochar production, it may be preferable to produce biochars alongside waste heat utilization or some form of bioenergy provided pricing is competitive. In-depth analyses and recommendations for enhancing char sustainability have been discussed in studies like Jeffery et al. (2013), Mohan et al. (2016) and Zhang et al. (2016).

2.6 Summary

Hydrochars and slow pyrolysis biochars are promising tools for nutrient recovery. Future research is geared towards blending low and high nutrient content feedstock materials to obtain chars with superior properties (Ippolito et al. 2015; Lin et al. 2013); blending biochars with hydrochars (Kambo and Dutta 2015) to maximise the properties of both char types; and thermal treatment of nutrient-rich biomass at lower temperatures to conserve nutrient forms like N (Lin et al. 2013); further optimization of cost-effective char post-treatment processes such as co-composting

and exposure to various industrial and agricultural wastewaters. In the foremost case, blending biochars from animal- and plant-based feedstock has been recommended as the former feedstocks possess higher nutrient contents (Chan and Xu 2009; Ippolito et al. 2015).

Ultimately, as hydrochars and biochars are produced from diverse feed-stocks at various processing conditions, it is possible to design chars that meet specific soil needs, aided by quantitative assessments on the influence of production parameters on char properties and functions, as recommended by Morales et al. (2015). In addition, it is generally accepted that longer-term char-soil field and incubation trials are essential for providing more accurate, comprehensive information on hydrochars and biochars interactions with soil. This has been demonstrated in studies like Gronwald et al. (2015, 2016) who compared laboratory and field trials to compare hydrochar and biochar mineralization. Based on char incorporation in three different soil types within regularly tilled mini-plot fields, the authors estimated that biochar decomposition would occur faster than previous laboratory incubation studies in the literature suggested, with predicted mean residence times far less than 250 years, and between 3–14 years for hydrochars derived from miscanthus. From field trials, Malghani et al. (2015) also estimated a half-life of about 19 years for hydrochar derived from agricultural waste (corn silage) and reported that hydrochar application to soil could result in positive priming due to easily mineralized carbon but only in the short term (≤ 3 months). As is often the case with chars, such dynamics are likely to be feedstock and process dependent.

CHAPTER 3

Materials, Equipment and Experimental Methods

3.0 Introduction

Information about the feedstock materials, equipment and analytical procedures used for the production and characterization of chars throughout this study are outlined in this section as presented in **Figure 3.1**. Feedstocks were chosen to represent waste materials typically found in the agricultural and municipal sectors. Bark-free wood feedstocks were also chosen for comparative purposes, and as these feedstocks were low in contaminants relative to the waste-based feedstocks, the resulting hydrochar and biochars were considered as reference chars.

All chemicals used for char and biomass treatment were of analytical grade and used as-received. Procedures used to assess char-compost and char-soil interactions during mesocosm laboratory trials are also outlined. In terms of CEC analysis, various studies have adapted different soil CEC procedures for measuring char CEC, making comparisons between studies challenging. Consequently, two of the four frequently used CEC methods which have been evaluated in this work are summarised here.

Improvements to char functionality in the literature involve physical, chemical, or biological modification or activation processes, with chemical activation being the preferred choice for a number of reasons, as summarised in **Section 2.4**. Chemical modification often requires the use of large quantities of chemical agents to achieve substantial improvements to char functionality. In this study however, mild chemical activation processes have been investigated, on the premise that lower quantities of reagent translate to lower costs associated with by-product disposal as well as lower activated char costs. As this study was specifically focused on enhancing char ammonia / ammonium and phosphate sorption capacities, chemical modification methods involving the incorporation of acid, alkali, and metal species were evaluated. Method development for such mild char chemical modification procedures are therefore outlined in this section.

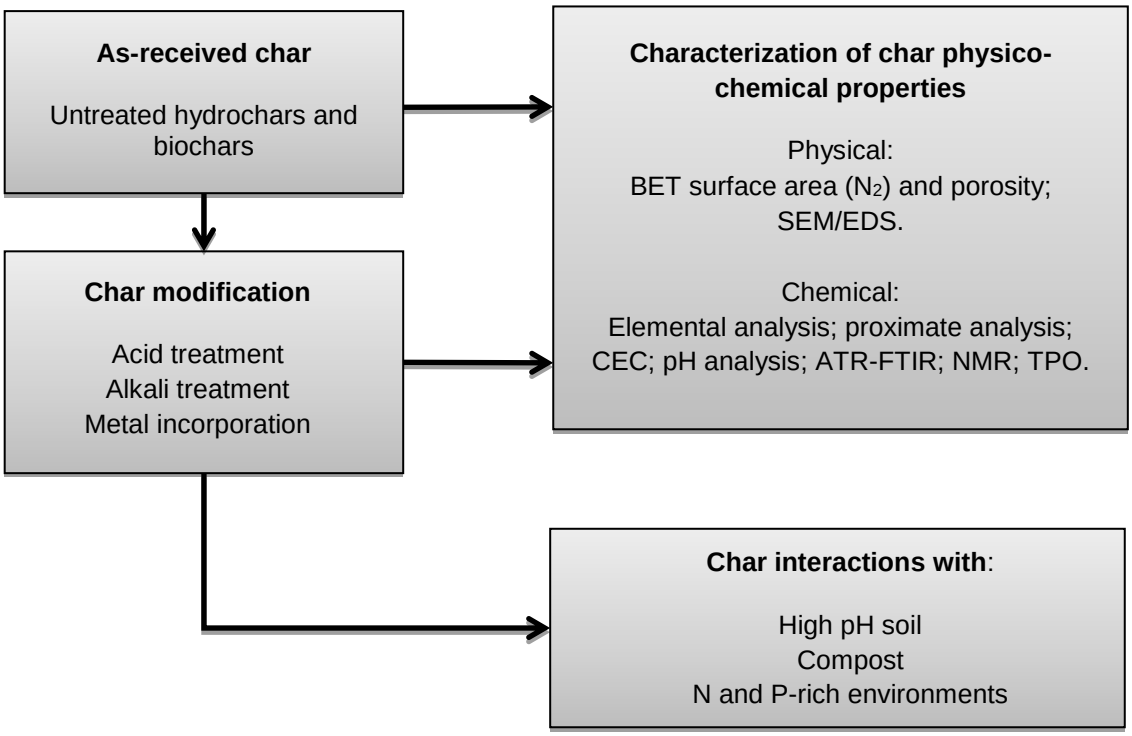

Figure 3.1 Overview of experimental setup.

3.1 Feedstock materials

The char samples analysed in this study originated from a set of five feedstocks within the Fertiplus Consortium (Grant Agreement N°: 289853), co-funded by the European Commission, Directorate General for Research & Innovation, within the 7th Framework Programme of RTD, Theme 2 – Biotechnologies, Agriculture & Food. Bark-free *Quercus ilex* (holm oak) wood, with particle sizes ranging from about 5–50 mm; paprika waste sourced from a greenhouse in Andalucia, Spain by Tecnova (Almeria); greenwaste supplied by Organic Waste Systems (OWS), Gent, Belgium; pre-treated organic wastes, namely: presscake, obtained after the anaerobic digestion (AD) of organic waste by OWS, Gent, Belgium; the unsorted organic fraction of municipal waste which was steam autoclaved at temperatures up to 160°C by Graphite Resources Ltd., Derwenthaugh, UK, resulting in a fibrous product commercially referred to as 'cellmat', free from large pieces of glass, plastic and metal. The range of biomass feedstocks are shown in **Figure 3.2**. Pig manure

sourced by the Energy research Centre of the Netherlands (ECN) was also used to produce a small set of biochars.

(a) (b) (c) (d) (e)

Figure 3.2 Biomass samples: (a) holm oak (b) greenhouse waste (c) treated municipal waste (cellmat) (d) presscake from AD (e) greenwaste.

3.2 Hydrochar and biochar production

Table 3.1 outlines the thermochemical processing conditions used for hydrochar and biochar production. Hydrochars were produced at the University of Leeds using a non-stirred hydrothermal reactor (**Figure 3.3)** fitted with a Type 'J' (iron constantan) thermocouple. Additional reactor specifications are provided in **Table 3.2**. An external heating jacket supplied heat for the reaction after programming the reactor to a specific temperature and heating rate using a *Parr 4836* controller. HTC was performed on feedstocks with about 10 wt.% feedstock to distilled water ratio. The mixture was briefly stirred manually before heating to 250°C and left to carbonize for 1 h at approximately 4 MPa after which the reactor and its contents were allowed to cool to about 50°C before recovering the residue (hydrochar) from the process water by filtration followed by air-drying.

Biochars produced via slow pyrolysis and gasification over a temperature range of 400–750°C were obtained from ECN and by Proininso S.A. (Málaga, Spain). Specifically, oak biochars used as reference biochars were produced at 450°C and 650°C by a commercial, mono retort pyrolysis reactor operated by Proininso over 12–18 h, further details of which are proprietary. ECN pyrolysis chars were produced using an auger screw thread *Pyromaat* reactor, full details of which are provided in Fryda and Visser (2015). Pyrolysis was performed over 60 min in an N_2 atmosphere unless otherwise stated, while fluidized bed gasifiers also operated by ECN were used to produce biochars at 600–750°C in air and N_2. As a small set of

pyrolysis chars were also produced by ECN at shorter residence times, at temperatures >600°C or in the presence of 1% O_2, Biochars produced by ECN via pyrolysis between 400–600°C in N_2 over 60 min residence times are referred to as chars produced under standard conditions to aid clarity. To minimise exposure to air and moisture, as-received biochars and air-dried hydrochars were stored in white 250–500 mL polyethylene plastic screw top jars fitted with inner seals.

Figure 3.3 Hydrothermal reactor and controller (*Parr*

3.3 Char modification

Chemical treatments were performed on oak and greenhouse waste-based chars as these chars possessed carbon contents >50%, thus classified as Class 1 biochars according to the EBC and IBI. As earlier stated, chemical modification involved soaking chars or char precursors in chemical reagents with or without further high heat treatment; chars from the latter treatment were referred to as surface activated chars. Furthermore, to investigate the effect of chemical treatment route on char performance in nutrient-rich environments, holm oak and greenhouse waste biomass samples were pre-treated with either KOH, $MgCl_2{\cdot}6H_2O$ or $FeCl_3{\cdot}6H_2O$ prior to pyrolysis at the University of Leeds and unless stated otherwise, pyrolysis was performed using a single vertical tube furnace (*Elite Thermal Systems Ltd.*, *Model TSV12/100/750*) under the flow of N_2 for 60 min. Bio-oils collected in the condenser catch pot and gases generated were not analysed. Details of the furnace shown in **Figure 3.4** are provided in **Table 3.2.**

Table 3. 1 Biochar nomenclature and processing conditions

Description	Temp. (°C)	Residence time (min)	Atmos-phere	Designation
HTC chars (University of Leeds)				
Holm oak	250	60	Air	OAK 250
Greenhouse waste (pepper/paprika waste from a greenhouse)	250	60	Air	GH 250
Municipal waste (cellmat)	250	60	Air	MW 250
Presscake from anaerobic digestion of organic fraction of municipal waste	250	60	Air	PK 250
Greenwaste	250	60	Air	GW 250
Pyrolysis chars (ECN)				
Holm oak from *Pyromaat*	400	60	N_2	OW 400
Holm oak from Proininso kiln (commercial)[a]	450	60	N_2	OAK 450
Holm oak from *Pyromaat*	600	60	N_2	OW 600
Holm oak from Proininso kiln (commercial)[a]	650	60	N_2	OAK 650
Greenhouse waste from *Pyromaat*	400	60	N_2	GH 400
Greenhouse waste from *Pyromaat*	600	60	N_2	GH 600
Municipal waste (Cellmat) from *Pyromaat*	400	60	N_2	MW 400
Municipal waste (Cellmat) from *Pyromaat*	600	30	N_2	MW6-30
Municipal waste (Cellmat) from *Pyromaat*	600	60	N_2	MW 600
Municipal waste (Cellmat) from *Pyromaat*	600	60	O_2	MW - 1%
Presscake from *Pyromaat*	400	60	N_2	PK 400
Presscake from *Pyromaat*	600	30	N_2	PK6-30
Presscake from *Pyromaat*	600	60	N_2	PK 600
Presscake from *Pyromaat*	600	60	O_2	PK - 1%
Presscake from *Pyromaat*	700	60	N_2	PK 700
Greenwaste from *Pyromaat*	400	60	N_2	GW 400
Greenwaste from *Pyromaat*	600	60	N_2	GW 600
Pig manure from *Pyromaat*	600	30	N_2	PM6-30
Pig manure from *Pyromaat*	700	30	N_2	PM7-30
Pig manure from *Pyromaat*	700	60	N_2	PM 700
Gasification chars (ECN)				
Greenhouse waste from fluidized bed	600	60	Air	GH-FA 600
Greenhouse waste from fluidized bed	600	60	N_2	GH-FN 600
Greenhouse waste from fluidized bed	750	60	N_2	GH-FN 750

[a] Reference biochar; biochars produced at non-standard conditions include: gasification chars, chars produced at shorter residence times (30 min), and chars produced in the presence of 1% O_2.

Table 3.2 Specifications of hydrothermal and pyrolysis reactors

Specifications of *Parr* hydrothermal reactor (University of Leeds)	
Reactor vessel capacity	0.6 L
Reactor construction	Type 316 stainless steel vessel
Temperature sensor	Type 'J' (iron constantan) thermocouple
Temperature controller	*Parr* 4836 manual controller
Gasket	Flat polytetrafluoroethylene (PTFE)
Maximum vessel temperature	350°C
Maximum vessel pressure	20 MPa
Closure	6 cap screws (split-ring)
Specifications of vertical tubular furnace (University of Leeds)	
Dimensions	Furnace bore: 90 mm O/D x 80 mm I/D x 1100 mm long; heated length: 750 mm
Reactor construction	Low thermal mass insulation; zinc-coated steel and outer mesh cover
Temperature sensor	Type 'N' thermocouple
Temperature controller	*Eurotherm* 2416CG dual display PID programmer
Gasket	Flat wire-reinforced graphite
Heating element	Resistance wire elements wound onto ceramic work tube
Maximum furnace temperature	1200°C
Maximum furnace pressure	Unknown
Closure	8 screw caps

Figure 3.4 Vertical tube furnace (*Elite Thermal Systems Ltd.*).

3.3.1 Acid treatment

For phosphoric acid treatment, 4 g char of particle size ≤ 2 mm was mixed with 2 g of 99% phosphoric acid in 20 mL of water. The mixtures were shaken briefly and left to stand for 24 h at room temperature as shown in **Figure 3.5**, after which the mixtures were heated for about 15 h at 80°C in an oven and rinsed with distilled water. Hydrochars and biochars were oven dried at 80°C and 100°C respectively.

For sulphuric acid treatment, 5 g char (≤2 mm) was mixed with 100 mL of 0.1 M H_2SO_4 and heated for 3 h at 80°C after which treated chars were washed with distilled water until a stable pH was attained and oven-dried at 80-100°C.

H_2O_2 treatment involved soaking 2 g char of particle size ≤2 mm in 20 mL of 10% or 30% H_2O_2 for 48 h at room temperature, using a methodology similar to that of Moreno-Castilla et al. (2000) and Xue et al. (2012) without agitation, after which biochars were heated at 80°C for 24 h, washed with distilled water until the pH was between 6–7 for biochars or close to the hydrochars' original pH before oven-drying at 80–100°C.

3.3.2 Alkali treatment

For surface activation with KOH, oak (particle size ≤ 2 mm) or greenhouse waste char was mixed in a solution of KOH using 1:1, 3:1 and 5:1 KOH to char ratios, corresponding to 2, 6, and 10 g KOH to 4 g char in 20 mL of distilled water. The mixtures were stirred for 2 h at 75°C with a magnetic stirrer. The treated biochars were subsequently rinsed with HCl followed by distilled water until the leachate pH values ranged between 6–7 then oven-dried for 2 h at 100°C. Treatments at 1:1 ratios were also performed for oak and greenhouse waste hydrochars.

For chemical activation with KOH, commercial oak biochars at the same procedure as outlined for surface modification was performed but with an additional pyrolysis step, where biochar-KOH mixtures were allowed to stand overnight before pyrolysis of chars for 1 h in a nitrogen atmosphere at 5 mL min^{-1}, heating rate of 10°C min^{-1} at 400°C and 600°C for Oak 450°C and Oak 650°C, respectively. Treated biochars were washed and dried as outlined above. To investigate the effect of activating agent/char contact time, the same chemical activation procedure was followed but chars were immediately pyrolysed at 600°C using the same conditions pyrolysis conditions and chars were washed and dried as normal. Finally, to compare the effect of KOH activation on raw biomass, 4 g holm oak and greenhouse waste were each soaked in 20 mL distilled water containing 2 g KOH followed by pyrolysis in an N_2 atmosphere at about 5 mL min^{-1} at 600ºC for 1 h at a heating rate of about 10°C min^{-1} using a bench-scale *Eurotherm* horizontal pyrolysis reactor. Biochars were rinsed with HCl followed by distilled water until the leachate pH values ranged between 6–7 and oven-dried for 2 h at 100°C.

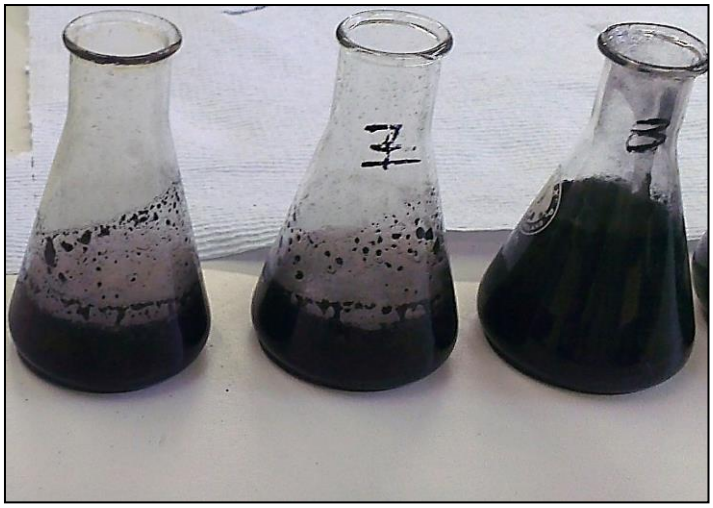

Figure 3.5 Chars soaked in chemical reagents (acid, alkali or salt) for hours to ensure adequate migration of reagents into interior and exterior char surfaces.

3.3.3 Metal incorporation

For surface activation, 8 mL of 2 M iron nitrate nonahydrate ($Fe(NO_3)_3 \cdot 9H_2O$) and 0.1 mL of 10 M sodium hydroxide was added to 4 g char of particle size ≤2 mm. The mixture was stirred, heated in an oven overnight at 105°C and rinsed with distilled water until orange iron precipitates shown in **Figure 3.6** were removed and oven-dried at 100°C. The iron contents of the treated biochars were determined using AAS following acid digestion with HCl.

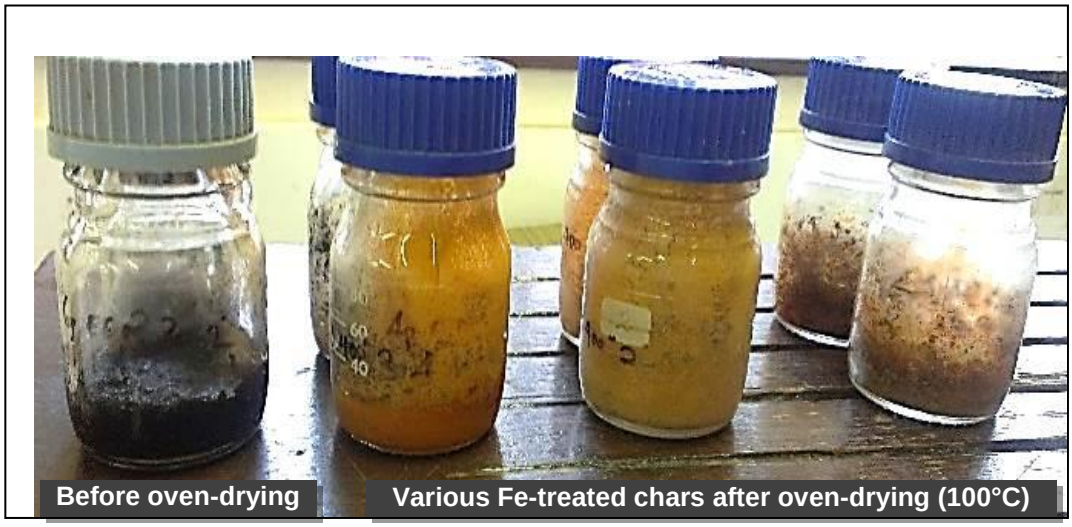

Figure 3.6 Enrichment of chars with iron nitrate nonahydrate.

For chemical activation, as high temperatures would be involved, iron chloride hexahydrate was used instead of iron nitrate, following a methodology similar to that of Zhang et al. (2012) in which 10 g oak biochars were mixed with 40 g $FeCl_3 \cdot 6H_2O$ in 60 mL distilled water. The mixture was stirred thoroughly and left to stand for 2 h at room temperature then heated for 24 h at 100°C on a Stuart hotplate before pyrolyzing the biochar for 1 h in an N_2 atmosphere at about 10 mL min^{-1} and heating rate of 10°C min^{-1} at 400°C or 600°C depending on the biochars' original production temperatures. That is, OAK 450 and GHW 400 were pyrolyzed at 400 °C while OAK 650 was pyrolyzed at 600 °C to correspond with temperatures slightly below initial production temperatures. Modified biochars were subsequently rinsed with distilled water and oven dried at 100°C for 2 h.

This procedure was repeated for biochars treated with magnesium chloride hexahydrate ($MgCl_2 \cdot 6H_2O$) on oak biochars with particle size ≤ 850 µm, ≤ 2 mm and ≤ 4.75 mm using both small and large tubular furnaces. To investigate the effect of pyrolysis temperature on magnesium loading onto biochars, OAK 650 was pyrolyzed at 400°C and 600°C as outlined above and stored for subsequent analysis. Additional magnesium treatments were performed: to compare the effect of magnesium treatment route (in situ treatment versus biochar post-treatment), as-received holm oak chips and greenhouse waste biomass were treated with $MgCl_2 \cdot 6H_2O$ as outlined above, as shown in **Figure 3.7**.

Figure 3.7 As-received (a) Oak and (b) Greenhouse (paprika) waste biomass and their respective magnesium-loaded chars: (c) Mg-Oak char; (d) Mg-Greenhouse waste char.

3.4 Char characterization

Details on the standard procedures for determining char elemental and functional groups are subsequently described.

3.4.1 Ultimate analysis

The C, H, N, and S contents of the various chars were determined by flash combustion using a *Thermo Instruments Flash EA 1112 Series* elemental analyser (**Figure 3.8**). 5 standards supplied by CE Instruments UK were used: 2,5-Bis(5-tert-butyl-benzoxazol-2yl)thiophene, BBOT (C=72.53 wt.%; H=6.09 wt.%; N=6.51 wt.%; S=7.44 wt.%; O=7.43 wt.%); Atropine; Methionine; L-cysteine and Sulphanilamide

while coal or oatmeal (C=47.76 wt.%; H=5.72 wt.%; N=2.09 wt.%; S=0.16 wt.%) were used as reference materials to monitor drift, and an empty folded tin foil capsule served as blank. In accordance with BS EN ISO 16948:2015 standards, approximately 2.5–3 mg of standards and finely ground samples were each placed in tin foil capsules along with <5 mg V_2O_5 for BBOT and samples, the latter added to aid combustion. Wrapped contents were combusted at 900°C in the reaction zone of the elemental analyser. Oxygen at 0.35 MPa and helium as carrier gas to sweep the resulting water vapour, oxides of carbon, nitrogen and sulphur into the instrument's detector while oxygen contents were determined by difference. Analyses were performed in duplicate and average values of dry weight percentages were reported unless stated otherwise.

Figure 3.8 Elemental analyser (*Thermo Instruments Flash EA 1112 Series*).

3.4.2 Proximate analysis

Proximate analysis involved determination of char moisture, ash, volatile and fixed carbon. In accordance with BS EN 14774-3:2009, hydrochars and biochars were heated at 60°C and 105°C respectively until constant mass was attained. Ash and volatile matter was determined according to BS EN 14775:2009, in which oven-dried samples were heated up to 550°C for 2 h in a muffle furnace and weighed when cooled. Fixed carbon was determined according to Equation (3.1):

$$\text{Fixed carbon} = 100 - (\%\ \text{Moisture} + \%\ \text{Ash} + \%\ \text{Volatile Matter}) \quad (3.1)$$

Temperature Programmed Oxidation (TPO) of the chars was done by thermogravimetric analysis (Mettler Toledo TGA/DSC1), where 5 µg of char was heated to 900 ^{o}C and recalcitrance values (R_{50}) were determined according to Equation (3.2) as outlined in Harvey et al. (2012b):

$$R_{50\ Char} = T_{50\ Char}/T_{50\ Graphite} \quad (3.2)$$

where $T_{50\ Char}$ and $T_{50\ Graphite}$ = temperature at which 50 wt.% char and graphite oxidise, respectively.

3.4.3 Micro- and macro-mineral analysis

Hydrochar and biochar micro- and macro-mineral contents were determined according to the BS EN ISO 16967:2015 method, in which Inductively-coupled Plasma-Mass Spectroscopy (*ICP/MS, Perkin Elmer ELAN DRC ICP-MS*) was used to determine mineral concentrations after acid digestion of about 0.2 g chars in about 10 mL 70% HNO_3 using an *Anton Parr Multiwave 3000* microwave.

3.4.4 pH analysis

For pH determination, 1:20 char/distilled water mixtures in 50 mL falcon tubes were hand shaken for 2 min and left to stand for 5, 15, 60, 75, and 120 min. A *Hach Lange* portable pH meter calibrated with pH 4, 7 and 10 buffers (Reagecon, UK) was used to measure pH values at room temperature (~22°C). As results indicated the pH readings were stable between 75 and 120 min, readings taken after 2 h were reported.

3.4.5 Cation Exchange Capacity

CEC can be determined using any of four main methods as outlined in **Section 2.2.5** but variations in laboratory procedures make comparative analysis of char CEC challenging in some cases, as alluded by McLauglin (2010) and Sumner and Miller (1996). Two of such methods were employed in this study for comparative purposes: direct displacement after washing (**Sections 3.5.5.1. 3.5.5.2** and **3.5.5.4**) and direct displacement (**Section 3.5.5.3**) alongside schematic diagrams summarising the sequence of saturation and leaching steps involved. Analyses were done at room temperature unless stated otherwise and at solution pH of about 7 for analyses involving ammonium acetate solutions. CEC analyses were performed in duplicate unless stated otherwise but when coefficients of variation

exceeded 25%, more repeats were performed and the average values reported. Most coefficients of variation were below 10% however.

3.4.5.1 CEC analysis by the Modified $BaCl_2 \cdot 2H_2O$ Compulsive Exchange

A summary of the procedure is presented in **Figure 3.9**, based on the procedure outlined in Gilman and Sumpter (1986), however due to the low density of the chars in this study, chars were separated via filtration as opposed to centrifugation. 2 g char was measured onto a funnel fitted with a *Whatman Grade 1* filter paper to which 20 mL of 0.1 M $BaCl_2 \cdot 2H_2O$ was added, letting the solution soak through completely before adding more reagent. The char was then leached with 10 mL of 2 mM $BaCl_2 \cdot 2H_2O$ six times, discarding 5 of the leachates obtained and retaining the last for pH analysis. The filter paper and biochar was transferred to a 100 mL flask to which 10 mL of 5 mM $MgSO_4 \cdot 7H_2O$ solution was added. This mixture was swirled occasionally for 1 h. The conductivity of 1.5 mM $MgSO_4 \cdot 7H_2O$ was determined to be 316 µS, and as the conductivity of the sample solution was to be 1.5 times this value (ie. about 450 µS), 0.1 mL of 0.1 M $MgSO_4 \cdot 7H_2O$ was added gradually, taking note of the amount of 0.1 M $MgSO_4 \cdot 7H_2O$ added. The pH of the sample solution was maintained within 0.1 units of the pH of the leachate analyzed earlier, otherwise 0.05 M H_2SO_4 was added drop-wise until pH was within the appropriate range. However, because the pH of the sample solution was more acidic than the pH of the leachate, the addition of sulphuric acid was discontinued.

Distilled water was added to the solution, after which the conductivity and pH of the solution was checked again and re-adjusted to the desired 450 µS and pH range desired. The flask was dried and weighed and the calculation for CEC was determined as outlined in Ross and Ketterings (1995) in Equations (3.3) – (3.6):

A: Total solution (mL) assuming that 1mL weighs 1 g =

$$\text{final tube weight (g)} - \text{tube tare weight (g)} - 2 \text{ g of char used} \quad (3.3)$$

B: Since 1.5 mM of $MgSO_4 \cdot 7H_2O$ has 0.003 mEq Mg^{2+} per mL,

$$Mg^{2+} \text{ in solution (mEq)} = \text{total solution (mL)} \times 0.003 \frac{\text{mEq}}{\text{mL}} \quad (3.4)$$

C: As 5 mM of $MgSO_4 \cdot 7H_2O$ has 0.1 mEq of Mg^{2+} and 0.1M $MgSO_4 \cdot 7H_2O$ has 0.2 mEq of Mg^{2+} per mL,

total magnesium added (mEq) =

$$0.1 \text{ mEq} + \left[(\text{mL of } 0.1\text{M } MgSO_4 \cdot 7H_2O \text{ added}) \times 0.2 \frac{\text{mEq}}{\text{mL}}\right] \quad (3.5)$$

D: Converting 2 g char sample analysed to 100 g, from (3.3) and (3.4):

$$\text{CEC (mEq/100 g)} = (C - B) \times 50 \quad (3.6)$$

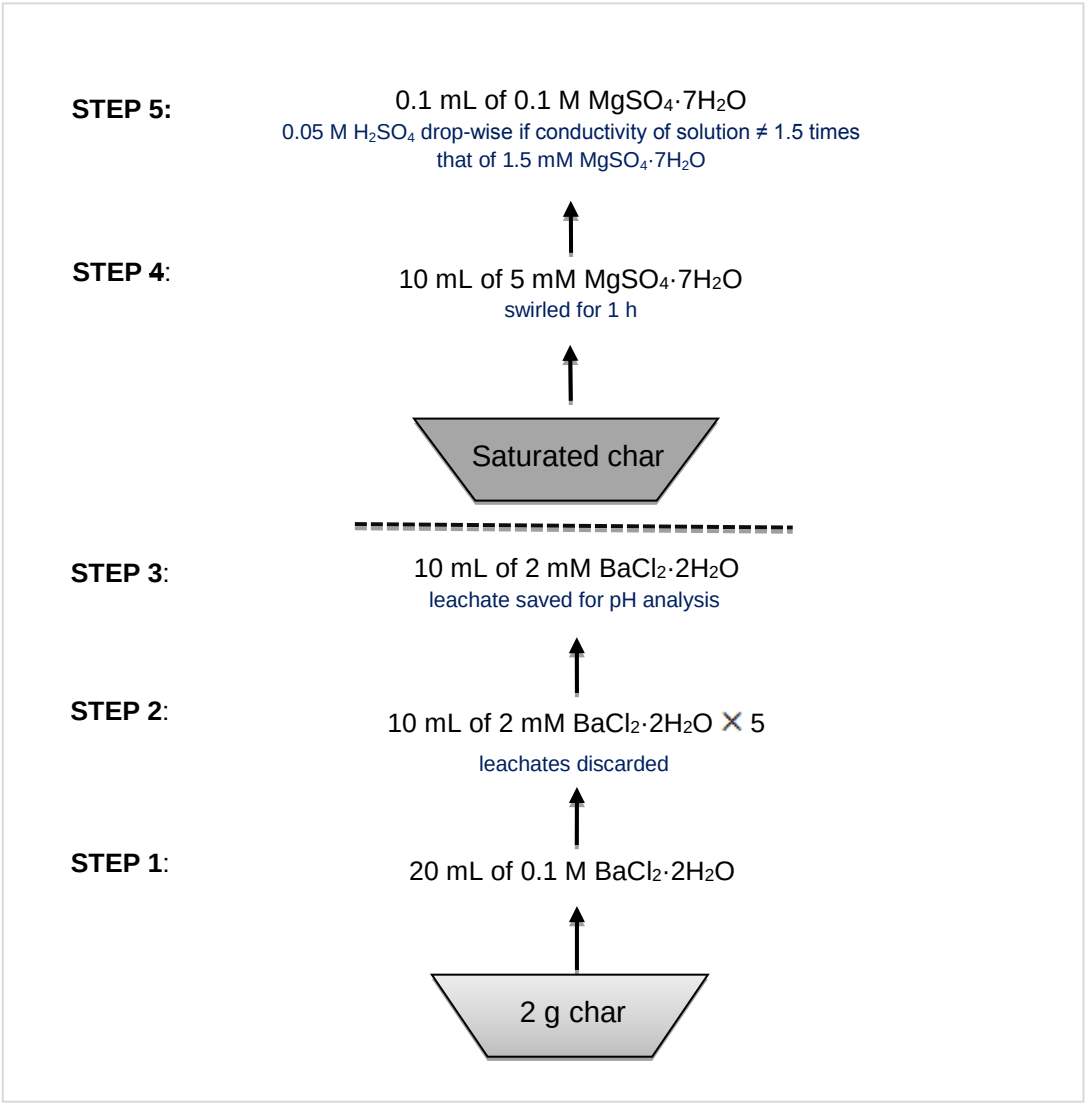

Figure 3.9 Schematic diagram of saturation and leaching process for barium chloride compulsive exchange CEC method.

3.4.5.2 CEC analysis using ammonium acetate (displacement after washing)

The method involved the adsorption of cations onto biochar surfaces followed by rinsing excess cations with alcohol before replacing with a different set of cations in accordance with the Chapman (1965) method and illustrated in **Figure 3.10**. The experimental setup used is shown in **Figure 3.12**. Due to low quantities of char available in this study, char and reagent quantities were scaled down by a factor of 10 whilst keeping reagent concentrations the same as in Chapman (1985). To confirm whether CEC values of original and scaled-down values would be similar, the CEC of commercial 450°C oak biochar was determined using both original and scaled-down ratios, and the former was higher by only 3.5 $cmol_c\,kg^{-1}$, thus 12.5 mL of 1 M of ammonium acetate solution adjusted to a pH of about 7 was added to 2.5 g char, shaken and allowed to stand overnight, after which the mixture was filtered through a *Whatman Grade 1* filter paper. The char was carefully washed with four more additions of 2.5 mL ammonium acetate solution, followed by eight additions of 2.5 mL 98% ethanol to remove excess ammonium acetate. Eight 2.5 mL additions of 1 M KCl solution were then added to the char sample to extract the adsorbed ammonium ions. In each leaching step, solutions were allowed to filter through the char completely. The leachate was transferred to a 25 mL volumetric flask and made up to volume with distilled water.

A 20 mL aliquot of this leachate was gently boiled with 5 mL of 60% NaOH, and ammonia present in the condensate was collected into a beaker containing 1 mL boric acid and trapped as ammonium according to Equation (3.7). Drops of bromcresol green screened with methyl red indicator were added and the solution was titrated with 0.01 M HCl until the indicator changed from green to pink due to the reaction shown in Equation (3.8). The distillation procedure was also performed with KCl solution to serve as a blank. Char CEC was determined according to Equation (3.9), similar to that used in Haluschak (2006). Here, single analysis was performed on biochars.

$$NH_3 + H_3BO_3 \rightarrow \underbrace{NH_4^+ : H_2BO_3^-}_{\text{ammonium borate complex}} + \underbrace{H_3BO_3}_{\text{excess boric acid}} \qquad (3.7)$$

$$NH_4^+ : H_2BO_3^- + HCl \rightarrow NH_4Cl + H_3BO_3 \quad (3.\ 8)$$

$$\text{CEC (mEq/100g)} = \frac{(V_1 - V_2) \times N}{V_a} \times \frac{V_L}{w} \times 100 \quad (3.\ 9)$$

where V_1 and V_2 = sample and blank titre (mL) respectively; N = normality of HCl (Eq L^{-1}); V_a and V_L = volume of aliquot and leachate respectively; w = sample mass.

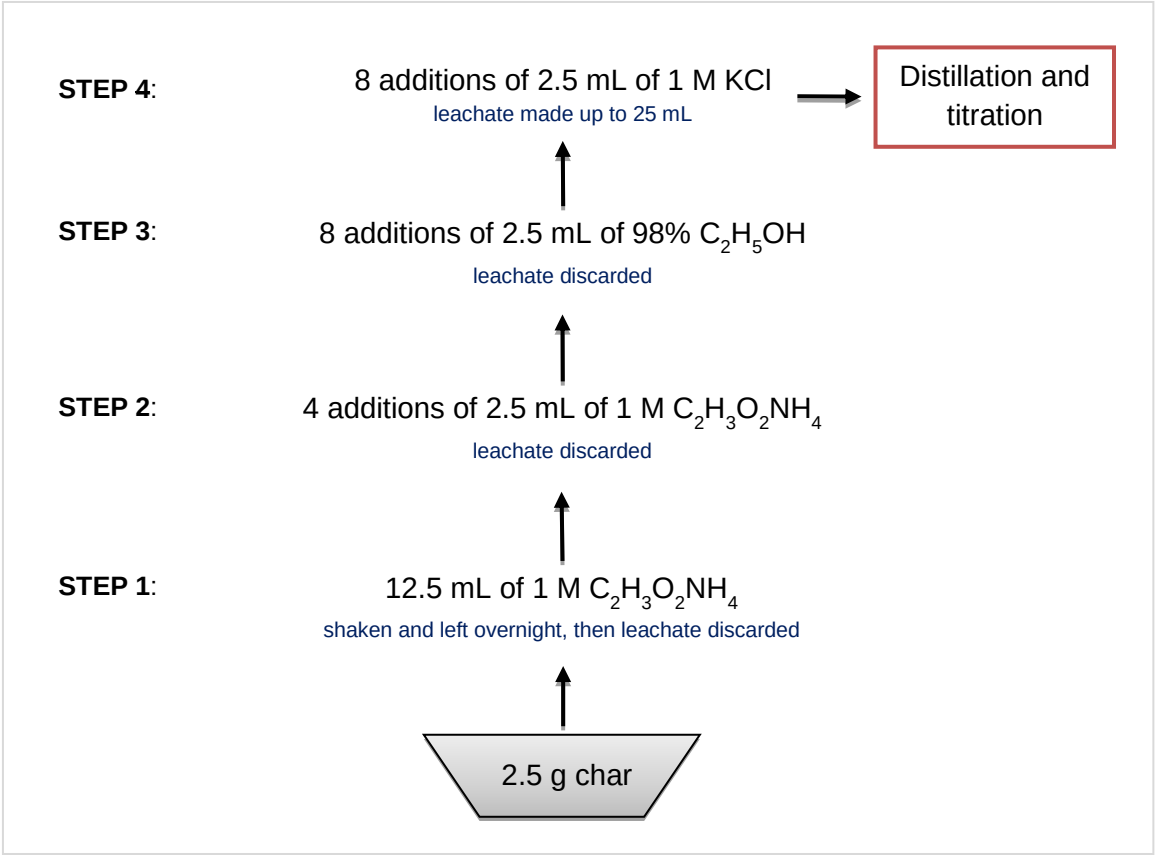

Figure 3.10 Schematic diagram of saturation and leaching process for CEC analysis via ammonium acetate displacement with KCl after washing with ethanol.

3.4.5.3 CEC analysis using ammonium acetate (direct displacement)

This method involved CEC determination after index cations adsorbed onto biochar exchange sites were displaced by cations from another saturating solution without rinsing excess cations from biochars with alcohol, following a methodology similar to that outlined in Sarker and Haldar (2005). 10 g of char into a 500 mL beaker to which 200 mL of 1 M ammonium acetate was added. The mixture was shaken and allowed to stand for 15 min after which the mixture was filtered through a Buchner

funnel fitted with a funnel and *Whatman Grade 1* filter paper. Both char and filter paper were transferred into a distillation flask containing 2 g magnesium oxide and 200 mL of tap water. The same distillation setup as shown in **Figure 3.12** was used, ensuring that the tip of the inverted funnel used to convey the condensate generated just dipped into a 500 mL beaker containing 50 mL of 4% boric acid and 5 drops of bromocresol green indicator. The distillation flask contents were gently boiled until 200 mL of condensate was obtained, and the condensate-indicator solution containing ammonium generated according to Equations (3.7) and (3.8) was titrated with 0.1 M hydrochloric acid until the indicator changed from blue to light green. A blank analysis involved the same procedure outlined above barring the addition of ammonium acetate. The procedure is outlined in **Figure 3.13** and CEC was determined according to Equation (3.10) as similar to that of Sarkar and Haldar (2005). Analyses were performed in duplicate or triplicate and average values ± standard deviation were reported.

$$\text{CEC (mEq/100 g)} = \frac{(V_1 - V_2) \times N \times 100}{w} \qquad (3.10)$$

where V_1 and V_2 = sample and blank titre (mL) respectively; N = normality of HCl (Eq L^{-1}); N = normality of HCl (Eq L^{-1}); w = sample mass (g).

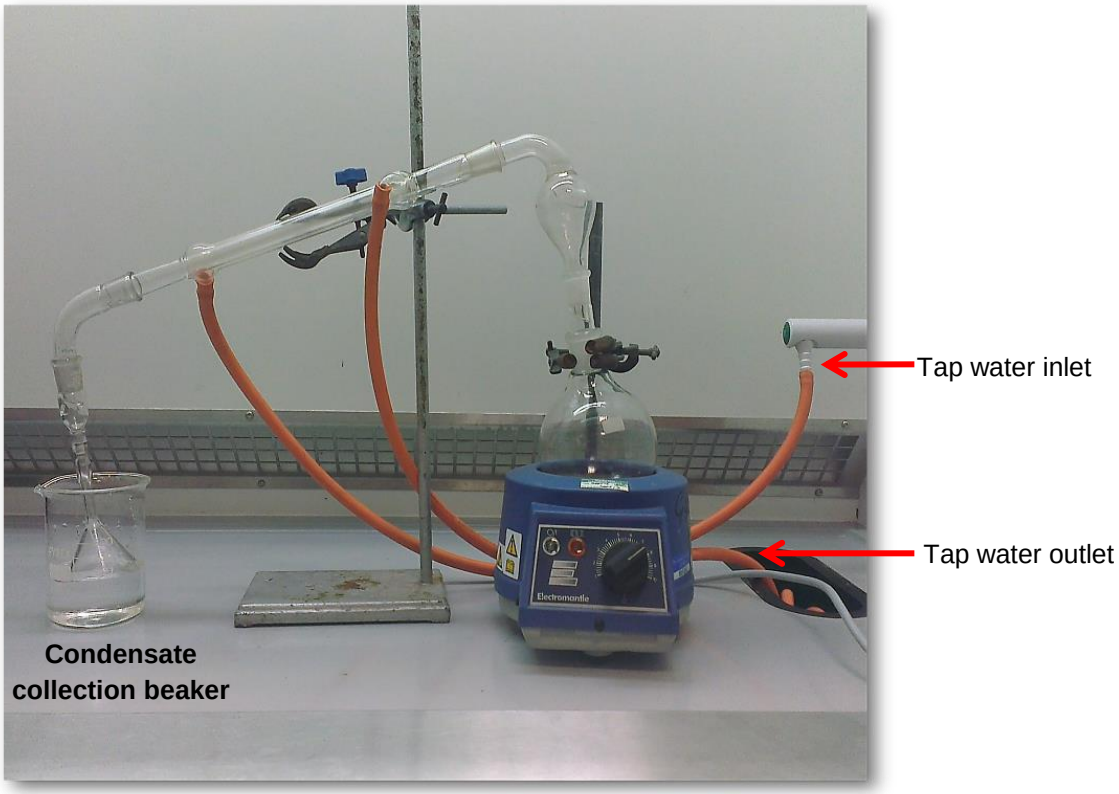

Figure 3.12 Distillation setup for CEC analysis.

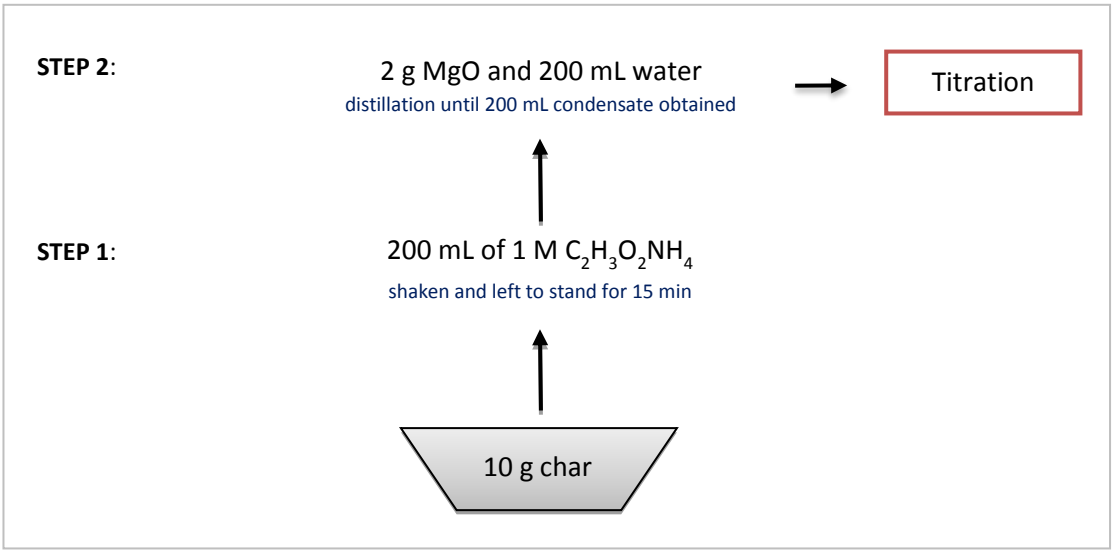

Figure 3.13 Schematic diagram of saturation and leaching process for CEC analysis using ammonium acetate (direct displacement without washing).

3.4.5.4 CEC analysis using the modified ammonium acetate compulsory displacement method

CEC was determined using a method similar to that of Brewer (2012), Gaskin et al. (2008) and Yuan et al. (2011). To remove soluble salts, 20 mL distilled water was added to 1 g of biochar and shaken at 160 rpm for 10 minutes each in a water shaker bath (*SW23 Julabo GmbH*) at room temperature and filtered through a Whatman Grade 1 filter paper. This was repeated four more times, discarding the leachates each time. Biochars were saturated with 10 mL of 1M sodium acetate (Alfa Aesar) with pH adjusted to 7 using a few drops of glacial acetic acid, shaken at 160 rpm for 16 minutes and filtered. This was repeated twice more, discarding the leachates each time, after which biochars were rinsed with ethanol thrice for 8 minutes each at 160 rpm. Three additions of 1 M ammonium acetate at pH 7 were used to displace sodium cations by shaking at 160 rpm for 16 minutes, storing the leachates for subsequent analysis. Analyses were done in duplicate or triplicate, and the average values reported, and a summary of the process is shown in **Figure 3.14**. To each 10 mL aliquot of the final leachates, 10 mL of 2000 mg K^+ as KCl was added to serve as an ionization suppressant before making up to 100 mL with distilled or deionised water and the concentration of displaced sodium cations were determined using a *Varian AA240FS* flame Atomic Absorption Spectroscopy (AAS) instrument as shown in **Figure 3.15**. Acetylene was used as fuel with air support and the lamp current was set at 5 mA. The wavelength chosen for the analysis was 330.3 nm with slit width of 0.5 nm. After obtaining a linear calibration plot from

prepared 400 mg L^{-1} Na standard solution, each of the samples were introduced into the nebulizer via a peristaltic pump. The concentration of Na^+ in the leachate was calculated using Equation (3.10) according to PerkinElmer (1996), and the resulting char CEC was determined using Equation (3.11):

$$Na^+ \text{ concentration } (\mu g\ g^{-1}) = \frac{(C \times V \times d.f)}{W} \qquad (3.\ 11)$$

where C = concentration of Na^+ detected by AAS (mg L^{-1}); V = volume of undiluted leachate generated (mL); d.f = dilution factor; W = char mass (g).

$$\text{CEC (meq/100 g)} = Na^+\ [\mu g\ g^{-1}] \times 10^{-3}\ [mg\ g^{-1}] \times \frac{1}{23}\ [mEq\ mg^{-1}] \times 100 \qquad (3.\ 12)$$

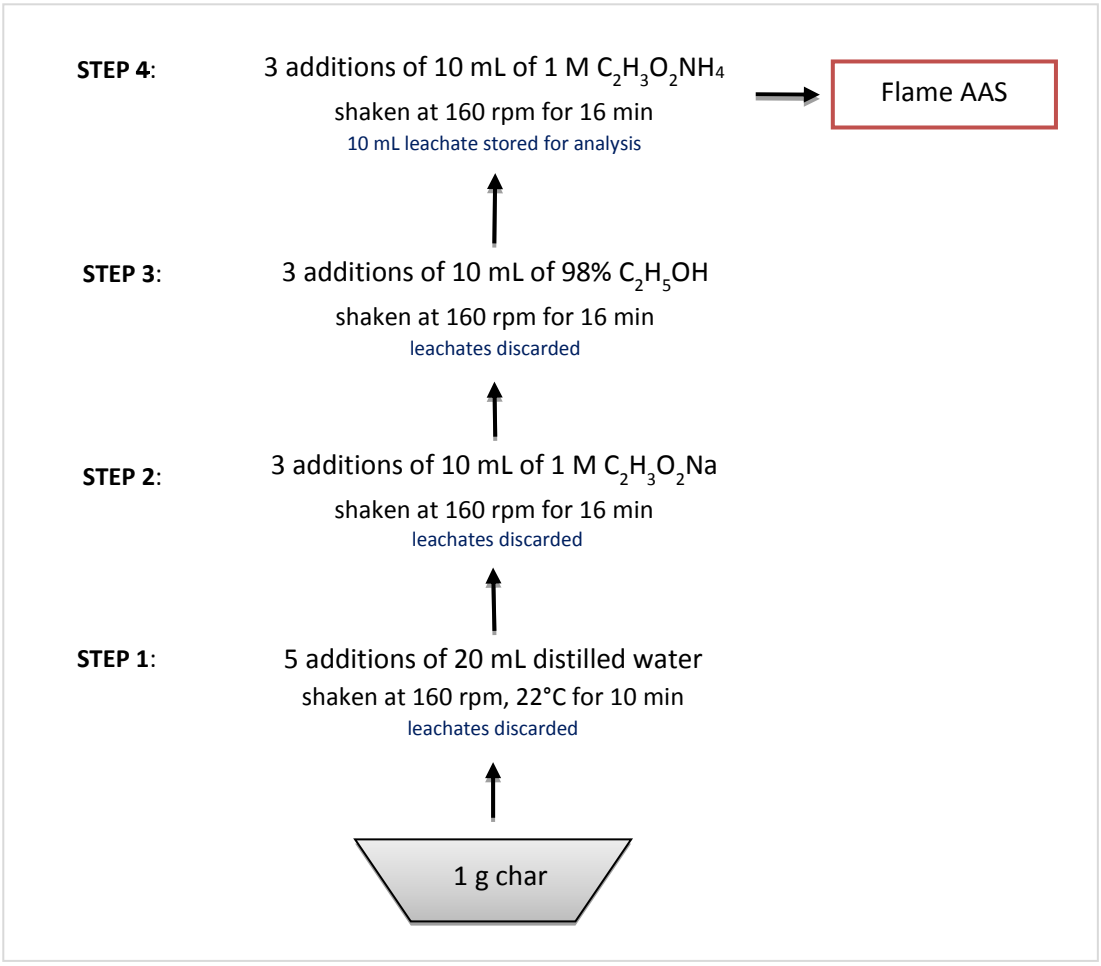

Figure 3.14 Schematic diagram of saturation and leaching process (ammonium acetate compulsory displacement method).

This method was chosen for CEC analysis of all char samples used in this study as it was relatively faster than the other methods considered and minimized the need for use of toxic reagents like barium chloride. Analysis was performed in duplicate as a minimum, and average values ± standard deviation were reported.

Analysis of the final leachate containing displaced K^+ ions was determined using AAS as it provides rapid quantitative information on elemental concentrations. AAS is reliant on the principle that as an atom is excited from its stable ground state orbital configuration by a specific wavelength of light energy, it emits radiant energy equivalent to the absorbed energy when returning from this less stable excited state (Beaty and Kerber 1993; PerkinElmer Inc. 1996; Robinson, 1960). The amount of element present in a substance can therefore be determined since the amount of light energy absorbed increases with the number of atoms present in a substance (Beaty and Kerber, 1993). A plot of absorbance versus concentration gives a straight line in accordance with Beer's Law until these variables increase to a point where non-ideal behaviour causes a curve (Beaty and Kerber 1993).

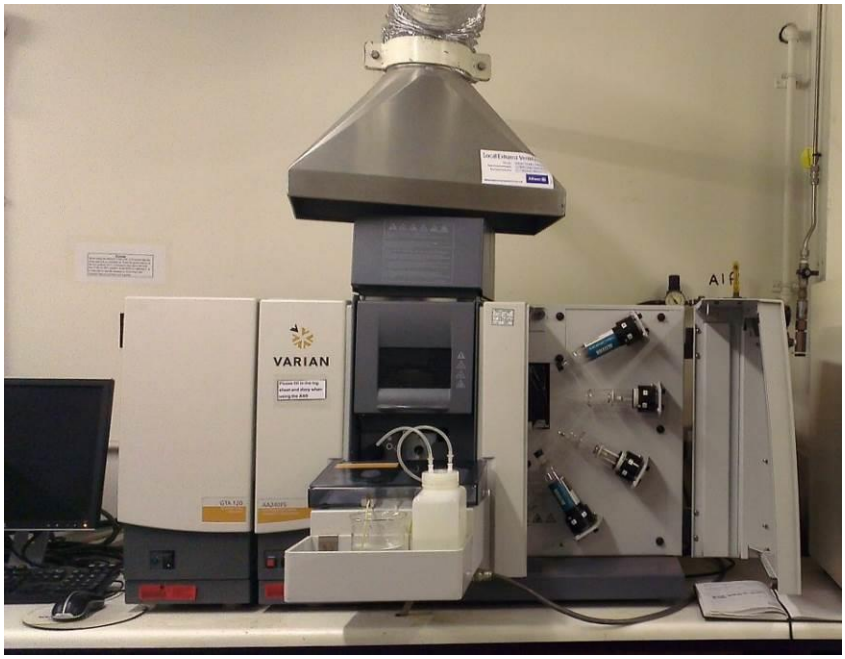

Figure 3.15 Atomic Absorption Spectrometer (*Varian AA240FS*).

3.5 Hydrochar humic-like substances and fulvic acids

Prior to humic acid extraction, hydrochars were ground in an agate mortar and oven dried at 60°C for 2 h. Hydrochar humic and fulvic acid contents were determined in

accordance with Sánchez-Monedero et al. (1996) and summarized by schematic presented in **Figure 3.16**, in which chars were extracted with 0.1 M NaOH in a 1:20 (w:v) ratio twice by shaking for 2 h in an end-to-end shaker bath at room temperature (~22–25 °C) followed by phase separation using a *Beckman Coulter Allegra X-22R* swinging bucket centrifuge at about 3100 × g for 15 min. The resulting supernatant was carefully decanted, and a portion of this was stored at 4 °C for total extractable carbon (EXC) analysis. Following a procedure similar to Jindo et al. (2016), the remaining supernatant was acidified with concentrated sulphuric acid to pH 2 and left to stand for 24 h at 4°C, resulting in a separation into two phases, a solid phase (humic-like acid) and aqueous phase containing fulvic acids and non-humic substances.

Fulvic acids were separated from non-humic substances by slowly passing the aqueous phase through a methanol-washed resin (*Supelite DAX-8, Supelco*). Fulvic acids were desorbed from the resin following the addition of 0.1 M NaOH, while 0.1 M H_2SO_4 was added to desorb the acid-soluble fraction (non-humic substances) (McCreary and Snoeyink 1980; Rashid and King 1969; Sánchez-Monedero et al. 1999). The leachates were each made up to 200 mL for soluble carbon and nitrogen analysis at Gorizia Research Unit (Italy), after which fulvic acid carbon (FAC) was determined from carbon analysis of the fulvic acids obtained while humic acid carbon (HAC) was determined as the difference between EXC, FAC and non-humic substance carbon. For comparative purposes, these are expressed in terms of ratios, as outlined in Sánchez-Monedero et al. (1999):

$$\% \text{ Humic acid} = (\text{HAC}/\text{EXC}) \times 100 \quad (3.13)$$

$$\text{Humification Ratio (HR)} = \text{EXC}/\text{TOC} \times 100 \quad (3.14)$$

$$\text{Degree of Polymerization} = (\text{HAC}/\text{FAC}) \quad (3.15)$$

$$\text{Humification Index (HI)} = \text{HAC}/\text{TOC} \times 100 \quad (3.16)$$

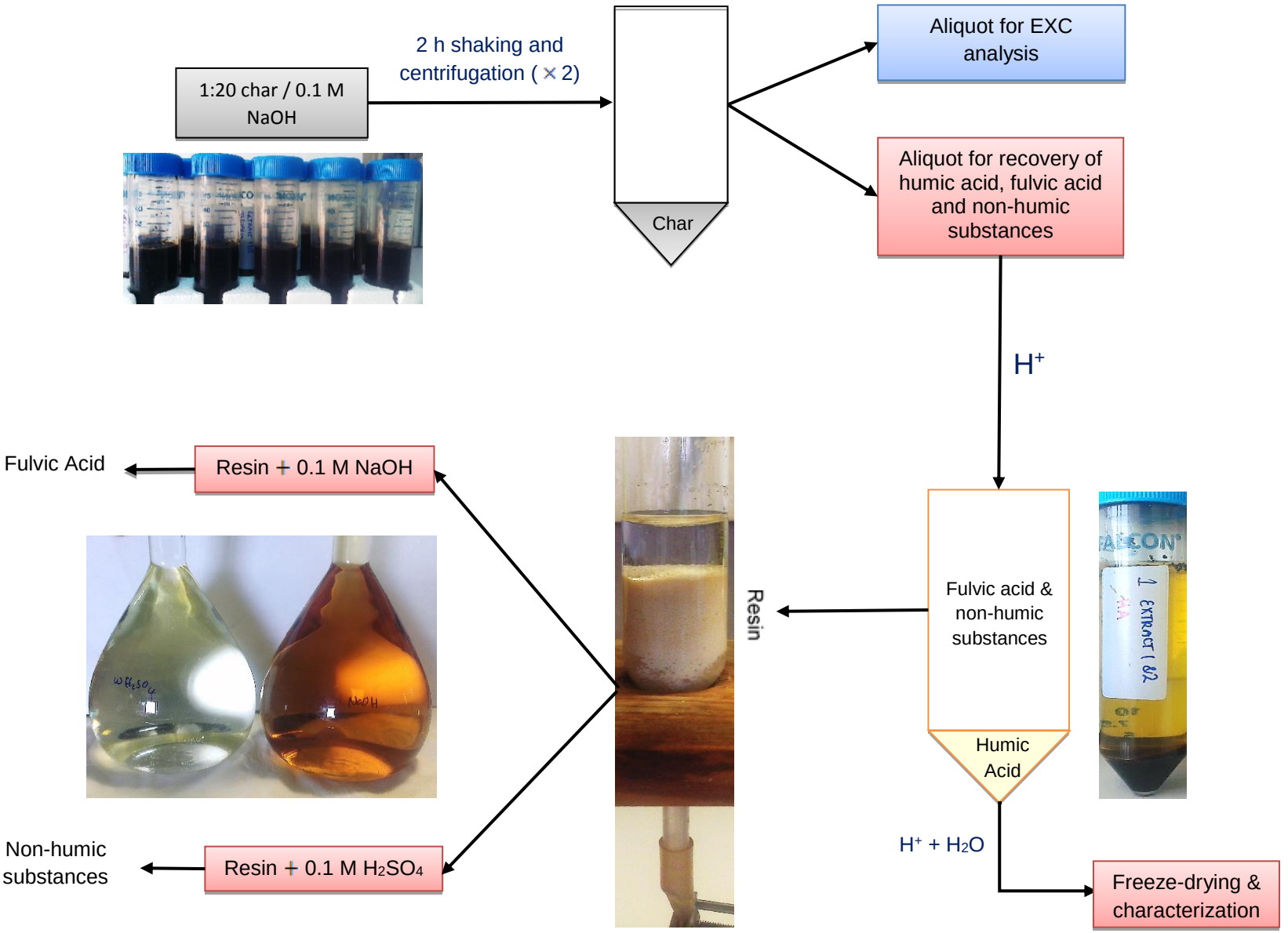

Figure 3.16 Outline of process used for recovery of humic acids, fulvic acids and non-humic like substances from hydrochars

3.6 Attenuated Total Reflectance-Fourier Transform Infrared (ATR-FTIR) analysis

Infrared analysis provides qualitative information on surface functional groups present on a sample. Each diatomic bond in a molecule undergoes unique stretching, bending, scissoring or rotational bond vibrational modes when infrared radiation is absorbed, the exact compound can be determined when compared with an existing or reference spectral database (Coates 2000). The intensity of given absorption peaks also provide information about sample molecular spatial properties (Coates 2000). In ATR-FTIR, samples are securely placed on a crystal possessing a high refractive index. When an infrared beam is passed at an angle through one end of the crystal, the intensity of the infrared beam exiting the other end of the crystal and into a detector is reduced (attenuated), depending on the energy absorption of the sample (Smith 2011).

In this study, ATR-FTIR analysis was performed using an *iS10 Nicolet* ATR-FTIR spectrophotometer fitted with a diamond crystal (**Figure 3.17**), taking 36–64 scans over a range of 4000–400 cm^{-1} and resolution of 4 cm^{-1}. Background readings were collected every 5 min and automatically subtracted from sample spectra to minimize interferences from atmospheric CO_2.

Figure 3.17 *iS10 Nicolet* ATR-FTIR.

3.7 Pyrolysis-Gas Chromatography (py-GC) analysis

A CDS series pyrolyser connected to a Shimadzu 2014 GC/MS was used to determine functional groups present in biomass feedstocks, chars and humic-like substances. Samples in fire-polished quartz tubes were pyrolysed at 500°C at a ramp rate of 20°C $(ms)^{-1}$ with a hold time of 20 s. An Rtx 1701 60 m capillary column with 0.25 i.d., 0.25 µm film thickness operating at a column head pressure of 30 psi was used to separate the resulting products, at a split ratio of 20/1 at 40°C maintained for 2 min, ramped to 250°C and maintained for about 30 min.

3.8 Surface area and porosity determination

Gas adsorption can occur by micro-pore filling, capillary condensation, monolayer and multilayer adsorption and these processes yield characteristic isotherm types, accurate interpretation of which is the first step in analysing the physisorption process (Sing et al. 1985). Physisorption isotherms are categorized into 5 or 6 IUPAC classification types as shown in **Figure 3.18** (Brunauer et al. 1940; Donohue and Aranovich 1999; Sing et al. 1985), partly based on Brunauer's findings**.** Type I isotherms occur on micro-porous solids with small external surfaces (Sing et al. 1985); Type II isotherms are exhibited in non-porous or macro-pore solids which undergo monolayer-multilayer adsorption (Schneider 1995; Sing et al. 1995); Type III and V isotherms are not very common and indicate weak gas-solid interactions; Types IV isotherms possess distinctive hysteresis loops arising from capillary condensation in meso-porous solids (Schneider 1995; Sing et al. 1985); Type VI isotherms are indicative of step-wise multilayer adsorption on non-porous materials (Schneider 1995; Sing et al. 1985). After identifying the adsorption process from the physisorption isotherm, statistical and empirical models are used to determine the surface area and pore size distribution, and these models include the Langmuir and Brunauer-Emmet-Teller (BET) models (Schneider 1995), Barrett, Joyner and Halenda (BJH), and Dubinin-Radushkevic (DR) models. Each model is based on kinetic theories which govern the number of molecules that would be adsorbed on a surface at a given pressure and temperature, hence obtaining the surface area of the solid; according to Lowell et al. (2004), surface areas is a product of the effective cross sectional area and number of adsorbate molecules in the monolayer. Each of these models has limitations however. For instance, the BET model can

provide actual surface area of Type II and IV isotherms if the C value is neither too high nor low, but is not as effective for Type I and III isotherms (Sing et al. 1985).

In this study, Brunauer-Emmett-Teller (BET) surface area and pore size distribution of treated and untreated oven-dried chars were determined by N_2 gas adsorption using two instruments, *Tristar 3000 Micromeritics* and *Quantachrome Nova 2200* at -196 °C after flow outgassing first at room temperature (~22°C) for 10 min and at 120 °C for 2-3 h to free any blocked pores within the chars. This low temperature range was chosen to prevent thermal decomposition of the samples, particularly so for the hydrochars. BET surface area was determined from linear fit adsorption data generated while pore volumes were determined using the t-plot model. Total pore volumes were obtained at relative N_2 pressures of 0.99.

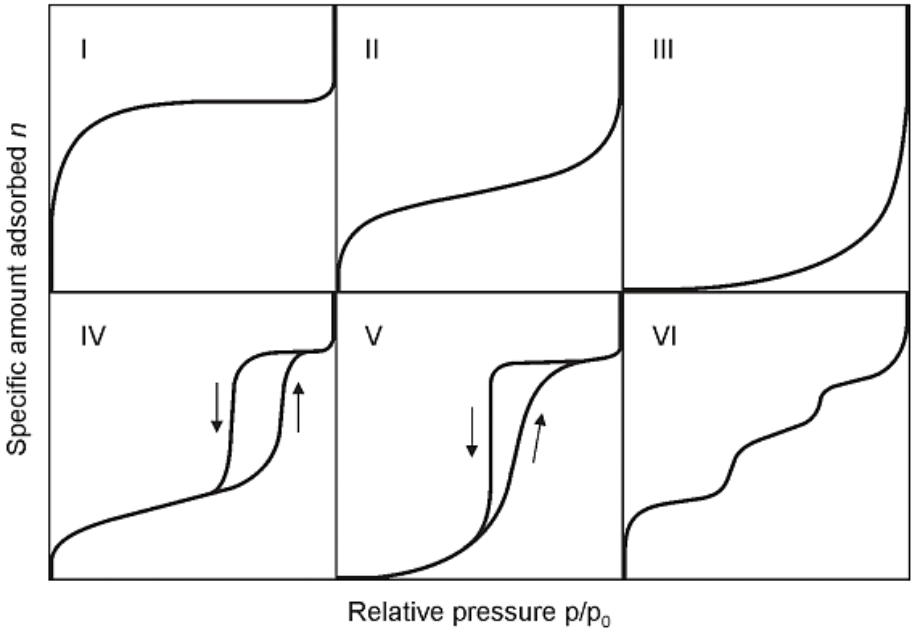

Figure 3.18 Physisorption isotherm types (Klobes et al. 2006; Sing et al. 1985).

3.9 Scanning Electron Microscopy (SEM) and Energy Dispersive X-ray Spectroscopy (EDS) analysis

SEM analysis of hydrochars and biochars was done using a *Carl Zeiss EVO MA15* microscope while qualitative information about biochar elemental composition analysis was done using *Oxford Instruments AZtecEnergy* EDS as shown in **Figure 3.19**. Prior to SEM and EDS imaging, chars were sputter-coated with gold and carbon, respectively.

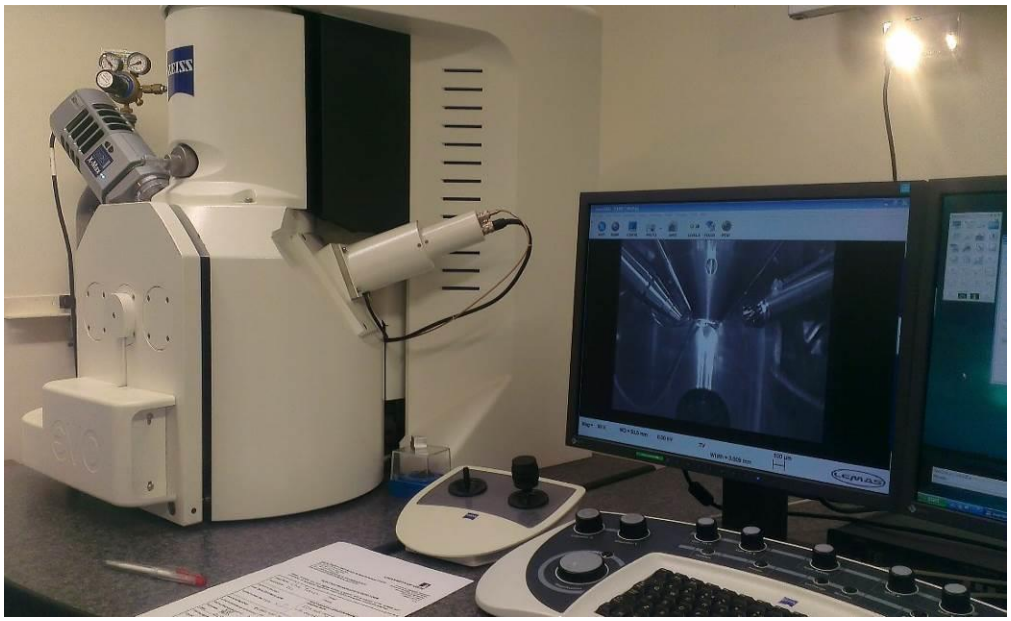

Figure 3.19 Scanning Electron Microscope (*Carl Zeiss EVO MA15*).

3.10 Ion Chromatography

As a substantial portion of the research relied on this analytical technique, its principle of operation is outlined. Ion Chromatography involves the quantitative determination of ions separated by virtue of differences in their migration or rate of movement through ion-exchange resins (Fritz and Gjerde 2000). Resin columns are often comprised of polymers (for example, polystyrene and divinyl benzene) possessing two ions – fixed or bound ions attached to the polymeric structure and unbound, oppositely charged ions (counter-ions) (Fritz and Gjerde 2000; Sigma-Aldrich n.d.) as shown in **Figure 3.20**. Ion exchange resins are categorised as cation or anion exchange resins based on the charge possessed by exchangeable counter-ions and bound ion ionic strength (Sigma-Aldrich n.d.). When the resin is in contact with insoluble solutions, the free ions are mobile and exchangeable with similarly charged ions in accordance with Donnan Exclusion, where a decrease in mobile ion concentrations occurs within an ion exchange membrane because of similarly charged bound ions present (IUPAC 2014).

Cation and anion exchange resins can be further categorised as weak and strong cation exchange resins, comprised of carboxylic and sulphonic acid groups or salts respectively, and as weak and strong anion exchange resins, comprised of ammonium chloride or hydroxide and quaternary ammonium groups respectively

(Fritz and Gjerde 2000; Sigma-Aldrich n.d.). Dilute carbonate salts or hydroxides and acidic solutions are used during anion and cation exchange chromatography, respectively (Fritz and Gjerde 2000).

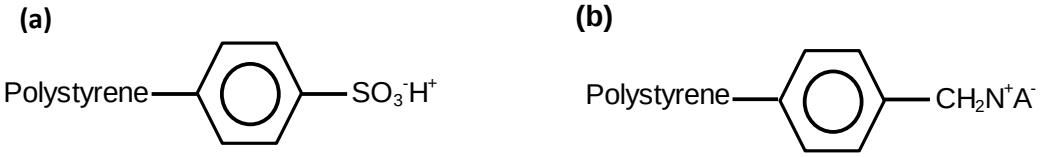

Figure 3.20 A typical (a) Cation exchange resin (Catex) (b) anion exchange resin (Anex) (Fritz and Gjerde 2000)

Fritz and Gjerde (2000) outlined the ion exchange process thus: sample ion separations are achieved by injecting sample into the chromatography system after appropriate eluent has been pumped though the system to achieve equilibration. Ion exchange occurs between the eluent and sample ions near the top of the column in a narrow zone or band however, continuous eluent flow creates competition for resin exchange sites which causes ions to move down the column. Ions however migrate at different rates due to their different affinities for exchange sites, thus separation into various bands is achieved. As eluent continues to flow through the column, sample ions and eluent exit the column to a detector. In suppressed ion chromatography however, sample ions and eluent flow into a suppressor before proceeding to the detector. The suppressor is a cation exchange system which serves a dual purpose of decreasing eluent signal (e.g. background conductivity) and increasing sample ion signal by protonating the ions (Fritz and Gjerde 2000; SeQuant 2007) as illustrated below, adapted from Fritz and Gjerde (2000):

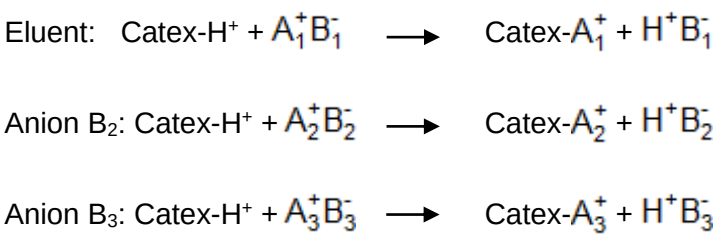

In this study, ammonium, phosphate and some alkaline earth metals were determined using a *Metrohm 850 Professional IC–AnCat* ion chromatograph as shown in **Figure 3.21**, with operating conditions provided in **Table 3.3**. A small set of samples were also analysed using a *Dionex DX100/LC20 Dionex* ion chromatograph fitted with an *IonPac CS12A, 250 × 4 mm* cation column and methyl

sulfonic acid solution (1.0 nN) as eluent, and a *Dionex IonPac AS14A, 250 × 4 mm* anion column with Na_2CO_3 (8.0 mM) and $NaHCO_3$ (1.0 mM) as eluent.

Table 3.3 Operating conditions of *Metrohm 850 Professional IC–AnCat* ion chromatograph

Cation exchange	
Eluent	1.7 mmol HNO_3 and 0.7 mmol Pyridinedicarboxylic acid (PDCA)
Pump flow rate	0.9 mL min^{-1}
Pump pressure	5.7 - 5.8 MPa
Column thermostat temperature	25.9 - 26.5°C
Conductivity	719.85 – 720.10 µS cm^{-1}
Anion exchange	
Eluent	3.2 mmol Na_2CO_3 and 1 mmol $NaHCO_3$; Regenerant:100 mmol H_2SO_4 and 100 mmol oxalic acid ($C_2H_6O_6$)
Pump flow rate	0.7 mL min^{-1}
Pump pressure	8.2 – 8.6 MPa
Column thermostat temperature	26.5°C
Conductivity	0.9 – 1.05 µS cm^{-1}

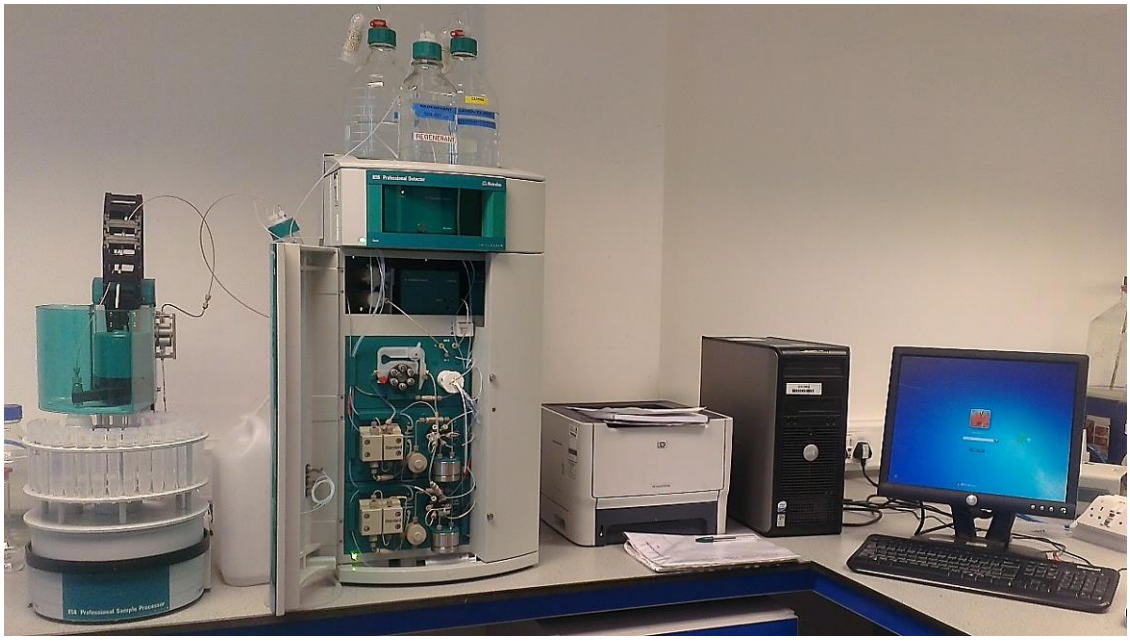

Figure 3.21 Ion chromatograph (*Metrohm 850 Professional IC–AnCat*) and data processing setup.

3.11 Soil incubation tests

Soil incubation tests were performed in triplicate with chars produced from holm oak, greenhouse (paprika) waste and presscake chars produced at 250–650°C. After adjusting the soil to 40% of its Water-Holding Capacity (WHC), pre-incubations were performed for 7 days in an oven at 25°C, after which a randomized block design was set up, consisting of three replicates of control (100% soil) and char-amended soil (98% soil + 2% char) in 200 mL plastic tubs as shown in **Figure 3.22**. The pre-incubation step was involved to return microbial communities to their unstressed state, since soil sampling results in a disruption of such microbial communities (Akagi et al. 2007; Creamer et al. 2014). Additionally, as soil moisture levels vary according to climatic conditions, pre-incubation could also serve to standardize soil water contents thus allowing for inter-site comparisons whilst allowing the aforementioned microbial communities to readjust to moisture content variations (Akagi et al. 2007). A range of pre-incubation temperatures and periods have been used in previous European studies, but Creamer et al. (2014) reported that generally, initial soil basal respiration rates were unaffected by these parameters although 20–25°C provided the most consistent results. Pre-incubation was therefore done at 25°C, after which all samples were incubated for a total of 21 days of incubation. As inorganic nitrogen analysis would be performed after specific days of incubation, tubs were arranged in parallel accordingly. Moisture contents were adjusted gravimetrically every other day and tubs were covered with polyethylene cloths to minimise excessive moisture loss.

Samples were arranged in a randomized block design and CO_2 evolution was measured with a Photo-Acoustic gas monitor (**Figure 3.23**), full details of which have been provided in Mondini et al. (2010). Jars were sealed with lids fitted with septa 1 h prior to CO_2 headspace measurements. To correct for atmospheric CO_2, jars containing distilled water filled to the same depth as the soil/soil-char samples were included at the beginning of each block as indicated in **Figure 3.22**. Two CO_2 measurements were taken within 8 h of the start of incubation followed by three evenly-spaced CO_2 measurements every 24 h for the next 3 days, then once daily for the next 7 days and less frequently until 21 days of incubation. CO_2-C fluxes were calculated as in Mondini et al. (2010) and related to total weights.

Inorganic N measurements were taken after 3, 7, 12, and 21 days of incubation as follows: NH_4-N and NO_3-N contents were determined after shaking a 1:10 mixture to

2 M KCl and distilled water respectively for 2 h, centrifuging for 15 min at about 3100 × g and filtering supernatants through 0.45 µm syringe filters. NH_4-N was determined spectrophotometrically according to Berthelot's reaction (highlighted in López-Cano et al. 2016) and NO_3-N was determined by Ion Chromatography.

Figure 3.22 Soil and soil-char incubation jars.

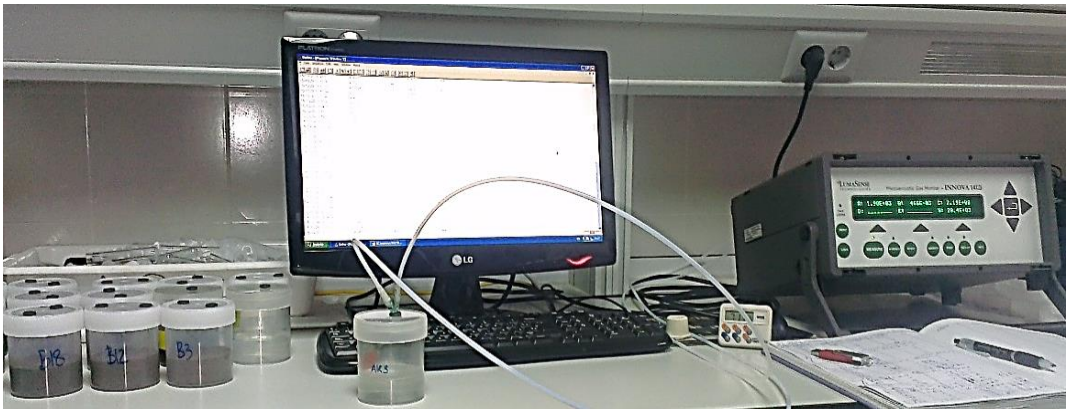

Figure 3.23 CO_2 measurements using a Photo-Acoustic gas monitor (*Lumasense Innova 1412i)*

3.12 Char interaction in nutrient-rich environments

Details on the procedures used to investigate char interaction in compost, nitrogen and phosphorus-rich synthetic wastewater and NH_3 gas are outlined subsequently.

3.12.1 Co-composting with hydrochars and biochars

$$2NH_4^+ : H_2BO_3^- + H_2SO_4 \rightarrow (NH_4)_2SO_4 + 2H_3BO_3 \qquad (3.17)$$

A 200 g dry basis mixture comprised of 60% a commercially available multipurpose compost (particle size ≤ 4.75 mm), and 40% shredded savoy cabbages as a source of nitrogen (≤ 9.50 mm) was mixed with 15% char (35 g dry basis, particle size ≤ 4.75 mm) and tests were performed in duplicate. Chars used were derived from holm oak at 250–650°C and from greenhouse (paprika) waste at 250°C and 600°C. Composting experiments with greenhouse waste produced at 400°C could not be performed due to its low quantity. Well-mixed char and organic matter samples were placed in perforated plastic vessels and placed in two ovens heated at 50°C to ensure sufficient generation of ammonia from the composting mixture and oven temperatures were constantly monitored with a thermometer. Moistened air was supplied to all composting mixtures at about 400 mL min^{-1}. The pH_{H2O} was measured as described in **Section 3.4.4** but using a 1:5 solid to water ratio. C/N ratios were determined from C and N values determined from elemental analysis of finely ground samples. Carbon dioxide and ammonia generated from the control and char-compost mixtures were collected in 1 M KOH and 0.65 M H_3BO_4 traps respectively, and the entire set up is shown in **Figure 3.24**. A total 17–21 days of incubation were performed, within which carbon dioxide and ammonia traps were changed daily for the first four days then every other day thereafter. Ammonia trapped in boric acid as in Equation (3.7) was titrated with 0.04 M H_2SO_4. Based on stoichiometric Equation (3.17), the concentration of ammonia in form of ammonium was calculated using Equation (3.18):

$$NH_3\ (mg\ L^{-1}) = \frac{(A - B) \times N \times 14 \times 1000}{V} \qquad (3.18)$$

where A and B = volume of sulfuric acid titrated for sample and blank respectively (L); V = volume of sample (L); N = normality of sulfuric acid, being 0.08 Eq L^{-1} in the present case.

Carbon dioxide trapped in KOH according to Equations (3.19)-(3.20) was precipitated with 0.5 M $BaCl_2$ and titrated with 1 M HCl as in Equation (3.22).

$$KOH + CO_2 \rightarrow KHCO_3 \quad (3.19)$$

$$KHCO_3 + KOH \rightarrow K_2CO_3 + H_2O \quad (3.20)$$

Prior to titration with HCl,

$$BaCl_2 + K_2CO_3 \rightarrow BaCO_3 + 2KCl \quad (3.21)$$

Milligrams of CO_2 emitted were calculated using Equation (3.18):

$$mg\ CO_2 = 22 \times \left\{\left[(B - A_i) \times \left(\frac{V_i}{50}\right)\right] + \left[(B - A_j) \times \frac{V_j}{50}\right]\right\} \quad (3.22)$$

where B = volume of hydrochloric acid titrated for blank (mL), A_i and A_j = volume of acid titrated for primary and secondary traps, respectively (mL); V_i and V_j = volume of alkali in primary and secondary traps respectively (mL).

Cumulative ammonia and carbon dioxide emissions were calculated based on total compost-char dry mixture weights.

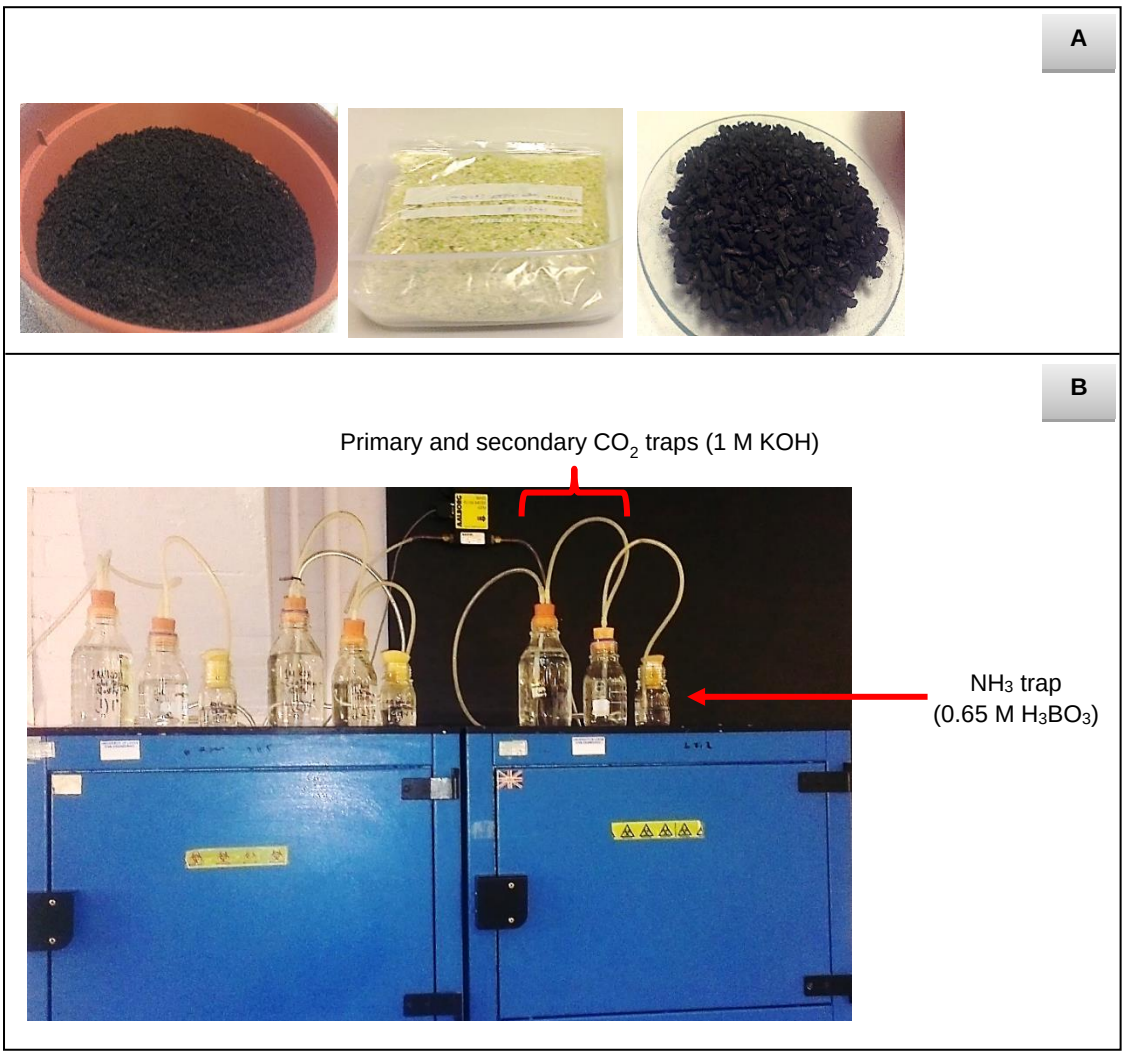

Figure 3.24 (a) Feedstocks (L-R: compost, *savoy* cabbage, char); (b) setup for char-compost incubation tests.

3.12.2 Ammonium and phosphate adsorption capacity determination

3.12.2.1 Batch adsorption

All containers were acid washed with 1 M HCl and rinsed with deionised water before use. 0.1 g biochar (≤850 µm) was transferred to plastic Nalgene containers and 100 mL of about 125 mg P L^{-1} phosphate solution prepared from potassium phosphate monobasic was added after its pH was adjusted to 7 with 1 M NaOH. The containers were tightly sealed and shaken at 160 rpm for 24 h in a water shaker bath (*SW23 Julabo GmbH*) (**Figure 3.25**) at room temperature (~22–25°C). 10 mL aliquots of each sample were taken after 24 h and filtered through 0.45 µm

Sartorius Minisart syringe filters for Ion Chromatography analysis (*Metrohm 850 Professional IC–AnCat*). This procedure was repeated for ammonium solutions, using about 1000 mg NH_4^+-L^{-1} prepared from ammonium chloride. Most analyses were done in duplicate and the average values reported. A number of tests were also performed using a synthetic wastewater solution to determine the effect of coexisting ions on ammonium and phosphate uptake. The concentrations of adsorbed ions were determined as:

$$q_e = (C_o - C_e)\frac{V}{M} \qquad (3.\ 23)$$

where C_o and C_e = initial and equilibrium liquid-phase phosphate or ammonium adsorbate concentrations respectively (mg L^{-1}); V = volume of solution (L); M = mass of char (g).

Removal efficiency was determined as:

$$\%\ \text{Removal} = \frac{C_o - C_e}{C_o} \times 100 \qquad (3.\ 24)$$

Figure 3.25 Shaker bath (*SW23 Julabo GmbH*).

3.12.2.2 Desorption studies

Adsorbed phosphate and ammonium in chars were extracted using a similar procedure as outlined above but using 0.01 M KCl solution. 10 mL aliquots of each sample were taken after 24 h then filtered through 0.45 µm *Sartorius Minisart* syringe filters for Ion Chromatography analysis.

3.12.2.3 Adsorption kinetics

To investigate possible phosphate and ammonium adsorption mechanisms, 0.1 g chars ($\leq$850µm) were each added to 125 mg P L^{-1} or 1000 mg NH_4^+ L^{-1} solutions respectively, as done in **Section 3.12.2.1** but 10 mL aliquots of each sample were taken at 2.5, 5, 7.5, 10 and 24 h. Samples were filtered, analysed by Ion Chromatography and the concentration of adsorbed ions were determined as in Equation (3.25):

$$q_t = (C_o - C_t)\frac{V}{M} \qquad (3.25)$$

where q_t = amount of PO_4^{3-} adsorbed (mg g^{-1}); C_o and C_t = liquid-phase adsorbate concentrations at initial conditions and time t respectively (mg L^{-1}).

3.12.2.3 Adsorption isotherms at varying initial concentrations

0.1 g of char with highest carbon contents (oak and greenhouse waste) was added to varying concentrations of phosphate solutions, specifically 50–200 mg P L^{-1}, and ammonium concentrations ranging from about 360–815 mg NH_4^+ L^{-1}. These concentrations were chosen to represent some real-case wastewater concentrations. The mixtures were shaken at 160 rpm for 24 h at room temperature, keeping all other parameters identical to batch adsorption tests. Samples were filtered, analysed by Ion Chromatography and the concentration of adsorbed ions were determined as in **Section 3.12.2.1**.

3.12.3 Char ammonia sorption capacity

Ammonia sorption was evaluated in a simple batch set-up, slightly modified from the methodology outlined in Taghizadeh-Toosi et al. (2012a). Briefly, 60 mL of NaOH was poured into a 250 mL Duran bottle after which a top containing about 0.2 g char was carefully placed into the bottle so it floated on top, as shown in **Figure 3.26**. The bottle was fitted with a septa was screwed tightly to obtain a closed atmosphere.

Carefully, 25 mL of 0.05 M $(NH_4)_2SO_4$ was injected into the bottle and gaseous ammonia was produced via the following chemical reaction:

$$2NaOH_{(aq)} + (NH_4)_2SO_{4(aq)} \rightarrow Na_2SO_{4(aq)} + 2H_2O_{(l)} + 2NH_{3(g)} \qquad (3.\ 26)$$

NaOH was present in excess such that a known amount of gaseous NH_3 was produced; in the current case this was 43 mg of NH_3 gas and average headspace volumes were equivalent to about 242.6 mL. After 7 days, the samples were removed from the bottles and CHNS contents were analysed via elemental analysis. The nitrogen content was adjusted for increased moisture content with respect to the char samples prior to NH_3 sorption. NH_4^+ contents were also determined by ion chromatography after shaking a 1:20 w/v mixture of char and 0.01 M $CaCl_2$ for 2 h at 160 rpm. For comparative purposes, NH_3 sorption capacities of holm oak and greenhouse waste feedstocks were evaluated following the same procedure outlined above, since unprocessed feedstocks are often used as litter material for NH_3 abatement in livestock systems. The NH_3 sorption capacities of oak hydrochar at various concentrations were further investigated following the same procedure as outlined above, generating about 450, 1000 and 1500 mg NH_3 by adjusting molar concentrations of $(NH_4)_2SO_4$ and NaOH according to Equation (3.26).

Figure 3.26 Simple batch setup for ammonia sorption tests.

CHAPTER 4

Influence of feedstock properties and processing conditions on char functionality

Abstract

Feedstock composition and processing conditions determine hydrochar and biochar properties, the organic, inorganic and textural properties of hydrochars and biochars produced from six biomass feedstocks were evaluated using various analytical techniques. Chars were produced from bark-free oak wood, paprika waste from a greenhouse, greenwaste, the treated organic fraction of municipal waste, and pig manure. Processing conditions included hydrothermal carbonization at 250°C for 60 min, slow pyrolysis at 400–700°C and gasification at 600–750°C over 30–60 min residence times. As oak wood and paprika waste chars possessed the highest carbon contents (>50%), these were categorised as Class 1 biochars in accordance with the International Biochar Initiative product specifications, while hydrochars and pyrolysis chars derived from municipal waste, presscake and greenwaste were Class 2–3. Despite substantial differences in carbon and inorganic matter content, degradation of lignocellulose structures were mostly similar in all feedstocks. However, char morphological properties were observed to be more dependent on processing temperature and reactor system than to feedstock property, based on the substantial differences in surface area of holm oak biochars produced using traditional kiln reactor (Proininso), screw conveyor and fluidized bed reactors. Biochar surface areas were generally low and were therefore comparable or even lower than hydrochars produced from the same feedstock. Conversely, with regard to char functional groups, both temperature and biomass feedstock property influenced char inorganic content and acidic oxygen groups. For instance, while oak hydrochar possessed more humic-like substances than hydrochars from other feedstocks, oak biochar produced at 650°C did not possess any humic-like substances.

4.0 Introduction

It is well understood that char properties are a function of feedstock properties and processing conditions, and temperature is often cited as one of the most influential processing factors governing both hydrochar and biochar properties. For instance, from a quantitative assessment of the effect of processing conditions on hydrochar yield and extent of carbonization, Suwelack et al. (2015) suggested that processing temperature was more influential than reaction time and process water acidity. Similarly, biochar recalcitrance, measured as a function of the energy needed to thermally oxidise biochar, appears to be influenced by pyrolysis temperature more substantially than bio-feedstock choice (Zhao et al. 2013). This is to be expected since processing temperature governs the loss of volatiles from feedstocks (Downie et al. 2009). Nevertheless, certain properties are likely to be more affected by feedstock properties; Zhao et al. (2013a) for instance suggested that more emphasis should be placed on feedstock properties if biochars are intended for enhancing soil nutrient content as this influences biochar mineral content to a greater extent than processing temperature. The relationships between feedstock properties and processing conditions on char properties are often non-linear however (Morales et al. 2015), thus further research is required to clarify these associations. In this chapter, the physicochemical properties of the hydrochars and biochars derived from the feedstocks described in **Section 3.1** are presented to evaluate the influence of HTC, slow pyrolysis and gasification on hydrochar and biochar elemental composition, surface functional groups and textural properties. This information can ultimately contribute to ongoing research involving the development of chars for specific purposes.

4.1 Feedstock composition

4.1.1 Ultimate and proximate analyses

The biomass feedstock compositions presented in **Table 4.1** show that carbon and oxygen contents of oak and greenhouse waste were within the range reported for hardwood and herbaceous biomass respectively (Jenkins et al. 1998). Their O/C atomic ratios as percent dry basis were also within the typical values observed for agricultural biomass, being 0.55–0.75 as outlined by Spokas (2010). Municipal waste (cellmat) had a comparable carbon content to oak and greenhouse waste, likely due to its cellulose-rich nature resulting from the steam autoclaving process.

Presscake and greenwaste possessed the lowest carbon contents, and their oxygen contents, determined as the difference between elemental C, H, N and S on a dry basis were likely overestimated given their high ash contents, although oxygen may have also been associated with these inorganics (Lawrinenko 2014). Compared to oak and greenhouse waste feedstocks, the inorganic contents in cellmat, presscake, and greenwaste feedstocks were considerably higher. Such inorganic matter, defined as diluents by IBI (2015), resulted in high ash contents for the waste-derived feedstocks. Although greenwaste possessed an exceedingly higher ash content than expected for yard waste feedstocks, the ash contents of oak, greenhouse waste and municipal waste were within the range reported for agricultural feedstocks. For instance, hardwoods possess ash contents < 3% while herbaceous crops and residues (straw, hulls, shells) tend to be much higher (Jenkins et al. 1998).

Table 4.1 Composition of biomass feedstocks

Property	Holm oak	Greenhouse waste	Municipal Waste (cellmat)	Presscake from AD	Greenwaste
Elemental content (db)					
C (%)	50.8	45.7	43.3	22.7	25.0
H (%)	7.4	6.6	6.6	2.5	3.0
N (%)	1.5	1.1	1.6	1.5	1.4
S (%)	0.0	0.3	0.5	0.0	0.0
O (%)	40.3	46.3	48.0	73.3	70.6
H/C	1.75	1.73	1.83	1.32	1.4
O/C (db)	0.59	0.76	0.83	2.42	2.1
Proximate analysis (a.r.)					
Moisture (%)	9.6	9.2	5.2	4.1	2.3
Ash (%)	2.6	10.0	26.8	61.3	75.7
Volatile matter (%)	65.5	74.6	66.7	31.5	22.0
Organic matter	87.8	80.9	68.0	34.6	22.0
Fixed carbon	22.3	6.2	1.3	3.1	0.0

Oxygen content determined as 100 – (%C + %H + %N + %S); db: dry basis; a.r.: as-received.

4.1.2 Feedstock nutrient contents

The macro- and micro-mineral contents of the five feedstocks are presented in **Figures 4.1** and **4.2**, respectively. Relative to other mineral elements, Ca contents were high in all feedstocks. This is not unusual since analysis of the ash

composition of various feedstocks by Jenkins et al. (1998) showed that CaO was one of the most abundant constituents present in hardwoods, nutshells, yardwaste, mixed paper and refuse-derived fuel (RDF), second only to SiO_2, while K_2O, MgO, P_2O_5 and SiO_2 were also present in appreciable quantities. Such inorganic elements are present in soil and are taken up by plants and trees during growth (Miles et al. 1995). In the waste-based feedstocks (municipal waste and presscake), Ca contents were especially high and such samples also possessed higher quantities of other macro- and micro-elements like Fe **(Figure 4.2**). Such elevated mineral concentrations are understandable particularly for municipal waste given its heterogeneous nature. Furthermore, the effect of pre-treatments such as autoclaving and anaerobic digestion may have resulted in a relative increase in inorganic matter content as a consequence of the degradation of some organic matter. Indeed, heat treatment of the unsorted municipal waste resulted in a more fibrous final product (cellmat), which provided evidence of some degree of organic matter decomposition. Yao et al. (2011) also observed an increase in cations following anaerobic digestion of sugar beet tailings.

The K content of oak biomass was 0.14%, lowest in of all feedstocks studied but was within the range reported for woody biomass; K contents of herbaceous (straw, grass) and ligneous (hulls, shells) feedstocks tend to be much higher than wood-based feedstocks (Jenkins et al. 1998). K can be bound to the organic matrix of biomass in form of alkali-carboxylic groups, complex ions or as dissolved salts (Miles et al. 1995). Na content was low for feedstocks with the exception of municipal waste and presscake. While steam, pressure and mechanical agitation was capable of separating large pieces of metal, plastic and glass from unsorted municipal waste, the resulting product (cellmat) still retained small glass and plastic fragments, evident from visual inspection and from elemental analysis. Glass and plastic are defined as contaminants according to the IBI. Moreover, chlorine was also present in municipal waste at higher concentrations than other feedstocks, second only to presscake. Specifically, chlorine contents in cellmat and presscake biomass were about three and five times higher than in oak biomass, being about 3600 mg kg^{-1} and 5300 mg kg^{-1} (db), respectively. These were still within the range observed for biomass however (Björkman and Strömberg 1997). Since chlorine is a precursor to dioxin formation at certain thermochemical processing temperatures (Björkman and Strömberg 1997; IBI 2015), monitoring chlorine concentrations in feedstocks is important. Na in cellmat may have been present in both soluble and insoluble form as NaCl and residual pieces of glass, respectively although further

analysis is required to confirm this. While plants require macro-minerals for optimal growth, high concentrations can have adverse effects. For instance, high Na contents initially affect crop growth negatively in some cases (Jeffery et al. 2013).

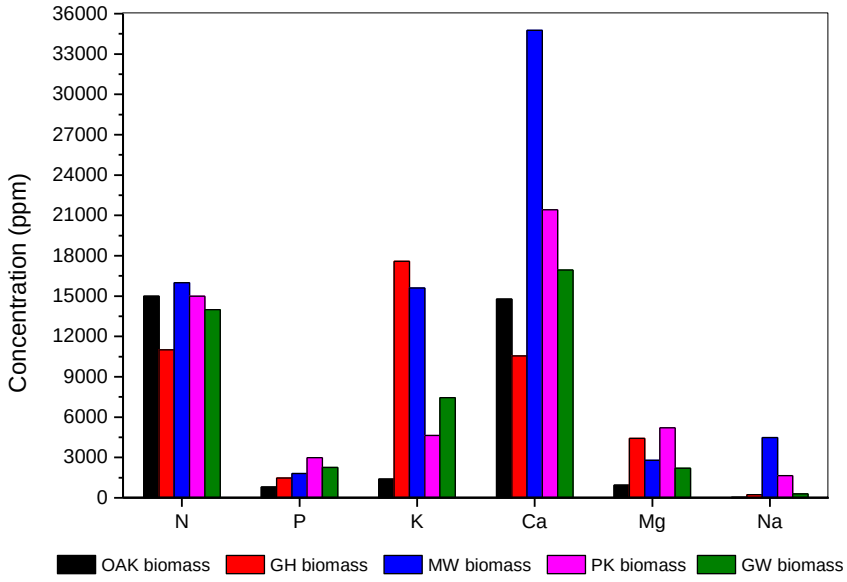

Figure 4.1 Macronutrient content of biomass feedstocks
GH: greenhouse (paprika) waste; **MW**: municipal waste (cellmat); **PK**: presscake from AD; **GW**: greenwaste.

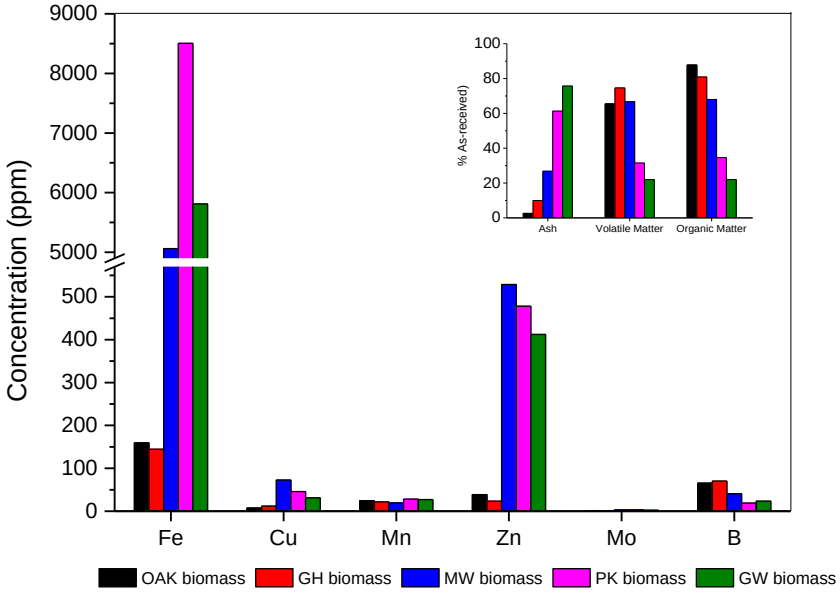

Figure 4.2 Micronutrient contents of the various biomass feedstocks.
(Molybdenum contents ranged from about 0.4–9.0 ppm).
GH: greenhouse (paprika) waste; **MW**: municipal waste (cellmat); **PK**: presscake from AD; **GW**: greenwaste. Inset: ash, volatile, and organic contents.

4.2 Effect of thermochemical processing on char inorganic content

4.2.1 Ultimate and proximate analyses

In **Section 4.1**, dissimilarities in carbon and inorganic contents were observed between two categories of feedstocks: oak, greenhouse and municipal waste feedstocks possessed higher carbon contents than presscake and greenwaste while inorganic (ash) contents were higher in the latter feedstock category. With the exception of greenwaste, HTC resulted in an increase in carbon content (**Table 4.2**), with the greatest increases observed for greenhouse waste followed by oak and municipal waste. The increase in carbon content following thermal treatment is expected since cellulose and hemicellulose-rich biomass carbonize during pyrolysis (Kizito et al. 2015). As there was only a small increase in carbon content in municipal waste hydrochar however, its carbon content of 45.2% would categorize it as a Class 2 char according to the IBI classification system or as a bio-carbon material according to EBC standards (IBI 2014) while presscake and greenhouse waste hydrochars would be termed Class 3 as their carbon contents remained below 30%. Following slow pyrolysis, the carbon contents of municipal waste, presscake and greenwaste were even lower than their original feedstocks likely due to the relative increase in ash content, and thus also termed Class 2–3 biochars. Commercial and non-commercial oak biochars had similar carbon contents regardless of difference in pyrolysis units, and the carbon contents of biochars produced at non-standard conditions (≠ 60 min, 0% O_2) are presented in **Table 4.3**. The few greenhouse waste gasification biochars investigated possessed slightly higher carbon contents compared to the greenhouse waste biochar produced at 600°C. Conversely, municipal waste and presscake pyrolyzed in the presence of 1% oxygen (MW-1% and PK-1%, respectively) had slightly lower carbon contents (3.8% and 1.4% lower, respectively) than their counterparts produced at 600°C under standard conditions, while oxygen contents increased by about the same proportion (4% and 1.4% higher respectively).

Predictions about char material stability are often made based on atomic O/C and H/C_{org} ratios preferably following acid-washing of chars, a recommended practice that corrects for the contributions of C and H from inorganics such as carbonates and H-bonded to silicates respectively (Kuhlbusch 1995). As hydrochars and biochars in this study were not acid-washed prior to elemental analysis, it is uncertain whether O/C and H/C ratios can serve as accurate predictors of their

stability. Nevertheless, for biochars produced at standard conditions, O/C ratios were below 0.4 in all chars with the exception of 400°C municipal waste biochar, suggesting that this char possesses the least stability. This is because O/C atomic ratios (% dry weight) < 0.2 are often thought to possess greater stability in soil (potentially over 1000 years) while O/C ratios >0.6 may possess far shorter stability of < 100 years, the latter suggested to be the transition point between biomass and char products (Crombie et al. 2013; Spokas 2010). Other frequently-used means of predicting char stability include chemical oxidation (Cross and Sohi 2013) and thermal (Temperature-Programmed) oxidation (TPO) (Harvey et al. 2012). From TPO analysis, the recalcitrance indices (R_{50}) of biochars produced at 400°C were similar and ranged from 0.47–0.49, with municipal waste biochar produced at 400°C being among the lowest at 0.47, while oak 400°C was 0.48; indices for 600°C pyrolysis and gasification chars were up to 0.55 (dataset not included). As anticipated, biochar stabilities were more similar to uncharred biomass than to graphite, whose R_{50} values are about 0.4 and 1.0, respectively (Harvey et al. 2012). Physical weathering by water action might also affect char stability, as Spokas et al. (2014) observed the disintegration of chars following 24 h agitation with water, particularly for wood/lignin-rich chars compared to cellulose-rich chars. Further discussions on char stability are provided in **Section 5.5.1**.

The ash contents of oak and greenhouse waste biochars were nearly twice higher than their hydrochar counterparts but only modestly higher for municipal waste, presscake and greenwaste. Hydrochars are expected to possess lower ash contents than biochars from the same feedstock due to the leaching of inorganics into process water during the former process, the degree to which appears to be dependent on carbonization temperature (Reza et al. 2013; Smith et al. 2016) and possibly the nature of bonds between inorganic matter and feedstock structures as implied in this study. In other words, the relatively smaller difference between hydrochar and biochar ash content for municipal waste, presscake and greenwaste compared to those of oak and greenhouse waste suggests that in the former group, inorganics may have been more strongly bound to the biomass structure. Alternatively, some inorganic elements may have been re-adsorbed from the process water into char pores that were formed, similar to observations by Reza et al. (2013). As porosity development was similar for all hydrochars however (ranging from 0.011–0.035 $cm^3\ g^{-1}$, **Section 4.4**, the latter hypothesis seemed unlikely but future analysis of hydrochars produced at varying carbonization temperatures are required to fully overrule this possibility.

Table 4. 2 Physicochemical properties of chars produced at standard conditions

Biochar	C (%)	H (%)	N (%)	S (%)	O[a] (%)	Ash content	Volatile matter	Organic matter[b]	pH
250°C hydrochars									
OAK	67.9	6.5	1.4	0.1	24.1	6.2	6.2	93.8	4.8
GH	66.4	6.8	3.1	0.2	23.5	5.2	61.6	91.1	5.8
MW	45.2	6.0	2.0	0.2	46.6	38.0	42.8	60.1	6.2
PK	22.8	2.0	0.9	0.1	74.2	69.8	20.7	28.4	7.2
GW	21.4	1.9	1.2	1.1	74.4	66.1	24.0	30.5	7.0
400–450°C biochars									
OAK (Comm.)	65.7	2.7	0.6	0.0	31.0	11.7	21.1	88.3	9.9
OW	70.9	3.6	0.4	0.0	25.1	12.1	20.8	87.9	9.7
GH	59.0	2.9	1.2	0.3	36.6	27.0	25.0	70.5	10.6
MW	39.9	3.7	1.7	0.3	54.4	50.1	26.2	49.5	9.5
PK	17.1	0.8	0.9	0.3	80.9	79.5	13.4	20.2	10.3
GW	16.1	1.1	1.3	0.0	81.5	77.5	15.5	21.7	11.1
600–650°C biochars									
OAK (Comm.)	76.5	1.4	0.8	0.0	21.3	14.3	11.8	85.7	10.3
OW	79.2	2.0	0.3	0.0	18.5	13.4	9.2	86.6	8.6
GH	63.0	1.2	0.9	0.4	34.5	17.0	13.0	80.0	11.0
MW	40.1	1.1	1.4	0.4	57.0	53.8	18.7	45.2	10.2
PK	18.5	0.5	0.6	0.3	80.1	83.4	7.6	16.2	10.1
GW	18.2	0.6	1.3	0.0	79.9	78.5	9.8	21.1	10.3

OAK (Comm.): commercial oak produced at 450°C and 650°C; OW: oak wood; GH: greenhouse (paprika) waste; MW: municipal waste (cellmat); PK: presscake from AD; GW: greenwaste. [a] Oxygen contents determined as 100 - (%C + %H + %N + %S) on dry basis; ash, volatile and organic matter expressed as as-received percentages.

Table 4.3 Physicochemical properties of chars produced at non-standard conditions

Biochar	C (%)	H (%)	N (%)	S (%)	O[a] (%)	Ash content	Volatile matter	Organic matter	pH
PK 700°C, 60 min, N_2	9.2	0.1	0.6	0.2	89.9	86.5	6.7	12.9	10.8
Gasification chars									
GH-FA 600°C (air)	73.8	1.1	0.9	0.0	25.0	22.6	19.0	75.4	10.8
GH-FN 600°C (N_2)	69.9	1.0	1.2	0.0	27.9	25.0	22.6	70.9	11.2
GH-FN 750°C (N_2)	72.2	0.7	1.6	0.0	25.5	22.0	26.3	76.4	12.3
Pyrolysis chars (30 min, N_2)									
MW 600°C, 30 min	39.1	1.1	1.4	0.8	57.6	59.9	18.7	39.3	9.7
PK 600°C, 30 min	24.2	1.1	0.6	0.2	73.9	81.5	7.6	18.4	10.3
PM 600°C, 30 min	63.0	1.0	2.8	0.0	33.2	32.6	22.5	93.2	11.4
PM 700°C, 30 min	65.8	0.7	2.2	0.0	31.3	28.7	17.3	68.4	10.2
Pyrolysis chars (600 °C, 60 min, 1% O_2)									
MW 600°C, 60 min	36.3	1.0	1.0	0.7	61.0	58.4	17.1	33.6	10.2
PK 600°C, 60 min	17.1	0.4	0.7	0.3	81.5	81.1	6.8	18.6	10.1

GH-FA and GH-FN refer to greenhouse waste gasification biochars produced in air and N_2 resp. [a]Oxygen contents determined as 100 - (%C + %H + %N + %S) on dry basis; ash, volatile and organic matter expressed as as-received percentages.

As expected, hydrochar pH values were mostly acidic and ranged between 4.8–7.2 while biochar pH values ranged from 8.6–12.3, highest in gasification chars. Studies by Rutherford et al. (2007) on cellulose, lignin, pine wood and bark chars revealed that more total acid surface functional groups and aliphatic alcohols were present in lower temperature chars (250–350°C, >8 h) at concentrations comparable to humic acids, but these groups were transformed to neutral or basic aromatic groups with increasing processing temperature (Mukherjee et al. 2011; Rutherford et al. 2007). Hydrochar pH was negatively correlated to oxygen content when evaluated on a dry ash-free basis (Pearson $r_)$ = -0.90) but was positively correlated to ash content (Pearson r = 0.93). This might be because both acidic and basic oxygen functional groups are present on carbon surfaces (López-Ramon et al. 1999; Yuan et al. 2011). Yuan et al. (2011) suggested that at lower temperatures, organic anions such as -$COOH^-$ and -O^- groups were predominantly responsible for biochar alkalinity while

carbonates of elements such as calcium and magnesium influence biochar alkalinity at higher temperatures. In hydrochars, oxygen functional groups may also be associated with inorganics like magnesium oxide or iron oxides, which might also explain why a very strong positive correlation between hydrochar pH and Mg and Fe was observed although further studies are required to confirm this. The relationship between biochar pH and char compositional properties such as oxygen, ash and elemental content are presented in **Table 4.4**. From the poor correlations between biochar pH and ash content in this study (0.52 and 0.18 in low and high temperature biochars, respectively), char pH is less a function of ash content. A significant positive correlation between the pH value of high temperature biochars (600–650°C) and Mg content were observed however (0.86). Fidel et al. (2017) similarly found positive correlations between total biochar alkalinity and specific acid-soluble base cations, rather than ash content, soluble and insoluble volatile matter, and fixed carbon content. Similarly, positive correlations between biochar pH and acid-soluble monovalent base cations were observed (Fidel et al. 2017).

Table 4.4 Pearson correlations between char pH and char compositional properties

Parameter	250°C hydrochars	400–450°C biochars	600–650°C biochars
Ash	0.93*	0.52	0.18
Volatile matter	0.08	-0.51	0.34
Organic matter	-0.94*	-0.54	-0.20
Oxygen[a]	-0.90*	-0.32	0.40
P	0.98*	0.12	0.54
K	0.11	0.26	0.64
Ca	0.61	-0.24	0.31
Mg	0.99*	0.60	0.86*
Na	0.85	-0.38	0.27
Fe	0.90*	0.27	0.12
Cu	0.66	-0.23	0.10
Zn	0.58	0.17	0.03
B	-0.70	0.31	0.78
Mn	0.49	0.66	0.36
Mo	0.91*	-0.49	0.06

*Two-tailed test of significance used and correlation is significant at the 0.05 level, based on ash content (%), elemental content (ppm, db) and [a]oxygen content determined by difference and evaluated here based on % daf basis.

4.2.2 Char nutrient content

Tables 4.5 and **4.6** compare the effect of thermochemical processing on biomass feedstock nutrient content. N contents decreased following thermochemical treatment of oak, presscake and greenwaste chars but the opposite was observed for greenhouse waste and municipal waste hydrochars. Most of the char inorganic content was comprised of Ca, followed by K and Mg, reflective of the starting feedstocks' inorganic compositions, and their concentrations generally increased following pyrolysis. This is understandable given that biochar mineral contents increase due to a relative loss in hydrogen and oxygen as pyrolysis temperature increases (Ippolito et al. 2015), although about 20% volatilization of alkali and alkaline earth metals occurs during slow pyrolysis depending on biomass composition, temperature, heating rate and element valency (Keown et al. 2005). For instance, K vaporises at lower temperatures in form of KCl depending on its proportion in biomass (Keown et al. 2005) while Ca, Mg, P and Si vaporise at higher temperatures (Amonette and Joseph 2009; Ippolito et al. 2015). Manure biochars possessed the highest inorganic contents as expected, thus Na contents were highest in biochars derived from pig manure followed by municipal waste (600°C). Relative to the biochars produced at standard conditions, no major differences were observed in municipal waste and presscake biochars pyrolysed for 30 min or in the presence of 1% oxygen. In municipal waste biochars however, some inorganics were somewhat higher following pyrolysis over 30 min compared to 60 min, notably Ca and Mg contents while pyrolysis in the presence of oxygen had a lower impact on mineral content. In terms of pollutant concentrations, a previous Fertiplus study revealed that in all the chars, the 16 priority polycyclic aromatic hydrocarbons, heavy metals, and chlorinated dioxin congeners were within the acceptable range recommended by the IBI.

Tables 4.5–**4.6** also show that with the exception of nitrogen content, hydrochar inorganic elemental contents were generally lower than the biochars'. As the main gas released during HTC is CO_2 (Benavente et al. 2015; Ramke et al. 2009), it is unlikely that micro- and macro-minerals were volatilized. Analysis of the HTC aqueous products confirmed that some minerals were leached into the process water, thus certain elements decreased relative to the original biomass. For oak, a 39–100% reduction in K, Mg, Na and Zn was observed in its hydrochar and this was also true for greenhouse waste with the exception of Zn which increased. For both municipal waste and presscake, only K and Na contents decreased and for greenwaste, K and Zn decreased while Na remained the same. The decrease in K

and Na in hydrochars from all feedstocks is expected given that these elements are readily leached from various biomass feedstocks using water even at room temperature (Saddawi et al. 2011). More inorganic elements were released from oak biomass compared to other feedstocks, suggesting that these elements were less strongly bound to the biomass structure. This was contrary to the findings of Saddawi et al. (2011) who observed woody biomass to release elements like Mg at lower proportions than herbaceous feedstocks. Leaching of inorganics may have been enhanced by the acidic aqueous phase during HTC, as organic acids are known to be present during HTC (Hoekman et al. 2011). Similar decreases in mineral content following HTC have been reported in the literature, such as a 48% reduction following HTC of plant-based biomass (corn stover, miscanthus, rice hull and switch grass) at 260°C for 5 min in Reza et al. (2013). Smith et al. (2016) noted up to 97% removal of elements like sodium but less dramatic decreases for multivalent elements following HTC of some of the same feedstocks used in this study, prepared under identical HTC conditions.

Table 4. 5 Standard condition hydrochar and biochar nutrient contents

	ppm (db)										
Char	P	K	Ca	Mg	Na	Fe	Cu	Zn	B	Mn	Mo
250°C hydrochars											
OAK	705	336	23200	290	100	169	10	15	82	107	0
GH	2110	6710	15500	1940	70	391	39	123	131	5	2
MW	2880	8500	23300	3800	430	8540	105	737	71	21	5
PK	4660	2140	26700	5570	295	10900	72	502	20	140	5
GW	5320	3000	29500	4800	269	9790	63	289	15	310	5
400–450°C biochars											
OAK (Comm.)	1700	11500	43800	2410	1410	1950	16	224	21	51	5
OAK	814	8840	27000	1560	1080	1410	16	103	9	30	3
GH	3610	40600	35600	9040	3610	2370	47	101	39	86	5
MW	4330	8210	59100	5110	7330	10200	173	540	33	180	8
PK	5760	11600	38400	5670	3690	8000	91	445	33	223	7
GW	2790	6050	41400	5150	1150	9780	36	544	26	391	3
600–650°C biochars											
OAK (Comm.)	1780	6140	50200	2710	361	415	11	56	32	426	<0.5
OAK	812	2000	30200	0	1560	1870	23	150	11	38	2
GH	4300	49000	43700	12000	4060	2160	27	68	47	80	2
MW	4750	8910	81000	290	14000	19900	188	901	46	223	7
PK	4830	11000	36000	4760	4000	16975	90	460	34	198	5
GW	2330	3830	31600	4660	981	9490	27	315	20	430	2

OAK (**Comm**) & **OW**: reference & ECN oak wood, respectively; **GH**: greenhouse waste; **MW**: Municipal waste; **PK**: presscake; **GW**: greenwaste. Concentrations presented as average of Fertiplus research group analyses (University of Leeds, CEBAS-CSIC Spain, and ECN).

Table 4. 6 Non-standard biochar nutrient contents

	ppm										
Char	P	K	Ca	Mg	Na	Fe	Cu	Zn	B	Mn	Mo
PK 700°C, 60 min, N_2	4330	6340	33800	6290	2690	10000	91	571	29	34	5
Gasification chars											
GH-FA 600°C (air)	4660	14000	15700	3290	6090	1850	0	57	19	2	2
GH-FN 600°C (N_2)	4490	2480	11800	2600	3900	1180	0	99	33	3	3
GH-FN 750°C (N_2)	6270	28600	29800	9730	8870	1200	0	90	44	5	4
Pyrolysis chars (30 min, N_2)											
MW 600°C, 30 min	5200	9920	87800	7630	14500	28850	252	950	55	213	9
PK 600°C, 30 min	4420	8170	28200	4740	2520	10800	67	410	28	140	5
PM 600°C, 30 min	31000	20500	38000	16800	31000	1420	68	321	36	238	2
PM 700°C, 30 min	20500	18600	33000	10200	28800	4000	0	1000	0	0	0
Pyrolysis chars (600°C, 60 min, 1% O_2)											
MW 600°C, 60 min	4890	9390	84600	6850	13000	13320	260	890	48	255	8
PK 600°C, 60 min	4860	9090	32600	4940	2840	11850	91	492	29	157	6

GH-FA and **GH-FN** refer to greenhouse waste gasification biochars produced in air and N_2, respectively. Concentrations presented as average of Fertiplus research group analyses (University of Leeds, CEBAS-CSIC Spain, and ECN).

4.3 Effect of thermochemical processing on char functional groups

4.3.1 Attenuated Total Reflectance Fourier Transform Infrared spectroscopy

ATR-FTIR spectra of the various biomass feedstocks are presented in **Figure 4.3** and their band assignments are provided in **Table 4.7**. Spectral characteristics were mostly similar between feedstocks even within the 'fingerprint' region (1300–650 cm^{-1}). Predominant bands were from alcohol or phenol groups (3600–3000 cm^{-1}), aliphatic groups (2985–2821 cm^{-1}), carboxyl or ketone groups (1700 cm^{-1}) and C-O from polysaccharides or inorganics such as silicates or phosphates (1025 cm^{-1}). Presscake, however, possessed the most aliphatic and carboxyl or amide groups followed by municipal waste, while greenhouse waste possessed the least aliphatics. Spectral characteristics of the hydrochars, pyrolysis and gasification chars are presented in **Figure 4.3(a)**–**(f)**. Most of the bands present in the original feedstocks were also present in the chars. Pig manure chars were also evaluated for comparisons with the plant-derived chars. Some differences were evident between feedstocks. For example, less sharp band intensities in oak and greenhouse waste biochars were evident, and a slower degradation of aliphatic groups in municipal waste was observed relative to the other feedstocks (**Figure 4.3(c)**). Processing temperature appeared to be the most influential factor governing the change in peak intensity compared to residence time, atmosphere (N_2 or 1% O_2) or even processing route. For instance, **Figure 4.3(b)**-**(d)** showed that there were no marked differences between chars pyrolyzed over shorter residence times (30 min), in 1% O_2 or between pyrolysis and gasification chars. Conversely, while hydrochars retained most of the spectral features of the original biomass, 600°C biochars were the least similar to the original biomass, with few discernible peaks.

Liu et al. (2015) attributed this loss of peaks to graphitization of the carbon material. Furthermore, the new band at about 870 cm^{-1} attributed to aromatic C-H vibrations only emerged at higher temperatures. At the same time, aliphatic groups (2925–2812 cm^{-1}) present in most of the unprocessed feedstocks which increased following HTC were absent in biochars with the exception of municipal waste pyrolysed at 400°C (**Figures 4.6(b)**–**(e)**). O-H groups (3600-3200 cm^{-1}) present in the feedstocks were absent in biochars. In pig manure, fewer aliphatic groups were likely present compared to other feedstocks (**Figure 4.3(f)**) and the most prominent band was at about 1000 cm^{-1}, attributable to either biomass polysaccharides or inorganic elements such as silicates or phosphates. Since peaks were still prominent even after pyrolysis at 600°C however, the former category was unlikely since hemicellulose and cellulose fractions are completely decomposed at

temperatures between 250–380°C (Liu et al. 2015; Reza et al. 2013; White et al. 2011). The reduction in peak number and intensity in higher temperature chars is indicative of increasing aromatization (Liu et al. 2015) and is in agreement with several studies which have shown that the degree of carbonization increases with processing temperature. Direct-excitation solid-state ^{13}C Nuclear Magnetic Resonance (NMR) spectra with composite pulse sequence suppression of background signals obtained from the EPSRC UK National Solid-state NMR Service at Durham also verified that the functionalities of oak 250°C and 650°C chars were markedly different. While the hydrochar had greater abundance of O-alkyl functional groups, the biochar possessed a dominant aromatic carbon signal (**Figure 4.5**). Such differences are likely attributable to the extent of carbonization rather than the form of thermochemical treatment employed, since Brewer (2012) observed similar changes in the peak characteristics of cross-polarisation NMR spectra for biochars produced at varying degrees of fast pyrolysis. With regard to the NMR method used in this study, long relaxation delays are experienced during direct excitation of nuclei, and several scans are often required to attain satisfactory signal-to-noise ratios (Bakhmutov 2011). Thus compared to cross-polarisation NMR, direct-excitation NMR is less rapid (Apperley et al. 2012). However, signal intensities for complex samples are not always proportional to the number of nuclei present during cross-polarisation NMR (Apperley et al. 2012).

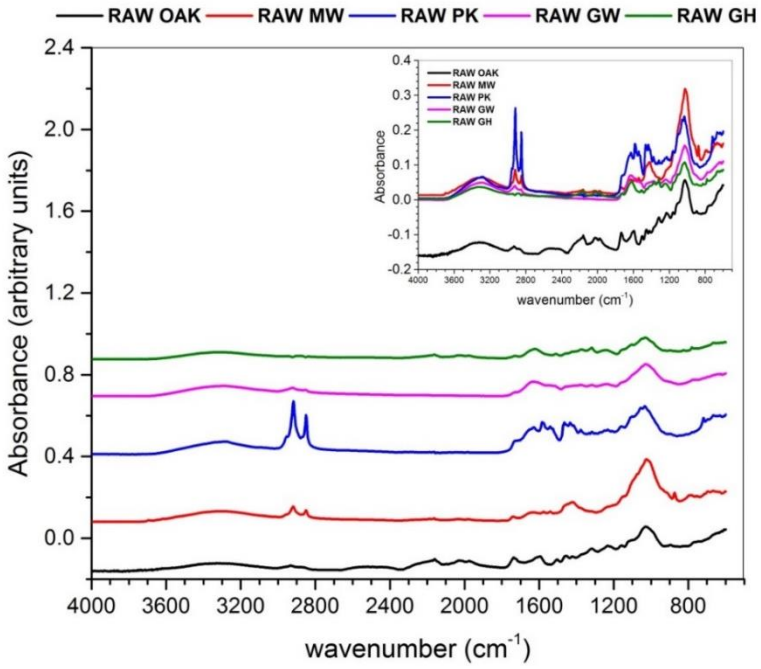

Figure 4.3 FTIR spectra showing band characteristics of biomass feedstocks: **MW**: municipal waste, **PK**: presscake, **GW**: greenwaste, **GH**: greenhouse waste. Inset: band characteristics as they occur at the exact absorbance intensities.

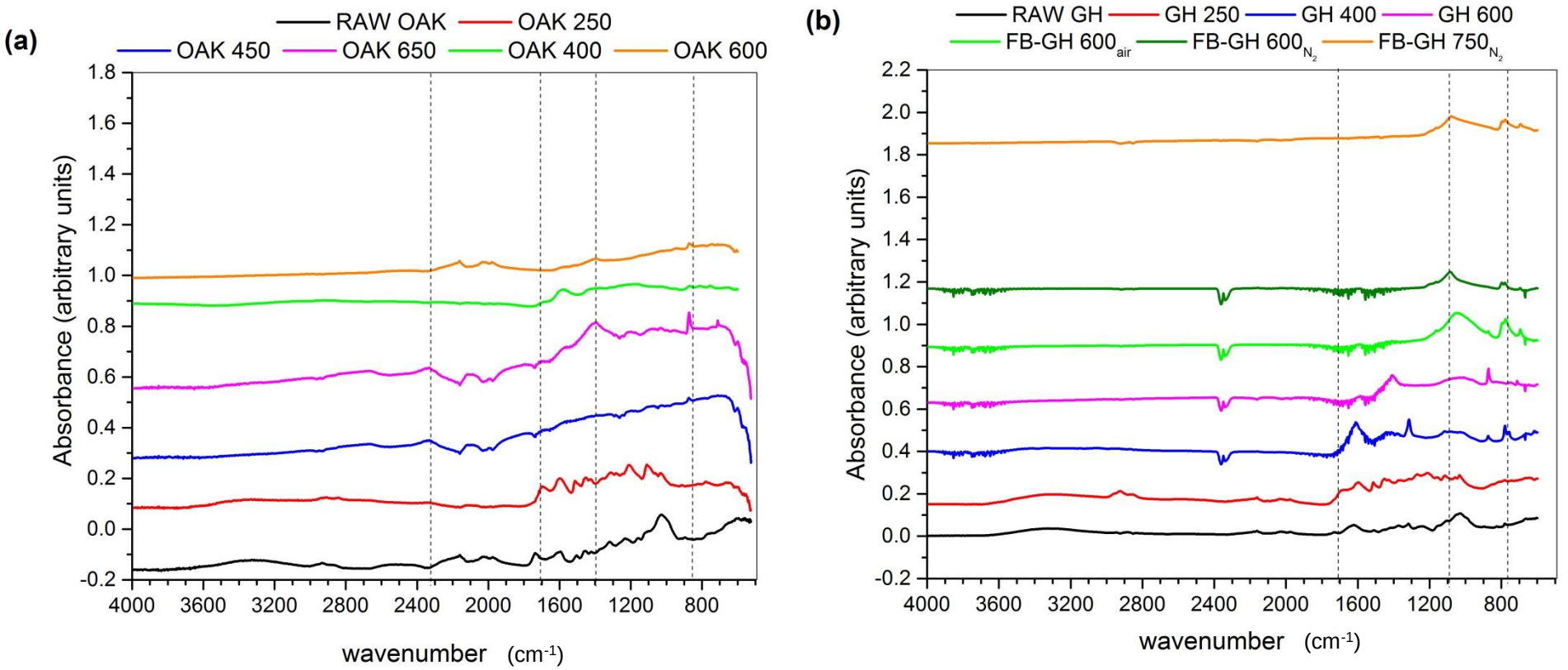
(a)
RAW OAK
OAK 250
OAK 450
OAK 650
OAK 400
OAK 600
Absorbance (arbitrary units)
wavenumber (cm-1)
(b)
RAW GH
GH 250
GH 400
GH 600
FB-GH 600air
FB-GH 600N2
FB-GH 750N2
Absorbance (arbitrary units)
wavenumber (cm-1)

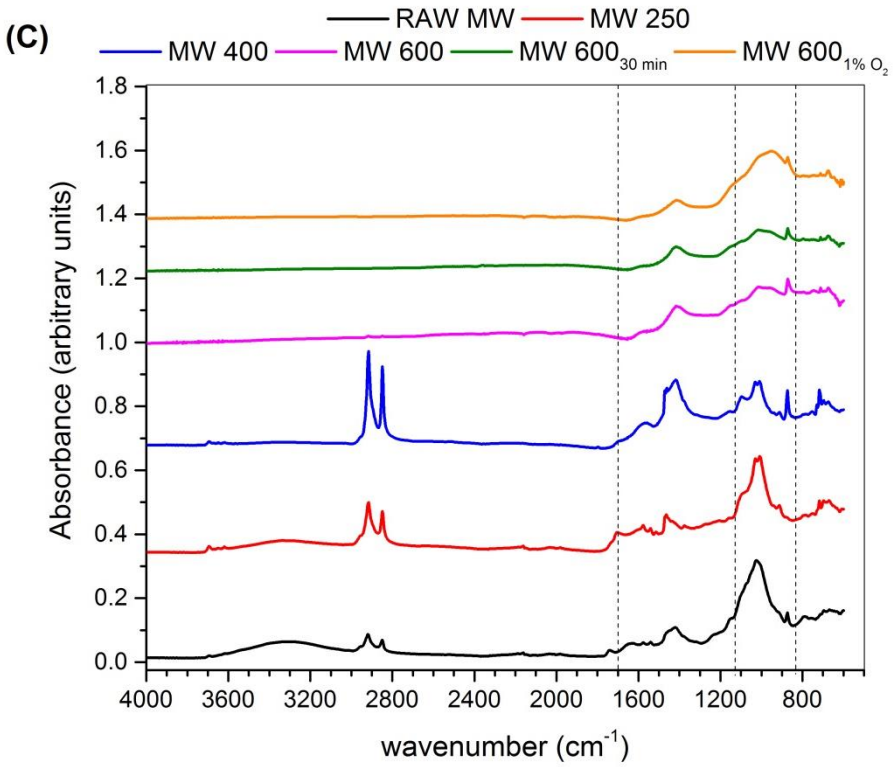
(C)
RAW MW
MW 250
MW 400
MW 600
MW 600 30 min
MW 600 1% O2
Absorbance (arbitrary units)
wavenumber (cm-1)

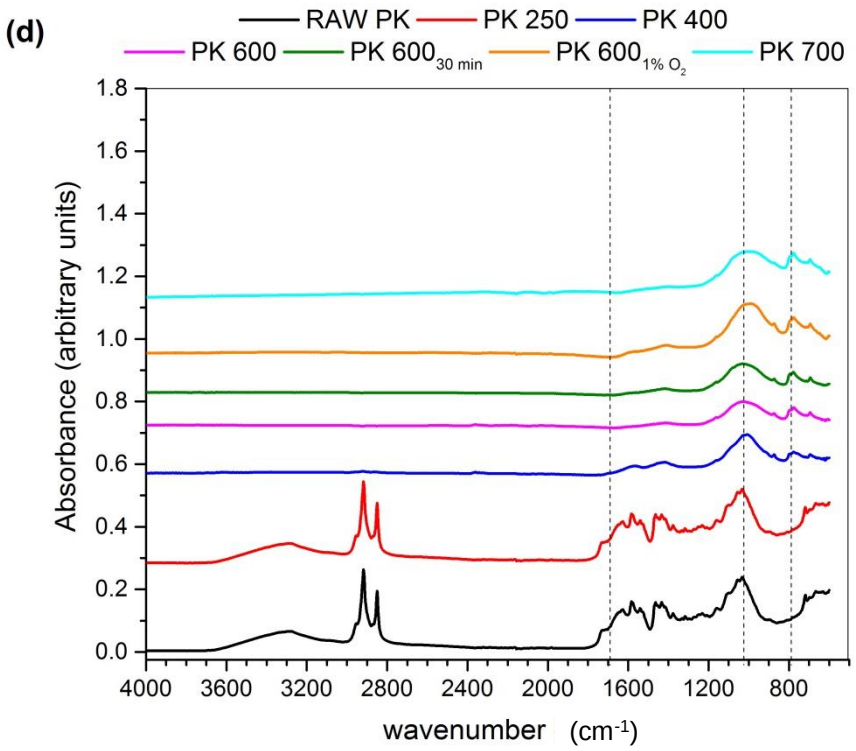
(d)
RAW PK
PK 250
PK 400
PK 600
PK 600 30 min
PK 600 1% O2
PK 700
Absorbance (arbitrary units)
wavenumber (cm-1)

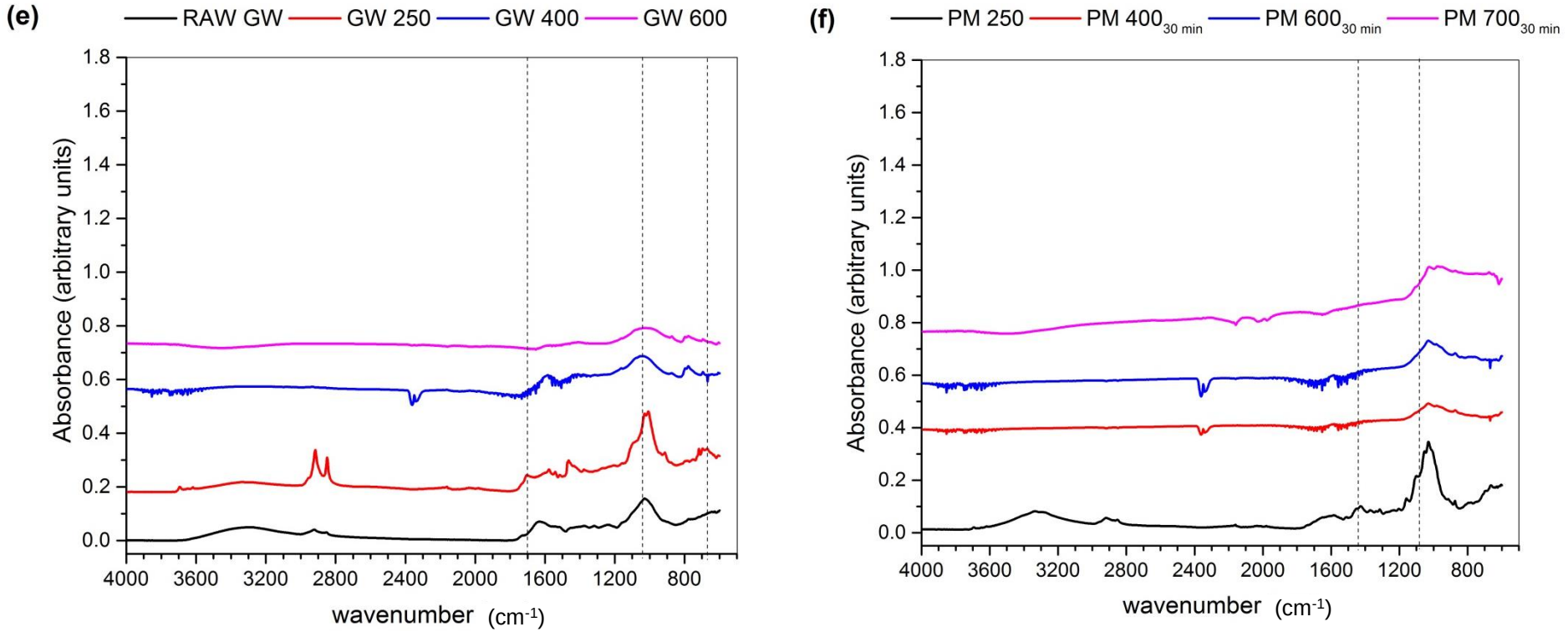

Figure 4.4 ATR-FTIR spectra showing bands within the 4000-600 cm^{-1} region for (a) oak (b) greenhouse waste (c) municipal waste (d) presscake (e) greenwaste (f) pig manure.

Table 4.7 ATR-FTIR functional group assignment of prominent spectral bands in biomass and chars

Band (nm)	Assignment	References
722	Amine group vibrations.	Cuetos et al. (2010)
765, 789	C-H out-of-plane bending of aromatic groups (765 cm^{-1}).	Wu et al. (2012)
800, 870	C-O out-of-plane vibrations or C-H vibrations of aromatic groups.	Provenzano et al. (2014); Wu et al. (2012).
1025, 1032	C-O stretch of polysaccharides, Si-O vibrations of silicates, or PO_4^{3-} vibrations.	Hsu and Lo (1999); Liu et al. (2015); Provenzano et al. (2014); Wu et al. (2011); Wu et al. (2012)
1050	O-H from aliphatic groups or stretching of PO_4^{3-}.	Cao and Harris (2010)
1048-988	CO_3^{2-} out-of-plane vibrations.	Zhao et al. (2013)
1100	C-C bending vibrations in aldehydes and ketones.	Reusch (2013)
1204	Phenolic O-H deformations and C-O stretching.	Pognani et al. (2010)
1288, 1271	C=C stretching.	Cao and Harris (2010)
1330	C-N vibrations of amines.	Wu et al. (2011)
1463, 1456	C-H bending of saturated hydrocarbons.	Zhao et al. (2013)
1403	Asymmetric COO^- deformation of polysaccharides; C=O stretching of phenols or O-H deformation; alpha-CH_2 bending in aldehydes and ketones.	Cuetos et al. (2010); Reusch (2013); Pognani et al. (2010)
1412-1477	Two peaks in some cases suggestive of C-H deformation from ignin components.	Hsu and Lo (1999); Wu et al. (2011)
1507	C=C stretching of aromatic compounds of lignin.	Pognani et al. (2010); Wu et al. (2011)
1589	Conjugated C=O stretching.	Provenzano et al. (2014)
1603, 1606	Asymmetric –COO stretching of amino groups, or amides.	Liu et al. (2015); Zhao et al. (2013)
1703, 1700	C=O stretching of carbonyl bonds. (ketone or carboxylic acid) e.g., lactones.	Cuetos et al. (2010); Merlic (1997); Rutherford et al. (2008); Wu et al (2011, 2012)
2152, 2093-1959	Stretching in nitrile C=N, C≅N, isocyanates, isothiocyanates, diimides, adzides and ketenes.	Reusch (2013); Merlic (1997)
2300, 2353	Alkynyl C-H or C=C stretching.	Merlic (1997)
2985-2821	Asymmetric -CH_2 and –CH_3 stretching vibrations indicative of aliphatic methylene groups.	Cao and Harris (2010); Cuetos et al. (2010); Pognani et al. (2010); Wu et al. (2011)
3600-3200; 3690	O-H stretching of alcohol or phenol groups.	Cuetos et al. (2010); Wu et al. (2012)

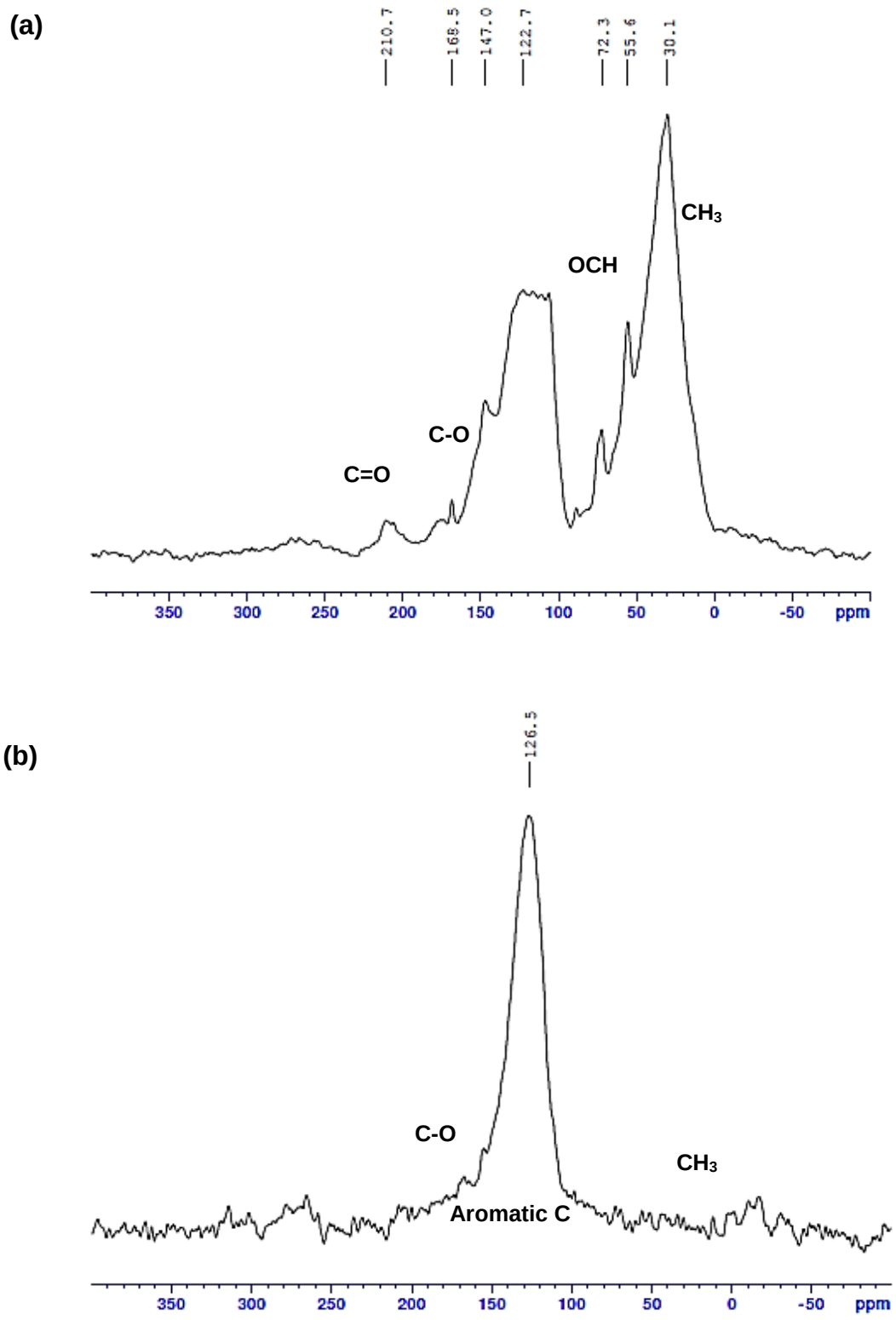

Figure 4.5 NMR spectra of (a) 250°C oak hydrochar and (b) 650°C commercial oak biochar showing differences in surface functionality.

4.3.2 Pyrolysis Gas Chromatography Mass Spectrometry (Py-GC-MS)

Pyrolysis-gas chromatography of the biomass feedstocks and hydrochars was performed at 500°C to evaluate some of the organic compounds present, and their respective pyrograms are presented in **Figures. 4.7** and **4.8**. As biochars possessed fewer functional groups compared to hydrochars, pyrograms of only the latter chars have been presented here. Full details of the biochar pyrograms have however been presented elsewhere (Anyikude 2016, *unpublished*). Furthermore, as only oak, greenhouse waste, and municipal waste samples had complete datasets (i.e., biomass, hydrochar, and humic-like acids extracted from hydrochars), pyrograms for only these three samples are presented subsequently. Py-GC-MS analysis of unprocessed municipal waste and its hydrochar were performed earlier using slightly different analytical conditions and are marked as (*).

As shown in **Figure 4.7**, complex mixtures of oxygenated organic species were present in all the biomass feedstocks, which is understandable as oxygen is the second major constituent of agricultural products, municipal waste and other lignocellulosic biomass (Jenkins et al. 1998; Pérez et al. 2002). Thermal degradation of lignin, cellulose, and hemicellulose yielded various forms and quantities of oxygenated species such as phenols, alcohols, amines and carbonyl groups (ketones, aldehydes, carboxylic acids) depending on the feedstock. For oak, predominant groups were phenols, indicative of lignin degradation, followed by carboxylic acids, alcohols, furans, and amines. Greenhouse waste pyrolysis products were similar to those of oak but there were differences in the forms of heterocyclic nitrogen compounds present; while oak comprised of more basic/Brønsted base nitrogen groups (pyrimidine derivatives), greenhouse waste possessed pyrrole and derivative groups, which are relatively weak bases (Brønsted acids). During high temperature treatment, aldehydes (e.g. furans) are known to react with ammonia at 450–500°C in the presence of certain inorganics (Al, Mo) to form pyrrole (Bishop and Denton 1946; Higasio et al. 2001), or from the dehydrogenation of pyrrolidine (Higaso et al. 2001). The reaction pathway of pyrrole formation from furane might have been more likely for greenhouse waste owing to its higher content of Al and to an extent, Mo (the former higher in greenhouse waste by 67.9 mg kg^{-1}; dataset not included). Alternatively, differences in the native nitrogen forms present in oak and greenhouse waste might have resulted in their distinctive decomposition characteristics. Further analysis of the nitrogen forms present in the feedstocks preferably using less destructive analytical procedures

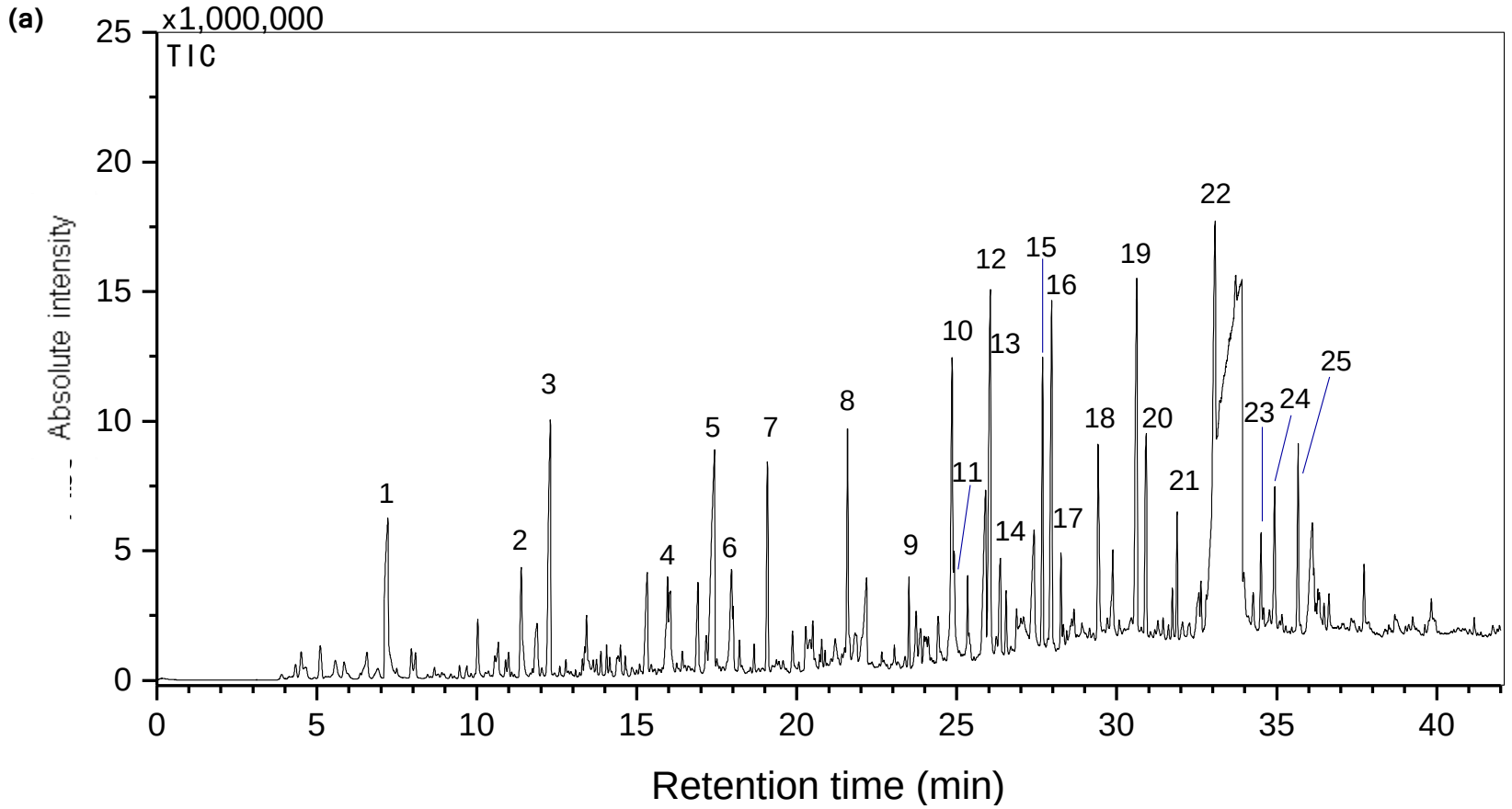

Figure 4.6 (a) Total Ion Chromatogram from Py-GC-MS of Oak biomass.

Peak identification: ***1****: Acetic acid;* ***2****: 2-Pentanone, 5-hydroxy-;* ***3****: Furfural;* ***4****: 2-Propenoic acid, 2-hydroxypropyl ester;* ***5****: 1,4-Butanediamine, 2,3-dimethoxy-N,N,N',N'-tetramethyl-, [S-(R*,R*)]-;* ***6****: 1,3-Cyclohexanedione;* ***7****: Phenol, 2-methoxy-;* ***8:*** *Creosol;* ***9****: Phenol, 4-ethyl-2-methoxy-;* ***10****: 4-Hydroxy-3-methylacetophenone;* ***11****: 1,2-Benzenediol, 3-methoxy-;* ***12****: 5-Hydroxymethylfurfural;* ***13:*** *Phenol, 2,6-dimethoxy-;* ***14****: d-Mannitol, 1,4-anhydro-;* ***15:*** *Phenol, 2-methoxy-4-(1-propenyl)-;* ***16:*** *1,2,4-Trimethoxybenzene;* ***17****: Benzaldehyde, 3-hydroxy-4-methoxy-;* ***18:*** *Benzene, 1,2,3-trimethoxy-5-methyl-;* ***19****: 3',5'-Dimethoxyacetophenone;* ***20****: Phenol, 2,6-dimethoxy-4-(2-propenyl)-;* ***21****: Phenol, 2,6-dimethoxy-4-(2-propenyl)-;* ***22****: Phenol, 2,6-dimethoxy-4-(2-propenyl)-;* ***23:*** *2,4,6(1H,3H,5H)-Pyrimidinetrione, 5-ethyl-5-(2-propenyl)-;* ***24****: Ethanone, 1-(4-hydroxy-3,5-dimethoxyphenyl)-;* ***25****:2,4,6(1H,3H,5H)-Pyrimidinetrione, 5-ethyl-5-(2-propenyl)-*

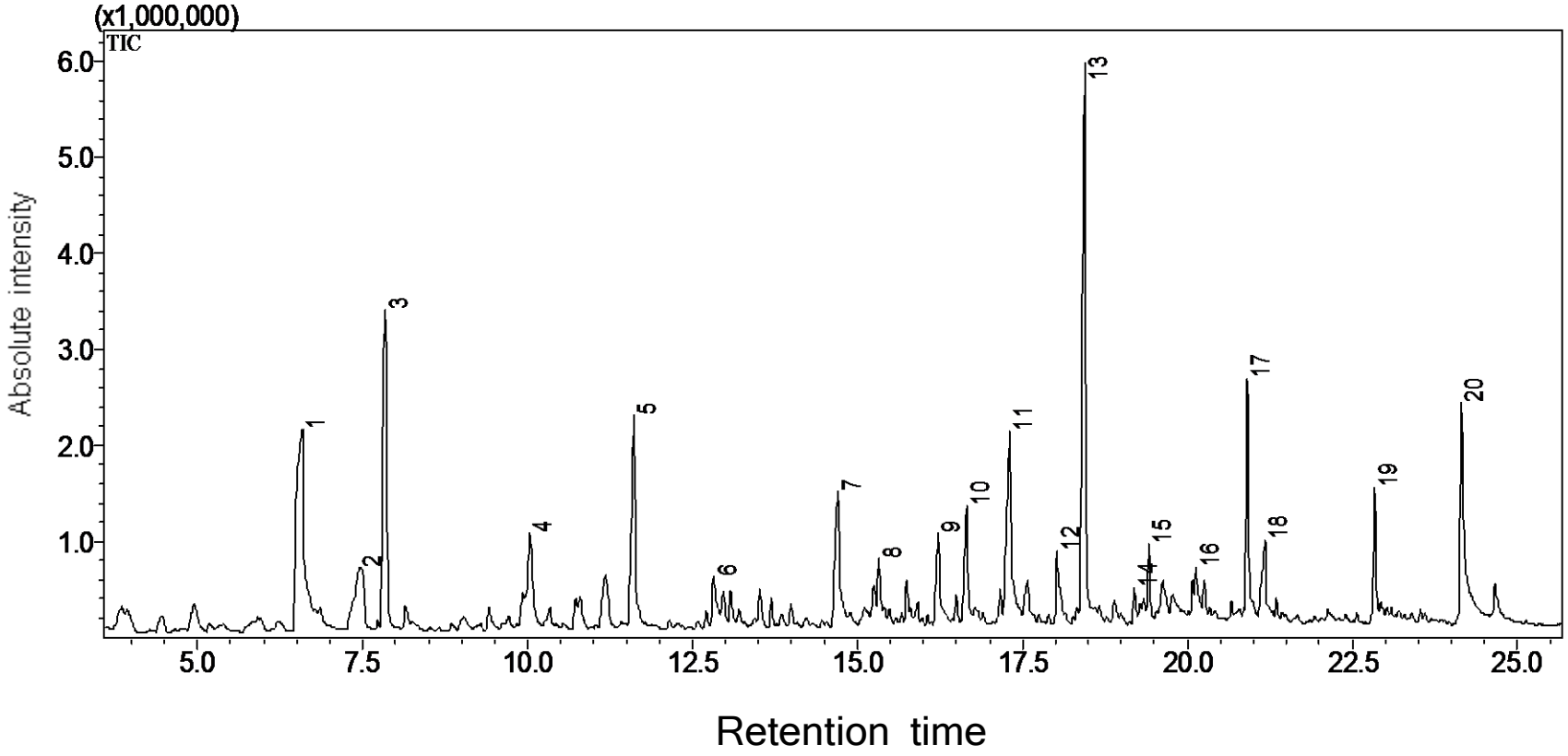

Figure 4.7 (b) Total Ion Chromatogram from Py-GC-MS of Greenhouse waste biomass (*).

*Peak identification: **1**: Acetic acid; **2**: Phenylalanine; **3**: undetermined; **4**: Pyrrole; **5**: Furfural; **6**: 2-Furanmethanol; **7**: 1,2-Cyclopentanedione; **8**: 2-Furancarboxaldehyde, 5-methyl-; **9**: undetermined; **10**: Oxazolidine, 2,2-diethyl-3-methyl-; **11**: 1,2-Cyclopentanedione, 3-methyl-; **12**: Phenol; **13**: Phenol, 2-methoxy-; **14**: Phenol, 2-methyl-; **15**: 2-Cyclopenten-1-one, 3-ethyl-2-hydroxy-; **16**: Phenol, 2-methoxy-3-methyl-; **17**: Phenol, 2-methoxy-4-methyl-; **18**: Disulfide, (1,1-dimethylethyl)(1-methylpropyl); **19**: Phenol, 4-ethyl-2-methoxy-; **20**: 4-Hydroxy-2-methylacetophenone*

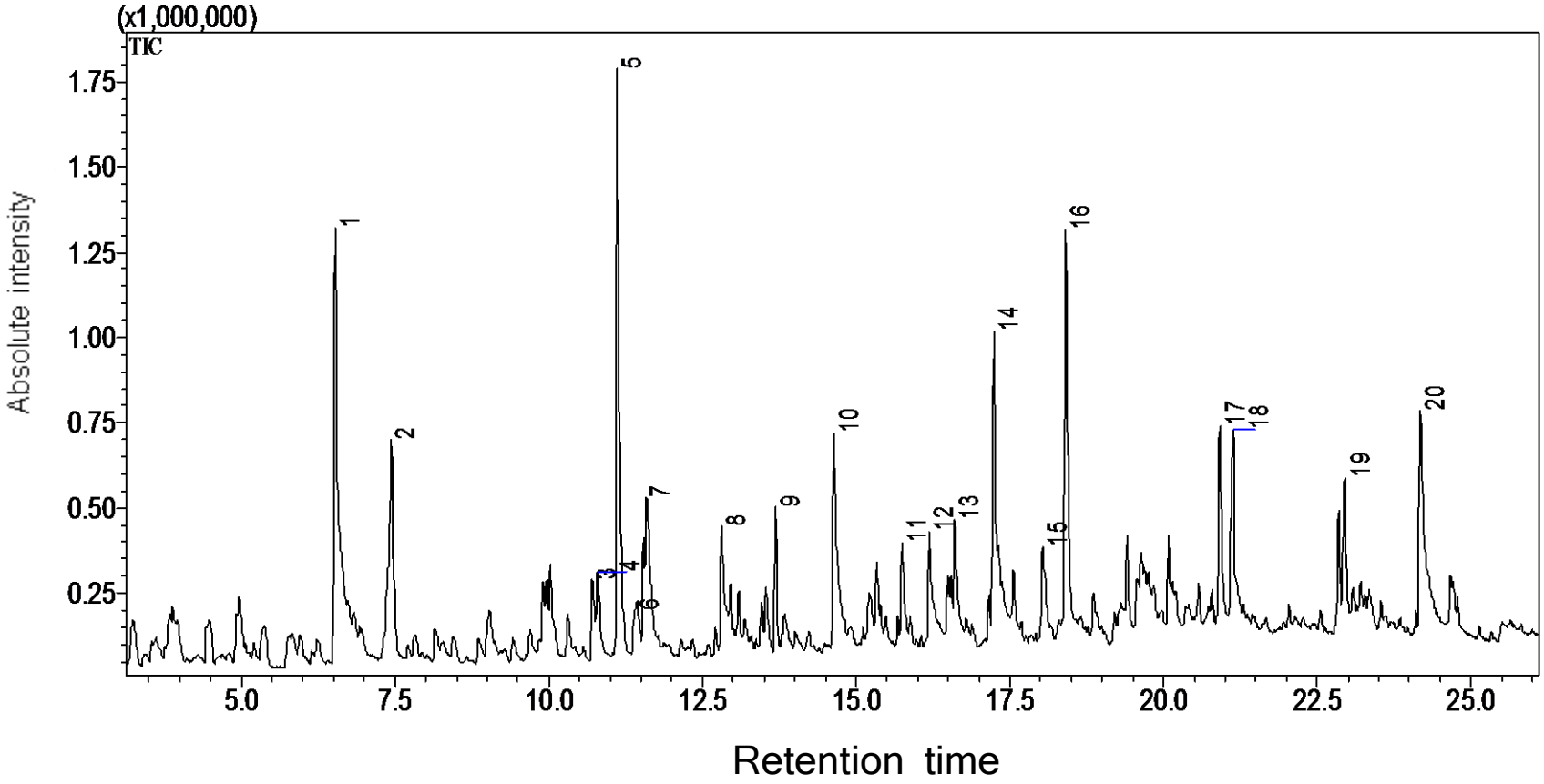

Figure 4.7 (c) Total Ion Chromatogram from Py-GC-MS of Municipal waste biomass (*)

*Peak identification: **1**: Acetic acid; **2**: Benzenepropanoic acid, .alpha.,.beta.-dimethyl-; **3**: 2-Methyl[1,3,4]oxadiazole; **4**: 3-Furaldehyde; **5**: Styrene; **6**: Butanoic acid; **7**: Furfural; **8**: 2-Furanmethanol; **9**: D-Limonene; **10**: 1,2-Cyclopentanedione; **11**: 1-Octyn-3-ol, 4-ethyl-; **12**: undetermined; **13**: Oxazolidine, 2,2-diethyl-3-methyl-; **14**: 1,2-Cyclopentanedione, 3-methyl-; **15**: Phosphonic acid, (p-hydroxyphenyl)-; **16**: Phenol, 2-methoxy-; **17**: Phenol, 2-methoxy-4-methyl-; **18**: Diazene, bis(1,1-dimethylethyl)-; **19**: (2,2-Dimethylcyclobutyl)methylamine; **20**: 2-Methoxy-4-vinylphenol*

may provide more information on native nitrogen forms. Greenhouse waste also appeared to possess fewer carboxylic acid groups than oak. Generally however, functional groups detected in both samples were similar to those observed via XPS in the literature (Amonette and Joseph 2009). In municipal waste, D-Limonene and styrene were among the main organic species present and were not observed in the former two feedstocks. D-Limonene is a cyclic terpene present in biomass extractives, and while some types of biomass have small amounts of styrene (ATSDR 2012), its high concentration in this feedstock was more suggestive of the degradation of polystyrene (plastic).

In the hydrochars, a reduction in number and intensity of peaks was observed suggesting decomposition of some organic species following HTC. Baseline drift was observed for some of the greenhouse waste samples. Peaks present in municipal and greenhouse waste feedstocks were absent in their respective chars, notably acetic acid, which is expected since it is one of the main organics found in the HTC aqueous phase (Reza et al. 2013). In place of pyrrolidine, the lower basicity thymidine was present in the oak hydrochar. Pyrograms for all three hydrochars revealed an increase in peak intensities for phenol compounds however, suggesting a relative increase in their concentration (**Figure 4.8**). This is in agreement with the literature as phenol compounds are derivatives of lignin which are more resistant to thermal degradation than hemicellulose and cellulose. n-hexadecanoic (palmitic) acid is one of many long-chained groups that are present in woody feedstocks as an extractive (Salehi 2012). For the municipal waste hydrochar, in addition to a relative increase in phenol group intensity, peak areas of styrene and D-Limonene groups relative to the unprocessed feedstock as expected.

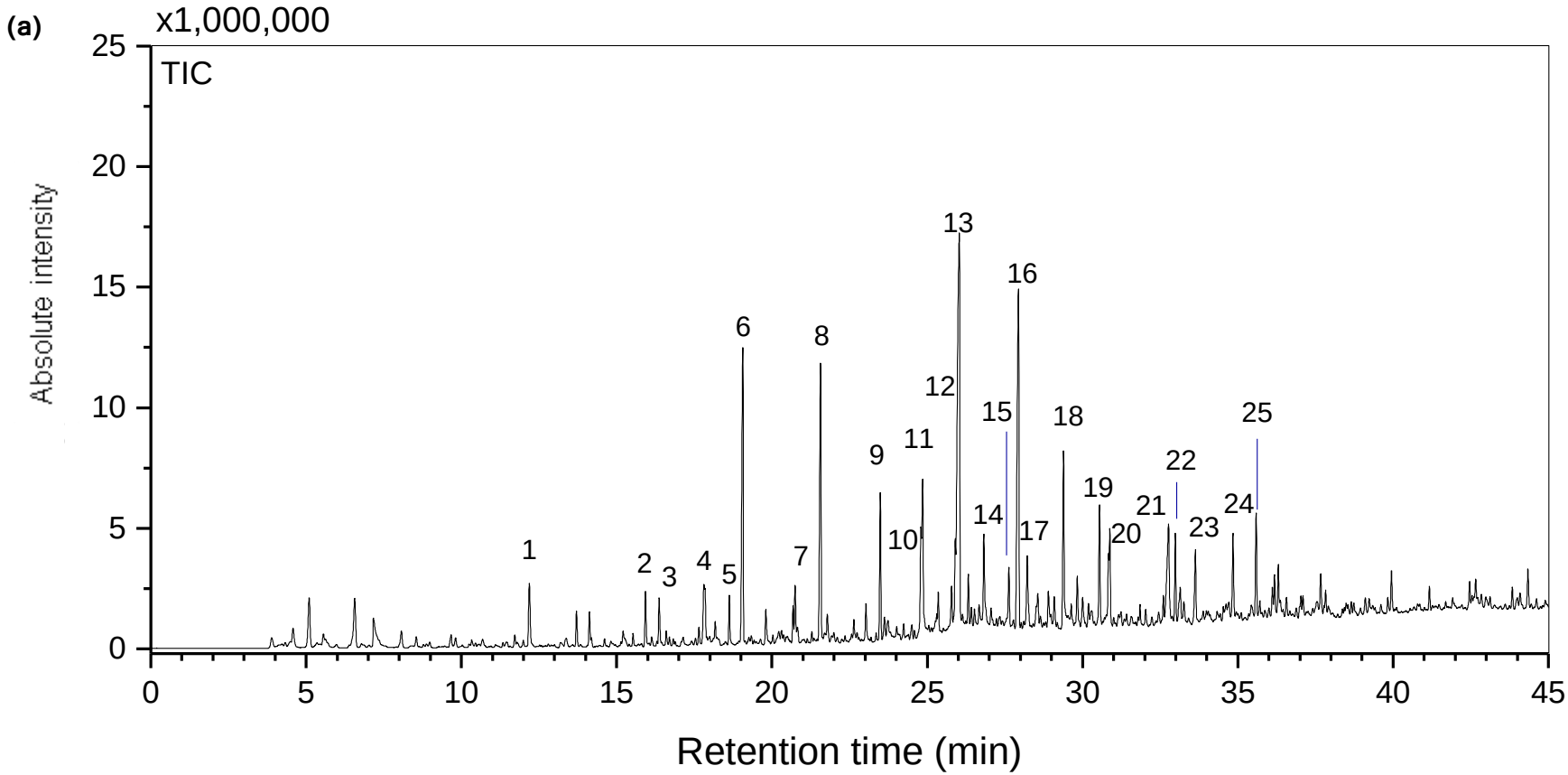

Figure 4.7 (a) Total Ion Chromatogram from Py-GC-MS of Oak 250°C hydrochar.
*Peak identification: **1**: 3,5-Dimethylpyrazole-1-methanol; **2**: 2-Furancarboxaldehyde, 5-methyl-; **3**: 2-Cyclopenten-1-one, 3-methyl-; **4**: 2-Cyclopenten-1-one, 2,3-dimethyl-; **5**: Phenol; **6**: Phenol, 2-methoxy-; **7**: Creosol; **8**: Creosol; **9**: Phenol, 4-ethyl-2-methoxy-; **10**: Ethanone, 1-(2-hydroxy-5-methylphenyl)-; **11**: 1,2-Benzenediol, 3-methoxy-; **12**: Catechol; **13**: Phenol, 2,6-dimethoxy-; **14**: Phenol, 3,4-dimethoxy; **15**: Eugenol; **16**: 1,2,4-Trimethoxybenzene; **17**: Benzaldehyde, 3-hydroxy-4-methoxy-; **18**: Benzene, 1,2,3-trimethoxy-5-methyl-; **19**: 3',5'-Dimethoxyacetophenone; **20**: Ethyl homovanillate; **21**: Phenol, 2,6-dimethoxy-4-(2-propenyl)-; **22**: Phenol, 2,6-dimethoxy-4-(2-propenyl)-; **23**: Benzaldehyde, 4-hydroxy-3,5-dimethoxy-; **24**: Ethanone, 1-(4-hydroxy-3,5-dimethoxyphenyl)-; **25**: 2,4,6(1H,3H,5H)-Pyrimidinetrione,5-ethyl-5-(2-propenyl)-*

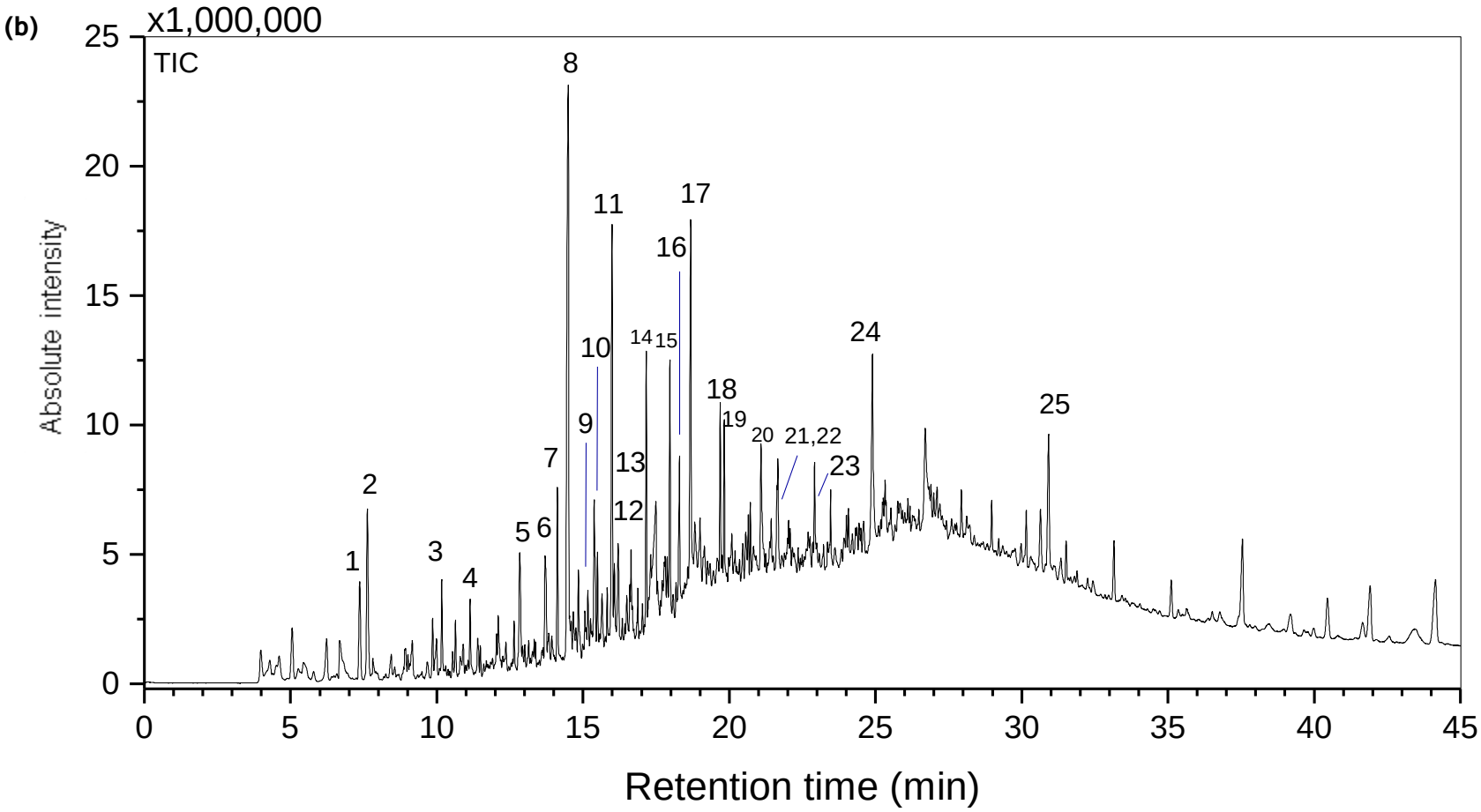

Figure 4.8 (b) Total Ion Chromatogram from Py-GC-MS of Greenhouse waste 250°C hydrochar.
*Peak identification: **1**: Toluene; **2**: 1H-Pyrrole, 1-methyl-; **3**: 2-Cyclopenten-1-one; **4**: 2-Cyclopenten-1-one, 2-methyl-; **5**: 2-Cyclopenten-1-one, 3-methyl-; **6**: 2-Cyclopenten-1-one, 2,3-dimethyl-; **7**: Phenol; **8**: Phenol, 2-methoxy-; **9**: p-Cresol; **10**: 2-Methoxy-5-methylphenol; **11**: Creosol; **12**: Phenol, 3,5-dimethyl-; **13**: Propane, 1-bromo-2,2-dimethyl-; **14**: Phenol, 4-ethyl-2-methoxy-; **15**: 4-Hydroxy-3-methylacetophenone; **16**: Phenol, 2-methoxy-4-propyl-; **17**: Phenol, 2,6-dimethoxy-; **18**: trans-Isoeugenol; **19**: 1,2,4-Trimethoxybenzene; **20**: Apocynin; **21**: Benzene, 1,1'-propylidenebis-; **22**: 2-Propanone, 1-(4-hydroxy-3-methoxyphenyl)-; **23**: Phenol, 2,6-dimethoxy-4-(2-propenyl)-; **24**: n-Hexadecanoic acid; **25**: Ethyl homovanillate*

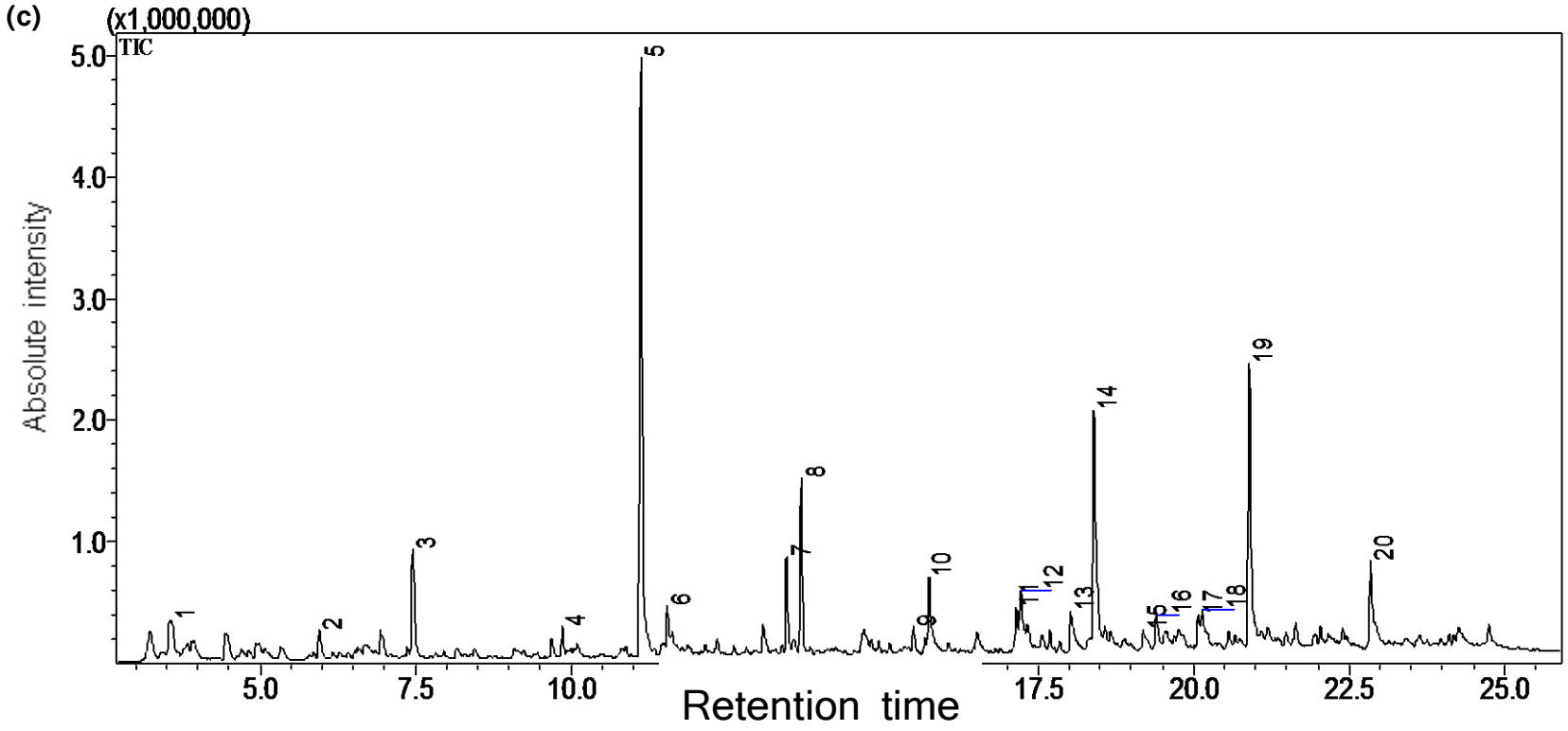

Figure 4.8 (c) Total Ion Chromatogram from Py-GC-MS of Municipal waste 250°C hydrochar (*)

*Peak identification: **1**: 1,3-Pentadiene, (Z)-; **2**: Furan, 2,5-dimethyl-; **3**: Toluene; **4**: 1-O-p-Nitrobenzoyl-2,3,4,6-tetra-O-benzyl-.beta.-d-galactose; **5**: Styrene; **6**: undetermined; **7**: .alpha.-Methylstyrene; **8**: D-Limonene; **9**: 2-Cyclopenten-1-one, 2,3-dimethyl-; **10**: 1,2-Cyclopentanediol, 3-methyl-; **11**: 2-Cyclopenten-1-one, 2,3-dimethyl-; **12**: 1,2-Cyclopentanedione, 3-methyl-; **13**: Phenol; **14**: Phenol, 2-methoxy-; **15**: Phenol, 2-methyl-; **16**: 2-Cyclopenten-1-one, 3-ethyl-2-hydroxy-; **17**: Phenol, 4-methyl-; **18**: Phenol, 2-methoxy-3-methyl-; **19**: Phenol, 2-methoxy-4-methyl-; **20**: Phenol, 4-ethyl-2-methoxy-*

4.3.3 Hydrochar fulvic and humic-like substances

Humification is the process by which low and high molecular weight organic matter from plant, animal and microbial cellular matter is decomposed in aerobic conditions (Epstein 1997). The resulting high molecular weight humic substances are comprised of 80% of humus and are categorised based on their solubilities in dilute alkali or acids into humic acid, fulvic acid and humin (Epstein 1997). That is, while humic acids are soluble in dilute alkali but not in dilute acids, the opposite is observed for humin, while fulvic acids are soluble in both dilute alkali and acid (Epstein 1997). Humic acids are defined by colour (dark brown), their insolubility in acidic conditions (pH < 1), and are comprised of aliphatic and partially methylated carboxylic acids, aliphatic acids (such as carbonyl and quinone groups), aromatic acid (phenolic acid) (Ishiwatari 1969; Sánchez-Monedero et al. 2002).

In hydrochars, humic-like substances may result from the condensation of polymeric sugars and amino acids, since sugars are formed during hydrothermal carbonization (Hoekman et al. 2011). Preliminary tests on oak 650°C revealed that humic-like substances were absent, so analysis of humic-like acids and fulvic acids was reserved for the hydrochars. As there was insufficient presscake biomass to generate more hydrochar for this analysis, only oak, greenhouse waste, municipal waste and greenwaste hydrochars were evaluated. However, given some similarities in organic functional groups between presscake and municipal waste hydrochar characteristics (**Figure 4.5 (c**,**d)**), it is speculated that presscake hydrochar might possess comparable quantities of humic-like substances and fulvic acids. Quantities of humic-like acids extracted from the hydrochars were generally low. Total carbon contents of the humic-like substances extracted from oak, greenhouse waste and municipal waste hydrochars presented in **Table 4.8** showed that the three samples were comparable although total carbon content was highest in the humic-like acid precipitated from oak, while greenhouse waste possessed the highest nitrogen content due to its inherently high nitrogen content. Due to the acid used for the precipitation of humic-like acid (0.1 M H_2SO_4), sulphur contents increased.

Table 4.8 Elemental contents of hydrochar humic-like acids and residual chars

Sample	HA Yield (%)	C (%)	H (%)	N (%)	S (%)	[a]O (%)
OAK 250-HA	13.6	59.3	4.9	0.2	1.7	34.0
GH 250-HA	3.7	56.4	5.6	2.5	2.5	33.0
[b]MW 250-HA	7.1	56.4	6.5	1.6	4.6	30.8
[c]OAK 250 residue	n/a	67.2	3.3	0.8	0.0	28.8
[c]GH 250 residue	n/a	58.7	3.7	1.6	0.0	36.1

- Elemental contents expressed as dry basis; [a]determined by difference; [b]single analysis performed; [c]OAK 250 and GH 250 residue refer to oven-dried (60°C) oak and greenhouse waste hydrochars after extraction of humic-like acid (HA), fulvic and non-humic like substances using NaOH; n/a: not applicable.
- While up to 4.5% humic-like acid was extracted from greenwaste hydrochar, elemental analysis of this extract could not be performed due to low sample quantity.

The total extractable carbon (EXC) determined from the supernatants obtained following NaOH extraction of the hydrochars are presented in **Table 4.9**, and showed that both EXC and humic acid-like Carbon (HAC) (the latter determined the difference between EXC, fulvic acid carbon and non-humic substance carbon) were positively related to their total carbon contents, the latter earlier presented in **Table 4.2**. Expressed relative to EXC, **Figure 4.8(a)** showed that humic-like substances accounted for a large proportion of this carbon for oak, greenhouse waste and municipal waste, while greenwaste was predominantly non-humic. In the case of nitrogen, no clear trend was observed between the hydrochars' fulvic, humic-like and non-humic components (**Figure 4.8(b)**) or to their total nitrogen contents. **Table 4.9** also included other humification indices for providing meaningful data interpretation, as recommended by Sánchez-Monedero et al. (1999): the degree of polymerization (HAC/FAC) is considered to be a good indicator of the humification process, and was highest in oak hydrochar. Furthermore, the higher humification ratio and humification index of the oak hydrochar, determined as a ratio of EXC and HAC to hydrochar TOC, respectively, suggested that the HTC process had a more pronounced effect on oak in terms of humification, followed by greenhouse waste. This was presumably due to their higher carbon contents, and further analysis is required to confirm whether lignin content was a contributory factor. For instance, previous studies exploring the origins of humic acids in terrestrial and aquatic

locations have suggested that lignin and to an extent hemicellulose degradation is partly responsible for humic acid formation (Wilson et al. 1983).

Table 4.9 Distribution of carbon and nitrogen in hydrochar extracts

	mg g^{-1} char				[a]DP	[b]HR (%)	[c]HI (%)
	EX Carbon	HA Carbon	FA Carbon	NHS Carbon			
OAK 250	157.3±2.5	127.7	14.7±0.4	14.9±0.7	8.7	41.6	33.7
GH 250	116.1±3.5	59.4	16.5±0.1	40.2±0.6	3.6	25.6	13.1
MW 250	42.6±24.9	21.9	9.6±2.4	11.1±1.3	2.3	13.0	6.7
GW 250	25.6±0.8	2.3	9.6±0.7	13.7±1.1	0.2	n.a	n.a

	mg g^{-1} char			
	EX Nitrogen	HA Nitrogen	FA Nitrogen	NHS Nitrogen
OAK 250	0.6±0.1	0.1	0.2±0.0	0.3±0.0
GH 250	8.1±0.2	2.9	0.6±0.0	4.6±0.0
MW 250	2.1±1.4	1.2	0.3±0.1	0.6±0.4
GW 250	0.9±0.0	0.5	0.3±0.0	0.2±0.0

- [a]Degree of Polymerization (DP) is the ratio of HAC to FAC; [b]Humification Ratio (HR) is the ratio of EXC/TOC x 100; [c]Humification Index (HI) is the ratio of HAC/TOC x 100
- EX, HA, FA and NHS refer to total extractable, humic acid-like, fulvic acid and non-humic substances respectively; n.a: unavailable data.
- GH: Greenhouse waste; MW: Municipal waste; GW: Greenwaste; n.a: unavailable data.
- TOC (mg g^{-1}) Oak 250 °C, GH 250 °C and MW 250 °C = 378.5, 453.0, and 328.0 respectively, determined by a Fertiplus research partner).
- Results reported as average of duplicates ± standard deviation.
- With the exception of (heterogeneous) municipal waste, coefficients of variation (%RSD) ranged from 0.9–17.1% and averaged 3.7% and 8.3% for carbon and nitrogen, respectively.

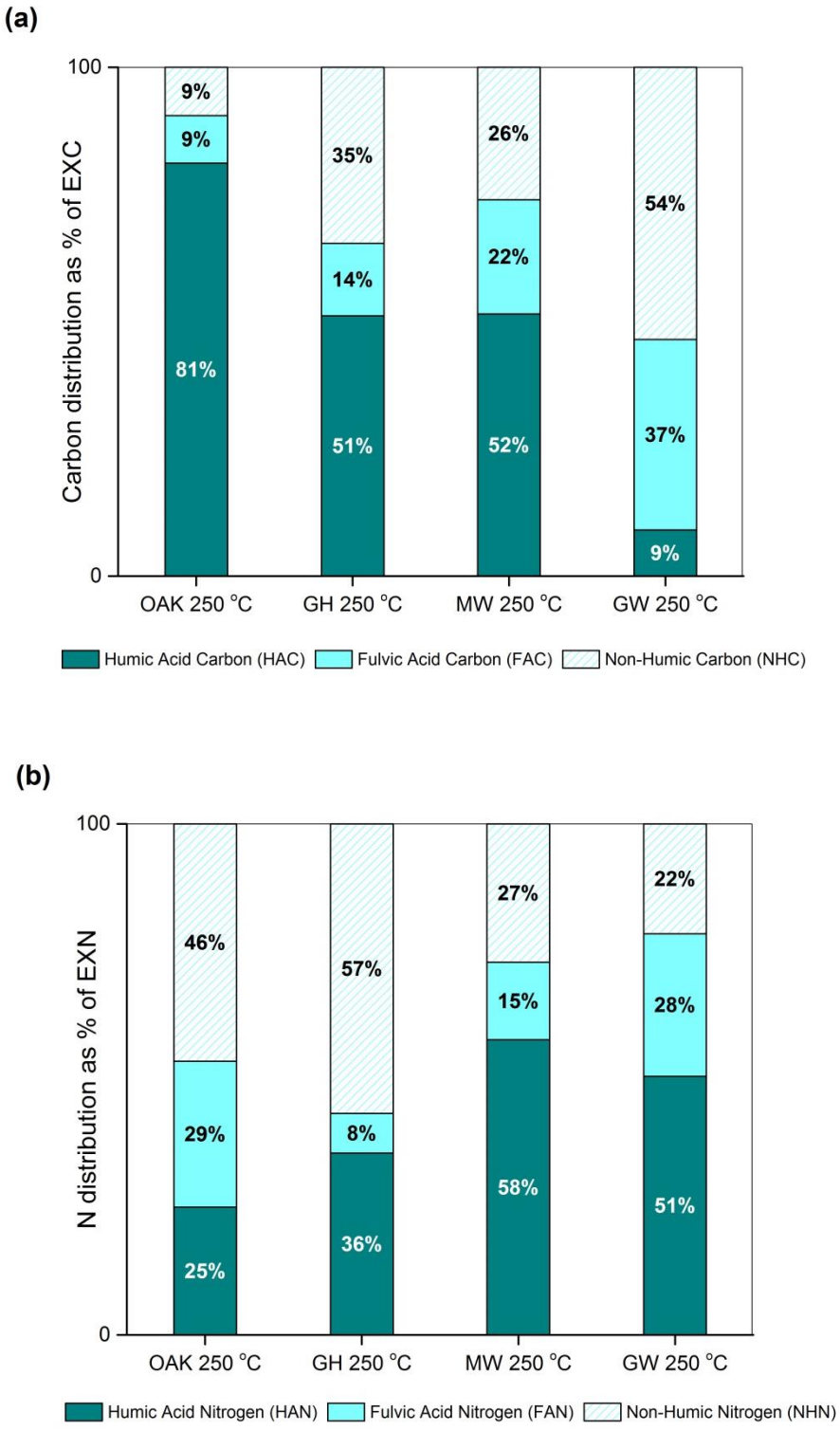

Figure 4.8 Distribution of a) carbon, and b) nitrogen in hydrochar humic-like acids, fulvic acids, and non-humic substances expressed as percentages of total extractable carbon and nitrogen contents, respectively.

FTIR spectra of the humic-like acids obtained from oak and greenhouse waste hydrochars were generally similar, and absorption bands were somewhat identical to various humic acid infrared spectra presented in Tan (2014). Tan (2014) further noted that bands at 1000 cm^{-1} in humic acids are often indicative of the presence of chelated SiO_2 impurities which could have otherwise been removed by washing with HCl-HF. In this study, strong bands were evident at around 1100 cm^{-1} however, possibly attributable to aldehyde, ketone or sulphate groups although the presence of some SiO_2 could not be ruled out as the humic-like acids were rinsed once with 0.1 M H_2SO_4 followed by distilled water rather than HCl-HF and distilled water. The spectra for oak hydrochar extracts and residue presented in **Figure 4.9(a)** revealed similarities in band characteristics but a relative increase in the band intensity was evident at around 1100 cm^{-1}. For greenhouse waste, a similar relative increase in band intensity also around 1114 cm^{-1}, in addition to a peak attributed to carbonyl groups (1700 cm^{-1}) which was absent in the post-alkali extracted hydrochar residue suggesting its removal from the hydrochar. The latter peak was much greater in intensity than in the un-extracted hydrochar however, suggesting that oxidation reactions occurred during extractions.

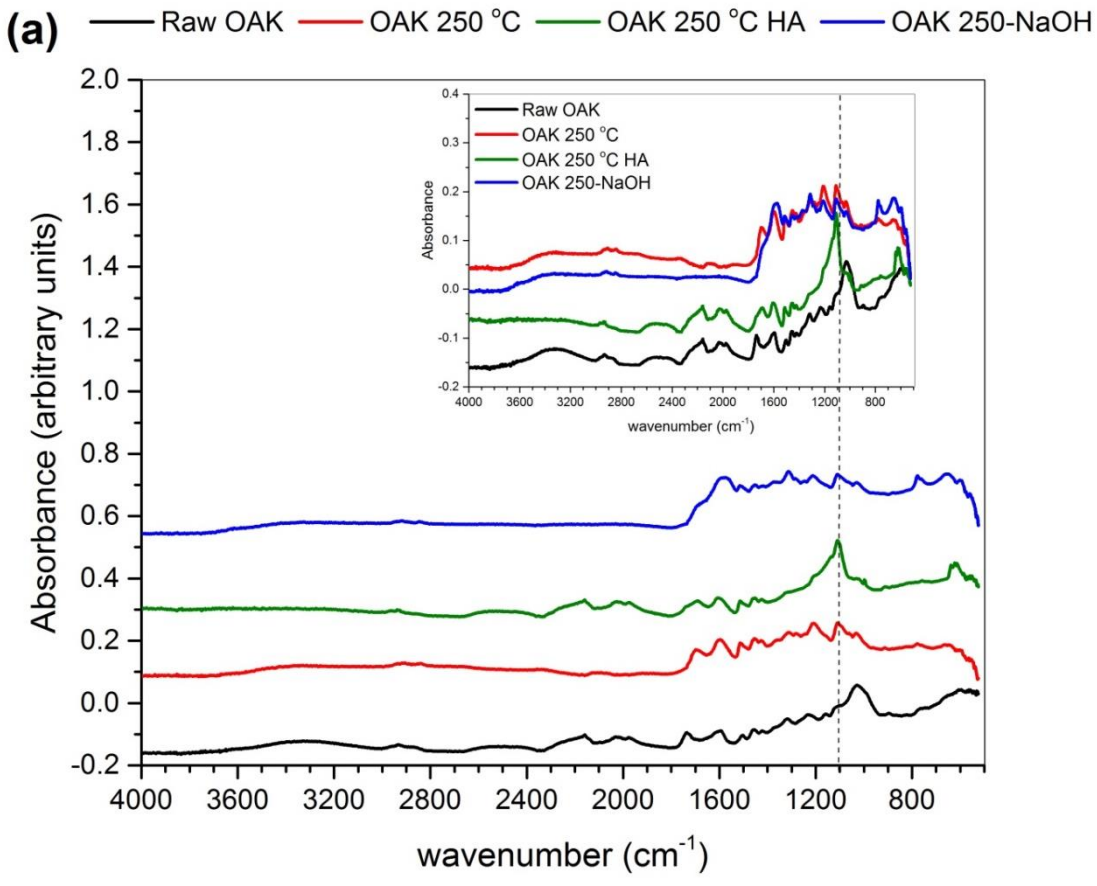

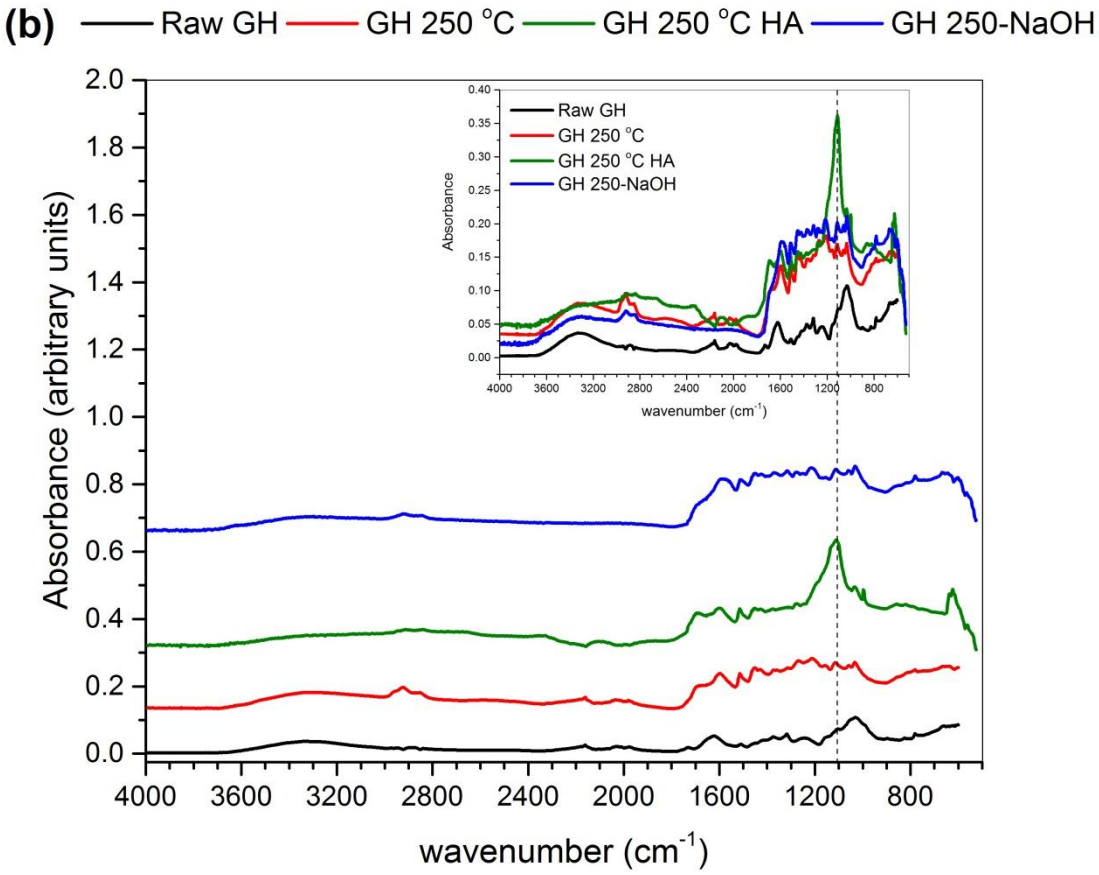

Figure 4.9 ATR-FTIR spectra comparing changes in band intensities between alkali-extracted and un-extracted a) Oak 250°C, and b) Greenhouse waste (GH 250°C) hydrochars. Suffixes 'HA' and 'NaOH' are used to specify the hydrochar humic-like acid extract and hydrochar residues obtained after alkali extraction respectively. Inset images of band intensities at original absorbance values.

To confirm the findings obtained from ATR-FTIR, Py-GC-MS analysis of the humic-like acid extracted from oak is presented in **Figure 4.10** for comparison with the pre- and post-alkali extracted hydrochar. As expected, the extracted hydrochar possessed fewer organic species compared to un-extracted hydrochar while humic-like substances comprised mainly of phenol, aldehyde and ketone compounds. In municipal waste humic-like acids, mostly saturated fatty acids and long chain aliphatics were detected. Peak areas peaks generally decreased in humic-like acids relative to their hydrochars. For example, the prominent peak attributed to 2,6-dimethoxy phenol was 6.58× greater in the oak hydrochar compared to its humic-like acid.

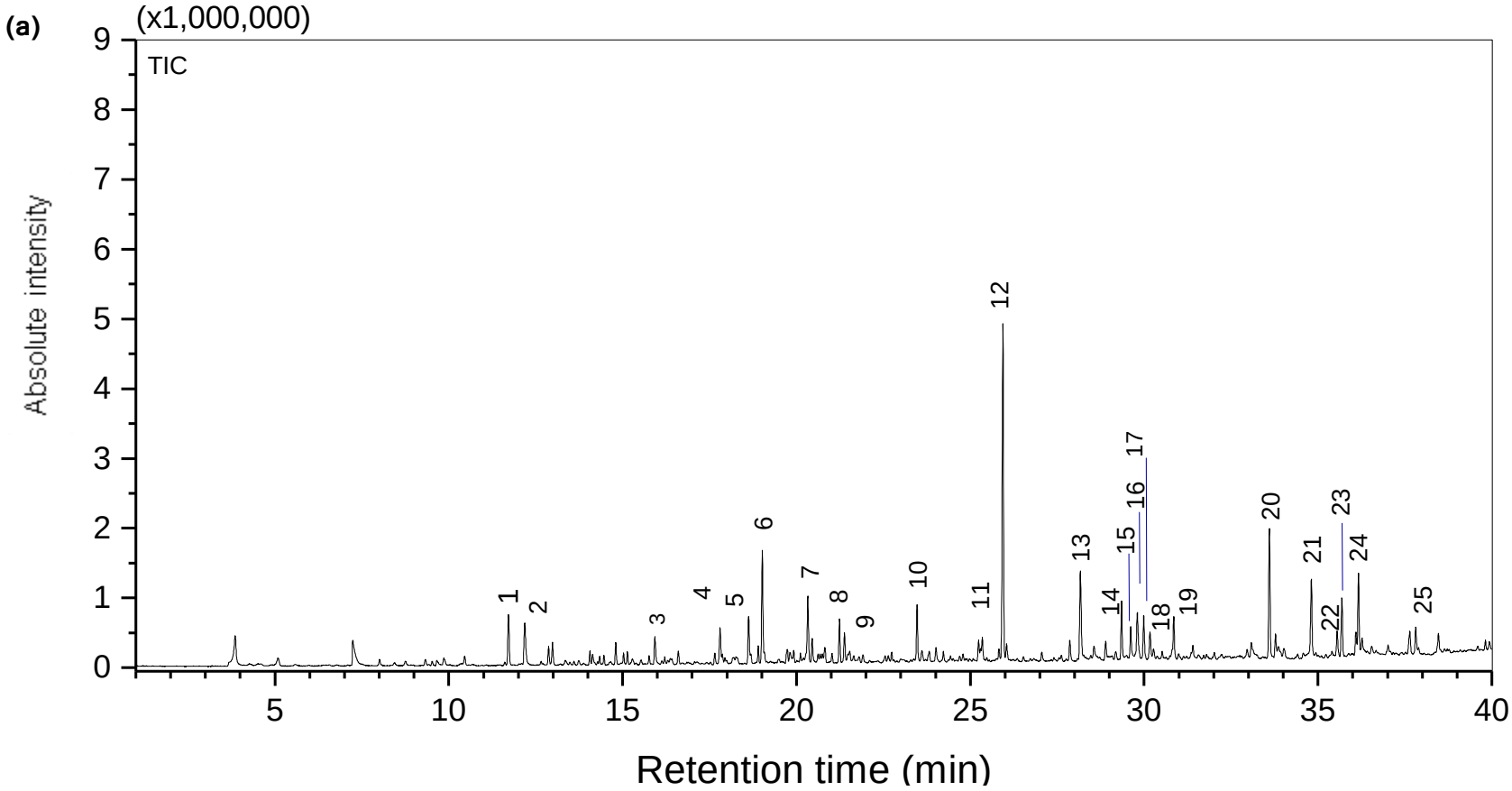

Figure 4.10(a) Total Ion Chromatogram from Py-GC-MS of Oak 250°C humic-like acid extract.

*Peak identification: **1**: Bicyclo[4.2.0]octa-1,3,5-triene; **2**: Cyclotetrasiloxane, octamethyl-; **3**: 2-Furancarboxaldehyde, 5-methyl-; **4**: 2-Cyclopenten-1-one, 2-hydroxy-3-methyl- one; **5**:Phthalan; **6**: Phenol, 2-methoxy-; **7**: Benzene, 1,3-bis(1,1-dimethylethyl)-; **8**: Bicyclo[3.2.1]oct-2-ene, 3-chloro-; **9**: 1-Propene, 3-chloro-2-(chloromethyl)-; **10**: Phenol, 4-ethyl-2-methoxy-; **11**: Homovanillyl alcohol; **12**: Phenol, 2,6-dimethoxy-; **13**: Vanillin; **14**: Benzene, 1,2,3-trimethoxy-5-methyl-;**15**: Dodecanoic acid; **16**: Apocynin; **17**: 1H-Inden-1-one, 2,3-dihydro-5-methoxy-; **18**: Ethanone, 1-(3-hydroxyphenyl)-;**19**: Benzene, 1,1'-propylidenebis-; **20**: Benzaldehyde, 4-hydroxy-3,5-dimethoxy- ; **21**: Ethanone, 1-(4-hydroxy-3,5-dimethoxyphenyl)-; **22**: 2,4,6(1H,3H,5H)-Pyrimidinetrione, 5-ethyl-5-(2-propenyl)-; **23**: 1H-Purine-2,6-dione, 3,7-dihydro-1,3,7-trimethyl-; **24**: Ethanone, 1,1',1''-(1,3,5-benzenetriyl)tris-; **25**: Pyrrolo[2,3-b]indole, 1,2,3,3a,8,8a-hexahydro-5-methoxy-3a,8-dimethyl-*

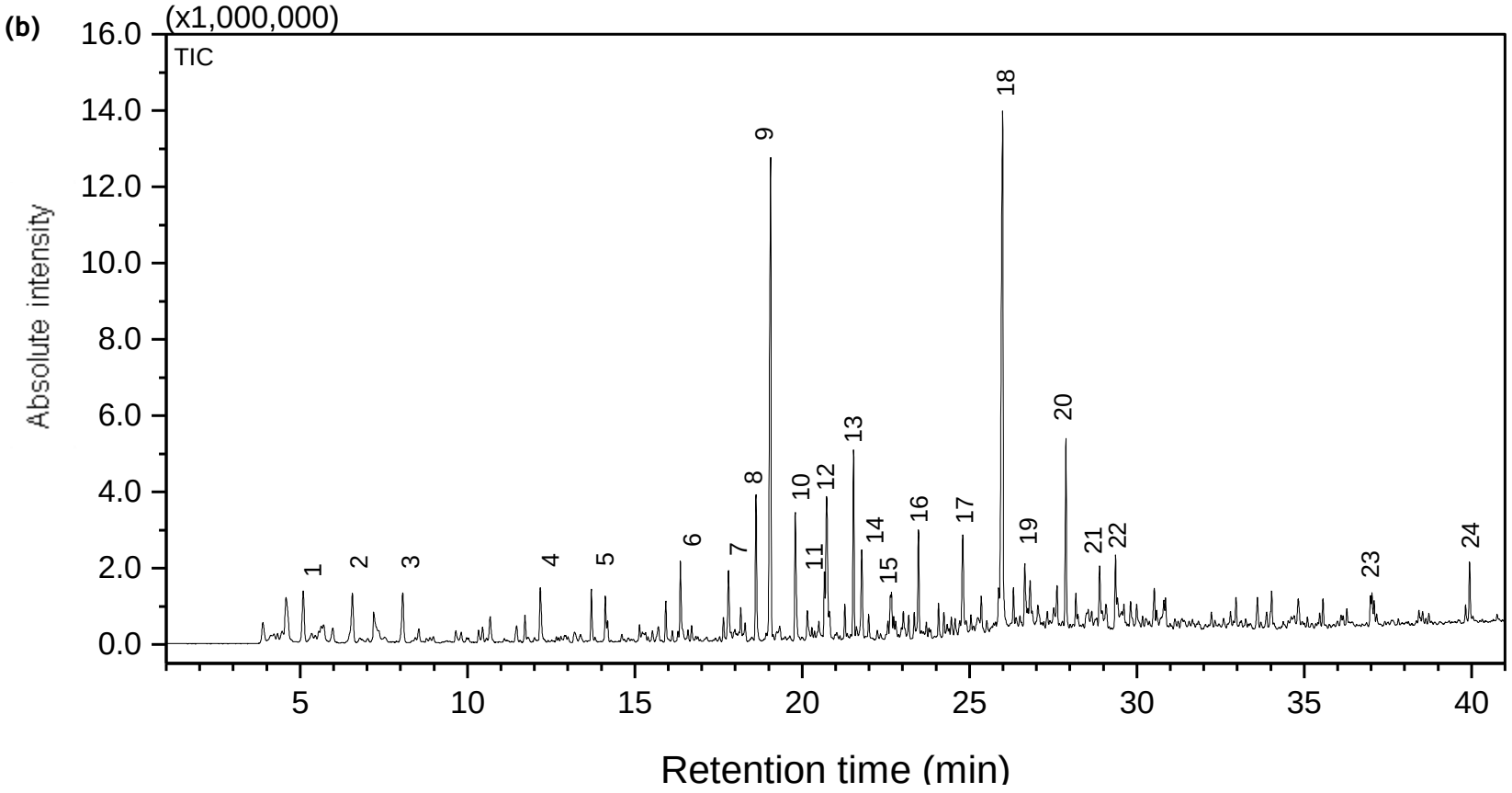

Figure 4.11 (b) Total Ion Chromatogram from Py-GC-MS of Oak 250°C residue following NaOH extraction.
*Peak identification: **1**: Furan, 2-methyl-; **2**: Furan, 2,5-dimethyl-; **3**: Toluene; **4**: 2-Cyclopenten-1-one; **5**: 2-Cyclopenten-1-one, 2-methyl-; **6**: 2-Cyclopenten-1-one, 3-methyl-; **7**: 2-Cyclopenten-1-one, 2,3-dimethyl-; **8**: Phenol; **9**: Phenol, 2-methoxy-; **10**: Phenol, 2-methyl-; **11**: p-Cresol; **12**: Benzeneethanol, 3-hydroxy-; **13**: Creosol; **14**: Phenol, 3,5-dimethyl-; **15**: Phenol, 3,5-dimethyl-; **16**: Phenol, 4-ethyl-2-methoxy-; **17**: 1,2-Benzenediol, 3-methoxy- ; **18**: Phenol, 2,6-dimethoxy-; **19**: 1,2-Benzenediol, 3-methyl-; **20**: 1,2,3-Trimethoxybenzene; **21**: Naphthalene, 2,3,6-trimethyl-; **22**: Benzene, 1,2,3-trimethoxy-5-methyl-; **23**: 1-Octadecanol; **24**: Behenic alcohol*

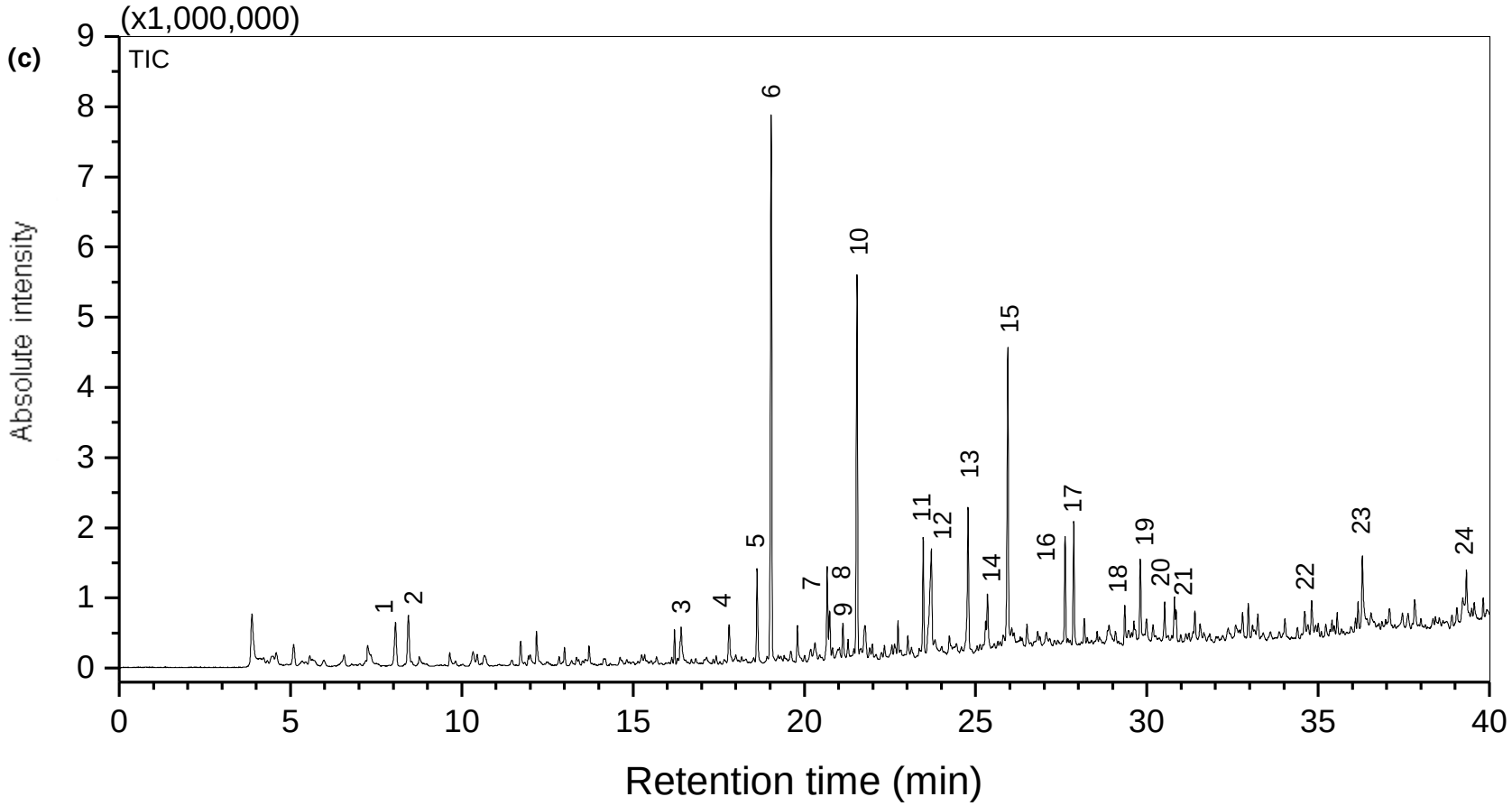

Figure 4.11 (c) Total Ion Chromatogram from Py-GC-MS of Greenhouse waste 250°C humic-like acid extract. *Peak identification: **1**: Toluene; **2**: 1H-Pyrrole, 1-methyl-; **3**: Ethanone, 1-(1H-pyrrol-2-yl)-; **4**: 2-Cyclopenten-1-one, 2,3-dimethyl-; **5**: Phenol; **6**: Phenol, 2-methoxy-; **7**: p-Cresol; **8**: Creosol; **9**: Phosphonic acid, methyl-, bis(trimethylsilyl) ester; **10**: Creosol; **11**: Phenol, 4-ethyl-2-methoxy-; **12**: 3-Pyridinol; **13**: 4-Hydroxy-3-methylacetophenone; **14**: Homovanillyl alcohol; **15**: Phenol, 2,6-dimethoxy-; **16**: Eugenol; **17**: 1,2,4-Trimethoxybenzene; **18**: Benzene, 1,2,3-trimethoxy-5-methyl-; **19**: Apocynin; **20**: 3',5'-Dimethoxyacetophenone; **21**: 2-Propanone, 1-(4-hydroxy-3-methoxyphenyl)-; **22**: Ethanone, 1-(4-hydroxy-3,5-dimethoxyphenyl)-; **23**: n-Hexadecanoic acid; **24**: Nalbuphine*

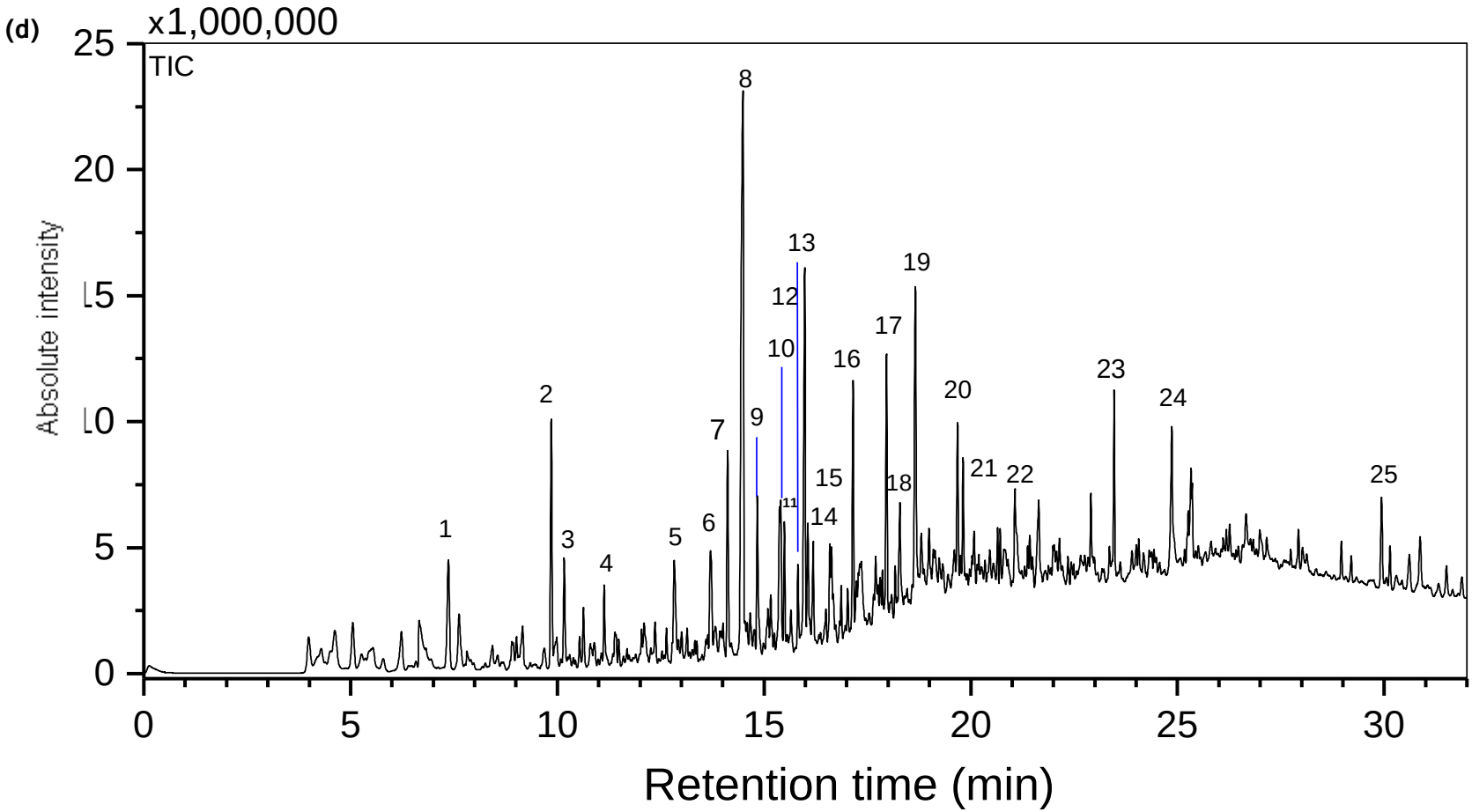

Figure 4.11 (d) Total Ion Chromatogram from Py-GC-MS of Greenhouse waste 250°C residue following NaOH extraction. *Peak identification: **1**: 8-Oxabicyclo[5.1.0]octane; **2**: 8-Oxabicyclo[5.1.0]octane; **3**: Toluene; **4**: Bicyclo[4.2.0]octa-1,3,5-triene; **5**: 2-Cyclopenten-1-one; **6**: 2-Cyclopenten-1-one, 2-methyl-; **7**: 2-Cyclopenten-1-one, 3-methyl-; **8**: 2-Cyclopenten-1-one, 2,3-dimethyl-; **9**: Phenol; **10**: Phenol, 2-methoxy-; **11**: Phenol, 2-methyl-; **12**: p-Cresol; **13**: 2-Methoxy-5-methylphenol; **14**: 2-Methoxy-5-methylphenol; **15**: Creosol; **16**: Phenol, 3,5-dimethyl-; **17**: 2,3-Dimethoxytoluene; **18**: Phenol, 4-ethyl-2-methoxy-; **19**: 4-Hydroxy-3-methylacetophenone; **20**: Phenol, 2-methoxy-4-propyl-; **21**: Phenol, 2,6-dimethoxy-; **22**: trans-Isoeugenol; **23**: 1,2,4-Trimethoxybenzene; **24**: Apocynin; **25**: Hexadecanoic acid, methyl ester*

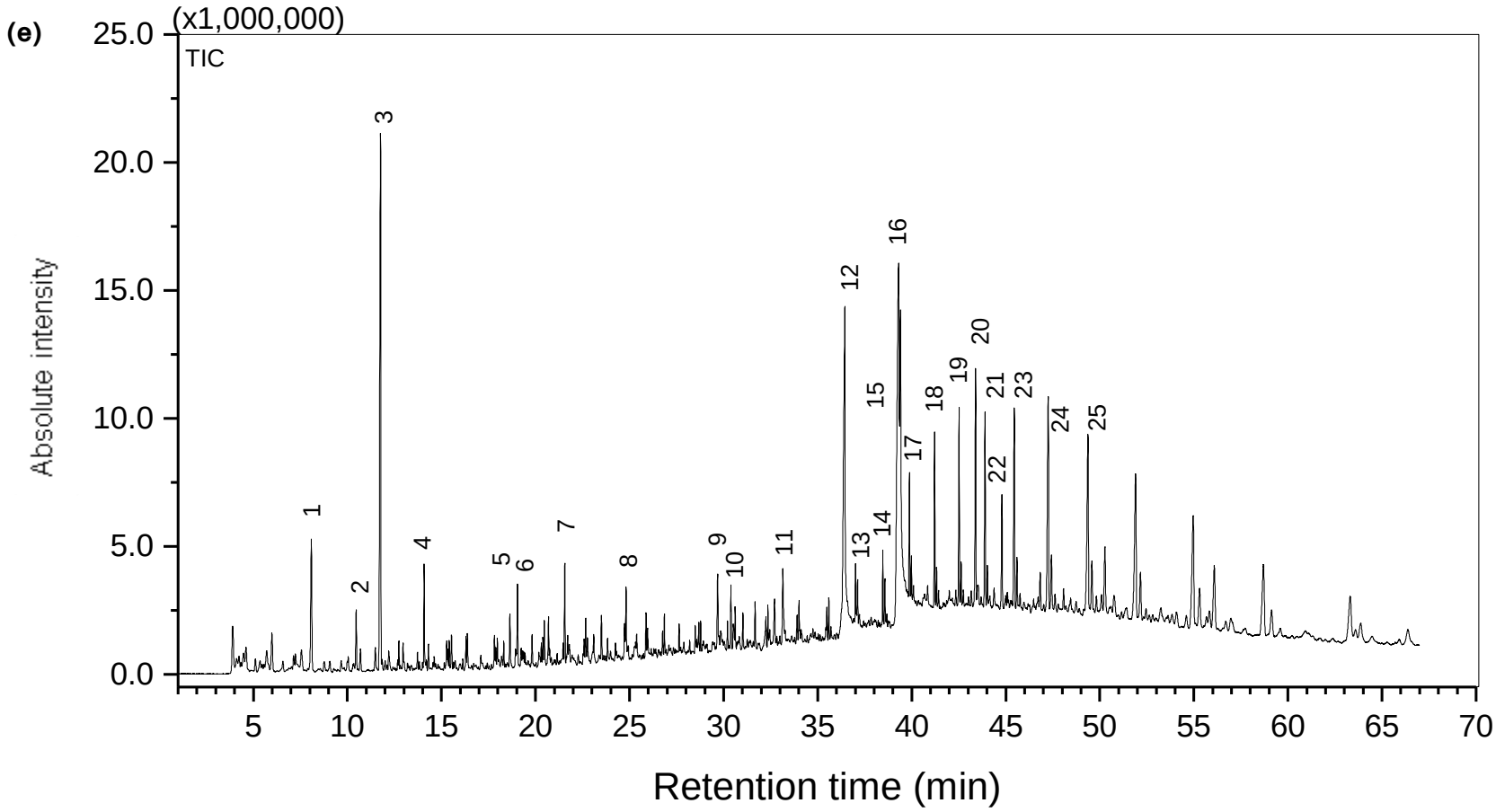

Figure 4.11 (e) Total Ion Chromatogram from Py-GC-MS of Municipal waste 250°C humic-like acid extract.
*Peak identification: **1**: Toluene; **2**: Ethylbenzene; **3**: Bicyclo[4.2.0]octa-1,3,5-triene; **4**: .alpha.-Methylstyrene; **5**: Phenol; **6**: Phenol, 2-methoxy-; **7**: Creosol; **8**: Decane, 1-bromo-; **9**: Dodecanoic acid; **10**: Benzene, 1,1'-(1,3-propanediyl)bis-; **11**: Tetradecanoic acid; **12**: n-Hexadecanoic acid; **13**: Octacosane; **14**: Heneicosane; **15**: 9-Octadecenoic acid, (E)-; **16**: Octadecanoic acid; **17**: Heneicosane; **18**: Heneicosane; **19**: Heneicosane; **20**: Benzenemethanamine, N-hydroxy-N-(phenylmethyl)-; **21**: Heneicosane; **22**: Bis(2-ethylhexyl) phthalate; **23**: Heneicosane; **24**: Heneicosane; **25**: Tetracontane*

4.4 Surface area and porosity

In agreement with literature, oak biochars possessed the highest surface areas compared to other feedstocks possibly due to its higher lignin and cellulose content. Hydrochar and pyrolysis char surface areas were comparable however, with the exception of the commercial (Proininso) oak biochars produced with the traditional kiln (450°C and 650°C). Such similarities in this study may have been caused by the processing reactors involved rather than feedstock properties, since biochars produced with the *Pyromaat* using the same feedstock (holm oak) as the traditional kiln had substantially lower surface areas (**Table 4.10** and **Table 4.11**). Fryda and Visser (2015) attributed the low surface areas to partial filling of char pores by condensable gases. This possibly occurred due to the nature of the reactor or flow of carrier gases during the reaction.

N_2 adsorption isotherms of oak biochars obtained from both traditional kiln and *Pyromaat* reactors reflected these differences (**Figure 4.11(a)-(d)**); while the traditional kiln (commercial oak) biochars exhibited Type IV isotherms indicative of mesoporosity (Schneider 1995; Sing et al. 1985), *Pyromaat* (non-commercial, ECN) biochars exhibited Type III isotherms. The presence of some hysteresis during the desorption phase in the latter biochars also suggested Type V isotherms however. Nevertheless, both Type III and V isotherms are often indicative of weak gas-solid interactions (Schneider 1995; Sing et al. 1985). Similar Type III/V isotherms were also observed in other *Pyromaat* biochars.

Adsorption isotherms for municipal waste biochars are also similar to Type V isotherms, and neither variations in pyrolysis processing temperature nor bleeding 1% O_2 changed isotherm shape and surface area (**Figure 4.12**). Similarly, gasification did not affect adsorption isotherms and surface areas until higher temperatures of 750°C were used as shown in **Figure 4.12** for greenhouse (paprika) waste biochars, where a Type IV isotherm was observed. Preliminary tests with greenhouse waste biochar pyrolyzed at 600°C in N_2 and in 1% O_2 revealed similar surface areas (2.0 and 1.9 $m^2\ g^{-1}$ respectively), thus sorption isotherms for the former char have been presented as a proxy for greenhouse waste 600°C pyrolyzed in the absence of oxygen.

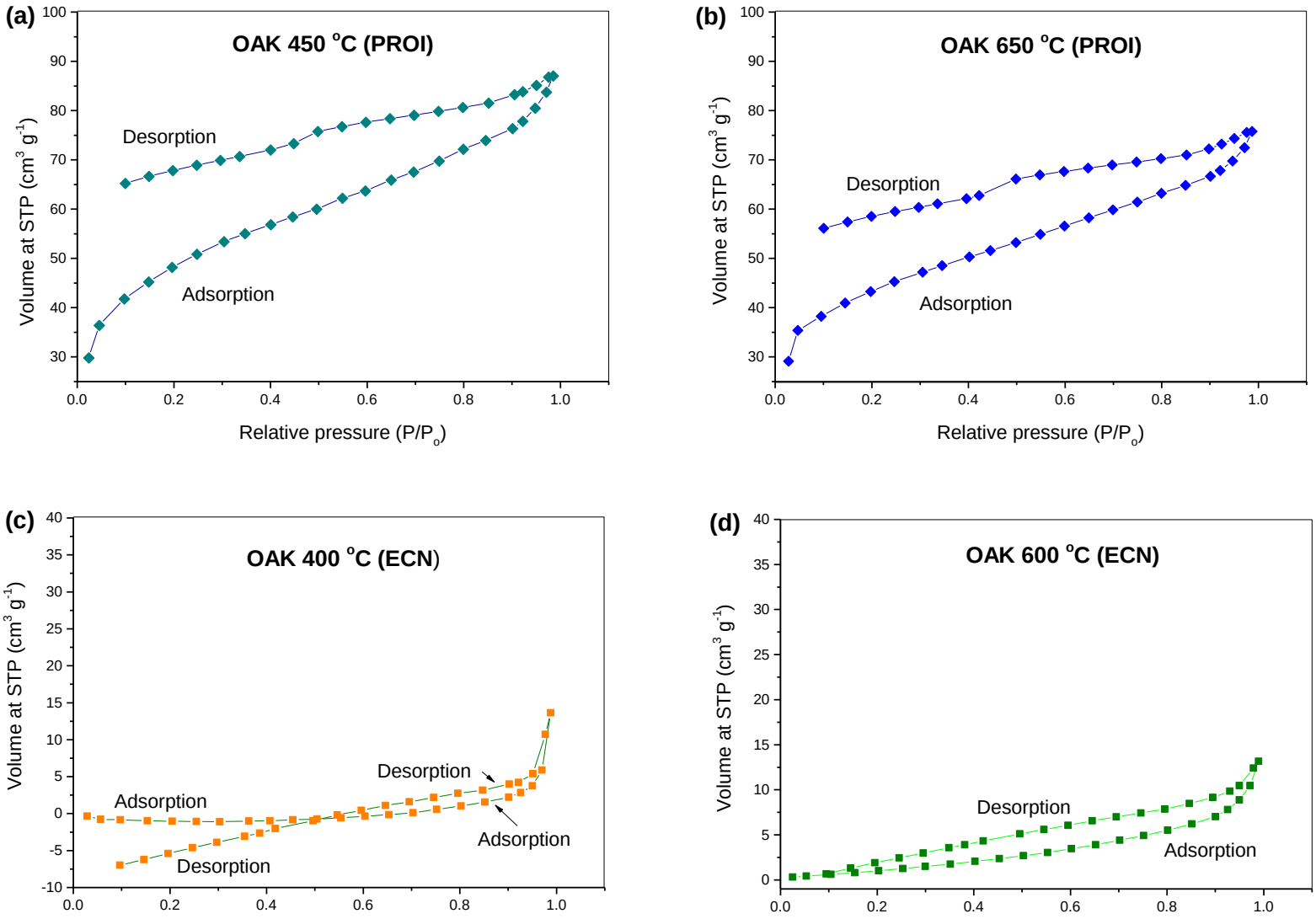

Figure 4.11 N_2 gas sorption isotherms for commercial and non-commercial oak biochars with manufacturer names in parentheses: a) Proininso Oak 450°C; b) Proininso Oak 650 °C; c) ECN Oak 400°C; d) ECN Oak 600°C.

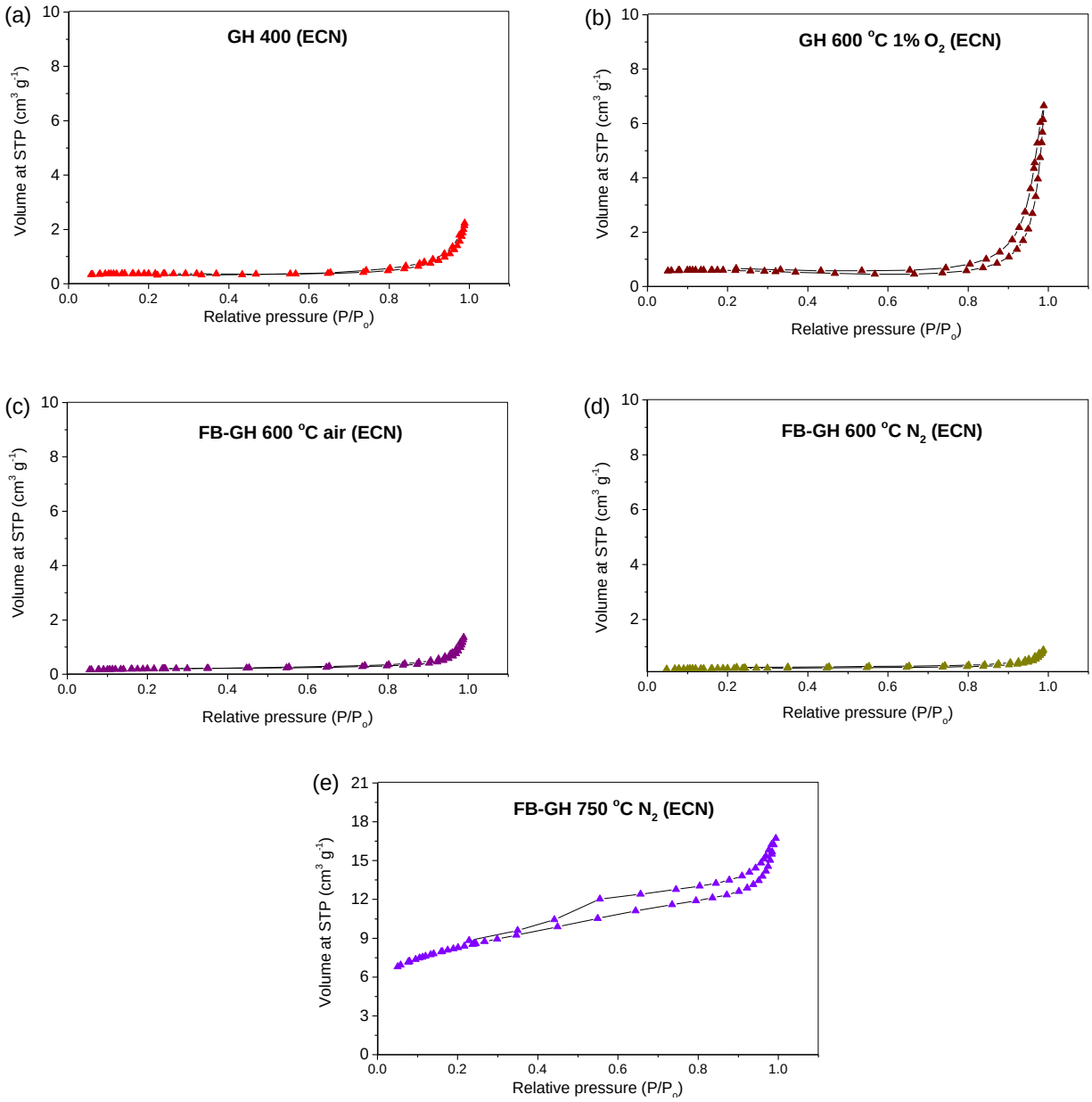

Figure 4.12 N_2 gas sorption isotherms for ECN greenhouse waste pyrolysis and gasification biochars: Pyrolysis biochars: a) GH 400°C; b) *GH 600°C; Gasification chars: c) FB-GH 600°C in air; d) FB-GH 600°C in N_2; e) FB-GH 750°C in N_2. $GH 600°C pyrolysed in 1% O_2 used as a proxy for GH 600°C as surface area and porosity development was similar for both.

Table 4. 10 Char surface area and porosity development of standard chars

Char	N_2 BET Surface area ($m^2\ g^{-1}$)	Total pore volume ($cm^3\ g^{-1}$)	[a]Average pore width (nm)
250°C hydrochars			
OAK (Comm.)	6.0	0.035	0.023
Greenhouse waste (GH)	2.5	0.011	0.021
Municipal waste (MW)	4.2	0.027	0.028
Presscake from AD (PK)	0.03	0.615	0.032
400–450°C biochars			
OAK (Comm.)	180.0	0.150	0.003
Oak wood (OW)	1.0	0.005	0.020
Greenhouse waste (GH)	1.3	0.003	0.904
Municipal waste (MW)	2.0	0.007	0.014
Presscake from AD (PK)	2.0	0.004	0.008
Greenwaste (GW)	2.0	0.011	0.022
600–650°C biochars			
OAK (Comm.)	280.0	0.160	0.023
Oak wood (OW)	2.0	0.010	0.020
Greenhouse waste (GH)	2.0	0.015	0.030
Municipal waste (MW)	4.0	0.029	0.029
Presscake from AD (PK)	2.5	0.017	0.027
Greenwaste (GW)	2.0	0.015	0.030

[a]Adsorption average pore width (4V/A by BET).

Table 4. 11 Char surface area and porosity development of non-standard biochars

Char	N_2 BET Surface area (m^2 g^{-1})	Total pore volume (cm^3 g^{-1})	[a]Average pore width (nm)
Gasification chars			
GH-FA 600°C (air)	0.7	0.002	2.866
GH-FN 600°C (N_2)	0.7	0.154	0.628
GH-FN 750°C (N_2)	29.0	0.017	0.331
Pyrolysis chars (600 °C, 30 min)			
MW 600°C, 30 min	6.0	0.031	0.017
PK 600°C, 30 min	3.1	0.014	0.002
PM 600°C, 30 min	1.9	1.500	0.016
Pyrolysis chars (600 °C, 60 min, 1% O_2)			
MW 600°C, 60 min	5.0	0.028	0.017
PK 600°C, 60 min	4.0	0.026	0.026

[a]Adsorption average pore width (4V/A by BET). **GH-FA** and **GH-FN** refer to greenhouse waste gasification biochars produced in air and N_2 respectively.

4.3.5 Char morphological properties

A typical microscope image of reference oak biochars (Proininso oak pyrolysed at 450°C and 650°C) were each presented in **Figure 4.13,** confirming the presence of various pores. Oak 650°C generally appeared to have a superior pore network which was in agreement with gas adsorption results.

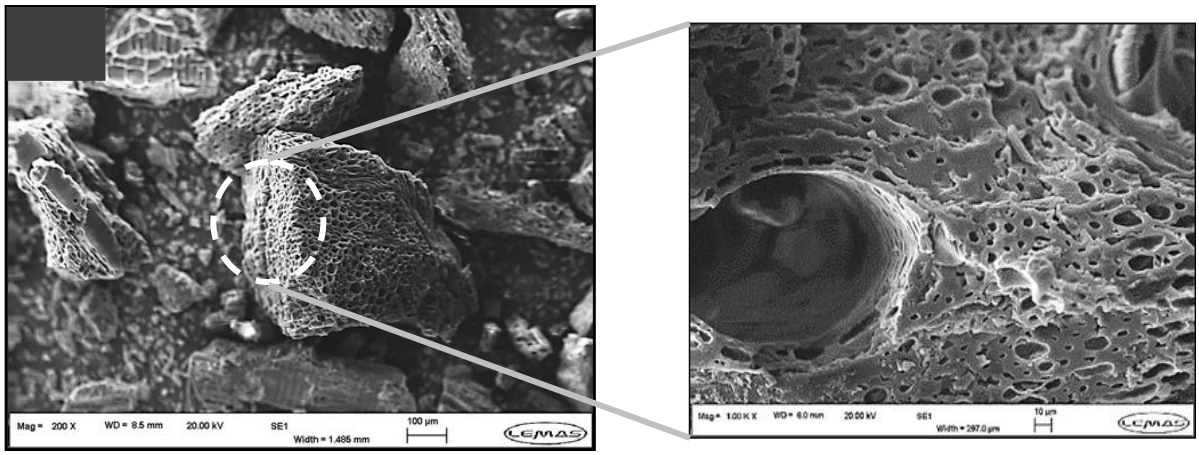

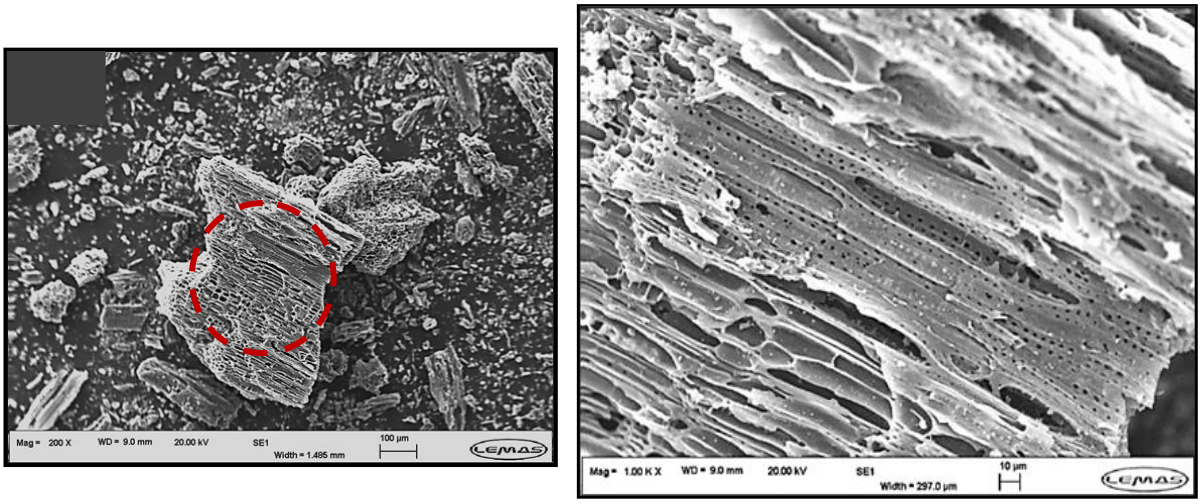

Figure 4.13 SEM imaging of commercial oak (Proininso) biochars produced at (a) 450°C (b) 650°C (L-R: 200× and 1000× magnification, respectively).

4.4 Conclusions

Details of char physico-chemical properties can provide vital information about potential char behaviour in various environments. In this study, the highest char carbon contents (>50%) were observed in oak and paprika waste chars and were categorised as Class 1 biochars, while hydrochars and pyrolysis chars derived from municipal waste, presscake and greenwaste were Class 2–3 as their carbon contents were lower. Char morphological properties were found to be a function of processing temperature and reactor system; using holm oak chars as a reference, substantial differences in surface area were observed in chars produced using hydrothermal, traditional kiln (Proininso), screw conveyor (Pyromaat) and fluidized bed reactors. In other cases, biochar surface areas were comparable or even lower than most hydrochars' possibly due to reactor-induced interactions between condensable gases and solid products.

With regard to char functional groups, both temperature and biomass feedstock property influenced char inorganic content and acidic functional groups such as humic-like substances. For instance, oak 250°C hydrochar possessed more humic-like substances than greenhouse waste, municipal waste and greenwaste hydrochars, while oak biochar produced at 650°C did not possess any humic-like substances. In spite of substantial differences in carbon and inorganic matter content however, the degradation of lignocellulose structures were mostly similar in all feedstocks investigated.

CHAPTER 5

Influence of functionality on char interaction in soil and nutrient-rich environments

Abstract

A number of adsorbents have been considered for ammonia/ammonium and phosphate recovery and this study was primarily aimed at contributing to growing research on some of the factors influencing char-adsorbent sorption capacity in nutrient-rich environments. Batch sorption tests involving hydrochars and biochars derived from bark-free oak wood, greenhouse (paprika) waste, treated municipal waste, presscake, greenwaste and pig manure showed that ammonium and phosphate sorption capacities were similar regardless of differences in char morphologies. However, char calcium and magnesium contents influenced phosphate sorption while oxygen groups were directly related to ammonium sorption. The ammonia removal efficiencies of two sets of chars with low and high nitrogen contents (chars derived from oak and greenhouse waste, respectively) were also evaluated from 7-day batch sorption tests in addition to small-scale co-composting trials over a period of 17–21 days. In both systems, oak hydrochar demonstrated the highest capacity for ammonia sorption compared to its biochar counterparts while greenhouse waste char sorption capacity was variable: in the 7-day batch ammonia sorption tests, greenhouse waste hydrochars showed the least potential for ammonia sorption compared to its biochar counterparts while the reverse was true in the co-composting system. Furthermore, a number of differences were observed between oak and greenhouse waste hydrochar ammonia removal efficiencies following extraction with alkaline and organic solvents; while a portion of nitrogen was recoverable as both ammonium and nitrate in greenhouse waste hydrochar, only ammonium was recoverable in oak hydrochar. Results from 21-day soil incubation tests with oak, greenhouse waste, and presscake chars were in general agreement with recalcitrance indices, O/C ratios and the literature, in that hydrochar-amended soils released the most CO_2-C and experienced higher inorganic nitrogen (NH_4-N and NO_3-N) mineralization, suggestive of their higher tendency to degrade in soils.

5.0 Introduction

Ammonium makes up a very high proportion of soluble nitrogen in animal waste are adsorbed onto negatively-charged sites or between clay interlayers in soils (Fernando et al. 2005). When released however, nitrifying bacteria convert this to nitrate in aerobic conditions which is eventually leached to groundwater (Fernando et al. 2005), excess quantities of which result in eutrophication. Furthermore, ammonia emission into the atmosphere result in nutrient deposition in nutrient sensitive ecosystems, formation of light–scattering aerosols resulting in haze and visibility impairment and formation of inhalable aerosol particles which are health concerns. High concentrations of ammonium and phosphates can be found in various wastewaters (Cai et al. 2013) and their recovery with chars increase the economic potential of hydrochars and biochars whilst minimising the risks of eutrophication. With growing concerns about its future availability (Rittmann et al. 2011), phosphorus recovery is also important. Consequently, the overarching aim of this chapter is to gain more insight on the factors influencing char nutrient sorption capacity, as a better understanding of such factors help to predict char suitability for nutrient recovery from certain nutrient-rich environments.

As a starting point, the CEC of various chars will be evaluated whilst identifying some of the relationships between char physico-chemical properties and CEC, ammonia / ammonium and phosphate sorption capacities. Furthermore, the potential for reducing ammonia and carbon dioxide emissions during laboratory-scale co-composting with selected hydrochars and biochars are explored. Finally, the effects of char physico-chemical characteristics on char mineralization in a high pH Mediterranean soil are evaluated in short-term soil incubation tests. Specifically, the carbon fluxes and inorganic nitrogen (NH_4-N and NO_3-N) mineralisation sorption capacity of 250°C hydrochars and 400°C biochars derived from oak, greenhouse (paprika) waste, and presscake from AD were used for soil incubation tests. Details of cation exchange capacity, various sorption tests, co-composting, and soil incubation procedures have been outlined in Chapter Three.

5.1 Hydrochar and biochar Cation Exchange Capacity (CEC)

5.1.1 CEC method development

As earlier mentioned in **Section 2.2.5**, variations in soil and biochar CEC procedures create challenges for biochar CEC comparisons across studies. **Table 5.1** summarises the four CEC methods evaluated in this study, with full descriptions of the methods earlier provided in **Sections 3.4.5.1**–**3.4.5.4**.

Table 5.1 Description of CEC procedures

Method No.	**Method description**	**Description section**
CEC-1	Modified $BaCl_2 \cdot 2H_2O$ compulsive exchange	3.4.5.1
CEC-2	Ammonium acetate pH 7 (displacement with KCl after washing)	3.4.5.2
CEC-3	Ammonium acetate pH 7 (direct displacement with MgO)	3.4.5.3
CEC-4	Modified ammonium acetate compulsory displacement pH 7	3.4.4.4

Figure 5.1 revealed some similarities in char CEC trend for oak biochars and waste-derived chars, yet substantial differences in the actual char CEC values were observed depending on the method employed. This variation was also observed in Skinner et al. (2001). CEC-1 was rejected due to challenges associated with char density as a portion of char tended to float to the top of the supernatant even after repeated centrifugation. From this method, low CEC values were obtained for oak 450°C and 650°C, being 1.1 and 3.1 $cmol_c\ kg^{-1}$ respectively. Skinner et al. (2001) similarly found that this method yielded the lowest CEC values compared to analysis performed with buffered pH and ammonium acetate and unbuffered ammonium chloride.

Of the three methods involving ammonium acetate, CEC-2 yielded the lowest CEC values but was most comparable with values often reported for similar biochars in the literature (Mukherjee et al. 2011). However, the relatively time-consuming nature of such a method (>14 h per sample, based on duplicate analysis and two distillation units) could be a potential drawback when analysis of large numbers of samples is required. CEC values obtained from this method were a factor of 10 lower than values obtained from CEC-3, and although a lower concentration of titrant (0.01 M HCl) was used in this method compared to 0.1 M HCl used in CEC-3,

such differences would likely only affect the volume of titrant used, which was accounted for in the final CEC calculations (c.f. Equations 3.9 and 3.10). The low CEC values obtained from CEC-2 may have been due to some hydrolysis of the saturating/index cation (NH_4^+ in this case) during the washing stage, a phenomenon that has been well discussed in the literature (Bower et al. 1952; Okazaki et al. 1961). As shown in **Figure 5.1**, similar CEC values were obtained from CEC-3 and CEC-4 in spite of differences in char mass, index cation, analytical technique (distillation and flame AAS respectively). However, linear regression plots of the two methods only showed a weak correlation (Pearson r = 0.389) as seen in **Figure 5.2**. but slightly better comparisons can be made between CEC-2 and CEC-3 (Pearson r = 0.724*, α=0.05) and between CEC-2 and CEC-4 (Pearson r =0.706*, α=0.05) in spite of numerical differences. Skinner et al. (2001) compared the CEC values of kaolinite, vermiculite and decomposed soil organic matter using various methods and observed that soil organic matter exhibited the greatest variation in CEC (c.f. **Figure. 2.4**) and attributed this to pH-dependent organic matter interactions. In terms of repeatability, most RSD values were below 20% for CEC-2, with *Proininso* oak 450°C and 650°C samples at 7.7% and 3.8% respectively. Precision was similar for CEC-4 in most cases, based on RSD values <10% in most cases, at 13.6% and 0.9% for *Proininso* oak 450°C and 650°C respectively analysed at different periods, but between 25-30% for more heterogeneous samples. Unfortunately, conclusions about the precision of CEC-1 and CEC-3 cannot be made as these were done as single analyses due to time constraints. CEC-4 was chosen for analysis of all the chars investigated in this study due to the relative speed with which several char samples could be analysed.

Findings from this study show that even when the same pH is maintained for all saturating solutions in order to control pH-dependent effects on char organic content, variations in char CEC still occur. Future comparisons between chars and standard materials of similar composition would therefore be beneficial in terms of confirming the accuracy of the CEC methods. For instance, Skinner et al. (2001) evaluated the CEC of soil samples alongside pre-washed humified organic matter, kaolinite and vermiculite whose effective CEC values were determined via saturation and subsequent summation of K, Na, Mg, Ca, and Al cations.

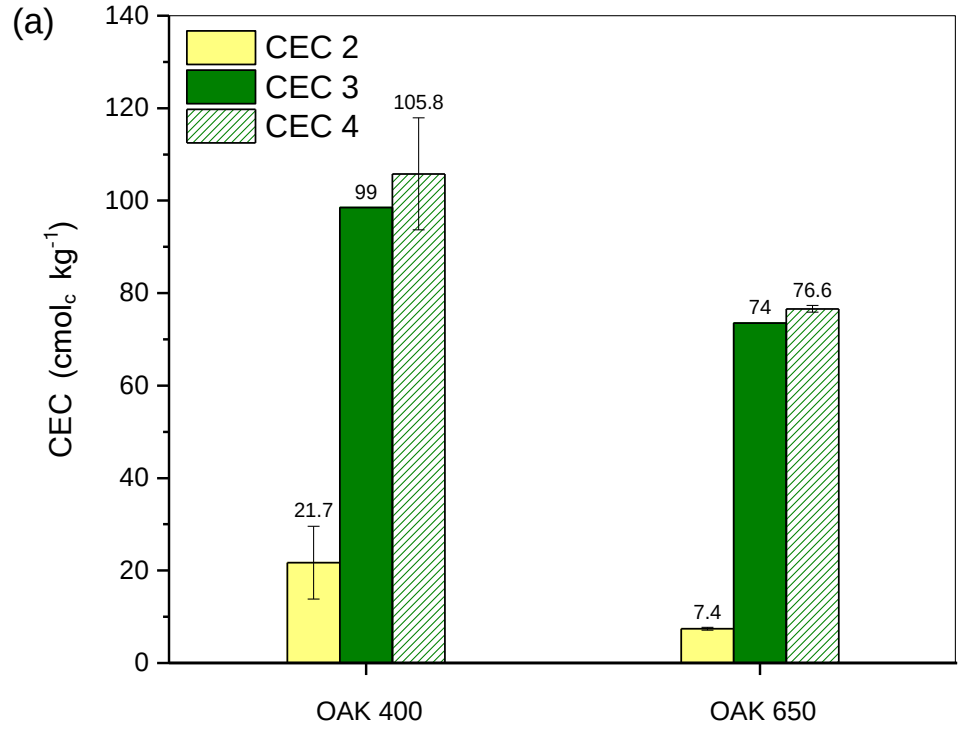
(a)
CEC 2
CEC 3
CEC 4
CEC (cmol$_c$ kg^{-1})
140
120
100
80
60
40
20
0
21.7
99
105.8
7.4
74
76.6
OAK 400
OAK 650

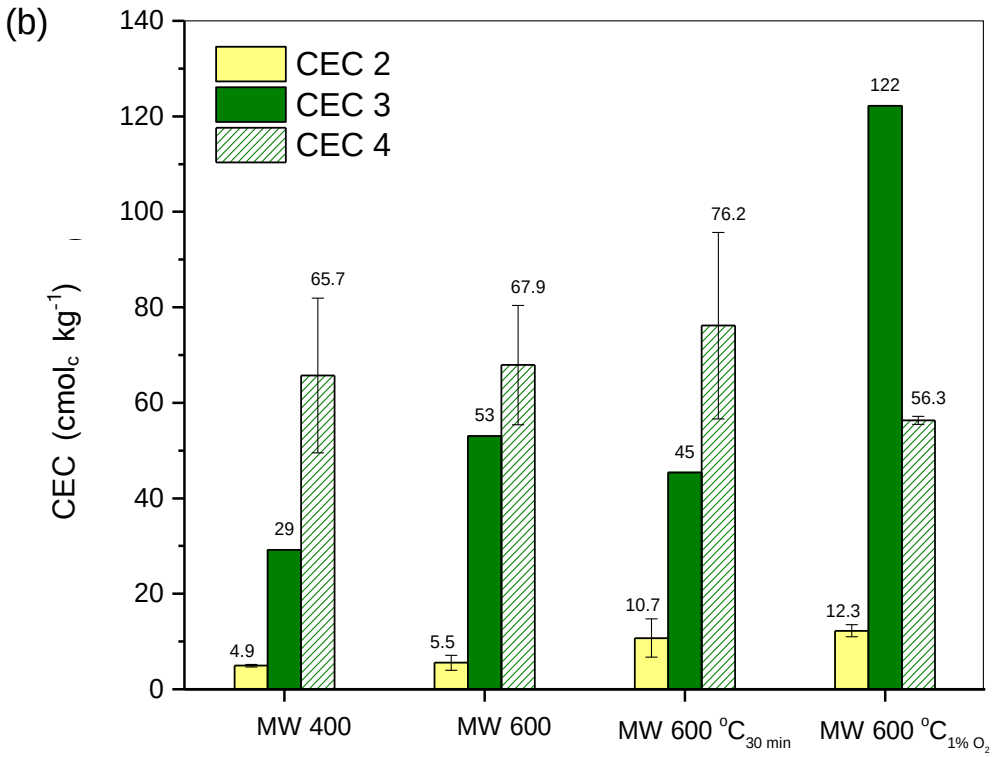
(b)
CEC 2
CEC 3
CEC 4
CEC (cmol$_c$ kg^{-1})
140
120
100
80
60
40
20
0
4.9
29
65.7
5.5
53
67.9
10.7
45
76.2
12.3
122
56.3
MW 400
MW 600
MW 600 °C$_{30\ min}$
MW 600 °C$_{1\%\ O_2}$

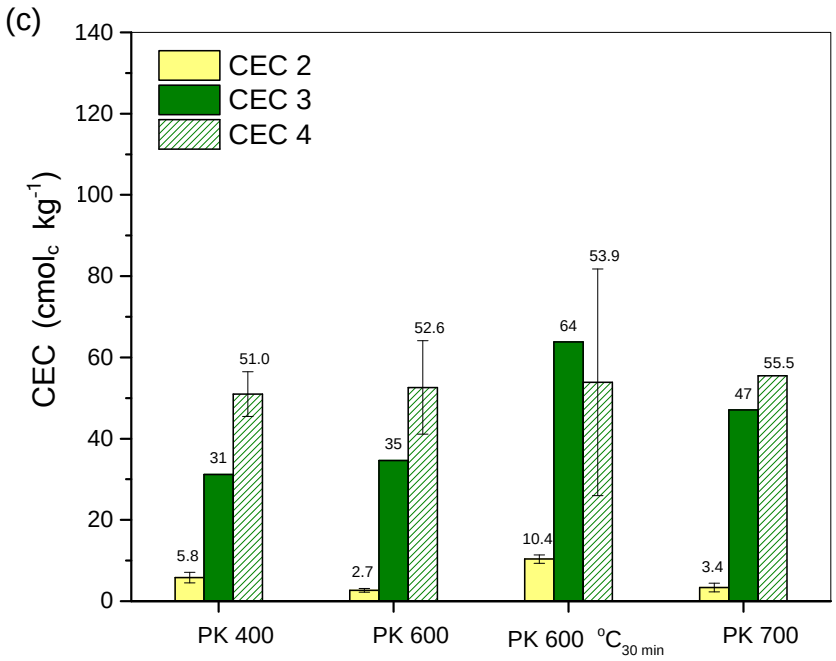

Figure 5.1 Comparison of 3 CEC methods for evaluating cation exchange capacities of a) oak b) municipal waste (MW) and c) presscake (PK) biochars at various pyrolysis temperatures. Suffixes '30 min' and '1% O_2' denote prevailing pyrolysis conditions: 30 min residence times and in the presence of 1% oxygen respectively. For CEC-3, single analysis performed only.

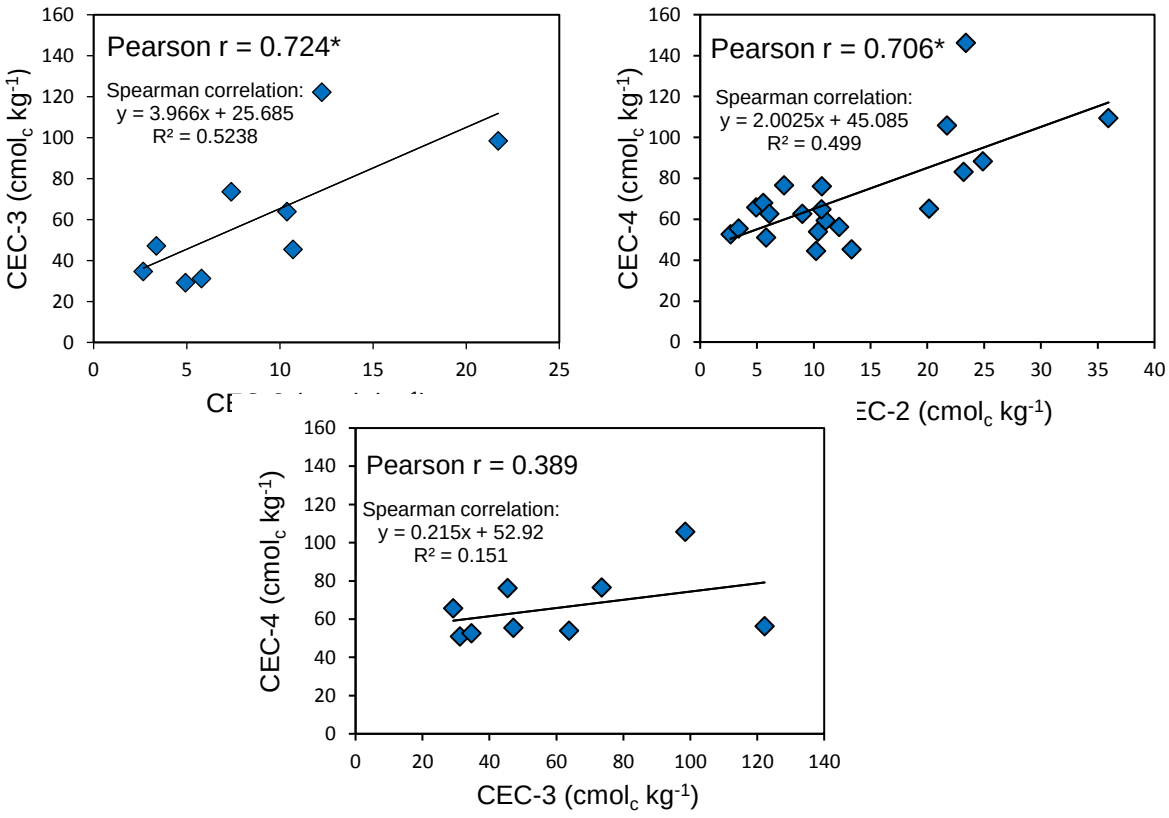

Figure 5.2 Relationship between char CEC Methods 2, 3, and 4.

5.1.2 Hydrochar and biochar CEC

CEC results for all chars determined using CEC-4 are presented in **Table 5.2** and showed that only non-commercial oak chars (OW) exhibited the trend of decreasing CEC with increasing pyrolysis temperature. Biochars produced between 600–650 °C generally possessed higher CEC values than lower temperature biochars (400–450 °C). Furthermore, hydrochar CEC values were lower than biochar CEC in spite of the higher oxygen contents in the former chars. CEC is known to be higher in chars produced at low temperatures (Lehmann 2007; Silber et al. 2010), and for this reason, acid functional groups are thought to influence char CEC as their quantities tend to diminish with increasing processing temperature. Yet Mukherjee et al. (2011) found no strong positive correlation between these parameters and put forth a number of reasons as to why this may be so.

Positive correlations between hydrochar and standard biochar oxygen contents (daf) and CEC were found in this study (Pearson r = 0.832 and 0.651* resp., α=0.05), as expected (Wang et al. 2015b). To some extent, positive correlations were also found between char CEC and organic matter: Pearson r = 0.731 and 0.537 resp., α=0.05 while no correlation was observed between CEC and volatile matter. The role of ash content on char CEC Is currently inconclusive; while Kirchmann and Witter (1992) and Morales et al. (2015) suggested that CEC may be independent of biochar elemental contents, other studies consider the relationship to be positively correlated (Gaskin et al. 2008; Zhao et al. 2013b), possibly facilitating the formation of oxygen groups (Mészáros et al. 2007). In this study, CEC was negatively correlated to ash content, albeit non-significant at the 0.05 level (Pearson r = -0.727 and -0.560 for hydrochars and biochars respectively). Following gasification of greenhouse waste, a sharp decrease in CEC was observed, which appeared unrelated to ash content. Similarly, both municipal waste and presscake biochars produced at non-standard conditions showed a decrease in CEC relative to biochars produced at standard conditions (**Table 5.2**). Additionally, no relationship between char CEC and surface area was evident; for instance, Oak 450 °C and PK 400 °C possessed similar CECs despite marked differences in surface area (180 m^2 g^{-1} and 2 m^2 g^{-1} respectively). Mukherjee et al. (2011) similarly found no substantial relationship between char CEC and surface area. Char negative surface charges were comparable although since presscake hydrochar possessed a comparable CEC but low surface area (0.03 m^2 g^{-1}), its negative charge was greatest.

Table 5.2 Hydrochar and biochar CEC and surface charge

CEC of chars produced at standard conditions			CEC of chars produced at non-standard conditions		
Char	CEC ($cmol_c\ kg^{-1}$)	Negative surface charge ($mmol_c\ m^{-2}$)	Char	CEC ($cmol_c\ kg^{-1}$)	Negative surface charge ($mmol_c\ m^{-2}$)
250°C hydrochars					
OAK	88.3 ± 9.7	0.15	**Gasification chars**		
GH	83.1 ± 19.4	0.33	GH 600°C (air)	45.8 ± 0.7	0.65
MW	44.5 ± 1.7	0.11	GH 600°C (N_2)	41.2 ± 1.6	0.59
PK	62.6 ± 3.5	20.87	GH 750°C (N_2)	51.0 ± 20.6	0.02
400-450°C biochars					
OAK (Comm.)	59.4 ± 8.1	0.003			
OW	105.8 ± 12.1	1.06	**Pyrolysis chars (600 °C, 30 min, N_2)**		
GH	109.5 ± 21.8	0.84	MW 600 °C, 30 min	76.2 ± 19.5	0.13
MW	65.7 ± 16.2	0.33	PK 600 °C, 30 min	24.4 ± 12.7	0.08
PK	51.0 ± 5.5	0.26	PM 600 °C, 30 min	79.1 ± 18.5	0.42
GW	64.8 ± 11.5	0.32			
600-650°C biochars					
OAK (Comm.)	76.6 ± 0.7	0.003	**Pyrolysis chars (600 °C, 60 min, 1% O_2)**		
OW	65.2 ± 20.2	0.33	MW 600 °C, 60 min	56.3 ± 0.8	0.11
GH	146.2 ± 32.3	0.73	PK 600 °C, 60 min	45.3 ± 0.4	0.11
MW	67.9 ± 12.5	0.17			
PK	52.6 ± 11.5	0.21			
GW	62.7 ± 2.1	0.31			

OAK (**Comm**.): commercial oak produced at 450°C and 650°C; **OW**: oak wood; **GH**: greenhouse (paprika) waste; **MW**: municipal waste (cellmat); **PK**: presscake from AD; **GW**: greenwaste. Negative surface charge determined as CEC/surface area.

5.1.3 CEC of solvent-extracted chars

Char volatile matter may directly or indirectly influence char CEC; for instance, Mukherjee et al. (2011) suggested that based on the strong positive relationship observed between volatile matter and total acid functional groups, the former influenced the pH-dependency of char CEC. Therefore, to better understand the reason behind CEC trends in this study, some chars were extracted with toluene and CEC measurements were repeated on these chars. This extraction had different effects on the two types of char: in hydrochars, the CEC in most cases increased (**Figure 5.3(a)**); in biochars, CEC either remained unchanged or decreased following solvent extraction, the latter more prevalent for the higher temperature biochars (**Figure 5.3(c)**). As CEC is thought to be a function of surface area and functionality, an increase in hydrochar CEC following solvent extraction could suggest either the unblocking of pores increasing porosity and surface area, or that a higher surface functionality is being revealed by removing tars. The latter effect may be more important as surface area had negligible influence on char CEC, with hydrochars possessing low surface areas (<6 $m^2 g^{-1}$). Based on the assumption that carboxyl and other functional groups increase CEC (Boehm 1994; Glaser et al. 2002; Warner 1977), the removal of volatile hydrocarbons from the surface of the biochar containing these groups by solvent extraction is expected to affect CEC by revealing a different surface functionality below.

As aforementioned, biochar CEC was generally similar before and after extraction but for the 600–650°C biochars, CEC was slightly higher for the as-received biochars indicating that solvent extraction reduced their surface functionality. There are some anomalies as observed in 400°C oak biochar, but the general emerging trend shows that hydrochar CEC is enhanced after extraction while biochars are either unaffected or lowered after extraction. This provides supporting evidence that CEC is potentially higher for hydrochar but the tars on its surface affect its CEC. Indeed, water-insoluble fatty acids were found sorbed onto hydrochars produced from microalgae (Heilmann et al. 2011) and brewer's spent grain (Poerschmann et al. 2015), based on analyses with ether and chloroform/methanol solvents respectively. Extracts analysed by GC-MS also confirmed the removal of oxygenated groups and hydrocarbons from hydrochars and biochars respectively (dataset not included). These findings are contrary to those of Mukherjee et al. (2011) who reported that volatile organic matter may be partly responsible for char CEC at near-neutral pH conditions.

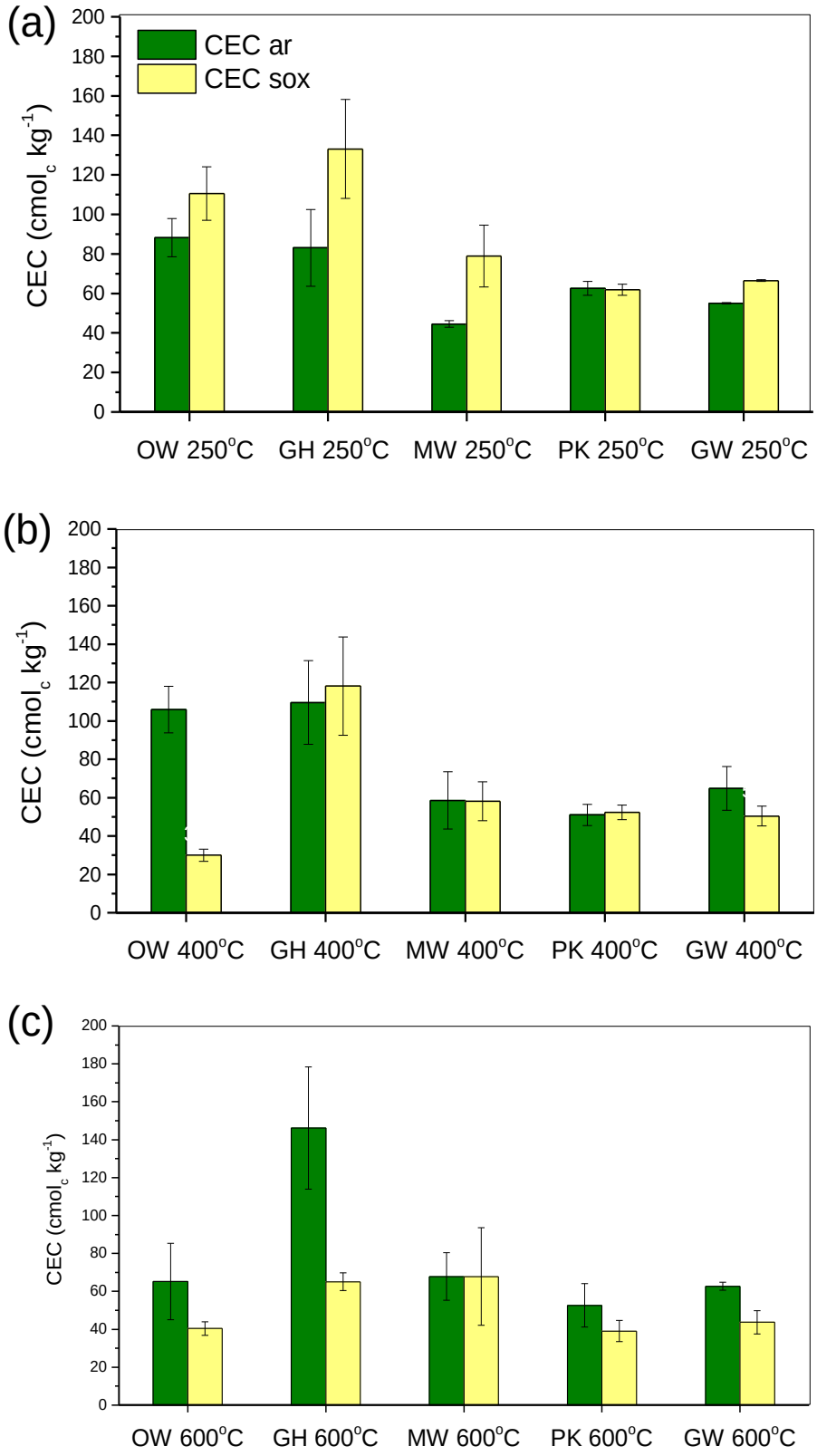

Figure 5.3 Effect of solvent extraction on char CEC
GH: greenhouse waste; MW: municipal waste; PK: presscake; GW: greenwaste
CEC_{ar} and CEC_{sox} refer to CEC before and after solvent extraction, respectively.

5.2 Char interactions in nutrient-rich environments

5.2.1 Char ammonium sorption

Details of ammonium sorption experiments have been outlined in **Section 3.12.2.** All containers were acid-washed prior to analysis.

5.2.1.1 Adsorption isotherms

Previous studies have shown that in addition to pH and time, initial ammonium concentrations are important factors that determine char adsorption capacity (Fernando et al. 2005; Kizito et al. 2015; Schlegel et al. 1999). Sorption tests were therefore performed on oak and greenhouse waste chars to determine the effect of different initial ammonium solution concentrations on char sorption capacities as shown in **Figure 5.4**. Some studies have reported that greater ammonium sorption occurs at increasing pH, but Kizito et al. (2015) observed optimal ammonium sorption within the pH range of 6.5–7. In this study, a pH of 7 was similarly used unless stated otherwise. For oak chars, ammonium sorption generally increased at higher initial solution concentrations in a somewhat S-shape (sigmoidal) trend (**Figure 5.5**), suggestive of low adsorbent affinity at lower solution concentrations. This was possibly due to NH_4^+-ligand interactions, which are overcome at higher solution concentrations (Limousin et al. 2007). In greenhouse waste chars, no discernible isotherm shape was observed and was therefore not presented.

Char ammonium sorption isotherm data were initially fitted to the linearized Langmuir and Freundlich models based on Equations 5.1–5.2:

Linearized Langmuir (Type II):
$$\frac{1}{q_e} = \left(\frac{1}{k_a q_m}\right)\frac{1}{C_e} + \frac{1}{q_m} \quad (5.1)$$

Linearized Freundlich:
$$\log q_e = \log K_F + \frac{1}{n}\log C_e \quad (5.2)$$

where q_e and q_m = amount of species adsorbed at equilibrium and saturated monolayer adsorption respectively (mg g^{-1}), C_e = equilibrium concentration (mg L^{-1}), n = adsorption intensity, K_a and K_F = Langmuir and Freundlich constants respectively (Ho 2004; Kumar and Sivanesan 2007).

Regression plots of the linearised Langmuir and Freundlich models are provided in Annex Fig A1 while their regression parameters are provided in **Table 5.3** and **Table 5.4**, which respectively show that model data parameters obtained over an

initial NH_4^+ concentration range of 360–1000 mg L^{-1} had lower R^2 values than those obtained over a wider initial NH_4^+ concentration range of 40–1000 mg L^{-1}.

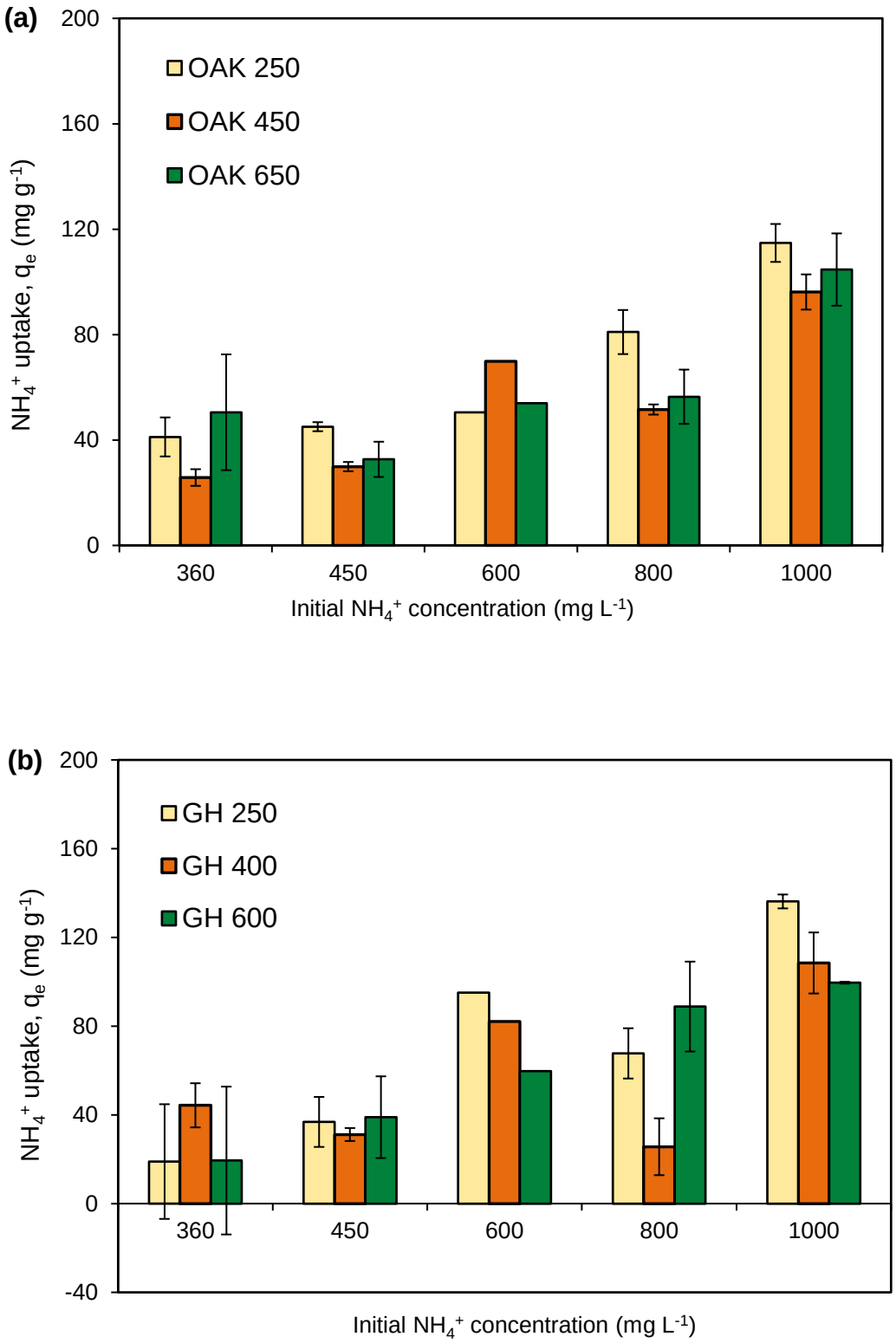

Figure 5.4 Effect of increasing concentration on NH_4^+ sorption by a) oak and b) greenhouse waste hydrochars and biochars. No error bars at 600 mg L^{-1} as only single analysis was performed. Sorption performed in triplicate at 1000 mg NH_4^+ L^{-1}.

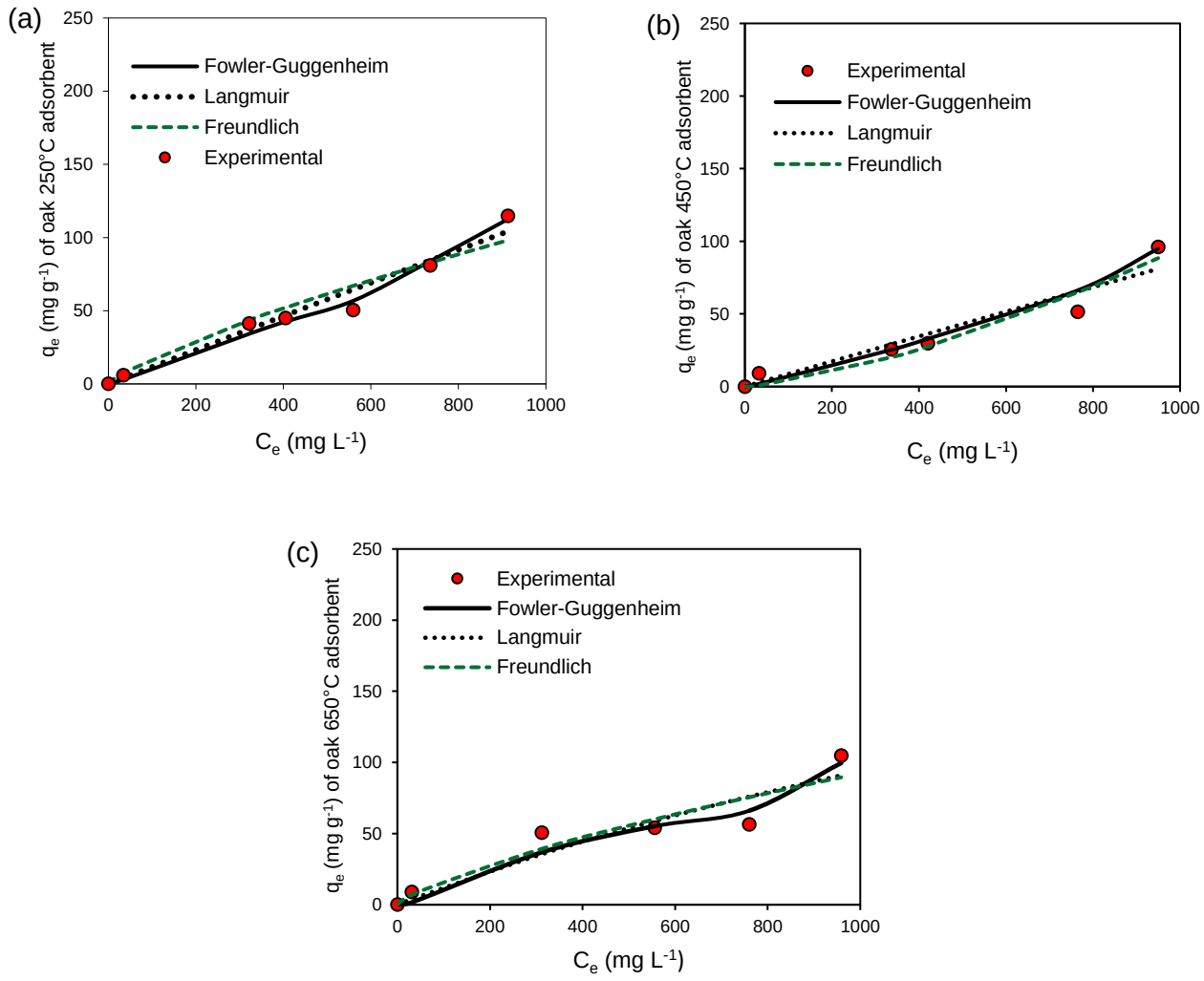

Figure 5.5 Oak char ammonium sorption (q_e) at various equilibrium NH_4^+ solution concentrations (C_e) for: (a) oak 250°C hydrochar, (b) oak 450°C biochar, (c) oak 650°C biochar. Experimental data fitted to nonlinear Langmuir, Freundlich, and Fowler-Guggenheim adsorption isotherm models.

This is expected, since a broader range of concentrations provide more accurate adsorption isotherm parameters (Kumar and Sivanesan 2006b). Langmuir *B* parameters between 0 and 1 were suggestive of favourable ammonium sorption while Freundlich n parameters greater than 1 suggested saturation of cation exchange sites (Foo and Hameed 2010; Hale et al. 2013). While the R^2 values suggested that the linearised Langmuir model described sorption better, its higher X^2 values suggested that the linearised Freundlich model described sorption better, a discrepancy which may have resulted from the model linearisation process (Ayoob and Gupta 2008) because this process distorts experimental error distributions (Kumar and Sivanesan 2006), as discussed in **Section 2.3.2.3**. This discrepancy

was further explored by fitting the experimental data to the nonlinear forms of both Langmuir and Freundlich models (Equations (2.5) and (2.8), respectively) using Solver nonlinear least squares method. However, while the nonlinear Langmuir model still possessed higher R^2 values than the nonlinear Freundlich model, maximum ammonium adsorption Langmuir (q_m) values were exaggerated, implying that both linear and nonlinear Langmuir models did not describe the experimental data accurately. Consequently, more complex nonlinear adsorption isotherm models were tested, as recommended by Limousin et al. (2007). Although not optimal, the Fowler-Guggenheim model (Equation 5.3) provided closer descriptions of the experimental data compared to the Langmuir, Freundlich, and Dubinin-Radushkevich nonlinear models, in keeping with earlier suggestions about lateral NH_4^+ adsorbate interactions. Nonlinear plots are presented in **Figure 5.5**, while the nonlinear Fowler-Guggenheim model parameters are summarised in **Table 5.4**.

$$q_e = q_m \frac{k_{FG} C_e \exp\left(\frac{\alpha q_e}{q_m}\right)}{1 + k_{FG} C_e \exp\left(\frac{\alpha q_e}{q_m}\right)} \qquad (5.3)$$

where k_{FG} = process adsorption constant (L mg^{-1}); α = constant describing inter-molecular interactions between adsorbate species; q_m = maximum adsorption capacity (Myśliwiec et al. 2016).

Table 5.3 Ammonium adsorption isotherm model data I (C_o = 360–1000 mg NH_4^+ L^{-1})

Char	Linearised Langmuir			Linearised Freundlich			X^2	X^2
	q_m (mg g^{-1})	B (L mg^{-1})	R^2	K_F	n	R^2	Lang	Freund
OAK 250	370.4	0.0004	0.871	0.13	1.03	0.898	8.6	4.9
OAK 450	-238.1	-0.0003	0.834	0.03	0.87	0.770	19.1	17.7
OAK 650	109.9	0.0018	0.357	0.72	1.45	0.553	26.7	17.7
GH 250	-52.6	-0.0009	0.797	0.00	0.61	0.756	110.6	86.3
GH 400	44.8	0.0614	0.001	7.68	3.35	0.046	140.1	81.9
GH 600	-58.8	-0.0008	0.881	0.00	0.64	0.932	42.6	6.2

Linearized Langmuir and Freundlich parameters respectively obtained from inverse and log plots of C_e values of approximately 360, 450, 600, 800, and 1000 mg L^{-1}. X^2_{Lang} and X^2_{Freund} refer to Chi-square values of q_e calculated from Langmuir and Freundlich parameters respectively.

Table 5.4 Ammonium adsorption isotherm model data II (C_o = 40–1000 mg NH_4^+ L^{-1})[a]

	Linearised Langmuir			Linearised Freundlich			X^2	X^2
Char	q_m (mg g^{-1})	B (L mg^{-1})	R^2	K_F	n	R^2	Lang	Freund
OAK 250	153.9	0.0012	0.998	0.28	1.17	0.983	19.2	6.6
OAK 450	57.5	0.0059	0.937	0.89	1.58	0.859	69.2	27.2
OAK 650	76.3	0.0042	0.979	0.96	1.56	0.910	37.4	18.2

	Nonlinear Langmuir			Nonlinear Freundlich		
	q_m (mg g^{-1})	B (L mg^{-1})	R^2	K_F	n	R^2
OAK 250	4175.5	0.00003	0.972	0.480	1.28	0.937
OAK 450	4175.6	0.00002	0.914	0.010	0.70	0.942
OAK 650	366.7	0.00034	0.881	0.580	1.36	0.894
[a]GH 250	6466.6	0.00020	0.593	0.0001	0.48	0.706
[a]GH 400	4934.4	0.00002	0.273	0.080	0.99	0.141
[a]GH 600	4934.4	0.00002	0.620	0.010	0.76	0.611

	Nonlinear Fowler-Guggenheim			
	q_m (mg g^{-1})	K_{FG} (L mg^{-1})	α	R^2
OAK 250	198.9	0.0004	2.1400	0.988
OAK 450	105.0	0.0004	3.5000	0.941
OAK 650	114.2	3.2500	0.0004	0.950
GH 250	154.5	4.0100	0.0002	0.988
GH 400	108.5	0.0001	9.2200	0.993
GH 600	113.2	0.0004	3.3800	0.999

[a]With the exception of GH data, whose parameters were obtained over C_o = 360–1000 mg NH_4^+ L^{-1}.
Linearized Langmuir and Freundlich parameters respectively obtained from inverse and log plots of C_e values of approximately 40, 360, 450, 600, 800, and 1000 mg L^{-1}. X^2_{Lang} and X^2_{Freund} refer to Chi-square values of q_e calculated from the linearised Langmuir and Freundlich isotherm parameters, respectively. K_F unit: $mg^{1-(1/n)}\,L^{1/n}\,g^{-1}$

5.2.1.2 Adsorption kinetics

The ammonium sorption kinetics of oak and greenhouse waste chars at an initial concentration of about 450 mg NH_4^+ L^{-1} were evaluated using the first, pseudo-first order, pseudo-second order and intra-particle diffusion models, the latter three being the frequently used models expressed in Equations 5.3-5.5:

Pseudo-first order: $$\log\left(q_e - q_t\right) = \log q_e - \frac{k_1}{2.303} t \quad (5.3)$$

Pseudo-second order: $$\frac{t}{q_t} = \frac{1}{q_e} t + \frac{t}{k_2 q_e^2} \quad (5.4)$$

Intra-particle diffusion: $$q_t = k_i t^{0.5} \quad (5.5)$$

Char ammonium sorption generally decreased with time as shown in **Figure 5.6** and

Table 5.5 shows key data obtained from the various plot models. Mohan et al. (2014) suggested that sorption kinetics obeying the pseudo-first order model were indicative of external mass transfer-controlled adsorption but as the pseudo-first order model gave very poor fits in most cases, it was excluded from this table. The pseudo-second order model generally had higher R^2 values compared to the pseudo-first order and intra-particle diffusion models although not an optimal fit in many cases based on R^2 values. Experimental and calculated q_e values were similar in the foremost model, however, k_2 values were negative.

5.2.1.3 Batch adsorption of NH_4^+ at 1000 mg L^{-1}

Ammonium sorption for oak and greenhouse waste chars were highest at initial concentrations of about 1000 mg NH_4^+ L^{-1} (about 780 mg NH_4-N L^{-1}). To compare the sorption capacities of other chars used in this study, subsequent adsorption tests were performed at this range to evaluate the proportion of ammonium removed by the chars, using a char/solution ratio of 1 kg char m^{-3}. **Tables 5.6–Table** 5.7 show that ammonium sorption capacities were generally comparable for chars produced at both standard and non-standard conditions, albeit slightly lower in the

Table 5.5 Adsorption kinetics model parameters

Char	Pseudo-second order				First order R^2	Intra-particle Diffusion R^2
	$q_{e\ exp}$ (mg g^{-1})	$q_{e\ cal}$ (mg g^{-1})	k_2 (min g mg^{-1})	R^2		
OAK 250	39.50	37.5	-0.0004	0.997	0.779	0.003
OAK 450	28.50	28.2	-0.0011	0.986	0.363	0.542
OAK 650	25.08	23.3	-0.0004	0.991	0.738	0.193
GH 250	28.90	27.3	-0.0003	0.986	0.149	0.162
GH 400	43.23	45.7	0.0001	0.914	0.038	0.353
GH 600	25.92	24.0	-0.0004	0.995	0.706	0.229

$q_{e\ exp}$ and $q_{e\ cal}$ refer to amount of NH_4^+ adsorbed by chars obtained from experimental data and from plots respectively. For Pseudo-second order model, parameters obtained from plot of t/q_t versus t. The Pseudo-first order model gave consistently low R^2 values and was therefore excluded.

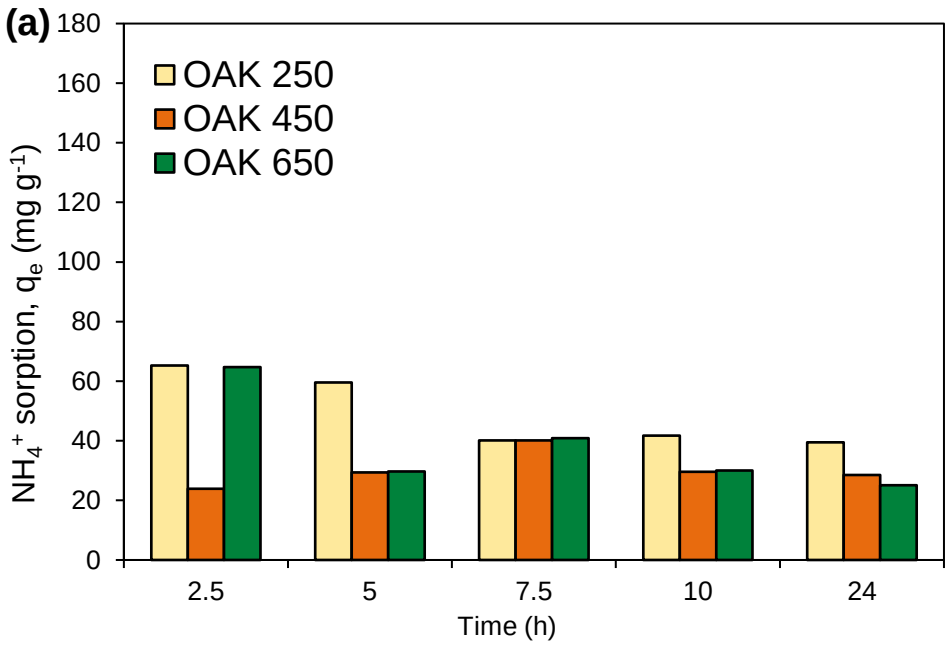

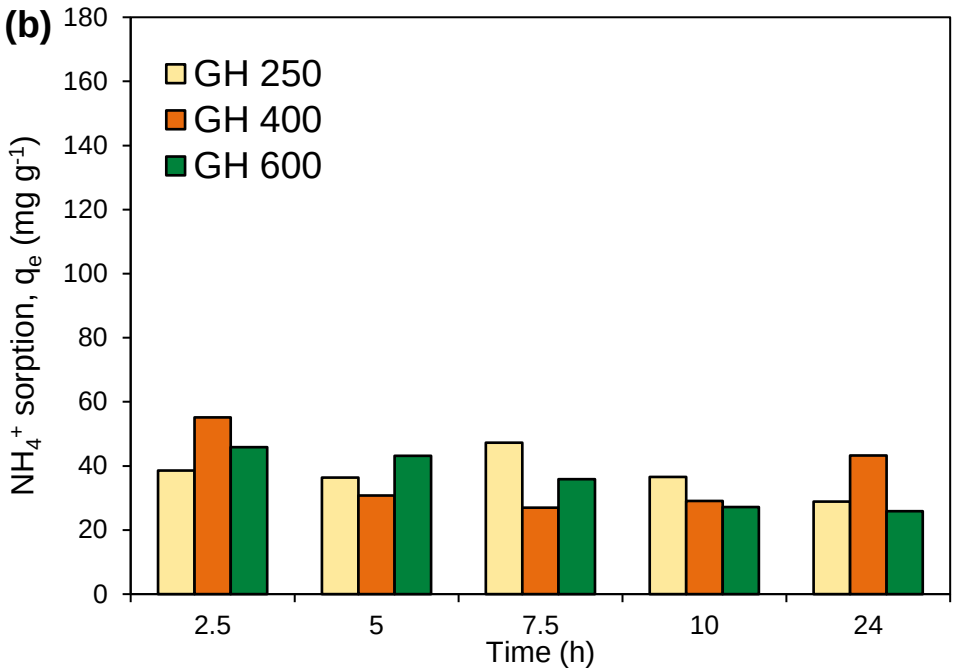

Figure 5.6 Adsorption kinetics of (a) oak and (b) greenhouse waste chars.

latter chars. For instance, both presscake and municipal waste biochars produced within 30 min had lower ammonium sorption capacities compared to those produced within 60 min. However, greenhouse waste biochars produced via gasification at 750°C (GH-FN 750) possessed marginally higher ammonium removal efficiency relative to GH 600°C. Conversely, ammonium sorption was marginally higher in most hydrochars and 400–450°C biochars compared to 600–650°C biochars thus the effect of treatment temperature was inconclusive. Yao et al. (2012) similarly found no trend between pyrolysis temperature and ammonium sorption. Char ammonium sorption capacities in this study were comparable to some reports in the literature for biochar. Wang et al. (2015a) reported 12.1–16.1% removal efficienciesof untreated and La-treated 300ºC biochars (initial ammonium concentration, C_o = 25.7 mg L^{-1}). Other studies reported higher ammonium removal efficiencies however: 37.3% sorption by activated phytoremediation plant char (C_o = 39 mg L^{-1}) in Zeng et al. (2013) and about 62–83% sorption by brewer's grains-sewage sludge biochar (C_o = 100 mg L^{-1}) in Zhang and Wang (2016).

Readily recoverable ammonium from post-sorption chars was determined using 0.01 M KCl, and a small number of chars were also extracted with 0.01 M $CaCl_2$ to compare the sorption capacity of both extractants. Ammonium desorption was found to be < 10 mg g^{-1} in both cases, thus desorbability ranged between 0.2–0.4. A number of studies also reported minimal ammonium release even when 1–2 M KCl

was used (Clough et al. 2013; Fernando et al. 2005; Jassal et al. 2015; Saleh et al. 2012). This may have resulted from a number of factors: ammonium was effectively trapped within the biochar pore structure (Clough et al. 2013) or organic matter (Fernando et al. 2005); ineffective extractants or extractant concentrations (Saleh et al. 2012); ammonia volatilization especially for high pH biochars (Wang et al. 2015b). Each of these possibilities were briefly explored in **Section 5.4.2**.

.

5.2.1.4 Possible mechanisms for char NH_4^+ sorption

Previous studies have reported a positive relationship between NH_4^+ sorption and adsorbent composition (acid functional groups, oxygen content, phenolic species associated with humic and fulvic substances, inorganic species) in addition to surface properties such as surface area (Canals-Batlle et al. 2008; Clough et al. 2013; Gai et al. 2014; Leuch et al. 2007; Fernando et al. 2005; Zeng et al. 2013; Zhang and Wang 2016). Thus the slightly lower NH_4^+ sorption capacities of the higher temperature (600–650°C) biochars was expected since NH_4^+ sorption capacities are often greater in chars produced at low temperatures due to their higher proportion of acid or oxygen functional groups (Bargmann et al. 2014; Spokas et al. 2012; Wang et al. 2015a; Zheng et al. 2010). Likewise, Zeng et al. (2013) noted that the disappearance of aromatic C=O and C=C, $-CH_2-$, CO and CC functional groups from a high temperature biochar (600°C) after NH_4^+ adsorption suggested that these functional groups reacted with NH_4^+. A positive relationship between biochar acid functional groups and ammonium sorption was also observed in Wang et al. (2015a) which corroborated earlier speculations by Zheng et al. (2010) that with increasing pyrolysis temperature, ammonium sorption decreased due to loss of biochar polar groups.

In addition to acid functional groups, other species present within chars have been found to enhance NH_4^+ sorption. For instance, the donation of lone pair electrons from N atoms to cationic adsorbent sites such as metal species occur at Lewis acid sites (Canals-Batlle et al. 2008; Le Leuch and Bandosz 2007; Petit and Bandosz 2009; Yin et al. 1999). Zhang and Wang (2016) recovered >60% NH_4^+ using a sewage sludge and Brewer's grains biochar partly due to the biochar composite's enhanced Mg and P content. In this study however, there was no correlation between % NH_4^+ sorption and char ash, P, Mg or Ca content.

Table 5.6 Ammonium sorption capacities of chars produced at standard conditions

Char	Negative surface charge ($mmol_c\ m^{-2}$)	$NH_4^+{}_{eq}$ ($mg\ g^{-1}$)	q_e ($mg\ g^{-1}$)	$\%NH_4^+$ ads.	K_d	Ammonium desorbed ($mg\ g^{-1}$)	Desorbability fraction
250°C hydrochars							
OAK	0.147	15.9	109.7 ± 14.1	12	0.12	n.d	0.00
GH	0.332	15.0	121.7 ± 0.3	13	0.13	4.8	0.03
MW	0.106	8.0	146.4 ± 5.8	14	0.16	4.0	0.03
PK	20.87	11.3	129.0 ± 19.5	13	0.15	4.2	0.03
GW	n.d	9.9	86.8 ± 27.1	8	0.09	n.d	0.00
400–450°C biochars							
OAK (Comm.)	0.003	10.7	100.9 ± 3.4	9	0.11	5.0	0.05
OAK	1.058	19.0	129.4 ± 34.8	13	0.11	5.0	0.05
GH	0.842	19.7	118.2 ± 26.9	12	0.13	4.8	0.04
MW	0.329	11.8	137.3 ± 0.6	13	0.15	3.0	0.02
PK	0.255	9.2	105.8 ± 11.5	9	0.11	4.0	0.04
GW	0.324	11.7	33.0 ± 17.3	3	0.03	2.2	0.02
600–650°C biochars							
OAK (Comm.)	0.003	13.8	114.4 ± 3.4	11	0.12	5.0	0.04
OAK	0.326	11.7	123.5 ± 28.7	12	0.16	n.d	0.00
GH	0.731	26.3	99.3 ± 28.5	10	0.11	n.d	0.00
MW	0.170	12.2	128.3 ± 6.7	13	0.14	2.8	0.02
PK	0.210	9.5	136.2 ± 18.1	13	0.15	2.2	0.02
GW	0.314	11.3	77.8 ± 33.6	8	0.08	3.8	0.01

Initial concentration (C_o) ≈1000 mg NH_4^+ L^{-1} (780 mg NH_4-N $L^{-1})^+$; OAK (Comm) and OW: reference & ECN oak wood respectively; GH: greenhouse waste; MW: Municipal waste; PK: presscake; GW: greenwaste. Desorbability = ratio of ammonium desorbed to ammonium adsorbed; n.d: not detected; n.a: unavailable data;

$NH_4^+{}_{eq}$ refers to the theoretical maximum amount of NH_4^+ a char can retain based on the number of cation exchange sites, since 1 $cmol_c\ kg^{-1}$ = 0.18 mg NH_4^+ per g char (alternatively, 1 $cmol_c\ kg^{-1}$ = 0.14 mg NH_4^+-N as frequently used in the literature, resulting in slightly lower $NH_4^+{}_{eq}$ values).

Table 5.7 Ammonium sorption capacities of chars produced at non-standard conditions

Char	Negative surface charge ($mmol_c\ m^{-2}$)	$NH_4^+{}_{eq}$ ($mg\ g^{-1}$)	q_e ($mg\ g^{-1}$)	% Ads.	K_d	Ammonium desorbed ($mg\ g^{-1}$)	Desor-bability fraction
PK 700 °C, 60 min, N_2	n.a	910.0[a]	99.3 ± 15.0	10	0.11	2.4	0.005
Gasification chars							
GH-FA 600°C (air)	0.654	8.2	80.6 ± 9.6	8	0.09	3.8	0.009
GH-FN 600°C (N_2)	0.588	7.4	57.5 ± 15.5	6	0.06	1.6	0.004
GH-FN 750°C (N_2)	0.018	9.2	101.8 ± 19.2	10	0.11	5.8	0.012
Pyrolysis chars (30 min, N_2)							
MW 600 °C, 30 min	0.127	13.7	92.6 ± 12.3	9	0.10	3.6	0.007
PK 600 °C, 30 min	0.079	4.4	100.1 ± 13.4	10	0.11	2.2	0.004
PM 600 °C, 30 min	0.416	14.2	127.1 ± 3.8	13	0.15	5.2	0.008
PM 700 °C, 30 min	n.a	n.a	52.1 ± 55.5	5	0.06	5.0	0.010
Pyrolysis chars (600 °C, 60 min, 1% O_2)							
MW 600 °C, 60 min	0.113	10.1	137.2 ± 3.1	14	0.16	3.6	0.005
PK 600 °C, 60 min	0.113	8.2	100.1 ± 15.8	10	0.11	4.6	0.010

Initial concentration (C_o) $\approx$1000 mg $NH_4^+\ L^{-1}$ (780 mg NH_4-N L^{-1}). GH-FA and GH-FN refer to greenhouse waste gasification biochars produced in air and N_2 resp.; n.a: unavailable data; 1 $cmol_c\ kg^{-1}$ = 0.18 mg NH_4^+ per g char; [a]based on single CEC of 55.5 $cmol_c\ kg^{-1}$.

Ammonium sorption onto soluble organic matter on char surfaces has also been suggested as a possible mechanism based on observations of increased ammonium adsorption in complex solutions (dairy or swine effluents) compared to simple solutions (ammonium chloride) (Fernando et al. 2005; Sarkhot et al. 2013) although the reverse effect has also been observed, as in Kizito et al. (2015). Moreover, Fernando et al. (2005) observed stronger soil retention of ammonium when leached with liquid slurry compared to pure ammonium solutions and suggested that dissolved organic carbon–soil complexes with ammonium were responsible. The liquid slurry comprised of different ions however, which may also have contributed to the observed differences. Fernando et al. (2005) further suggested that in certain conditions, organic matter might increase ammonium retention; in soils with high humic and fulvic acid content, complexes with

ammonium may be formed in alkaline conditions due to deprotonation of the carboxylic and phenolic groups within such species. Based on these findings, it was expected that chars with higher organic contents in this study would possess greater ammonium sorption capacities, and that oak hydrochars, previously found to possess the highest amounts of humic-like subtances (**Section 4.3.3**), would adsorb the most ammonium. Yet this was not the case, as no strong correlation between % ammonium sorption and char organic content was observed and the sorption capacities of oak hydrochar was similar to the other chars. This trend was observed even at lower initial ammonium concentrations; at about 43 mg L^{-1}, % ammonium sorption ranged from 15.1–23.3% in the order:

Oak 450 °C (9.2±0.2 mg g^{-1}) ≅ Oak 650 °C (8.9±0.8 mg g^{-1}) > Oak 250 °C (6.0±0.5 mg g^{-1})

An additional trend from the literature which was not observed in this study was the influence of surface area. Adsorbents with high surface areas are thought to possess better ammonium removal efficiencies (Ismadji et al. 2016) but char surface areas had little impact here as presscake and commercial oak biochars possessed similar ammonium sorption capacities in spite of very different surface areas (2.5 m^2 g^{-1} and 280 m^2 g^{-1} respectively). This suggested that physisorption/ion exchange was not a dominant mechanism for ammonium sorption. Similarly, as presscake hydrochar possessed the highest negative surface charge, it was expected that its ammonium sorption capacity would be highest but this was not the case; the general relationship between char negative surface charge and ammonium sorption was also very weak (Pearson r = 0.206). Similar results was also observed by Tian et al. (2016) who reported that ammonium sorption was negatively correlated with char BET surface area. Following solvent extraction, hydrochar sorption of ammonium increased in four of six hydrochars (**Figure 5.7**) as was observed for their CEC. A positive relationship between hydrochar oxygen content and ammonium sorption was also observed, with Pearson r = 0.962* (α=0.05 level) as opposed to Pearson r = -0.887 for un-extracted chars, but this relationship remained weak for the biochars.

Based on the number of cation exchange (negative) sites available on the chars, their theoretical maximum ammonium sorption capacities were calculated and presented as $NH_4^+{}_{eq}$ in **Table 5.6** which showed that CEC-predicted ammonium sorption was considerably lower than actual ammonium sorption for all the chars. Comparing the maximum ammonium sorption capacities as determined from Langmuir q_m values, this trend was also true for oak 250°C, oak 650°C and GH 400°C. Bolan et al. (2004), Jassal et al. (2015), Taghizadeh-Toosi et al. (2011b) and

Zeng et al. (2013) also observed that CEC underestimated actual ammonium sorption capacities. Jassal et al. (2015) and Zeng et al. (2013) attributed this discrepancy to physical sorption of N into char pores partly because the adsorbed ammonium was not readily extractable with 1 M KCl, which should have ensued if ion exchange had occurred (Jassal et al. 2015). Alternatively, Bolan et al. (2004) reported that both NH_4^+ and K^+ sorption capacities were comparable to CEC-predicted values for zeolites, while bark had higher ammonium sorption capacities than CEC-predicted values which the authors attributed to ion exchange in the former and ammonium conversion to organic nitrogen in the latter. In this study however, no strong relationship between char organic content and ammonium sorption was observed as aforementioned. On the other hand, Nguyen and Tanner (1998) observed maximum NH_4^+ sorption by zeolite to be substantially lower than CEC-predicted values.

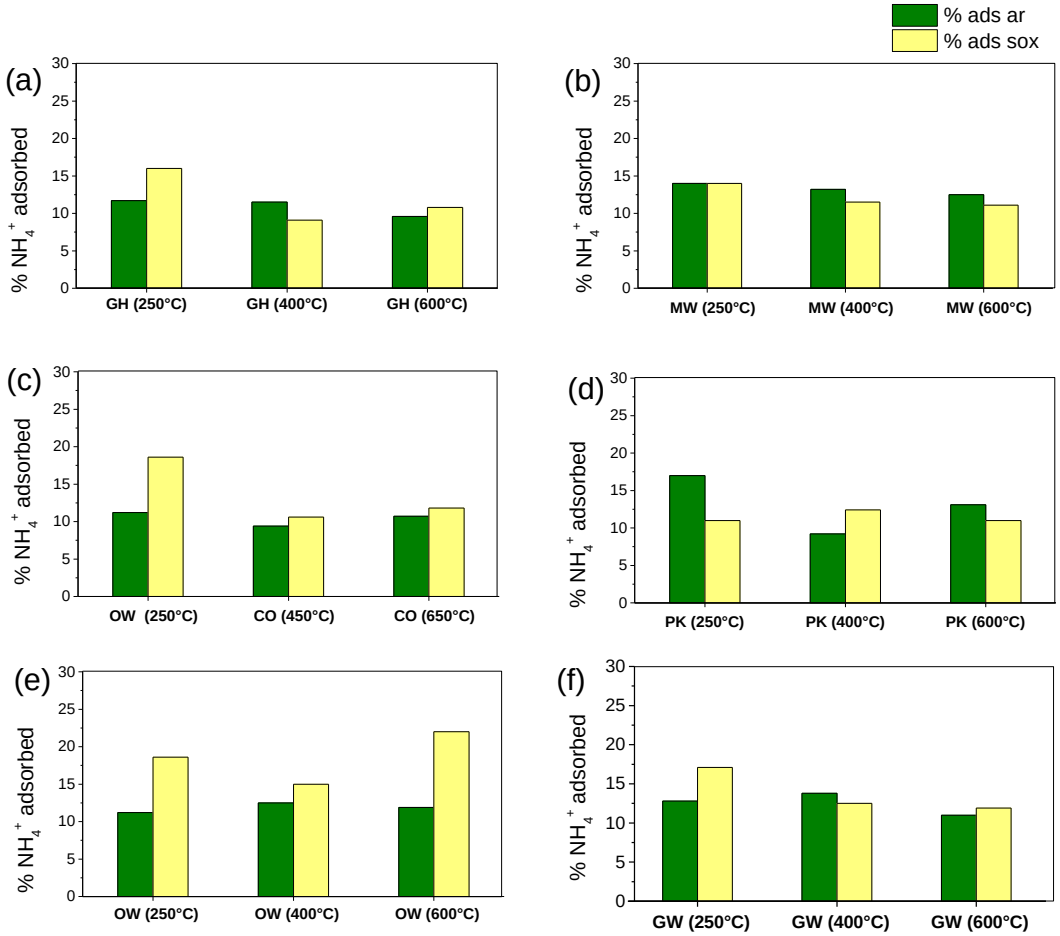

Figure 5.7 Ammonium sorption capacities of as-received and solvent extracted (sox) chars: a) GH: greenhouse waste; b) MW: municipal waste; c) CO: commercial oak; d) PK: presscake from AD; e) OW: oak wood; GW: greewaste chars.

Overall, as factors such as adsorbent composition, particle size and coexisting ions understandably influence adsorbent ammonium sorption (Bolan et al. 2004), these findings suggest that CEC is not always a reliable predictor of ammonium sorption.

5.3.2 Char phosphate sorption

Details on phosphate sorption experiments have been outlined in **Section 3.12.2**.

5.3.2.1 Adsorption isotherms

The phosphate sorption capacities of oak and greenhouse waste chars were compared at various phosphate concentrations as shown in **Figure 5.8**. Due to increasing concentration gradients, phosphate sorption (mg g^{-1}) increased with increasing initial phosphate concentration, resulting in better filling of reactive adsorption sites (Chen et al. 2013; Krishnan and Haridas 2008; Wang et al. 2011; Xue et al. 2009). However, Chen et al. (2013) and Wang et al. (2011) found that while mg phosphate^{-} sorption per gram of char increased with initial concentration, adsorption efficiency (i.e. removal ratio) decreased, possibly because fewer active adsorption sites were available at higher initial phosphate^{-} concentrations. This was also the case for chars in this study, with adsorption efficiencies (% sorption) highest at 170 mg PO_4^{3-} L^{-1} in most cases**.**

While pyrolysis temperature and feedstock composition did not affect char adsorption capacity substantially, hydrochars generally exhibited lower adsorption capacities. The linearized Langmuir isotherm models fitted to experimental data from 170–700 mg PO_4^{3-} L^{-1} did not fit the data for any of the chars, particularly as its adsorption constant (B) values were negative. Similarly, the linearised Freundlich isotherm model described the sorption mechanism only slightly better, based on R^2 values and a better agreement between experimental and calculated q_e values (

Table 5.8). Even oak 450°C, oak 650°C, and GH 400°C evaluated over a wider concentration range of 67–700 mg PO_4^{3-} L^{-1} (22–230 mg PO_4-P L^{-1}) possessed comparable R^2 values. From the literature, the Freundlich model is considered to suit phosphate sorption better; as adsorbents become saturated, adsorption affinity decreases exponentially (Sakadevan and Bavor 1998), or because precipitation reactions occur (Zeng et al. 2013). Conversely, the Langmuir model fitted better than Freundlich model in Wang et al. (2011) and Zeng et al. (2013), possibly due to biochar P release (Zeng et al. 2013).

Table 5.8 Phosphate sorption isotherm model data

Char	Langmuir			Freundlich			X^2 Lang	X^2 Freund
	q_m (mg g^{-1})	B (L mg^{-1})	R^2	K_F	n	R^2		
OAK 250	-4.2	-0.001	0.423	16.8	-2.3	0.594	-7.0	-9.5
OAK 450	-5.4	-0.003	0.898	0.0	0.6	0.860	-810.3	-0.1
OAK 650	-3.0	-0.003	0.886	0.0	0.5	0.862	-4442.4	-0.1
GH 250	1.3	-0.002	0.576	8.1	-3.3	0.125	138.7	-7.2
GH 400	6.3	-0.004	0.763	0.0	0.5	0.960	-1145.8	-0.1
GH 600	-2.4	-0.008	0.021	0.9	7.0	0.011	-25.5	-0.5

Linearized Langmuir and Freundlich parameters respectively obtained from inverse and log plots of C_e values of approximately 67, 170, 250, 500 and 700 mg PO_4^{3-} L^{-1} for oak 450°C, oak 650°C, and GH 400°C and the latter four concentrations for other chars.
X^2 Lang and X^2 Freund refer to Chi-square values of q_e calculated from Langmuir and Freundlich parameters respectively.

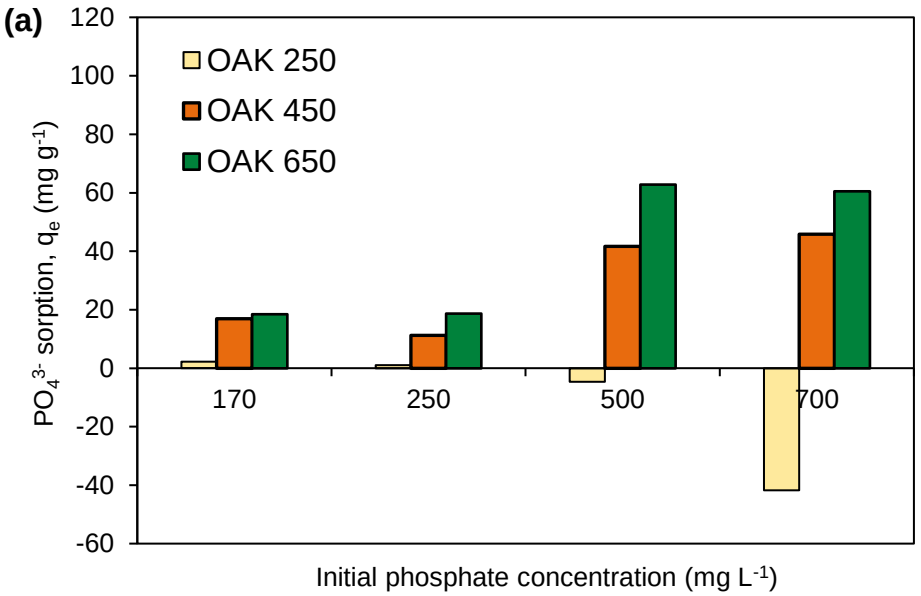

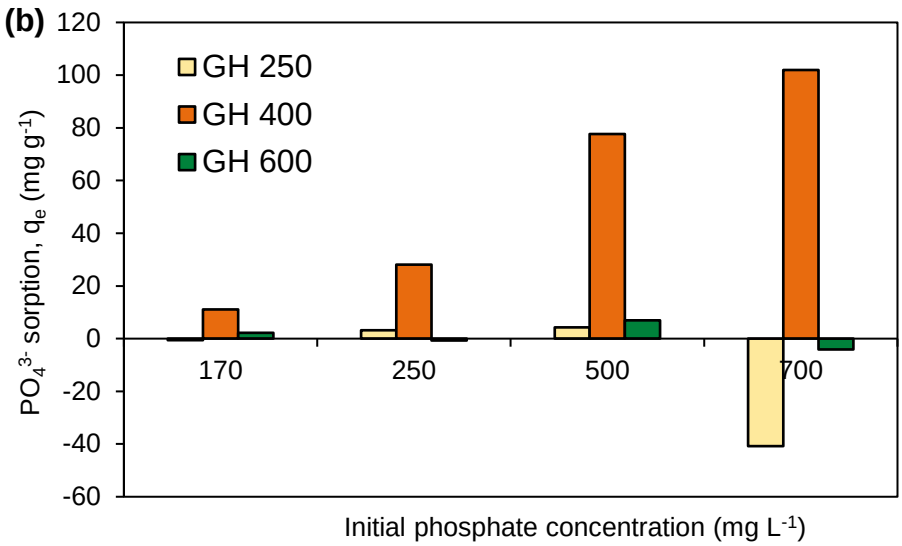

Figure 5 8 Effect of increasing concentration phosphate sorption in chars from (a) oak (b) greenhouse waste.

5.3.2.2 Adsorption kinetics

Oak chars reached maximum, phosphate sorption after 5 h while this took slightly longer for the greenhouse waste chars produced at 250°C and 600°C (**Figure 5.** 9). Other studies have reported far shorter maximum sorption times of 5 min (Ye et al. 2015) and 30 min (Su et al. 2013). Ye et al. (2015) similarly found that adsorption of PO_4^{3-} onto acid-treated red mud (rich in iron and aluminium oxides) occurred very rapidly, wherein over 90% sorption occurred within the first 5 min and then slowed until equilibrium was reached, presumably after 20 min. On the contrary, other studies showed that adsorption equilibrium was attained after 24 h at room temperature (Wang et al. 2011; Zhang et al. 2012). Su et al. (2013) demonstrated that with an increase in initial solution concentration, time to reach equilibrium increased, 8 h in their case. Due to such variations, adsorption tests were maintained at 24 h in this study. Here, oak char kinetics followed a more predictable pattern than greenhouse waste biochars. fitted to kinetic models showed that the pseudo-second order model consistently gave a closer fit compared to the pseudo-first order and intra-particle diffusion models based on linear regression analysis (**Table 5.9**) although k_2 values were negative possibly due to phosphate release in at some initial (C_o) concentrations. Previous studies have also observed many metals and heavy elements follow this pattern (Limousin et al. 2007). Wang et al. (2011) also found this model fitted better than the intra-particle diffusion model but

also suggested that simultaneous rapid surface sorption of phosphate and slower intra-particle diffusion through the adsorbent occurred simultaneously.

Table 5.9 Adsorption kinetics model parameters

Char	Pseudo-Second order				Pseudo-First order R^2	Intraparticle Diffusion R^2
	$q_{e\ exp}$ (mg g^{-1})	$q_{e\ cal}$ (mg g^{-1})	k_2 (min g mg^{-1})	R^2		
OAK 250	9.41	8.22	-0.0006	0.980	0.870	0.773
OAK 450	24.08	22.62	-0.0005	0.996	0.548	0.009
OAK 650	24.14	22.17	-0.0004	0.995	0.758	0.369
GH 250	18.06	17.12	-0.0005	0.969	0.434	0.103
GH 400	16.57	15.13	0.0003	0.651	0.090	0.022
GH 600	28.24	27.78	0.0166	0.981	0.068	0.696

$q_{e\ exp}$ and $q_{e\ cal}$ refer to amount of phosphate adsorbed by biochars obtained from experimental data and from plots respectively. For Pseudo-second order model, all parameters obtained from plot of t/q_t versus t. The pseudo-first order model generally had higher R^2 values than the first order model.

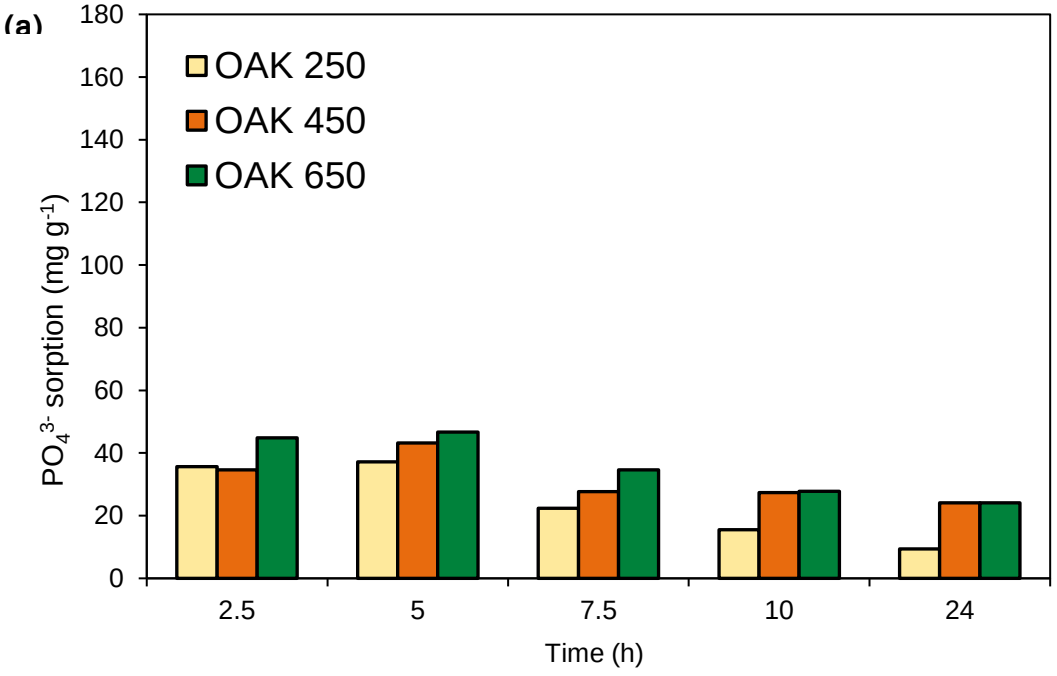

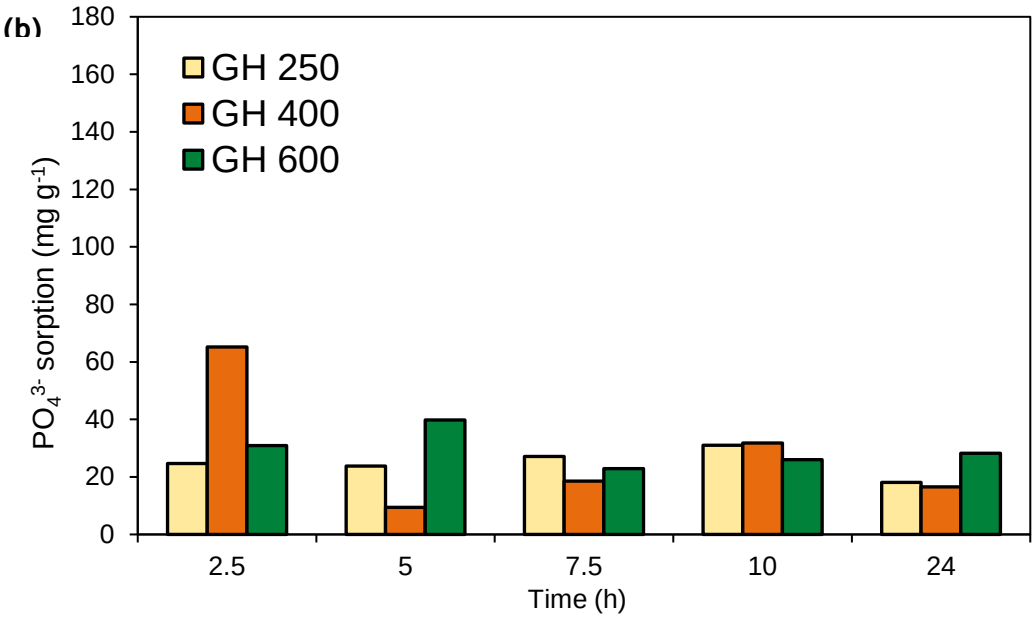

Figure 5. 9 Phosphate sorption kinetics for (a) oak and (b) greenhouse waste chars.

5.3.2.3 Char phosphate sorption at 400 mg L^{-1}

Char adsorption tests were performed at about 400 mg PO_4^{3-} L^{-1} (about 130 mg PO_4-P $^{L-1}$) to evaluate the proportion of phosphate removed by other chars in this study, using a char/solution ratio of 1 kg char m^{-3}, as presented in **Table 5.10**. Most results had coefficients of variation < 5% but greenhouse waste samples consistently showed much higher percent variations, likely due to sample heterogeneity. Phosphate release occurred in hydrochars derived from greenhouse waste and presscake and 450°C oak biochar. Such release has also been observed in low and high temperature biochars elsewhere (Zeng et al. 2013). phosphate sorption capacity increased with pyrolysis temperature with the exception of commercial oak and greenhouse waste biochars. This is in agreement with findings of Wang et al. (2015a) who observed an increase in phosphate asorption with pyrolysis temperature up to a certain point (500°C). Phosphate release from some chars at certain concentrations did not appear to be due to char P content, as extraction of chars with water to ascertain water-soluble phosphate showed that oak hydrochars and commercial oak biochars produced at 450°C and 650°C respectively released 1.18 ± 0.04, 0.55 ± 0.00 and 1.19 ± 0.03 mg g^{-1} PO_4^{3-} while greenhouse waste biochars produced at 400°C and 600°C released 2.1 ± 0.1 and 3.5 ± 0.2 mg g^{-1} phosphate, respectively. On the other hand, char P might not

always be completely extractable with concentrated acid (Mukherjee and Zimmerman 2013) or by water.

Recoverable phosphate, obtained by desorbing chars with 0.01 M KCl was minimal hence phosphate the ratio of desorbed phosphate to total adsorbed phosphate (desorbability) could not be determined in all but two biochars. Xue et al. (2009) and Ye et al. (2006) also found that basic oxygen furnace slag and palygorskite adsorbents respectively did not desorb a lot of phosphate regardless of initial phosphate concentration, although desorbabilty increased to some extent with an increase in amount of adsorbed phosphate. Low phosphate desorption might have been because the extracting solution (0.01 M KCl) was insffiecient; for instance, while salt solutions of KCl or $NaNO_3$ are frequently used as extractants, Su et al. (2013) found that phosphate release was most effective when using high pH solutions such as 0.1 M NaOH. On the other hand, easily desorbed phosphate would have suggested physical adsorption rather than strongly bound (chemical) sorption (Xue et al. 2009).

5.3.2.4 Possible reaction mechanisms for char phosphate sorption

Phosphate sorption has been reported to occur via physical (ion-exchange) and chemical (chemisorption) reactions. Generally, char phosphate sorption capacities in this study were found to be lower than other adsorbents, but some positive correlation between phosphate sorption and Ca or Mg contents were observed in hydrochars and biochars, and to a lesser degree with ash content. Xue et al. (2009) also found that adsorbent chemical composition was most influential, leading to simultaneous chemical precipitation and ligand exchange between adsorbent and phosphate. Furthermore, Yao et al. (2011) compared biochars produced from raw and from anaerobically digested sugar beet tailings and found that phosphate sorption capacities increased in the latter biochars possibly due to the presence of surface MgO as this compound was absent in the former. Studies like Su et al. (2013) further established that phosphate sorption occurred via inner-sphere complex reactions, based on increases in phosphate sorption with increasing ionic strength and from differences in adsorbent iso-electric point before and after sorption.

Table 5.10 Char phosphate sorption capacities

Char	q_e (mg g^{-1})	% PO_4^{3-} ads.	K_d	Desorbed (mg g^{-1})
250°C hydrochars				
Oak wood	26.6 ± 10.3	6.28	0.07	n.d
Greenhouse waste	-9.6 ± 7.6	0.00	-0.02	n.d
Municipal waste	5.1 ± 3.8	1.21	0.01	n.d
Presscake from AD	37.0 ± 7.1	9.41	0.10	n.d
Greenwaste	9.6 ± 11.2	2.22	0.02	n.d
400–450°C biochars				
Oak wood (commercial)	-0.3 ± 6.1	0.00	-0.001	n.d
Oak wood	5.5 ± 19.0	1.33	0.01	n.d
Greenhouse waste	18.7 ± 1.9	4.42	0.05	n.d
Municipal waste	11.9 ± 4.3	2.76	0.03	n.d
Presscake from AD	7.8 ± 1.4	1.81	0.02	n.d
Greenwaste	-10.3 ± 6.8	0.00	-0.02	n.d
600–650°C biochars				
Oak wood (commercial)	15.1 ± 5.9	3.64	0.04	n.d
Oak wood	3.6 ± 6.1	0.86	0.01	n.d
Greenhouse waste	9.1 ± 6.5	2.14	0.02	8.5
Municipal waste	14.3 ± 0.6	3.46	0.04	n.d
Presscake from AD	30.0 ± 24.9	6.97	0.08	n.d
Greenwaste	13.1 ± 13.7	3.17	0.03	n.d

Initial PO_4^{3-} $C_o \approx 400$ mg L^{-1}; n.d: not detected.

Other cations including Ca^{2+}, Al^{3+} and La are known to increase phosphate sorption as well (Bolan et al. 2004; Wang et al. 2015a; Xue et al. 2009; Yao et al. 2013; Ye et al. 2015; Zeng et al. 2013), particularly if they are present as basic functional groups. Wang et al. (2015a) for instance observed that biochar phosphate sorption capacity was a function of ketones, pyrones and chromens based on a positive

correlation of these groups with phosphate removal efficiency, although R^2 values of 0.73 suggested that these groups were not solely responsible. As such, phosphate sorption mechanisms are thought to be dependent on metal ion reactions (precipitation, surface deposition), surface area and surface functionality (Wang et al. 2015a; Yao et al. 2013; Zeng et al. 2013). Other studies however suggested that since biochars tend to be negatively charged, surface functionality may not influence phosphate sorption a great deal (Yao et al. 2011; Zeng et al. 2013) although Su et al. (2013) suggested that adsorbent OH^- groups interact with phosphate. Phosphate sorption capacity was better at lower solution pH in Wang et al. (2012) however, owing to the presence of more positively charged atoms (H^+) on adsorbent surfaces of Fe-treated activated carbons.

The influence of biochar surface area on phosphate sorption is unclear but some studies suggest that its influence may be minor compared to adsorbent elemental composition. Wang et al. (2015a) for instance found that the best performing biochars did not possess superior surface areas compared to other biochars. Conversely, despite similar mineral contents in presscake biochars produced at varying slow pyrolysis conditions in this study, greater sorption of phosphate was observed following pyrolysis at shorter residence times (PK-30) and in the presence of 1% O_2 (PK-1%) compared to presscake biochars produced at standard conditions (PK) as shown in **Figure 5.10(a)**. With q_e values of 47.2 ± 32.3 mg g^{-1} and 66.3 ± 0.63 mg g^{-1} for PK-30 and PK-1% respectively, a positive relationship between surface area and phosphate sorption was observed:

PK 600 (2.5 m^2 g^{-1}) < PK-30 (3.1 m^2 g^{-1}) < PK-1% (4.0 m^2 g^{-1})

Differences in thermochemical processing also influenced phosphate sorption in greenhouse waste biochars (**Figure 5.10(b)**). In this case however, the relationship between biochar surface area and phosphate sorption was not as clear between greenhouse waste biochars produced at standard conditions (GH 600) and non-standard conditions (GH-FA 600, GH-FN 600 and GH-FN 750 corresponding to gasification in air at 600 °C, N_2 at 600°C and 750°C respectively) with similar mineral contents:

GH-FA 600 (0.7 m^2 g^{-1}) < GH 600 (2.0 m^2 g^{-1}) < GH-FN 600 (0.7 m^2 g^{-1}) < GH-FN 750 (29.0 m^2 g^{-1})

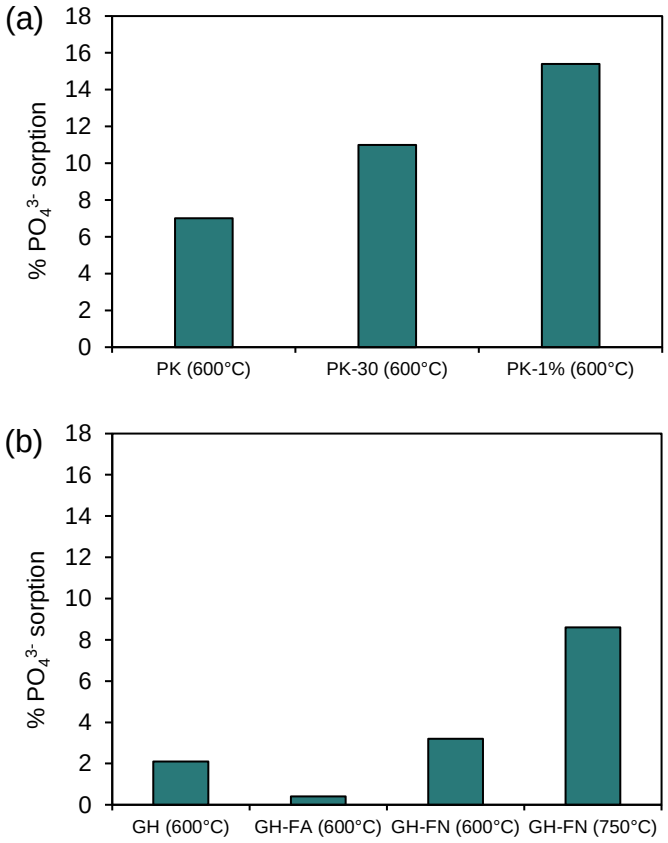

Figure 5.10. Comparison of phosphate sorption capacities of (a) presscake produced at standard conditions (**PK**), slow pyrolysis at 600°C for 30 min (**PK-30**) and slow pyrolysis in 1% O_2 at 600°C, 60 min (**PK-1%**); (b) greenhouse waste biochars produced via slow pyrolysis (**GH**), gasification in air (**GH-FA**), and gasification in N_2 (**GH-FN**).

Solvent extraction had variable effects on char phosphate sorption (**Figure 5.11**). For all but one hydrochar (presscake), solvent extraction (denoted as 'sox') increased phosphate removal efficiencies. Phosphate removal efficiencies also increased in 4 of 6 low temperature biochars (400–450°C); 400°C oak biochar which released phosphate into solution prior to extraction performed marginally better after extraction. It is currently unclear whether such increases may have been due to the creation of more sites for phosphate sorption. However, for four of the six biochars produced at 600–650°C, solvent extraction decreased % sorption capacity.

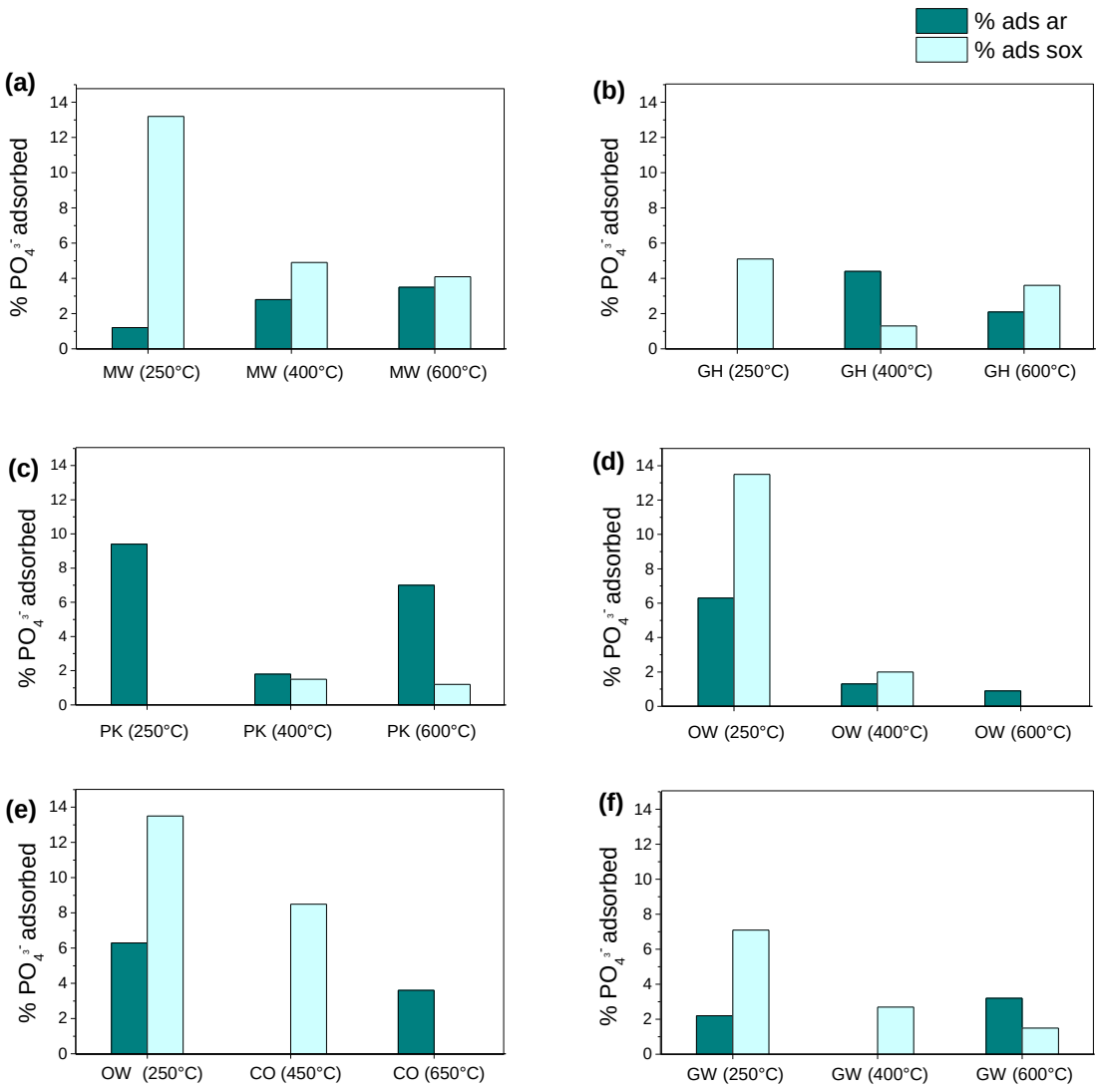

Figure 5.11 Comparison of PO_4^{3-} sorption capacities of as-received and solvent extracted ('sox') chars: a) **MW**: municipal waste; b) **GH**: greenhouse waste; c) **PK**: presscake; d) **OW**: oak wood; e) **CO**: commercial oak; f) **GW**: greenwaste biochars.

Finally, with regard to method suitability, various methods have been used to estimate char ammonium and phosphate sorption, ranging from flow analysis, ion chromatography to colorimetry/spectrophotometry. Owing to the number of samples to be analysed, batch-wise IC analysis was performed. In addition to calibration standards, each batch included reference biochars (*Proininso* oak 450°C and 650°C). Blank ammonium and phosphate solutions were analysed alongside samples to confirm that no losses occurred due to volatilisation. Results showed that while phosphate$^-$ results were consistent when using ion chromatography, ammonium determination appeared to be partly affected by eluent conditions or by residual ammonium carried-over from previously analysed sample regardless of the deionised water samples run after every four samples.

5.4 Char ammonia sorption capacity

Batch ammonia sorption tests as described in **Section 3.12.3** were performed as a simple means of screening char ammonia sorption capacity and comparing batch sorption tests with ammonia emissions reduction during laboratory-scale co-composting. Equivalent ammonia sorption capacities were calculated by converting the increase in total nitrogen to NH_3 using a conversion factor of 1.21.

5.4.1 Char ammonia sorption during batch sorption tests

The ammonia sorption profiles of oak and greenhouse waste hydrochars and biochars are presented in **Figure 5.13** for ammonia levels equating to (a) 43 mg and (b) 450 mg NH_3. The different conditions were used to assess the influence of concentration of N species on sorption capacity and to simulate low to high levels of N species that may be present in real-case scenarios. For oak, the increase in total N content after exposure to 43 mg ammonia was 11.0±0.4 mg g^{-1} for the biomass and between 0.58–15.4 mg g^{-1} for the chars. Char sorption was comparable to those observed in previous studies. For instance, Taghizadeh-Toosi et al. (2012a) reported an average increase of about 6.7±0.6 mg g^{-1}. **Figure 5.13(a)** indicated that the % sorption of ammonia was higher for the hydrochar than the respective biochars (45% and < 10% respectively), equivalent to 18.8 mg g^{-1} for the hydrochar and < 1 mg g^{-1} for oak 650°C.

The comparable ammonia sorption capacity of the raw feedstock with the hydrochar appeared to be independent of the inorganic concentrations present as **Figure 4.1** showed that oak biomass possessed a lower mineral content compared to all the chars. Moreover, minerals such as Mg and P would perhaps need to be present in soluble form to facilitate ammonium sorption similar to that observed by Zhang and Wang (2015). Boron contents were highest in the unprocessed Oak and hydrochar however, which are known to be good sites for ammonia (Doonan et al. 2010). Ammonia sorption by both samples were slightly higher when using the higher initial ammonia concentration (450 mg L^{-1}), with the hydrochar still maintaining a higher capacity than the biochar (c.f. 28.5 mg g^{-1} for the hydrochar and 8.1 mg g^{-1} for oak 650°C). For greenhouse waste samples, an entirely different trend was observed (**Figure 5.12(c)**); greenhouse waste hydrochar, which possessed the highest nitrogen content, released the most total nitrogen followed by GH 600°C.

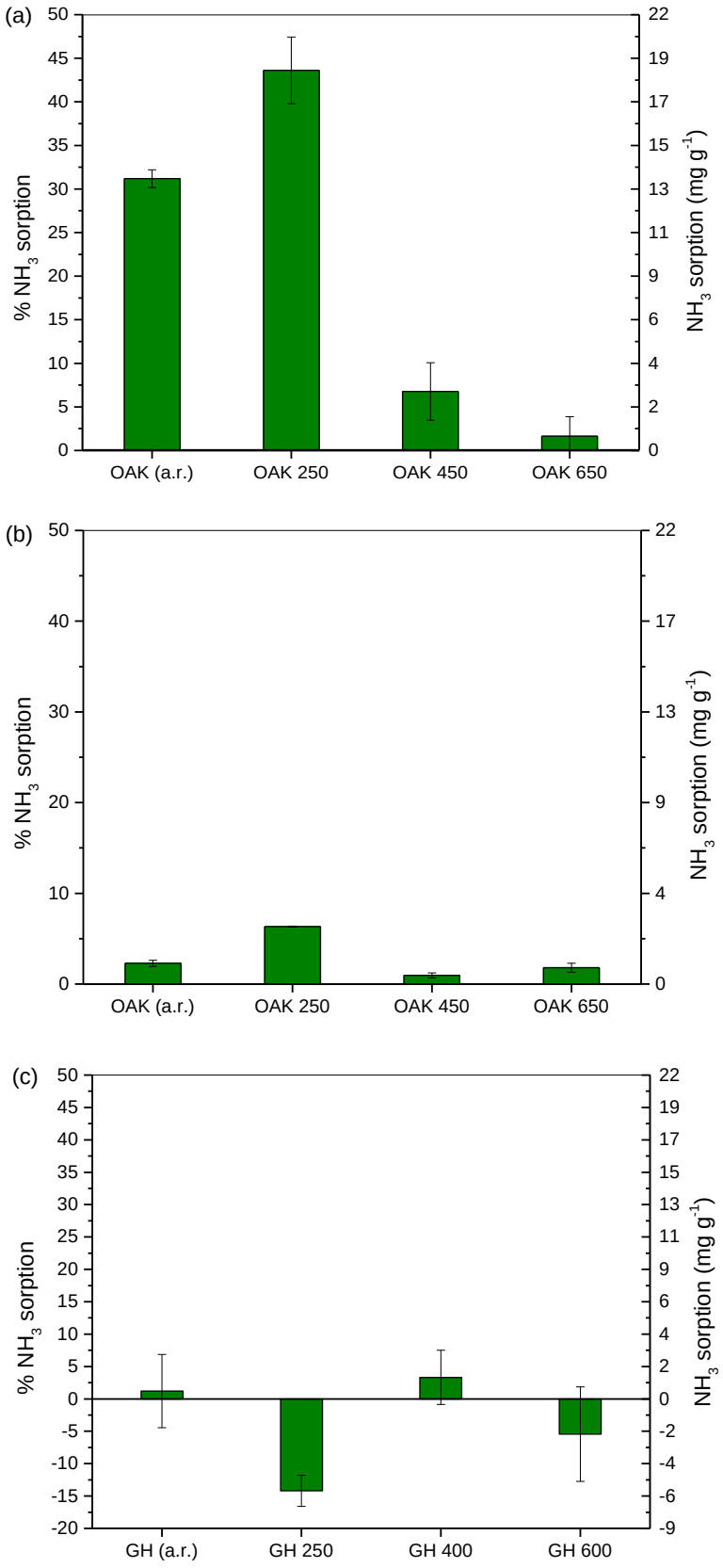

Figure 5.12 Effect of increasing ammonia concentration on the performance of oak chars: (a) hydrochar and biochar uptake at about 43 mg NH_3; (b) hydrochar and biochar uptake at about 450 mg NH_3; (c) greenhouse waste at about 43 mg NH_3.

Figure 5.13 shows the change in ammonia sorption for the hydrochar with increasing ammonia concentration indicating that while a greater capacity was attained at higher initial ammonia concentration, the % sorption reduced considerably, suggesting that while sites were available for ammonia sorption even at 1500 mg ammonia, its removal efficiency was greatly reduced. Ammonia sorption appeared to start levelling off at higher concentration suggesting a maximum sorption in the order of 40–50 mg g^{-1} ammonia for the hydrochar. Also notable was the fact that the hydrochar ammonia sorption capacities were higher than their ammonium sorption capacities, whereas for the biochars, the opposite was true. This might be linked to the increased surface area and porosity of the biochars compared to the hydrochar, and the propensity of the former chars for water retention.

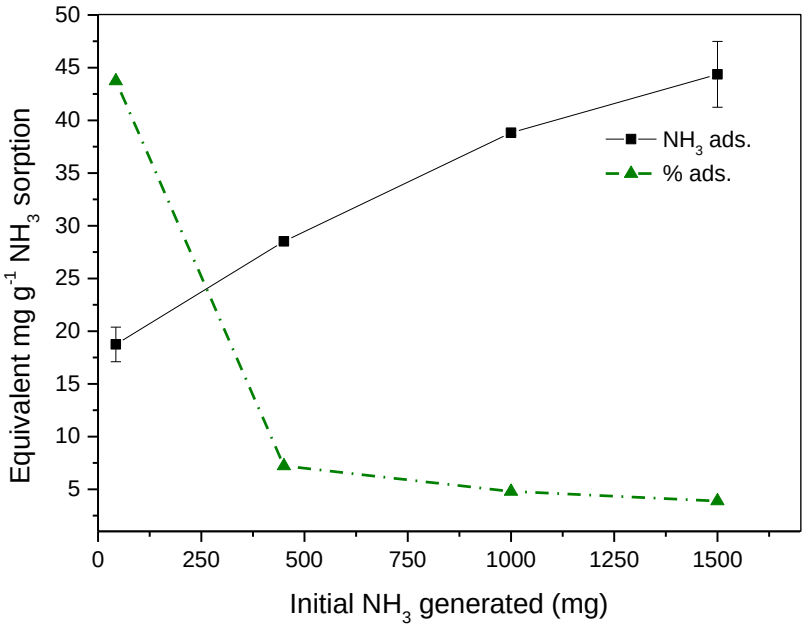

Figure 5.13 Hydrochar uptake over a range of about 43–1500 mg NH_3 generated according to Equation (3.26) and analyses performed in duplicate. To obtain equivalent NH_3 sorption capacities, increases in total nitrogen contents multiplied by N to NH_3 conversion factor of 1.21.

Further analyses revealed more differences between oak and greenhouse waste samples: a comparison of the two sets of biomass and hydrochars showed that exposure to ammonia resulted in some increase in NO_3^- for greenhouse waste hydrochar whereas no similar increase was detected in the oak hydrochar (**Figure 5.14**(**a**)). Furthermore, analysis of oak and greenhouse waste hydrochars which were subjected to NaOH treatment in order to extract humic-like substances

showed that NaOH extraction decreased the ammonia sorption capacity of oak hydrochar presumably due to loss of humic and fulvic-like substances (**Figures 4.12 (c)** and **(d)**). The reverse was however observed for the greenhouse waste hydrochars; while elemental analysis showed that less nitrogen was present in the hydrochar following exposure to ammonia gas, both ammonium and nitrate contents increased (**Figure 5.14**) in spite of the fact that both analyses were performed within the same period (within 24 h). Ammonia sorption experiments performed on a different batch of GH 250°C hydrochar prepared under the same conditions but on different days revealed a similar result. The most feasible explanation for this discrepancy might be linked to its high nitrogen content (3.0±0.3%), as ammonia sorption tests using microalgae biomass with a high nitrogen content (7.5±0.4%) also exhibited similar sorption capacity. It was therefore speculated that upon exposure to ammonia, nitrogen forms in some high-nitrogen samples might be transformed into less stable forms thus becoming volatilized at elevated temperatures; in this case, greater N losses following elemental analysis at temperatures >900°C compared to samples prior to ammonia exposure. In-depth investigations are required to confirm this however.

The high nitrogen content of GH 250°C might also explain why its sorption capacity increased following extraction with both NaOH and toluene, in spite of the fact that the former treatment is known to decrease char and biomass ability to adsorb ammonia (Dorward et al. *in prep.*). After both treatments, char nitrogen content decreased from about 2.8% to < 1.8% which suggested that high nitrogen samples might not be suitable for ammonia recovery although further studies on other high nitrogen samples are required to confirm this.

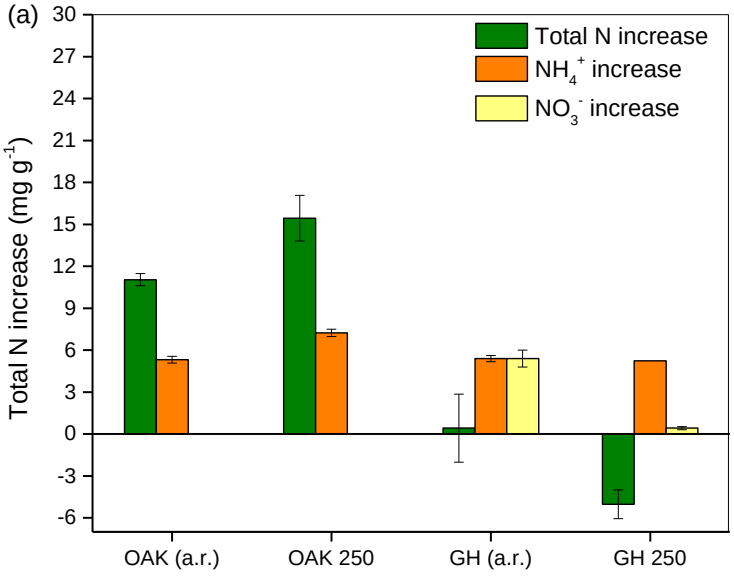

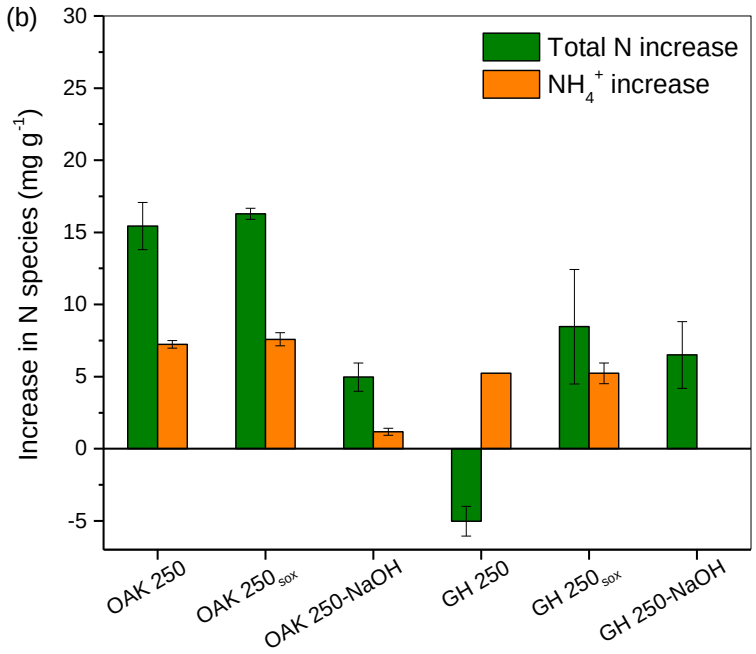

Figure 5.14 (a) Increase in total nitrogen content in oak and greenhouse waste hydrochars exposed to 43 mg NH_3 for 7 d; (b) effect of alkali (NaOH) and organic solvent ('sox') extraction on the NH_3 uptake capacities of oak and greenhouse waste hydrochars. Total N determined by elemental analysis and NH_4 from IC and differences before and after sorption calculated accordingly.

5.4.2 Recoverable nitrogen

Whilst the levels of ammonia sorption listed in **Table 5.11** indicated an increased sorption for hydrochar, subsequent washing of the chars in $CaCl_2$ did not release the entire adsorbed N. $CaCl_2$-extractable ammonium contents were highest for the hydrochar and generally decreased in proportion to ammonia gas concentration exposure. Following exposure to 1000 mg and 1500 mg ammonia, only 6.7±0.3 and 8.6±2.0 mg of ammonium was recoverable per gram of oak 250°C hydrochar respectively. For NH_3 sorption, both concentrations showed a similar trend and indicated that typically 30–40% of the N was released upon washing with $CaCl_2$ in form of ammonium. Taghizadeh-Toosi et al. (2012a) similarly observed that 2 M KCl-extractable ammonium represented only a fraction of the increase in total N following exposure to ammonia.

Further investigations are required to confirm whether even more ammonium can be recovered with serial extractions using 2 M KCl and water (Haider et al. 2016; Wang et al. 2015b), although N species other than inorganic N may be present in post-

ammonia sorption chars (Taghizadeh-Toosi et al. 2012b) which are not easily recoverable with such extractants. For instance, Petit et al. (2010) showed that ammonia retention in form of amines is also possible, and extensive studies by Thorn and Mikita (1992) on ammonia fixation by organic matter presumably at ambient temperatures suggested that matter rich in phenolic and hydroxyl groups are likely to retain ammonia in form of heterocyclic nitrogen (indole, pyrrole, pyridine). As $CaCl_2$-extractable ammonium is considered plant-available (Houba et al. 1986; Lazányi and Loch 2006), these results suggest that hydrochar may be the most beneficial in terms of release of N in soils or soil amendment products. No changes in nitrate were observed following ammonia sorption tests in either oak hydrochar or biochars in agreement with the findings of Taghizadeh-Toosi et al. (2012a,b).

Table 5.11 Untreated (as-received) char NH_3 and NH_4^+ sorption and release profile

Char	NH_3 sorption (mg g^{-1})	$CaCl_2$-extractable NH_4^+ (mg g^{-1})	NH_4^+ sorption (mg g^{-1})	NH_4^+ desorbed (mg g^{-1})
	[a]43 mg NH_3		43 mg NH_4^+ L^{-1}	
OAK 250	18.8±1.6	7.2±0.3	6.0±0.5	0.0±0.0
OAK 450	2.9±1.4	1[b]	9.2±0.2	1.1±1.6
OAK 650	0.7±0.9	1[b]	8.9±0.8	0.0±0.0
	[a]450 mg NH_3		450 mg NH_4^+ L^{-1}	
OAK 250	28.5±0.3	6.1±0.8	45.1±1.7	9[b]
OAK 450	4.3±1.2	2.68±0.04	29.9±1.8	12[b]
OAK 650	8.1±2.2	2.1±0.1	32.7±6.7	11[b]

[a]43 and 450 mg NH_3 generated based on Equation (3.36); [b]single analyses reported while other values are reported as mean sorption ± standard deviation; undetected NH_4^+ concentrations reported as zero.

5.4.3 Small-scale co-composting with chars: Effect on NH_3 and CO_2 emissions

Details on the co-composting experimental setup have been provided in **Section 3.12.1**. **Table 5.12** summarises the elemental content and pH of the 200 g (db) control the mixture comprised of 60% commercial multipurpose compost (particle size $\leq$ 4.75 mm) and 40% shredded savoy cabbage ($\leq$ 9.50 mm), the latter added as a source of nitrogen. Identical mixtures were amended with 15% char to give a total mass of about 235 g (db). However, the compost used for tests with oak 450°C and oak 650°C was of a different brand to the batch used for other chars, and even

though the same ratios of chars and cabbages were maintained in all cases, direct comparisons between the two batches were therefore not possible. Controls from both batches predictably showed an increase in pH with the addition of the biochars while hydrochar addition had the opposite effect. After 17 days of composting, pH increased in all cases, while moisture content of the mature mixtures decreased despite maintaining a steady flow of humidified air. C/N ratios expressed on mass basis for the starting materials ranged from 18.1–28.7, and generally decreased after the composting process.

Table 5.12 Characteristics of composting mixtures

Sample	C (%)	N (%)	C/N mass ratio	pH
Prior to composting				
OAK 450	24.5±4.9	0.9±0.1	19.0	6.5±0.1
OAK 650	14.2±4.4	0.7±0.2	26.1	6.5±0.6
Control 2	37.1±0.8	2.1±0.1	19.2	6.0±0.6
OAK 250	46.6±2.7	1.6±0.0	18.1	5.7±0.1
GH 250	42.2±0.2	2.2±0.0	28.7	5.5[a]
GH 600	43.6±1.1	1.6±0.1	19.5	6.4[a]
After composting				
Control 1	9.0±0.8	0.5±0.0	17.7	7.2±0.4
OAK 450	18.3±1.3	0.8±0.2	22.1	7.5±0.0
OAK 650	9.5±2.4	0.6±0.1	15.9	7.2±0.1
Control 2	33.7±0.5	1.8±0.0	18.5	6.8±0.1
OAK 250	42.8±1.8	1.6±0.1	26.7	6.3±0.1
GH 250	41.8±1.9	2.2±0.1	18.8	7.2±0.1
GH 600	44.0±5.4	1.5±0.4	29.6	7.5±0.1

C and N values average (n=4) ± SD; pH values read after shaking a 1:5 w/v mixture and average (n=2) ± SD reported; [a]single analysis performed only.

5.4.2.1 Ammonia emissions

To ensure sufficient generation of ammonia, composting was maintained at 50°C as studies have shown that ammonia volatilization commences at temperatures >45°C and high pH levels, also being within the temperature range which microbes flourish (Epstein 1997). Ammonia and carbon dioxide generated during the composting

process are shown in **Figure 5.15** and **Figure 5.16**, respectively. Ammonia emissions peaked at 2–3 days of composting in mixtures amended with oak 450°C and oak 650°C while controls within the same batch still had slightly elevated ammonia emissions until after 6 days of composting. In the second batch, maximum ammonia emissions were observed around 6 days of composting for mixtures amended with oak 250°C, GH 250°C and GH 600°C while the associated control peaked around 8 days. This time difference between both controls and indeed the quantities of ammonia released from both composting batches was likely a function of the starting compost characteristics.

Malińska et al. (2014) reported lower ammonia emissions in biochar-amended feedstocks relative to un-amended feedstocks during the first week, but an increase by the second week. With the exception of GH 600°C, all chars resulted in some decrease in ammonia, with the greatest reduction observed for hydrochar-amended mixture and showed no signs of increasing in subsequent days. **Figure 5.15** showed that feedstocks co-composted with oak 650°C had slightly lower ammonia emissions than mixtures amended with oak 450°C, in agreement with the lower surface area and CEC in the latter. On the other hand, oak 250°C which possessed a far lower surface area relative to both oak 450°C and oak 650°C outperformed both biochars, suggesting that surface area was not a factor behind the lower sorption capacity of oak 450°C. Chen et al. (2010) attributed reduction in total kjehldahl nitrogen losses to the high specific surface area and microporosity of bamboo charcoal while the organic acids present in bamboo vinegar neutralised ammonia generated from the composting sample. Corre et al. (2013) however suggested that surface acidity influenced the adsorption of ammonia on carbon-graphene composites more significantly than surface area and micro-pore volume. While all the chars in this study possessed comparable ammonium sorption capacities, Langmuir q_m values over a range of initial ammonia concentrations showed that ammonia sorption capacity followed the order: OAK 250 > OAK 650 > GH 250 > GH 600 > OAK 450 (**Table 5.4**) which reflected the magnitude of ammonia emission reduction relative to the controls during co-composting to some extent.

This small-scale composting study would have benefitted from a comparison of the mixtures' inorganic N contents at the start and end of composting to determine the organic and inorganic nitrogen species present in the chars, as this may have explained why differences between batch ammonia sorption tests and composting tests were observed for the greenhouse waste hydrochar while both experimental

tests were comparable for the other chars. Furthermore, while this study was primarily aimed at assessing hydrochar and biochar potential for minimising ammonia emissions while co-composting, additional analyses involving a comparison of the mixtures' inorganic nitrogen contents at the start and end of composting would have provided further information on the ammonium and nitrate dynamics. Longer-term composting trials performed by López-Cano et al. (2016), Sánchez-Garcia et al. (2016) and Vandecasteele et al. (2016) provided useful information on the effect of co-composting with one of the biochars used in this study (*Proininso* oak 650°C): López-Cano et al. (2016) reported an increase in NO_3^--N content following *Proininso* oak 650°C biochar amendment. Similarly, Sánchez-Garcia et al (2016) reported an increase in nitrifying bacteria population with the application of biochar-amended compost material compared to the application of compost or biochar only, which was in agreement with previous studies showing an increase in NO_3^--N content with biochar amendment (Khan et al. 2014; Prommer et al. 2014), of which Prommer et al. (2014) outlined a number of possible mechanisms.

On the other hand, in Vandecasteele et al. (2016), NO_3^--N contents were comparably low in biochar-amended and un-amended composts; the authors also noted that the NH_4^+-N content of biochar-amended composting matter was lower than un-amended composting matter from the onset of co-composting which was maintained up to 27 days of composting but gradually exceeded un-amended compost in the maturation phase. Differences between these three studies may have resulted from the composting materials and experimental setups. The outdoor 31-week co-composting study by López-Cano et al. (2016) involved co-composting *Proininso* oak 650°C with olive mill waste and sheep manure, and while similar amendments were evaluated in Sánchez-Garcia et al. (2016), the field study composting was completed in 2 years. In Vandecasteele et al. (2016), full-scale co-composting studies incorporated the same biochar into greenwaste and treated municipal waste.

5.4.2.2 Carbon dioxide emissions

In both batches, maximum carbon dioxide emissions occurred after 2 days, and the lower carbon dioxide evolution observed in the second composting batch used for oak 250°C, GH 250°C and GH 600°C may have resulted more from the substantially higher moisture content (>70%) rather than differences in topsoil, as Epstein (1997) noted that microbial activity is affected by moisture content. In both

batches, a similar trend was however observed, where decreases in carbon dioxide emissions were observed within 17 days, with a sharp drop in carbon dioxide within the first 5 days of composting as also reported elsewhere (Epstein 1997; Malińska et al. 2014; Steiner et al. 2010). **Figures 5.15** (**a**) and (**c**) show similarities in carbon dioxide evolution between char-amended and un-amended feedstocks. Similarities in carbon dioxide emissions between control and char-amended composting matter were also observed by López-Cano et al. (2016), while in Vandecasteele et al. (2016), composting with biochar resulted in a decrease in carbon dioxide emissions during the bio-oxidative stage. Conversely, Malińska et al. (2014) also observed a slight increase in carbon dioxide evolution from sewage sludge composted with woodchip biochar. Although differences were marginal in this study, the highest total carbon dioxide emissions per gram material relative to the controls followed the order:

Batch 1: OAK 650 > Control > OAK 450

Batch 2: GH 600 > Control > OAK 250 > GH 250

Thus if carbon dioxide emission is used as a measure of microbial activity (Fang et al. 2016; Khan et al. 2014), then it appeared that the oak 650°C and GH 600°C biochars may have provided more conducive conditions for microbial activity to a greater extent than hydrochars. Microbial biomass was not assayed in this study however, and as none of the chars were recovered from the composted mixtures for further analysis, it remains unclear whether the lower carbon dioxide emission by oak 250°C and GH 250°C may have resulted from some interaction between ammonium adsorbed on hydrochar surfaces and carbon dioxide. Reactions with NH_3 and CO_2 could have occurred at about 30–60°C according to the equation: $2NH_{3(g)} + CO_{2(g)} \leftrightarrow (NH_4)_2CO_{3(s)}$. Vandecasteele et al. (2016) observed that in spite of the 53% reduction in cumulative carbon dioxide emissions in oak 650°C biochar-amended feedstock relative to un-amended feedstock in the bio-oxidative stage, the rate of organic matter degradation increased in the former. This discrepancy was

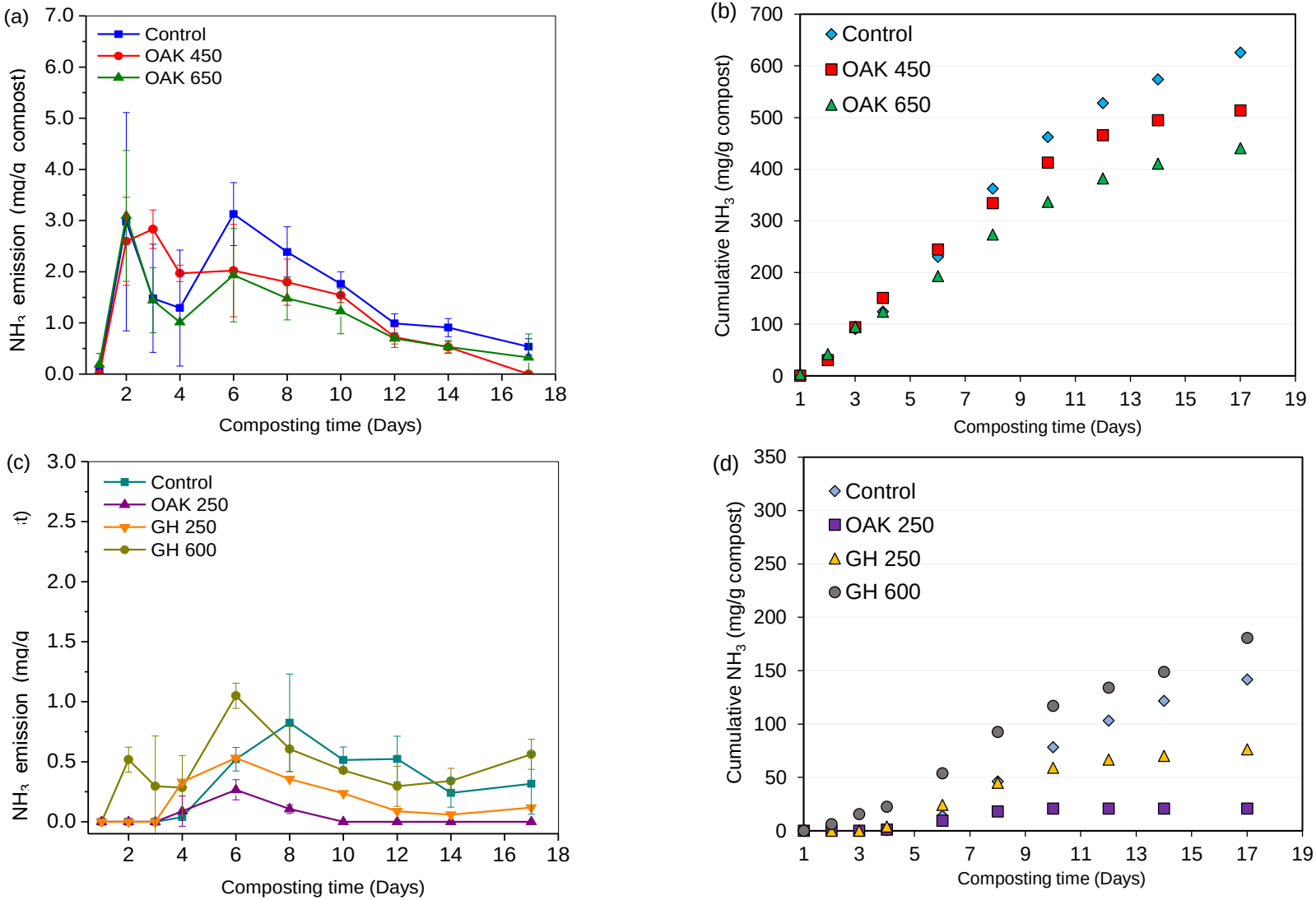

Figure 5.15 NH_3 emissions during co-composting with various chars, including cumulative emissions during 17 days of composting showing lower NH_3 emissions from composting matter amended with oak and greenhouse waste chars. Cumulative NH_3 emissions were calculated based on total compost-char dry mixture weights.

suggested to be due to sorption of carbon dioxide by the alkaline biochar although by the end of the composting process both amended and un-amended composts had similar losses in organic matter (Vandecasteele et al. 2016). Field composting trials by Sánchez-Garcia et al. (2016) similarly showed an increase in organic matter decomposition in composts amended with *Proininso* oak 650°C.

5.5 Char mineralisation

Char mineralisation in a moderately high-pH soil over short-term incubation studies are described here, with CO_2 fluxes and inorganic nitrogen dynamics used as a measure of this degradation. Details of the experimental setup used have been provided in **Section 3.11**. Jumilla sandy soil from Murcia, Spain (C = 7.41%; H = 0.30%; N = 0.23%; S = 0.00%) was used for soil incubation tests. Its pH was about 7.8–8.0 and other chemical/biochemical properties were previously described in Mondini et al. (2010).

5.5.1 Hydrochar and biochar soil respiration

The rate of soil respiration was higher in hydrochar-amended soils in agreement with previous studies (Fang et al. 2016; Khan et al. 2014; Suliman 2015) and notably in soil amended with GH 250. In all char-amended soils, CO_2 evolution peaked after 1–2 days of incubation, which generally agreed with earlier composting results. CO_2 evolution was in the order: GH 250 > OAK 250 > GH 400 > PK 250 and as such was not strongly related to char volatile content but generally corroborated trends in elemental O/C (daf) atomic ratios:

OAK 650 (0.07)	=	PK 400 (0.07)	<	OAK 450 (0.10)	<	GH 400 (0.12)	<	OAK 250 (0.21)	=	GH 250 (0.21)

To some extent, CO_2 evolution in char amended soils was also in agreement with recalcitrance indices as determined by TPO analysis:

OAK 650 (0.52)	>	OAK 450 (0.50)	>	OAK 250 (0.49)	>	PK 400 (0.48)	>	GH 400 (0.47)	>	GH 250 (0.44)

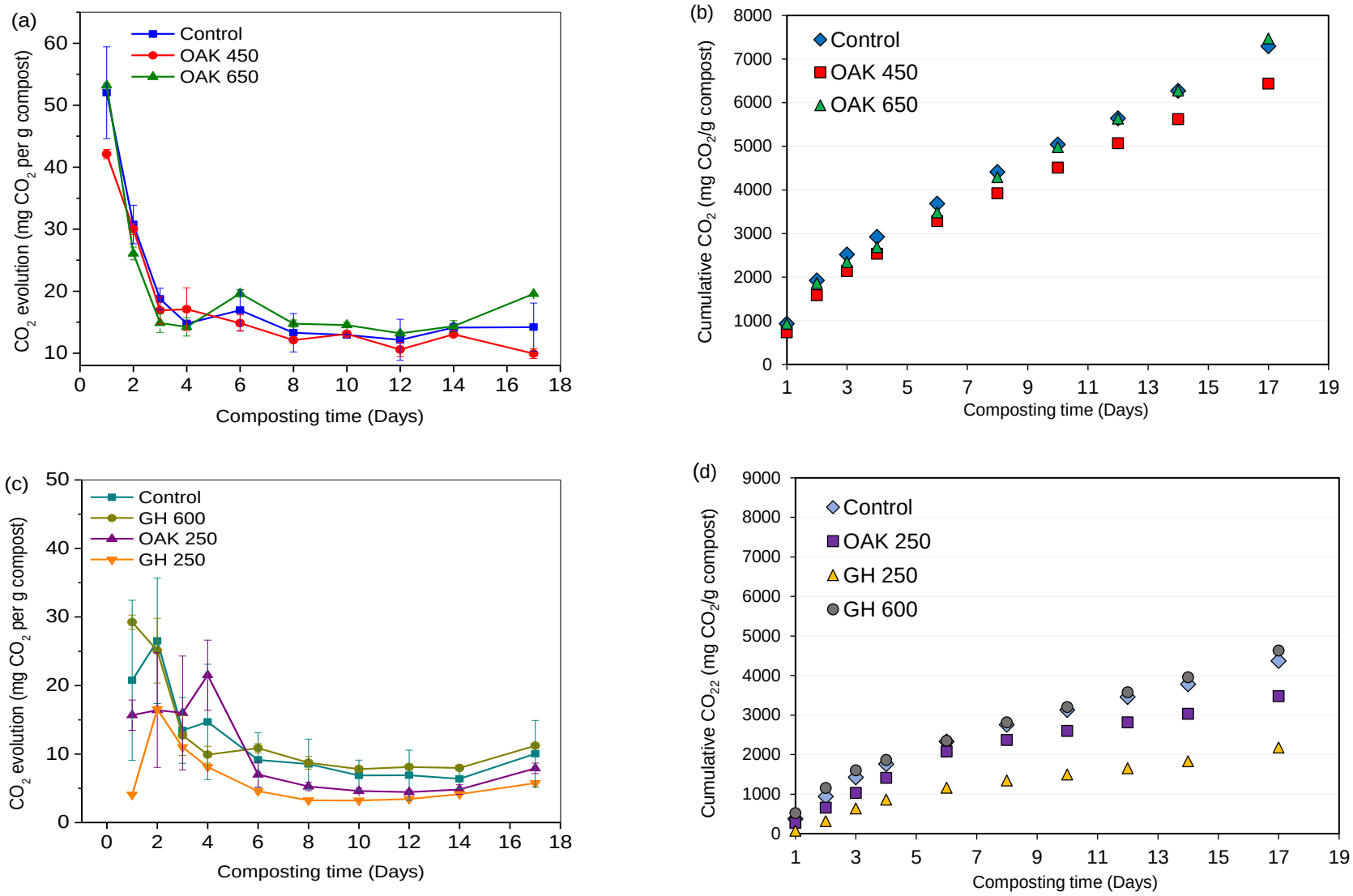

Figure 5.16 Carbon dioxide emissions during co-composting with various chars, including cumulative emissions during 17 days of composting showing lower carbon dioxide emissions from composting matter amended with oak and greenhouse waste chars. Cumulative carbon dioxide emissions were calculated based on total compost-char dry mixture weights.

Hydrochar respiration rates could be attributed to their more easily degradable carbon form or high volatile matter content (Malghani et al. 2015; Subedi et al. 2015; Quayyum et al. 2012). This suggests that substantial amounts of hydrochar C might be lost over longer periods of time although some studies (Malghani et al. 2015) have shown that two-thirds of hydrochar C still remains in soil after one year. Moreover, Malghani et al. (2015) projected a hydrochar C half-life of 19 years in soil based on C mass balance and thermogravimetric analyses, and further suggested that hydrochar C mineralization may occur in two stages: a fast initial decomposition stage whereby a third of the C is lost within the first months following hydrochar application followed by a slower decomposition stage. This timeframe is likely hydrochar and soil dependent. Carbon dioxide evolution was slightly lower in OAK 650 relative to the control (**Figure. 5.18**) which was contrary to co-composting trends outlined earlier but in agreement with the findings of Vandecasteele et al. (2016).

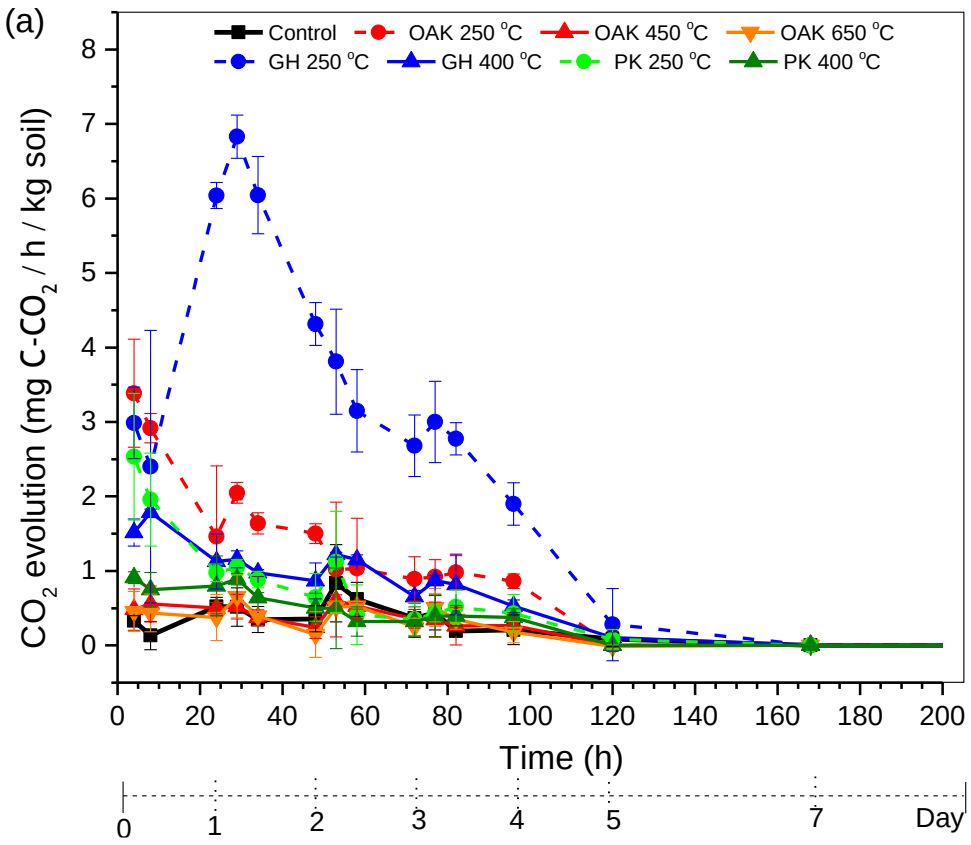

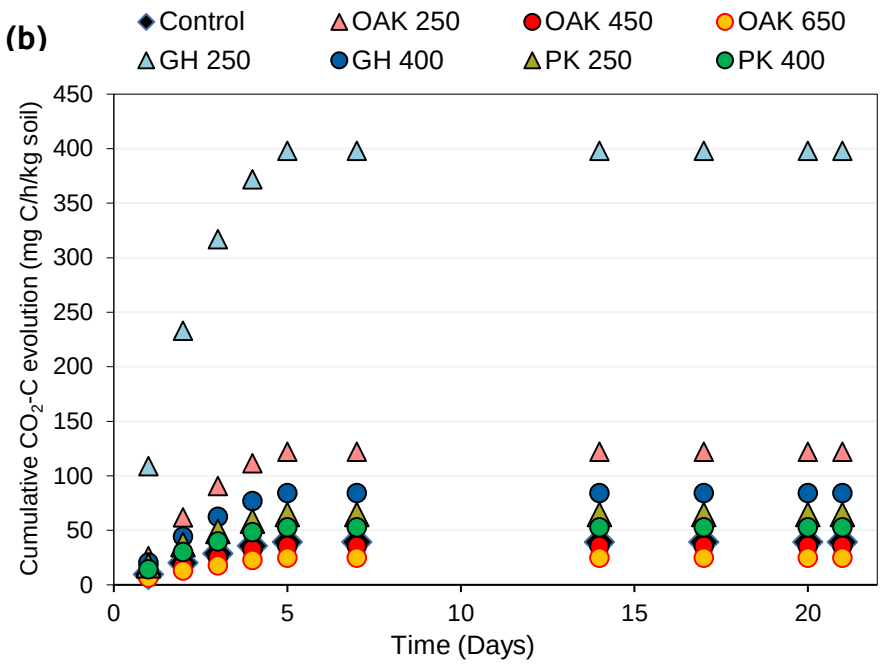

Figure 5.17 (a) CO_2-C fluxes from soils amended with hydrochars and biochars derived from oak, greenhouse waste and presscake. Cumulative CO_2-C fluxes determined based on daily carbon dioxide evolution over the 21 days of incubation.

5.5.2 Hydrochar and biochar N dynamics

As shown in **Figure 5.18**, ammonium contents of char-amended soils were higher than controls until about 12 days of incubation whereas the opposite trend was observed for nitrate content, in that it was after 12 days of incubation that char-amended soils displayed higher nitrate contents. This was in agreement with the findings of Sánchez-Garcia et al. (2016) and Khan et al. (2014) who reported that char-amended feedstocks possessed higher nitrate contents, speculated to be due to biochars' positive effect on nitrifying bacteria or some adsorption of nitrate by biochar. These trends were most obvious for hydrochar-amended soils, with GH 250°C in particular but after 21 days of incubation, ammonium contents decreased substantially in GH 250-amended soil. This is in agreement with studies like Quayyum et al. (2012) who observed similar decreases in ammonium content, which were attributed to N immobilization of easily-mineralizable amendments after 365 days of incubation. Further differences between hydrochar- and biochar-amended soil characteristics included the period of maximum ammonium availability. For hydrochar-amended soils, ammonium generally peaked later than biochar-amended soils, at about 7–12 days of incubation in the former case compared to about 3 days in biochar-amended soils. In the control (soil only), ammonium content

peaked after 12 days of incubation while nitrate concentrations peaked earlier at 7 days of incubation. With the exception of oak 250°C, maximum nitrate concentrations was also extracted from hydrochar-amended soils after 7 days of incubation. In soils amended with oak 450°C, oak 650°C and GH 400°C biochars, this occurred after 3 days of incubation.

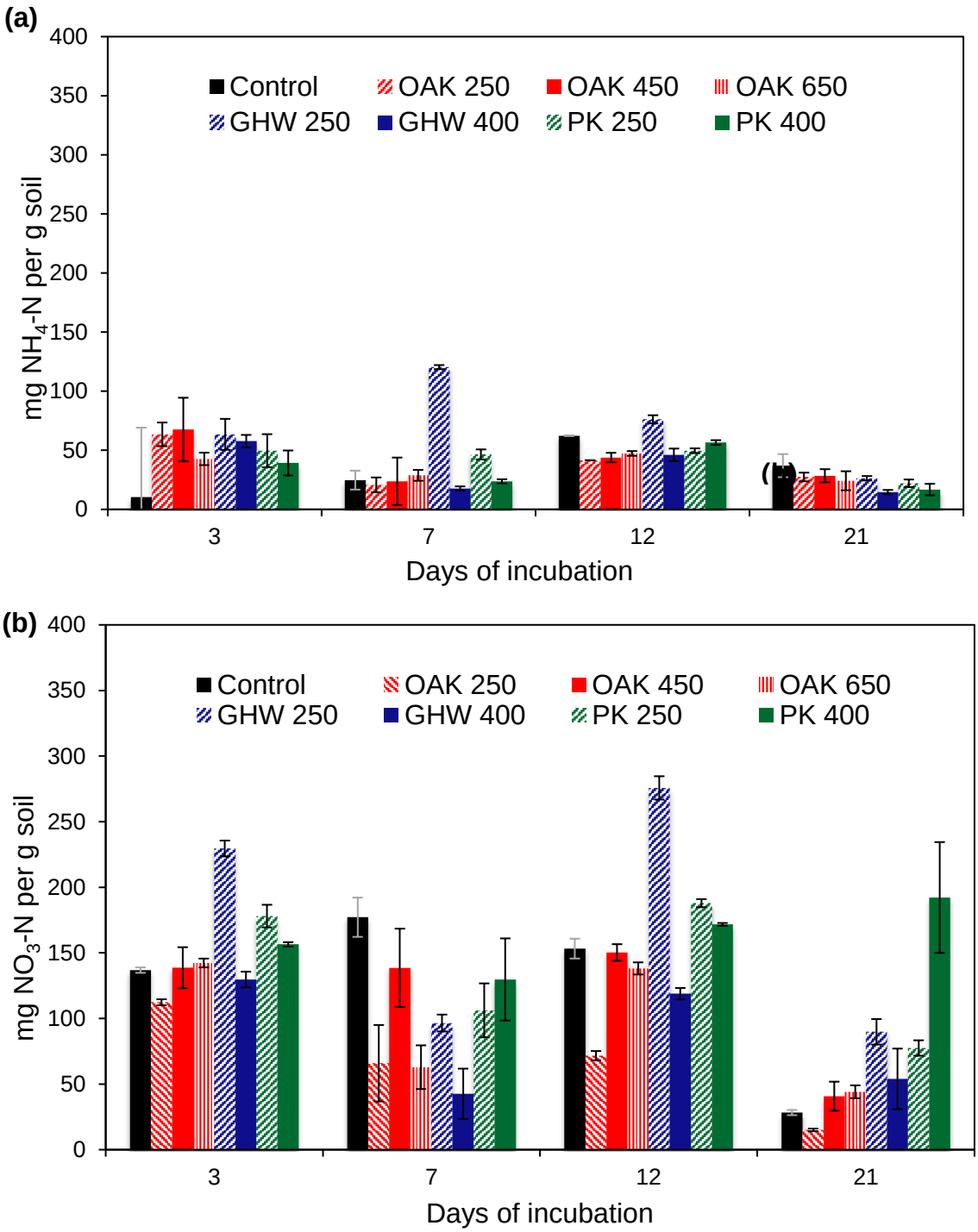

Figure 5.18 Inorganic nitrogen dynamics during soil incubation showing: (a) gradual decrease in NH_4^+-N contents; (b) variable NO_3^--N contents.

5.6 Conclusions

This study investigated the phosphate and ammonium adsorption capacities of biochars derived from various waste biomass feed-stocks, comparing key physicochemical properties such as surface area, CEC, ash and mineral content. Solvent extraction increased hydrochar CEC, possibly due to removal of hydrophobic compounds. Conversely, slow pyrolysis biochar CEC generally decreased following solvent extraction. Ammonium and phosphate sorption capacities ranged from about 105.8–146.4 mg g^{-1} and 0–30 mg g^{-1}, equivalent to about 15% and 7%, respectively and of which only a fraction of which was 0.01 M KCl-extractable. Biochar phosphate sorption capacity increased with pyrolysis temperature possibly due to metal ion precipitation reactions between phosphate and char calcium and magnesium. A positive relationship between char oxygen functional groups, CEC and ammonium sorption suggested that ammonium sorption may have occurred mainly via chemical reactions with oxygen-containing functional groups rather than ion-exchange/physisorption. Results from this study show oak hydrochars possessed much higher ammonia and ammonium sorption capacities relative to oak biochars. Despite differences in physicochemical properties and processing conditions, all chars had comparably low ammonium and phosphate sorption capacities, and would benefit from some form of modification to increase their sorption capacities.

An assessment of the impact of biochars and hydrochars on inorganic nitrogen dynamics and carbon dioxide evolution from a high pH sandy soil over 21 days of incubation showed that the addition of biochars and hydrochars had comparable impact on nitrogen dynamics with the exception of greenhouse waste hydrochar (GH 250), which generated ammonium after 7 days of incubation, reflecting its degradation in soil, as was confirmed by its marked CO_2 evolution relative to other biochars and hydrochars studied. Most ammonium was transformed in soil to nitrate after 12 days of incubation. Similarly, carbon dioxide measurements suggested low degradation and organic matter mineralization by most biochars and hydrochars excluding GH 250°C. Overall however, hydrochar-amended soils generated higher amounts of inorganic nitrogen and carbon dioxide compared to 400°C biochars due to higher mineralization rates in the former.

CHAPTER 6

Recovery of ammonia/ammonium and phosphate with chemically modified hydrochars and biochars

Abstract

The potential for increasing hydrochar and biochar properties to enhance their ability for nutrient recovery has been widely researched. Following chemical modification of biomass (in-situ modification) or biochars (post-treatment) with metal salts, acids and alkali at mild activation conditions, the ammonia / ammonium and phosphate sorption capacities of oak and greenhouse (paprika) waste chars were evaluated using laboratory batch sorption tests. Results indicated that phosphate sorption could be increased from relatively low (2.1–3.6%) to high (66.4–70.3%) proportions by impregnation with magnesium while increases to biochar surface area had no substantial effect on char phosphate or ammonium sorption. Modest increases in both ammonia and ammonium sorption were observed following chemical modification of biochars and hydrochars. Furthermore, neither ammonium nor phosphate sorption capacities were adversely affected by coexisting ions during sorption tests with synthetic wastewater. Treatment with phosphoric acid showed the greatest potential for enhancing ammonia and/or ammonium sorption in biochars, while KOH and H_2O_2 treatment enhanced ammonia sorption in the hydrochar. These findings suggest that char surface functionality is more influential than surface area, and modification processes able to change the surface functionality enhance char ammonia / ammonium sorption. Findings from this study suggest that char composition is a key property influencing char nitrogen and phosphorus recovery potential while surface area has less influence on sorption.

6.1 Introduction

Activated carbon has been the standard adsorbent used for recovering a variety of contaminants (Pollard et al. 1992) owing to its well-developed pore structure and high surface area (Kastner et al. 2009; Pollard et al. 1992; Steiner et al. 2010). However, due to the high costs associated with traditional activated carbon, alternative waste-derived feed-stocks have been considered, ranging from agricultural by-products to industrial waste materials (Kastner et al. 2009; Pollard et al. 1992). To be considered suitable however, such alternative feed-stocks are required to be abundant, carbon-rich, and possess appreciable pore development, (Pollard et al. 1992). Hydrochars and biochars show potential as suitable alternatives to traditional activated carbon as they are carbon-rich products that are obtainable from various kinds of organic waste, although Nguyen et al. (2014) rightly observed that most agricultural by-products considered for such nutrient recovery require some form of modification.

Studies have demonstrated that the presence of basic oxygen functional groups such as metal oxides, ketones, pyrones and chromens on adsorbents are advantageous for phosphate recovery (Chen et al. 2011; Nguyen et al. 2012, 2014; Park et al. 2015; Wang et al. 2015a; Xue et al. 2009; Yao 2013; Zeng et al. 2013). Various processing temperatures, activating agents and loading ratios have been employed, which understandably produce adsorbents with different phosphate sorption capacities even when similar chemical activation agents are used. For instance, while some studies have reported increases in adsorbent phosphate sorption following Fe-treatment (Krishnan and Haridas 2008; Nguyen et al. 2013), a 51% decrease has been observed in other studies (Yao 2013).

With regard to ammonium sorption capacities, low temperature chars tend to have higher sorption capacities possibly due to their higher proportion of acid functional groups (Wang et al. 2015a; Zheng et al. 2010), char ammonium removal efficiencies may be increased by introducing acidic species. Incorporation of cationic species also enhance char ammonium sorption, as the donation of lone pair electrons from N atoms to cationic adsorbent sites such as metal species occur at Lewis acid sites (Canals-Batlle et al. 2008; Le Leuch and Bandosz 2007; Petit and Bandosz 2009; Yin et al. 1999). Zhang and Wang (2016) recovered >60% ammonium using a sewage sludge and Brewer's grains biochar partly due to the biochar composite's enhanced Mg and P content. These studies suggest that hydrochars are likely to possess greater ability for ammonia and ammonium sorption compared to biochars, given the higher proportion of acidic functional groups in the former. On the other

hand, the higher surface areas of biochars may compensate for their lower acidic functionalities since some studies have reported that high adsorbent surface areas and pore volumes increase ammonia and ammonium removal efficiencies (Ismadji et al. 2016; Petit and Bandosz 2009). Moreover, the high surface areas of some biochars may provide more sites for the loading of acidic or cationic species which can increase Brønsted and Lewis acid sites respectively.

This study was therefore aimed at enhancing char potential for nitrogen and phosphorus recovery based on mild activation conditions adapted from frequently used char chemical modification methods. It is anticipated that this study will contribute to growing research on the factors influencing char nutrient recovery. To eliminate uncertainties arising from matrix interferences, wood-based chars with carbon contents >50% were used owing to their low contaminant concentrations, while selected treatments were performed on greenhouse waste chars. Furthermore, the effects of treatment route (i.e., biomass pre-treatment versus biochar post-treatment as outlined in **Chapter Three**) were investigated for chemical treatments which demonstrated the greatest increases in char ammonium and phosphate sorption capacity.

6.2 Physicochemical properties of modified hydrochars and biochars

As two types of chemical treatment were used to modify biochars, activating agents are prefixed with “SA” and “CA” to represent surface activation and chemical activation respectively, the latter treatment involving an additional calcination step. Various chemical treatments understandably had variable effects on biochar functionality as outlined henceforth. Most treatments focused on oak biochars but for comparative purposes, selected treatments were replicated for greenhouse (paprika) waste chars produced at 400°C and for oak hydrochars. A range of activating agent concentrations were used in preliminary studies as outlined in **Chapter Three** but as further nutrient sorption tests were performed using the lowest concentrations (1:1 activating agent/char ratios), only these are reported subsequently unless stated otherwise.

6.2.1 Treated char elemental content

Elemental contents of the treated chars listed in **Table 6.1** revealed a decrease in carbon and nitrogen contents for treated oak 250°C, oak 650°C and most of the GH 400°C chars, while oxygen contents increased. This was somewhat similar to findings of Yakout (2015) who observed a decrease in carbon content while oxygen, hydrogen, nitrogen contents increased following acid and KOH treatment, and to Latham et al. (2013) after acid and base treatment of hydrothermally treated sucrose. Conversely, the carbon contents of most treated oak 450°C treatment increased, as found elsewhere (Gai et al. 2014; Zheng et al. 2013) while oxygen contents decreased. Zheng et al. (2013) similarly observed increases in carbon, hydrogen and nitrogen contents in acid-washed biochars while oxygen content decreased. Acid treatment generally resulted in an increase in H and O which suggested presence of stable carbon-oxygen complexes and available activated sites (Guerrero et al. 2005). This anomaly could also be related to the relative ease of leaching of inorganics and the difference in reactivity of the surface towards decarboxylation and hydrolysis. Hydrochar yields following the various surface treatments ranged from 67.1–86.2%, with H_2O_2 treatment resulting in the greatest material loss while H_2SO_4 treated hydrochar experienced the least material loss. This suggested that surface treatment severity for oak hydrochars followed the order: H_2O_2 > H_3PO_4 > KOH > H_2SO_4. Biochar yields following chemical activation with KOH were about 56%, while oak 650°C treated with Mg had a yield of about 51%.

6.2.2 Char CEC and functional groups

The CEC values of the oak biochars following surface and chemical activation were compared in **Figure 6.1** which showed that the former treatment increased char CEC the most; of these, SA-KOH treatment yielded the most substantial increases. Oak 450°C and oak 650°C CEC values increased by about 82 and 56 $cmol_c\ kg^{-1}$, respectively but the reverse was observed in oak biochars after CA-KOH treatment.

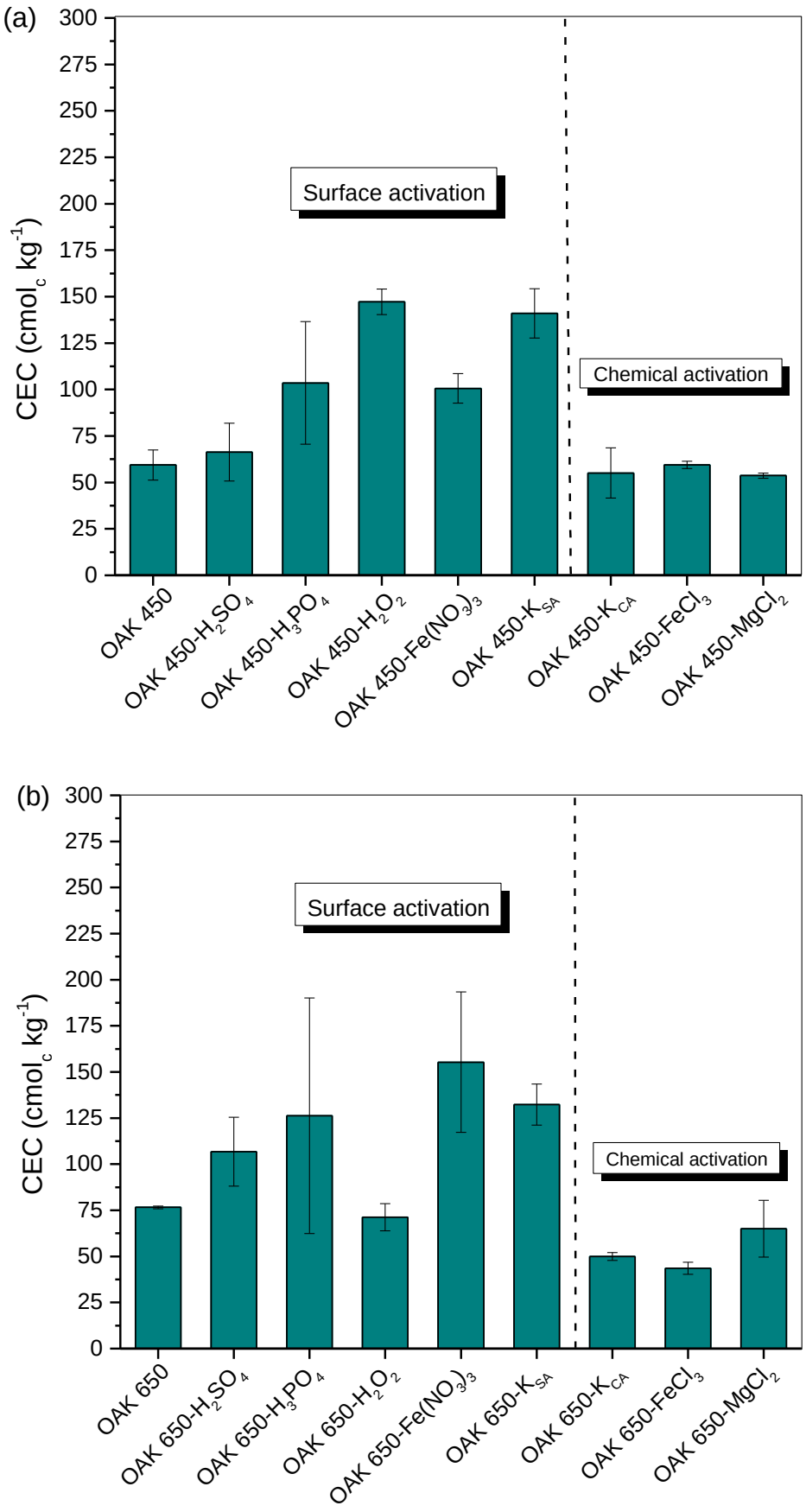

Figure 6.1 Effect of various chemical treatments on char CEC (a) Oak 450 °C; (b) Oak 650°C.

Table 6.1 Elemental content and CEC values for a selection of modified chars

Char	CEC ($cmol_c\ kg^{-1}$)	[a]$NH_4^+{}_{eq}$ ($mg\ g^{-1}$)	C (%)	H (%)	N (%)	S (%)	[b]O (%)
Surface activated ("SA") chars							
OAK 250	88.3±9.7	15.9	67.9	6.5	1.4	0.1	24.1
OAK 250-H_2SO_4	81.1±4.6	14.6	61.3	4.9	0.4	0.04	33.4
OAK 250-H_3PO_4	86.8±4.7	15.6	60.2	4.8	0.3	0.0	34.6
OAK 250-H_2O_2	102.4±7.3	18.4	56.1	4.5	0.3	0.0	39.1
OAK 250-KOH	102.0±8.2	18.4	62.0	4.9	0.4	0.0	32.7
OAK 450	59.4±8.1	10.7	65.7	2.7	0.6	0.0	31.0
OAK 450-H_2SO_4	66.3±15.6	11.9	73.6	4.8	0.5	0.0	21.1
OAK 450-H_3PO_4	103.5±33.0	18.6	70.0	4.1	0.4	0.0	25.5
OAK 450-H_2O_2	147.2±6.9	26.5	71.3	3.9	0.5	0.0	24.3
OAK 450-KOH	141.0±13.2	25.4	74.1	3.2	0.5	0.02	22.2
OAK 450-Fe	100.6±7.9	18.1	64.6	2.9	1.3	0.0	31.2
OAK 650	76.6±0.7	13.8	76.5	1.4	0.8	0.0	21.3
OAK 650-H_2SO_4	106.8±18.7	19.2	62.9	2.4	0.6	0.0	34.2
OAK 650-H_3PO_4	126.3±63.9	22.7	50.5	3.6	0.5	0.0	45.4
OAK 650-H_2O_2	71.2±7.4	12.8	63.7	2.3	0.5	0.0	33.5
OAK 650-KOH	132.3±11.2	23.8	59.5	3.1	0.5	0.03	36.9
OAK 650-Fe	155.3±38.1	28.0	59.3	1.9	1.6	0.0	37.2
GH 250	83.1±19.4	15.0	66.4	6.8	3.1	0.2	23.5
GH 250-KOH	226[c]	41	55.2	3.5	2.2	0.0	39.1
GH 400	109.5±21.8	19.7	59.0	2.9	1.2	0.3	36.6
GH 400-H_2SO_4	120.3±9.5	21.7	68.0	4.5	1.2	0.0	26.3

Table 6.1 Elemental content and CEC values for a selection of modified chars

Char	CEC ($cmol_c\ kg^{-1}$)	[a]$NH_4^+{}_{eq}$ ($mg\ g^{-1}$)	C (%)	H (%)	N (%)	S (%)	[b]O (%)
GH 400-H_3PO_4	150.8±15.2	27.1	67.4	5.1	1.0	0.03	26.5
GH 400-H_2O_2	156.7±45.9	28.2	68.8	4.6	0.9	0.46	25.2
GH 400-KOH	366.1±9.1	65.9	70.3	4.0	0.9	0.05	24.8
GH 400-Fe	162.3±13.7	29.2	49.1	3.2	2.8	0.0	44.9
Chemical activated ("CA") chars							
OAK 450-Mg 400	53.7±1.4	9.7	57.1	2.6	3.6	0.00	36.7
OAK 650-Mg 600	65.0±15.4	11.7	65.1	1.8	0.7	0.11	32.3
OAK-Mg 600	50[c]	9.0	53.6	2.5	0.3	0.20	43.5
GH-Mg 600	n.a	n.a	43.4	1.6	0.9	0.00	54.1

[a]$NH_4^+{}_{eq}$ refers to the maximum equivalent char NH_4^+ sorption capacity since 1 $cmol_c\ kg^{-1}$ = 0.18 mg $NH_4^+\ kg^{-1}$ char; [b]Oxygen content determined as difference between % C, H, N and S from 100 (dry basis); [c]single analysis only; CEC expressed as average of duplicates ± standard deviation; n.a. = unavailable data.

The greatest increase in CEC was observed for KOH-activated GH 400°C as shown in **Table 6.1**. Min et al. (2004) also observed CEC increases following surface modification with bases, but it is uncertain whether the increase in GHW 400 CEC following SA-KOH treatment could be attributed to oxidation of the biochar surface resulting from the presence of K and O following Equation (6.1) as outlined in Viswanathan et al. (2009), because while potassium salt complexes are formed even without carbonization (Ehrburger et al. 1986; Lillo-Ródenas et al. 2003). Equation (6.1) might only occur at much higher temperatures (Ehrburger et al. 1986; Lillo-Ródenas et al. 2003; Viswanathan et al. 2009):

$$K_2O + C \rightarrow C-O-K + K \quad (6.1)$$

It is more likely that CEC increases resulted from an increase in carbonyl groups. This hypothesis is based on the increase observed following SA-KOH treatment of GH 400°C compared to oak biochars, the former biochar possessing more carbonyl groups as seen in **Figure 6.2** (1760–1665 cm^{-1} bands). Mallampati and Valiyaveettil (2013) reported ester bond cleavage into hydroxyl groups following NaOH treatment. Yakout (2015) also found that KOH treatment increased biochar phenolic groups; such base treatment increases char CEC (Han et al. 2005). SA-H_2O_2 treatment also

increased CEC although not as greatly as SA-KOH treatment. This increase was possibly due to the formation of oxygen-containing species following acid-catalysed hydrolysis reactions (Lin et al. 2012; Marsh and Rodríguez-Reinoso 2006). Acid treatment similarly had varying effects on char CEC: while there was little change in hydrochars treated with H_2SO_4 and H_3PO_4, all other treatments had a positive impact on CEC. For instance, following H_2O_2 treatment, a two-fold increase in the CEC of oak 450°C was observed although the increase for the oak hydrochar was less obvious. Previous studies (Huff et al. 2016; Liang et al. 2006) have attributed this effect to an increase in oxygen functional groups due to oxidation of aromatic carbon and increase in carbonyl groups. Also apparent was that the increase in CEC cannot be attributed to changes in surface area since H_2O_2 treatment resulted in a drastic reduction in surface area (>50%) for both oak biochars as discussed subsequently.

6.2.2 Treated char functional groups

Char functional groups as determined by ATR-FTIR, solid-state NMR and TPO analysis all showed that treated chars did not differ substantially from their untreated counterparts. Relative to unprocessed oak biomass, additional peaks were observed in treated and untreated chars reflective of the biomass degradation to carbonyl, hydroxyl and other reactive functional groups (**Figure 6.2**). Amongst treated and untreated chars, no major differences in functional group intensities are observed, suggesting that chemical treatment does not alter char functionality substantially. A slight relative increase in the intensity of carbonyl functional groups (1700 cm^{-1}) is however observed following H_2O_2 treatment.

FTIR spectra confirmed that some band intensities increased following some surface activation treatments, notably the 1700 cm^{-1} and 1440 cm^{-1} bands in GH 400°C following SA-KOH treatment (**Figure 6.2**). SA-KOH oak 450°C also possessed a marginally higher peak at 1585 cm^{-1} relative to untreated oak 450°C. These suggest an increase in C=O groups. Following H_2O_2 and Mg treatment, absorbance intensities either had no marked effect on biochar functional groups or decreased their intensities. In the 1800–600 cm^{-1} region, four bands were observed in all biochars: sharp peaks around 1714–1698 cm^{-1} attributable to C=O stretching of carbonyl groups (Pradhan and Sandle 1999; Wu et al. 2011); 1440 cm^{-1} likely corresponding to ketone stretching as observed in lignocellulosic materials (Keiluweit et al. 2010); 1400 cm^{-1} likely due to aromatic C=C stretching (Park et al. 2015); 875 cm^{-1} possibly due to out-of-plane bending vibrations for β-glucosidic

linkages or for C-O groups, aldehydes and benzene derivatives (Krishnan and Haridas 2008; Sricharoenchaikul et al. 2008). Additional bands were also present in oak 450°C and GH 400°C biochars at 1610 cm^{-1}, attributable to aromatic C=C stretching or conjugated ketone and quinone C=O stretching vibrations (Keiluweit et al. 2010; Park et al. 2015). A band at 1583-1575 cm^{-1} resulting from conjugated C=O stretching vibrations of hemicellulose or aromatic rings (Krishnan and Haridas 2008; Sricharoenchaikul et al. 2008). Overall, the observed changes in elemental and organic composition, CEC and surface area suggest that benefits are derived from chemical treatment in terms of increased CEC and in some cases surface area without a great deal of material loss.

6.2.3 Physical characteristics of treated chars: Surface area and morphology

Chemical activation is thought to enhance char surface area and porosity development to a greater extent compared to surface activation due to the higher activation temperatures employed (>450°C). Despite the lower temperatures used in surface modification (60–80°C) however, comparable increases to surface area have been observed by Sricharoenchaikul et al. (2008). In this study, SA-KOH treatment increased the surface area of GH 400°C by 55% while a drastic decrease of >75% was observed in SA-KOH treated oak biochars. An increase in GH 400 surface area may have resulted from demineralization by KOH or HCl (the latter introduced during the rinsing stage of the procedure), as is known to occur following alkali or acid treatment of feedstocks (Mahmoud et al. 2012; Mukherjee 2003; Yakout 2015). Demineralization from KOH action is more likely, since preliminary tests showed that increasing KOH/biochar loading ratios whilst maintaining the same HCl concentration increased surface areas in all 3 biochars. For instance, SA-KOH treated oak 650°C at 1:1 and 5:1 KOH/char loading ratios had a surface area of 59.3 $m^2\ g^{-1}$ and 67.8 $m^2\ g^{-1}$ respectively as shown in **Table 6.2**. The demineralization was possibly more pronounced in GH 400°C owing to its higher ash content, especially if such inorganics were more loosely bound to its carbon structure than in oak biochars. Dislodgement of these inorganics would consequently increase pore spaces, although more studies are required to confirm this. Increasing KOH/carbon ratios result in greater microporosity while converse is true for increasing H_3PO_4/carbon ratios. In the latter case, while low ratios result in micropore development, increasing ratios result in mesoporosity development (Marsh and Rodríguez-Reinoso 2006).

The decrease in oak biochar surface areas following SA-KOH treatment likely occurred because surface activation was not followed by high temperature

treatment. This was validated by the fact that an additional pyrolysis step performed on oak 650°C increased its surface area to 344.3 m^2 g^{-1} (**Table 6.2**). Yet a similar KOH surface activation process on physic nut waste biochar without further heat treatment resulted in an increase in surface area from about 200 m^2 g^{-1} to >500 m^2 g^{-1} in Sricharoenchaikul et al. (2008). As this study was aimed at increasing biochar ammonium and phosphate removal efficiencies however, less emphasis was placed on increasing biochar surface area as it was observed that high and low surface area biochars performed comparably. This was further demonstrated by CA-KOH oak 650°C (i.e., oak 650°C pyrolyzed after KOH treatment) whose higher surface area did not increase its PO_4^{3-} removal efficiency as briefly discussed in **Section 6.4.3** KOH treatment

Generally however, KOH treatment is known to significantly increase surface areas in feedstock (Azargohar and Dalai 2008; Gu and Wang 2012; Sricharoenchaikul et al. 2008) owing to intercalation of K atoms within carbon lamella. This results in an increase in char porosity following their removal in a rinsing step (Sricharoenchaikul et al. 2008; Viswanathan et al. 2009) but such reactions typically occur at high temperatures through the series of reactions outlined in Viswanathan et al. (2009). Indeed in terms of porosity development, while chars benefit from H_3PO_4 and $ZnCl_2$ treatment at temperatures of < 450°C and < 500°C respectively, KOH treatment requires higher activation temperatures (Marsh and Rodríguez-Reinoso 2006). Furthermore, increases in char surface area during KOH treatment is also time-dependent as shown in **Table 6.2**, where suffixes A and B refer to KOH treatment involving pyrolysis at 600°C after shaking the char-KOH mixture; in treatment A, the char-KOH mixture was allowed to stand for some hours before pyrolyzing at 600°C and in treatment B, chars were immediately pyrolyzed at 600°C after shaking. The substantial increase in char surface area following the latter treatment likely because there was less time for KOH-treated char to react with atmospheric CO_2.

Following a similar trend to SA-KOH treatment, H_2O_2 treatment resulted in a decrease in oak biochar surface areas by about 53.3% and 73.1% for oak 450°C and oak 650°C, respectively, with even greater reduction following 30% H_2O_2 treatment. Pereira et al. (2003) and Pradhan and Sandle (1999) respectively reported a 12% and 9.2% reduction in surface area following surface activation of activated carbon with <10% and 30% H_2O_2. It is not unusual for char surface areas to decrease following chemical treatment due to pore wall collapse (Moreno-Castilla et al. 2000; Pereira et al. 2003; Pradhan and Sandle 1999) or blockage of micropores by newly formed surface oxygen groups (Pradhan and Sandle 1999).

However, Xue et al. (2012) and Yakout (2015) respectively reported that peanut hull hydrochar and rice straw biochar treated with 10% and 30% H_2O_2 increased char surface area by 7.7% and 55.4%. It remains unclear why H_2O_2 surface treatment has such variable effects, and further investigations are required to confirm whether compositional differences in ash content are influential factors.

Table 6.2 Surface areas of selected treated chars

Treatment	Concentration	BET surface area N_2 (m^2 g^{-1})	t-Plot micropore volume (cm^3 g^{-1})	[a]Average pore width (nm)
H_2O_2				
	10% OAK 450-H_2O_2	65.4	0.018	3.126
	30% OAK 450-H_2O_2	53.6	0.015	3.418
	10% OAK 650-H_2O_2	64.5	0.016	3.241
	30% OAK 650-H_2O_2	45.4	0.002	0.191[b]
KOH				
SA-KOH				
	1:1 KOH-OAK 450	0.2	0.001	1.572
	5:1 KOH-OAK 450	3.3	0.002	1.895
	1:1 KOH-OAK 650	59.3	0.013	3.462
	5:1 KOH-OAK 650	67.8	0.019	2.862
	1:1 KOH-GH 400	2.0	0.001	7.522
	5:1 KOH-GH 400	2.5	0.001	5.484
CA-KOH				
	1:1 KOH-OAK 650 A	43.3	0.012	3.030
	1:1 KOH-OAK 650 B	344.3	0.125	2.096
Untreated chars				
	GH 400	1.3	0.003	0.904
	OAK 450	180.0	0.150	0.003
	OAK 650	280.0	0.160	0.023

SA-KOH and CA-KOH refer to KOH treatment via surface and chemical activation respectively; [a]adsorption average pore width (4V/A by BET); [b]based on desorption average pore width 4V/A by single point analysis; [c]based on BJH adsorption average; the surface areas of 1:1 OAK 450-KOH were measured thrice and found to be low on each occasion.

SEM imaging of a selection of treated oak biochars presented in **Figure 6.3** showed that chemical treatment did not alter char morphologies substantially; at best, CA-KOH treated oak 450°C had somewhat rougher edges compared to untreated oak 450°C (**Figure 6.3(ii)**). A visible difference in oak 650°C following magnesium

treatment at 600°C was evident however, although magnesium was unevenly distributed, ranging from 1.45–5.95% in the sample points analysed. SEM/EDS imaging of a section of Mg-treated oak 650°C presented in **Figure 6.4** showed the distribution of Mg on the char. No differences in Mg-treated OAK 450 were evident and as such SEM images were not included. Generally, the SEM results corroborated ATR-FTIR (**Figure 6.2**) and NMR findings (**Figure 6.5(a)**) which showed no distinctive differences between treated and untreated char surface functional groups. TPO analysis of a selection of chars showed that chemical modification increased recalcitrance indices of oak and greenhouse waste biochars however: while recalcitrance indices for GH 400°C, oak 450°C and oak 650°C biochars were 0.47, 0.50 and 0.52 respectively, KOH-treated greenhouse waste and oak biochars ranged from 0.52–0.55; similarly, H_2O_2-treated biochars were between 0.47–0.56, lowest in GH 400°C. **Figure 6.5(b)** showed an example TPO plot for KOH-treated oak biochars.

6.3 Influence of chemical treatment on char ammonia / ammonium sorption

6.3.1 Ammonia / ammonium sorption by treated hydrochar and biochars

The nitrogen contents of the untreated chars are presented in Annex Table A4 and ranged from 4.3–23.8 mg N g^{-1} char, highest in the greenhouse waste hydrochar. The N contents of the treated chars decreased with the exception of H_2SO_4 and KOH treated biochars, equivalent to 5.4–5.9 and 6.3–7.0 mg N g^{-1} respectively. This reduction was possibly due to modification disrupting N-containing compounds in the biomass thus increasing N release while the relative increase in N content for the few chars was speculated to be primarily due to loss of carbon. There was an increase in sample weights of post-ammonia sorption chars while carbon contents decreased in all cases, likely due to sorption of moisture by the chars. This was expected since moisture is known to enhance ammonia sorption (Chou et al. 2006; Le Leuch and Bandosz 2007). The ammonia sorption capacities of the treated chars

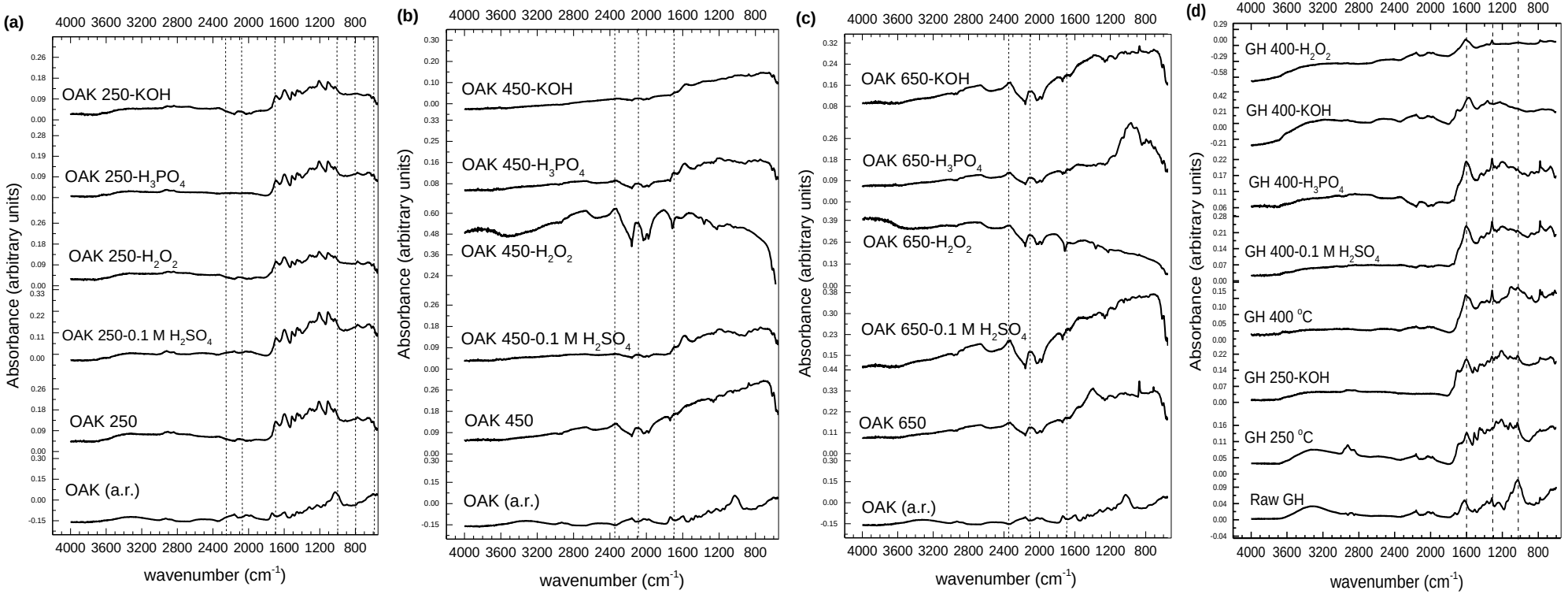

Figure 6.2 ATR-FTIR spectra of treated chars showing no substantial differences in functional groups.

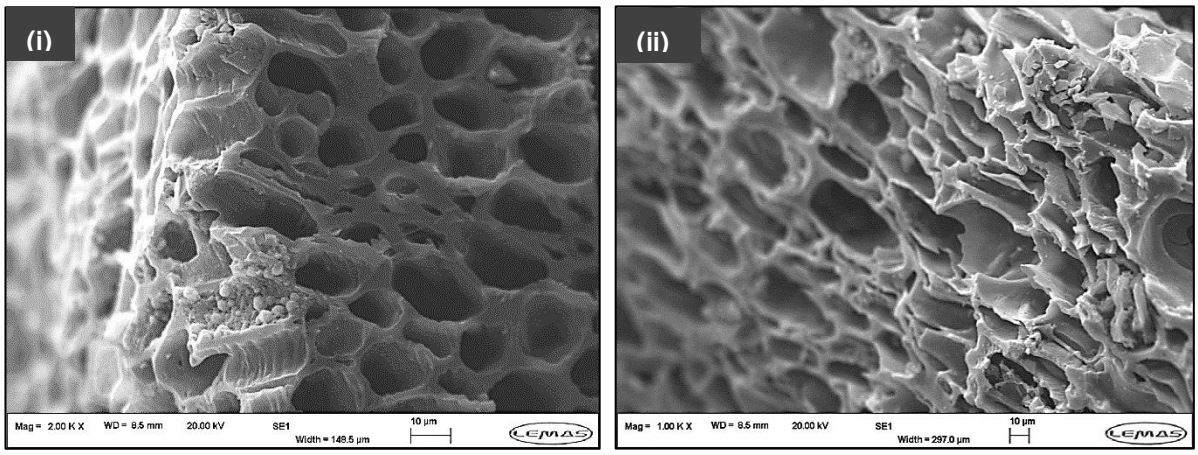

OAK 450 **CA-KOH OAK 450**

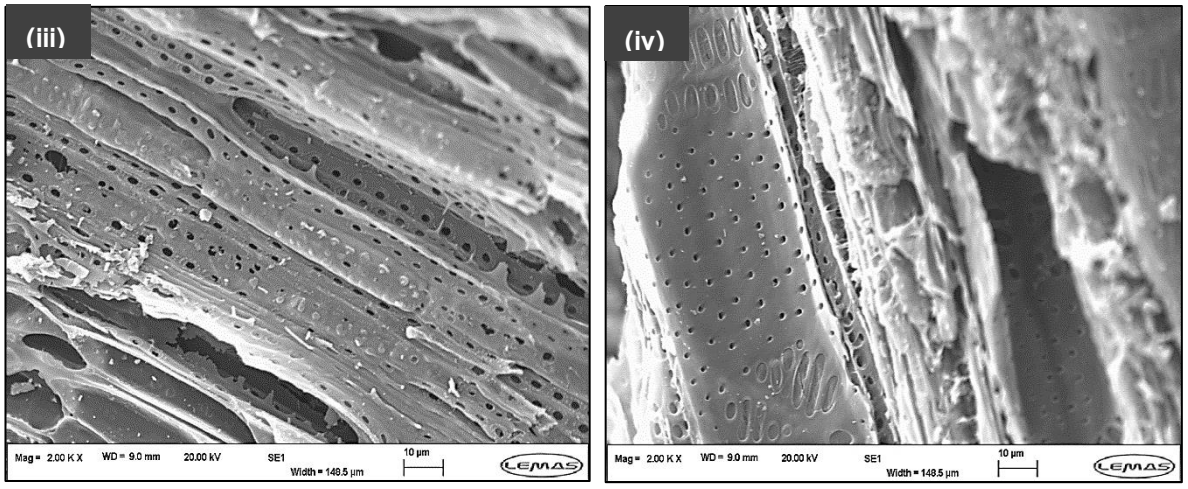

OAK 650 **CA-KOH OAK 650**

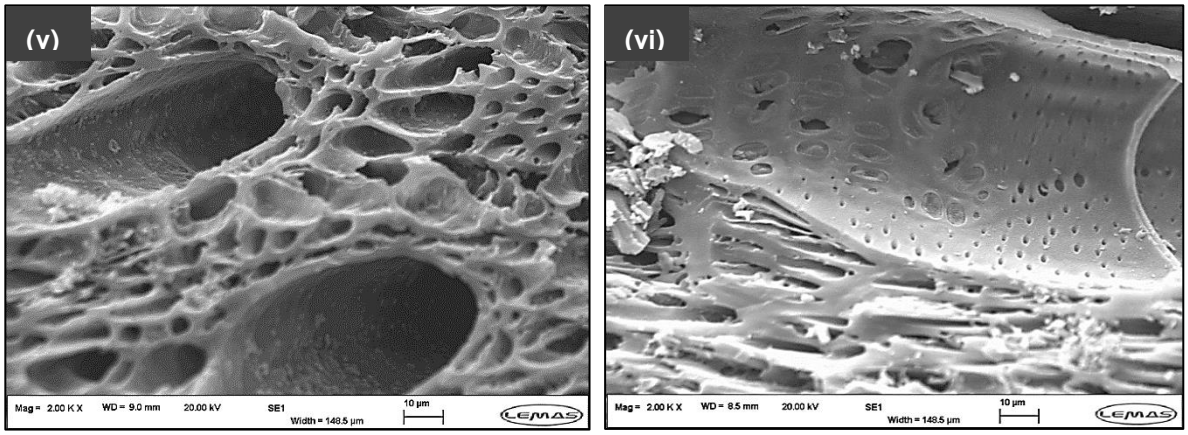

OAK 650-$MgCl_2$ **OAK 650-$FeCl_3$**

Figure 6.3 SEM imaging (1000-2000x magnification) of a selection of oak biochars showing similarities in char morphology before and after chemical treatment. CA-KOH refers to chemical activation of chars using KOH.

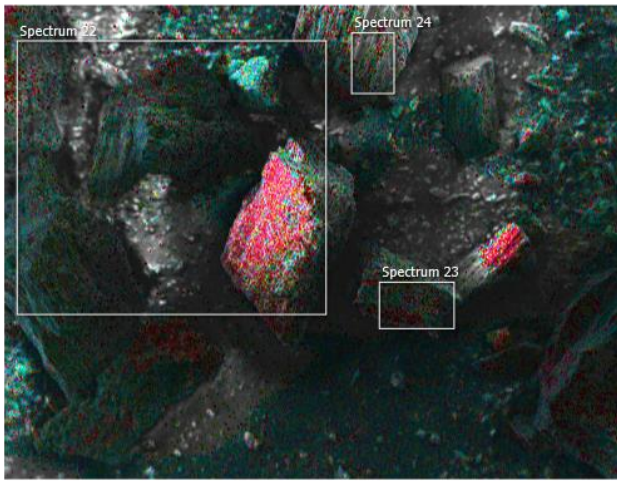

Spectrum 22

Element	Wt%	Wt.% Sigma
C	76.11	0.24
O	16.08	0.21
Mg	5.95	0.05
Si	0.09	0.01
P	0.13	0.02
S	0.09	0.01
Cl	0.38	0.02
Ca	0.94	0.03
Cu	0.23	0.07
Yb	0.01	0.14
Total:	100.00	

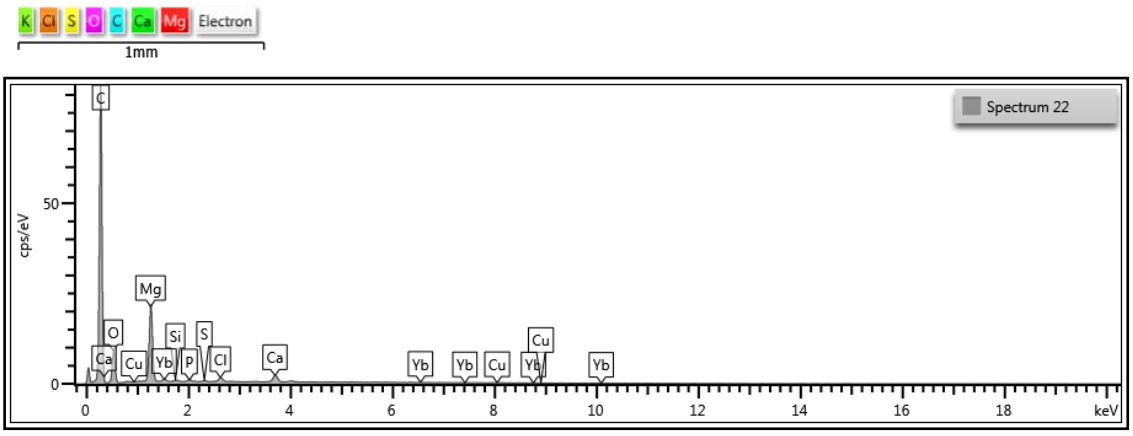

Figure 6.4 SEM/EDS imaging of magnesium-treated oak 650°C.

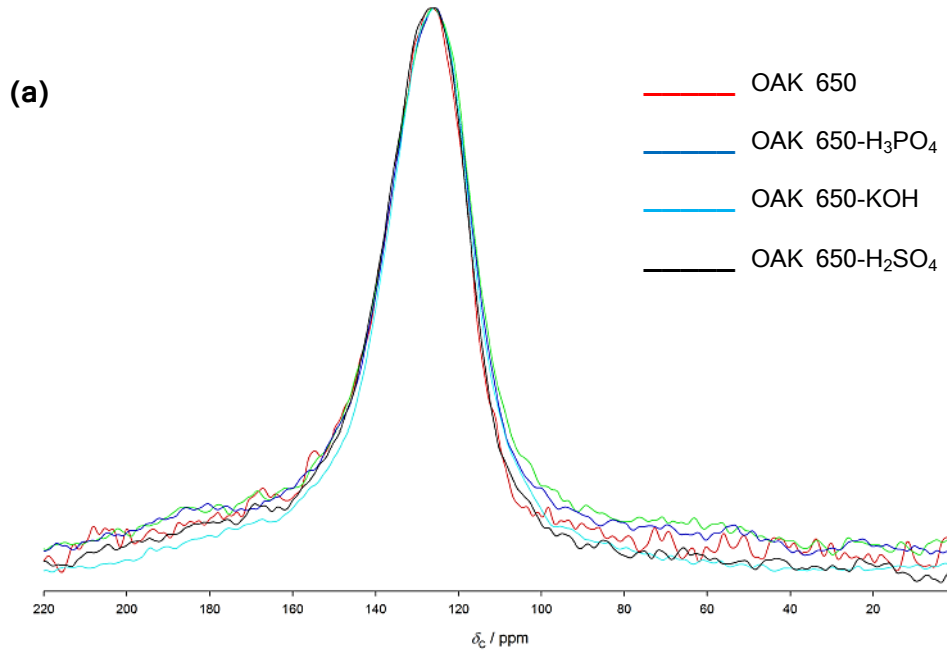

(b)

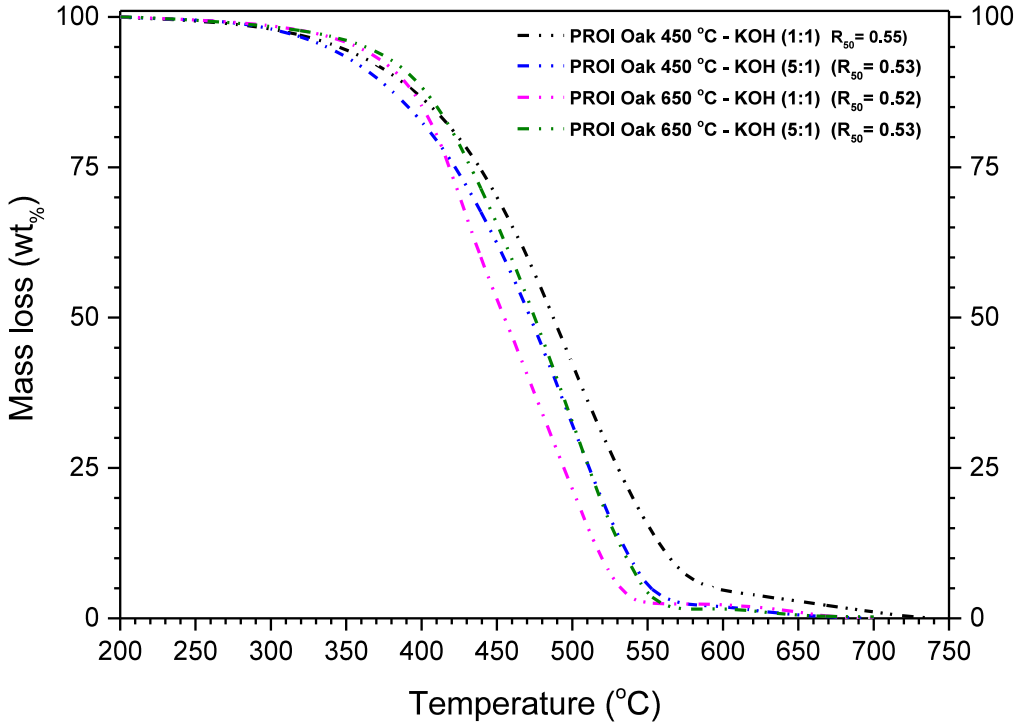

Figure 6.5 (a) Solid-state direct-excitation ^{13}C NMR analysis of various treated OAK 650 biochars showing similarities in aromatic functional groups; (b) TGA-Temperature-Programmed Oxidation (TPO) plot for KOH-treated chars.

shown in **Figure 6.6** and **6.7** showed that treatment with KOH increased ammonia sorption in oak 250°C and GH 250°C and 400°C. For the oak biochars, acid treatment appeared more influential, resulting in a two- to three-fold increase in ammonia sorption by acid-treated oak 450°C and some increase in H_3PO_4-treated oak 650°C. Comparatively, chemical treatment had a greater impact on oak biochars compared to oak hydrochar.

Conversely, ammonium sorption following char modification yielded variable results as shown in **Figure 6.6**; ammonium sorption capacities were evaluated at 450 mg NH_4^+ L^{-1} to investigate their potential for ammonium recovery from a representative concentration range encountered in real-case conditions (Cai et al. 2013). In general, modification of the chars resulted in a reduction in ammonium sorption capacity, particularly for H_2O_2 and KOH treatment. Some studies have noted that the presence of cationic (metal) species enhance ammonium sorption so this was tested for both ammonia and ammonium sorption. **Figure 6.7**(**b**) revealed that Mg incorporation had negligible effect on char ammonia sorption and a detrimental

effect on char ammonium sorption (**Figure 6.8)** but in the presence of coexisting ions, Mg-treated chars outperformed their untreated counterparts (**Table 6.4**). Preliminary sorption tests done with Mg-treated oak and greenhouse waste biomass in pure ammonium solutions were similar to untreated oak 650°C and GH 600°C biochars. These results were not included here as sorption tests were done at initial concentrations of about 1000 mg NH_4^+ L^{-1} whereas values reported in this section were obtained following sorption tests at about 450 mg NH_4^+ L^{-1}.

As observed in untreated chars, ammonium release from treated chars were low following desorption tests. For instance, KOH-treated oak 450 and 650°C respectively released 8.5 and 9.7 mg g^{-1}; H_2O_2-treated oak 450 and oak 650°C released 9.4 and 6.7 mg g^{-1}, respectively. As blank sorption tests performed alongside char sorption tests showed negligible ammonium losses during sorption tests, it is speculated that ammonium release from chars was low either due to strong interactions between ammonium and chars or due to the low extractant concentrations (0.01 M KCl or 0.01 M $CaCl_2$) used as aforementioned.

6.3.2 Possible mechanisms for ammonia sorption by treated chars

Mechanisms for ammonia sorption involve interactions at Brønsted and/or Lewis acid sites; in the former case, protonation of ammonia occurs as it dissociates in water or via acid-base neutralization reactions with carbonyl and phenolic OH^- groups present on adsorbents to form NH_4-complexes (Corre et al. 2013; Le Leuch and Bandosz 2007; Long et al. 2008; Petit and Bandosz 2009; Steiner et al. 2010; Taghizadeh-Toosi et al. 2012a). Acid treatment generally showed the greatest potential for increasing biochar ammonia and ammonium sorption capacities, particularly for oak 450°C resulting from acid-catalysed hydrolysis of polymeric units in lignocellulosic materials and labile carbon in biochars lead to ketone formation after H_3PO_4 treatment (Lin et al. 2012; Marsh and Rodríguez-Reinoso 2006). Additionally, the formation of ammonium complexes with H_3PO_4 may have occurred as observed by Oya and Iu (2002) whose extensive studies confirmed the presence of $NH_4H_2PO_4$ and/or $(NH_4)_2HPO_4$ depending on the H_3PO_4 loading ratio employed. Substantial variability in ammonium sorption by all H_3PO_4-treated chars was observed in this study however (**Figure 6.8**), possibly due to uneven distribution of reagent onto chars. H_2SO_4 treatment had variable effects on char ammonia and ammonium sorption capacities: for oak 450°C, increases in both ammonia and ammonium sorption capacity were observed while no substantial increase in ammonium sorption was observed in oak 250°C and oak 650°C sorption relative to their untreated counterparts. Ammonia sorption decreased in oak 250°C but

marginally increased in oak 650. The increase in ammonia sorption of H_2SO_4-treated biochars was in agreement with Petit et al. (2010) who showed that sulphur-containing groups may be as influential as oxygen functional groups for ammonia sorption.

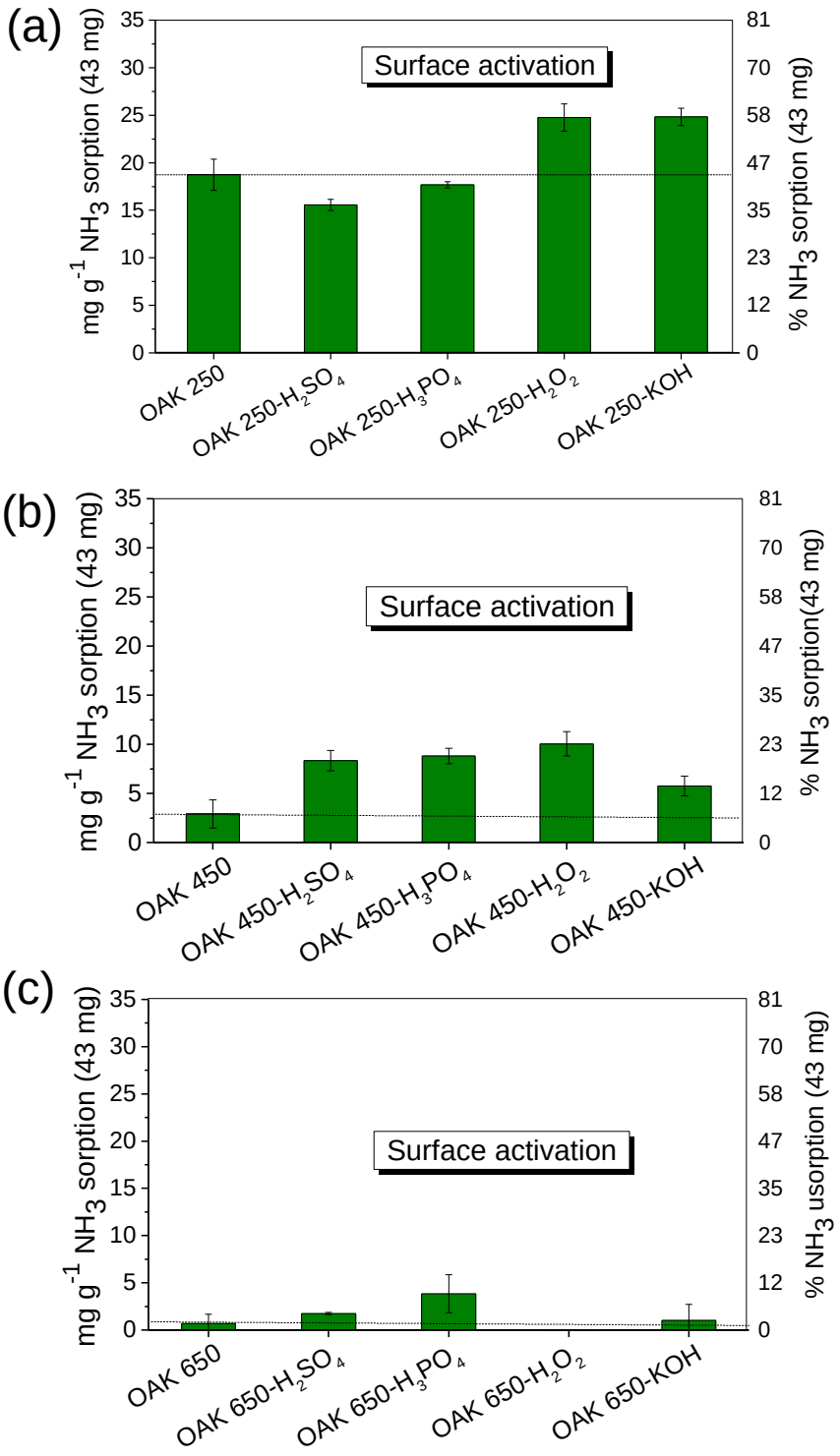

Figure 6.6 Ammonia sorption capacities of various treated chars relative to untreated chars showing: (a) marginal increase in treated oak hydrochars; (b) considerable improvements in treated oak 450°C biochars; (c) variable effects for treated oak 650°C biochars.

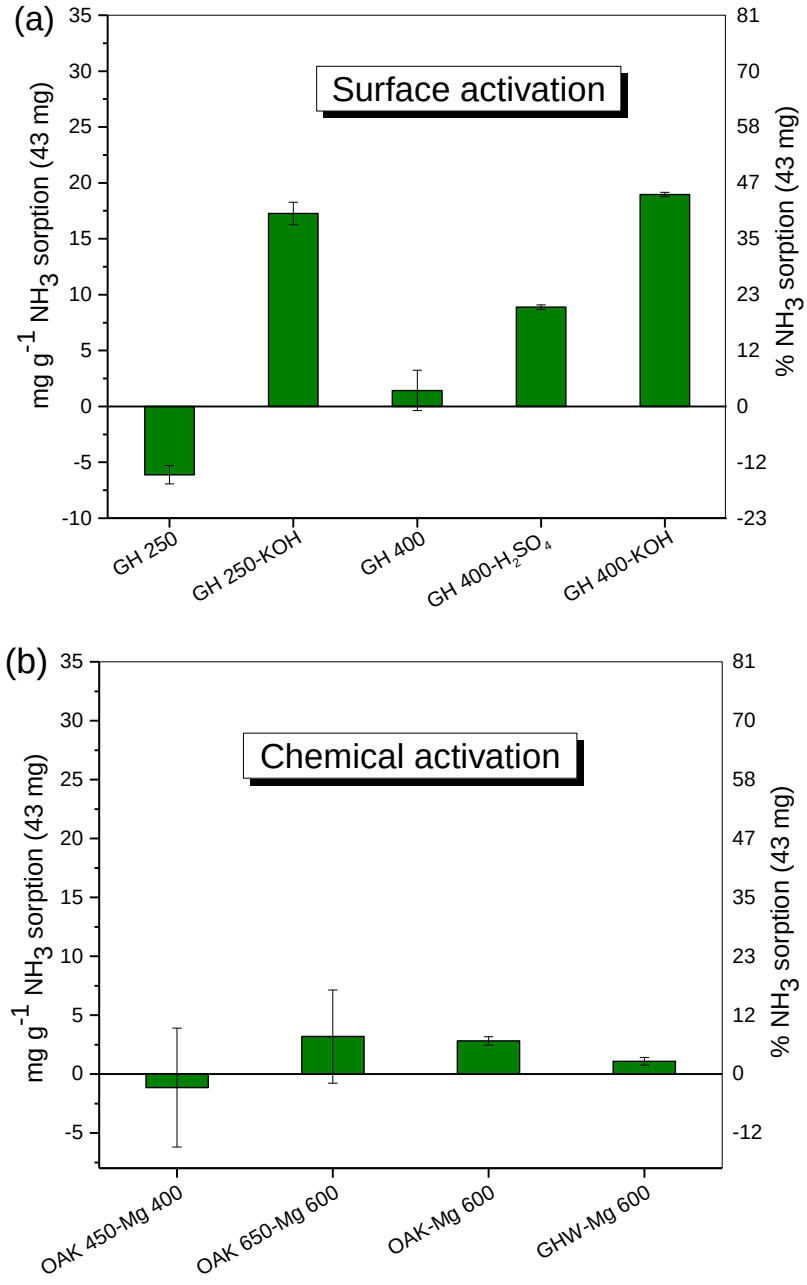

Figure 6.7 Ammonia sorption by treated chars: (a) Increases in greenhouse waste char ammonia sorption; (b) variable effects following Mg treatment of oak and greenhouse waste biochars (OAK 450-Mg and OAK 650-Mg) and biomass (OAK-Mg and GH-Mg). All KOH treatments here involved surface activation only.

Similar increases in ammonia sorption have also been reported by Chou et al. (2006) and Ritz et al. (2011). Such increases likely resulted from the formation of recoverable ammonium sulphate salts on adsorbent sites possibly following similar

reactions to those outlined in Chou et al. (2006). It is also likely that increasing H_2SO_4 concentration up to a certain point could enhance ammonia sorption capacity based on findings of Chou et al. (2006). H_2O_2 treatment also has variable effects on char ammonium and ammonia sorption capacities; a marked increase to the ammonia sorption by H_2O_2-treated oak 250°C and oak 450°C is evident. H_2O_2 modification done by Gómez-Serrano et al. (1994) resulted in an increase in hydroxyl and carbonyl groups with increasing treatment time. This suggested that increases to ammonia sorption capacity by H_2O_2-treated chars might have occurred due to interactions between ammonia and OH or CO groups.

All oak chars experienced a reduction in ammonium sorption by KOH- and H_2O_2-treated chars (**Figure 6.8**). regardless of substantial increases in char CEC. Huff et al. (2016) similarly noted that while H_2O_2 treatment increased CEC, methylene blue adsorption capacity decreased, which emphasises that CEC may not be a suitable predictor of char sorption capacity. This might possibly be because ion exchange was not the dominant mechanism for char ammonium sorption, based on ammonium sorption kinetics which generally followed pseudo-second order kinetic model (**Table 6.3**), suggestive of chemisorption reactions. Conversely, in the presence of coexisting ions, a 6-fold increase in ammonium sorption by H_2O_2-treated oak 450°C is observed while that of H_2O_2-treated oak 650°C decreases relative to untreated oak 450°C and 650°C respectively (**Table 6.4**). This is contrary to expectations since increases to ammonium sorption by H_2O_2–treated chars are anticipated when there is less competition between ammonium, other protonated species and metals for adsorption sites (Wang et al. 2015b). Compared to other treatments, both low and high temperature biochars responded better to H_3PO_4 treatment with regard to ammonia sorption, with greater effects in oak 450°C, with about 6.8% to 20.5% ammonia removal efficiency. Such an increase was still lower than untreated and treated oak hydrochars however, with 43% and 57% ammonia removal efficiencies respectively. Optimization of the chemical treatment processes may yield greater increases.

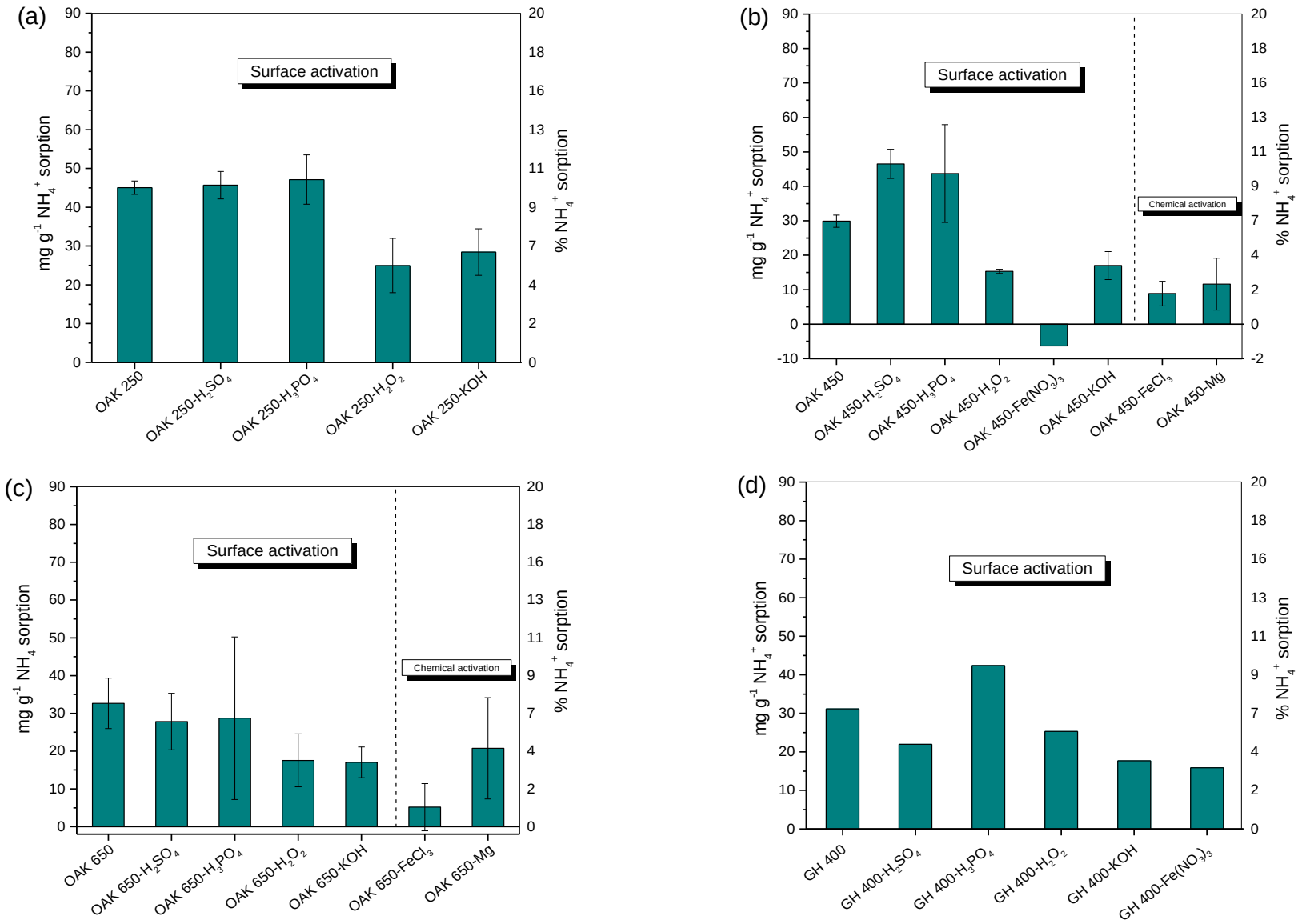

Figure 6.8 Variable effects of surface and chemical activation on the char ammonium sorption capacities of (a) oak 250°C hydrochar; (b) oak 450°C biochar; (c) oak 650°C biochar; (d) GH 400°C biochar. Error bars not included in GH samples because single analysis done only.

Table 6.3 Adsorption kinetics model parameters

Char	Pseudo-second order				First order	Intra-particle Diffusion
	$q_{e\ exp}$ (mg g^{-1})	$q_{e\ cal}$ (mg g^{-1})	k_2 (min g mg^{-1})	R^2	R^2	R^2
OAK 450-KOH	-5.97	-5.2	0.0003	0.166	0.003	0.830
OAK 650-KOH	14.10	12.3	-0.0004	0.976	0.673	0.640
GH 400-KOH	17.70	16.4	-0.0003	0.933	0.306	0.014
OAK 450-H_2O_2	14.90	13.8	-0.0006	0.999	0.965	0.297
OAK 650-H_2O_2	8.50	7.1	0.0004	0.117	0.144	0.114
GH 400-H_2O_2	25.32	26.5	0.0005	0.707	0.026	0.110
OAK 450-$Fe(NO_3)_3$	-6.30	5.1	0.0005	0.841	0.215	0.045
OAK 450-$FeCl_3$	8.90	8.4	-0.0010	0.955	0.345	0.033
OAK 650-$FeCl_3$	5.20	4.5	-0.0009	0.956	0.509	0.889

$q_{e\ exp}$ and $q_{e\ cal}$ refer to amount of NH_4^+ adsorbed by chars obtained from experimental data and from plots respectively. For Pseudo-second order model, parameters obtained from plot of t/q_t versus t. The Pseudo-first order model gave consistently low R^2 values and was therefore excluded.

Table 6.4 The effect of co-existing ions on char ammonium sorption capacity

Char	NH_4^+ equilibrium concentration (C_e) mg L^{-1}	NH_4^+ adsorbed (Q_e) mg g^{-1}	% NH_4^+ adsorbed	K_d
OAK 250	536.5±27.5	24.5	4.4	0.046
OAK 450	554.7±20.9	6.3	1.1	0.011
OAK 650	544.6±3.1	16.4	2.9	0.030
GH 250	544.9±3.8	16.1	2.9	0.030
GH 400	534.5±19.9	26.5	4.7	0.050
GH 600	533.5±20.8	27.6	4.9	0.052
OAK 450-H_2O_2	524.6±12.1	36.4	6.5	0.069
OAK 650-H_2O_2	549.9±12.9	11.1	2.0	0.020
OAK (a.r.)-Mg 600 °C	498.4±29.9	62.6	11.2	0.126
GH (a.r.)-Mg 600 °C	485.6±15.8	75.4	13.4	0.155

Synthetic wastewater concentration (mg L^{-1}): NH_4^+: 561.0±5.4; Mg^{2+}: 28.6±5.3; Ca^{2+}: 150.2±0.6; Na^+: 318.7±14.3; K^+: 513.5±6.0; SO_4^{2-}: 27.5±0.5; NO_2^-: 46.4±0.5; PO_4^{3-}: 67.4±4.2; NO_3^-: 889.1±7.3.

6.3.2 Recoverable nitrogen

Figure 6.9 shows the proportion of ammonium recovered for selected treated chars, amounting to a little under half of the total adsorbed ammonium. 0.01 M KCl-extractable ammonium suggests that some ammonium may be readily available for plants when treated chars are in contact with soil water although specific pot trials are required to confirm this.

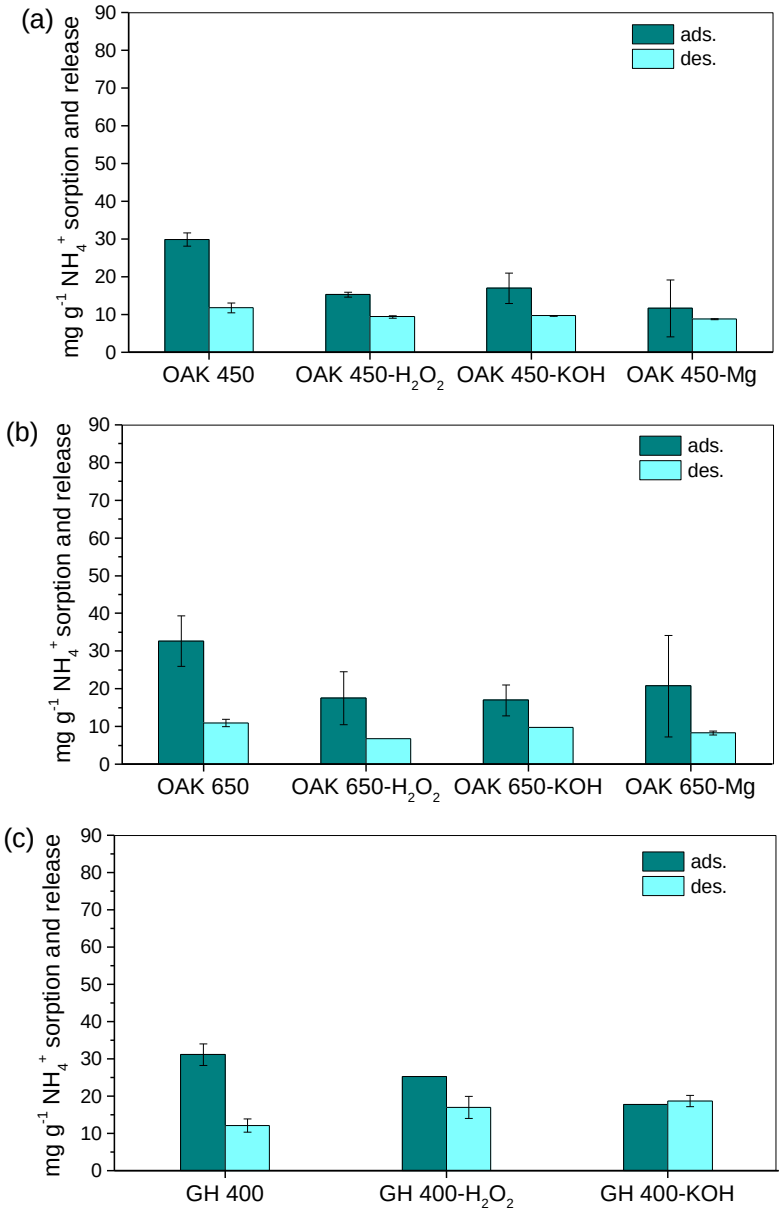

Figure 6.9 Similarities in amounts of 0.01 M KCl-extractable ammonium from some treated chars: (a) oak 450°C; (b) oak 650°C; (c) GH 400°C. Columns without error bars are single analyses only.

6.4 Influence of chemical treatment on char phosphate sorption

The phosphate sorption capacities of biochar derived from traditionally used biomass (oak) and agricultural waste (paprika waste) with comparable carbon contents (>40%) were evaluated following activation with various chemical agents to understand the effect of these treatments on biochar phosphate recovery.

6.4.1 Chemical activation with magnesium

Figure 6.10 shows that biochars treated with magnesium salts adsorbed the highest phosphate, with Mg-OAK 650 adsorbing more phosphate than Mg-oak 450°C. Mg treatment of oak biochar resulted in much greater phosphate sorption, particularly smaller particle size ($\leq$850 µm) biochars (**Figure 6.11**). To identify whether this was due to differences in biochar properties or to temperature, the phosphate removal efficiencies of oak 650°C pyrolyzed at 400ºC and 600ºC were compared. Phosphate sorption was found to be lower in the former suggesting that temperatures >400°C are required for developing adequate phosphate adsorbents. SEM/EDS of oak 650°C following Mg treatment at 600ºC confirmed the presence of Mg (**Figure 6.12)** while no visible differences were observed in oak 450ºC after 400°C Mg treatment (data not included). Some Mg^{2+} was leached into the phosphate solution during the test, as evidenced by the slightly lower count number and from ion chromatography data (data not included). As there was a marked increase to phosphate sorption observed for 600°C Mg treatment, this temperature was used for Mg-treatment of unpyrolyzed oak and greenhouse waste. Both Mg-treated biomass samples showed even greater phosphate sorption compared to their Mg-treated biochar counterparts and compared favourably with adsorbents from previous studies (**Table 6.5**). Thus in-situ magnesium modification is more reasonable than biochar post-treatment in terms of phosphate sorption and cost, as a single-step modification and pyrolysis process is involved which reduces energy requirements.

Following desorption tests, 8.9 mg g^{-1} phosphate was released from Mg-treated oak biomass, but was undetected in the case of greenhouse waste biomass. Only a small portion of phosphate was recoverable by 0.01 M KCl as shown in **Figure 6.11**, regardless of the particle size of oak biochar treated with magnesium. Further investigations are required to better understand why phosphate release was low, as this impacts its potential for use as a soil fertilizer, or for repeated use in wastewater. Alternatively, the incorporation of post-sorption Mg-oak 650°C biochars in composts shows potential for minimising nitrogen losses that arise during the composting process. For instance, Wong et al. (2017) recommended the addition of

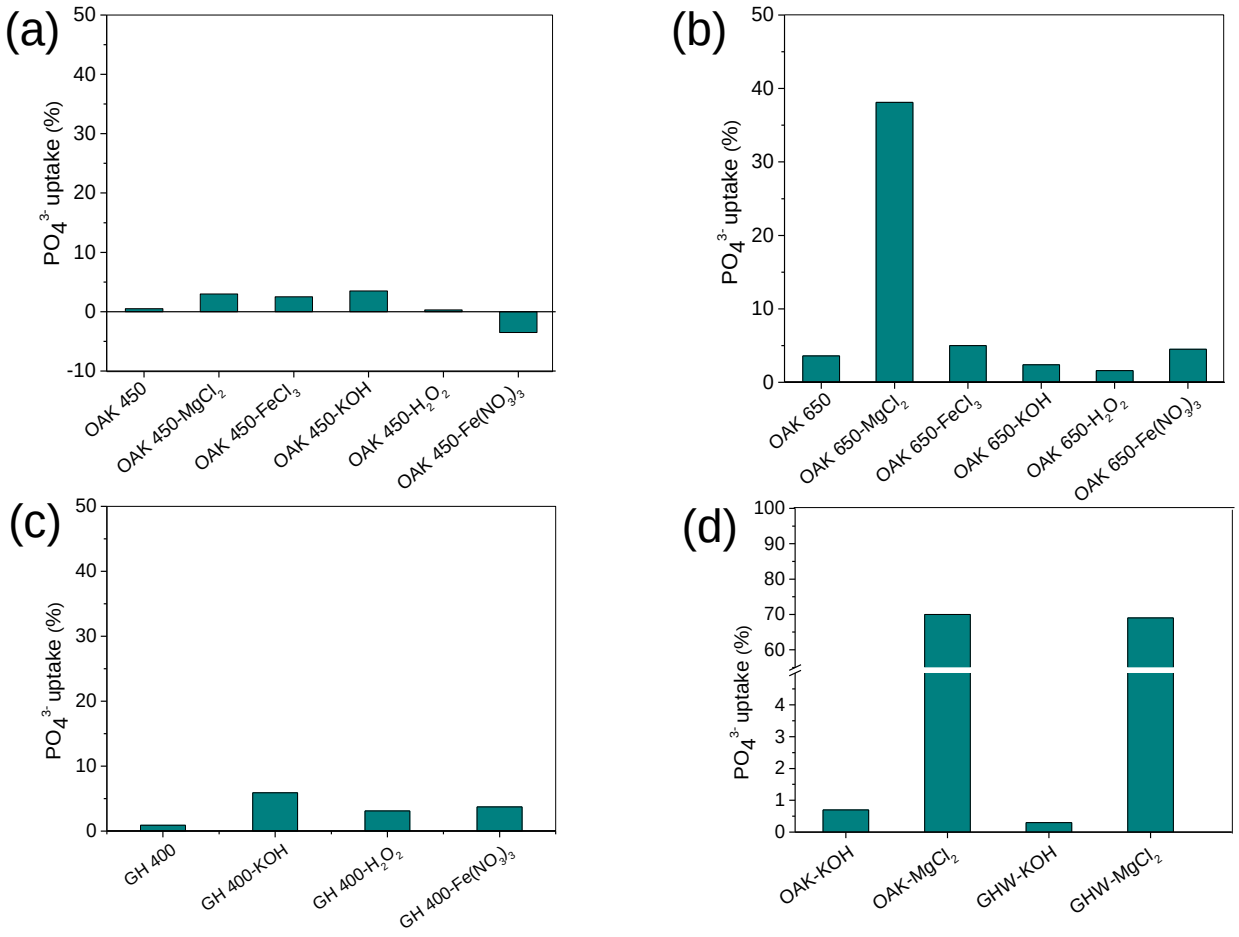

Figure 6.10 Effect of various chemical treatments on char phosphate sorption.

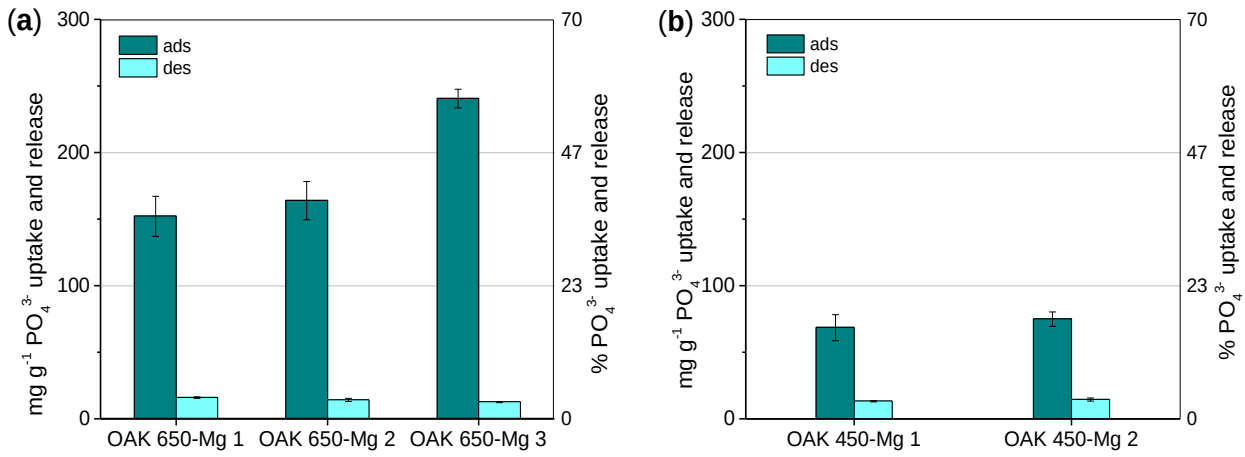

Figure 6.11 Effect of biochar particle size on sorption of phosphate: (a) oak 650°C; (b) oak 450°C where suffixes 1, 2 and 3 refer to Mg treatments performed thus; (1): biochars (≤4.75 mm) left to stand for 2 h in Mg solution, filtered and pyrolysed; (2): biochars (≤ 4.75 mm) left to stand for 2 h in Mg solution, heated overnight at 90°C, filtered and pyrolysed; (3): biochars (≤850 µm) treated as in (2).

Mg and P salts to composts to facilitate struvite precipitation to minimise such nitrogen losses, but also noted some of the challenges associated with this option, such as the insolubility or pH of some of the magnesium salts or oxides suggested. EDS imaging shows that some Mg is still present in the post-sorption Mg-treated oak 650°C biochar (**Figure 6.12**). Although the ammonium sorption capacity of the post-PO_4 sorption Mg-oak 650°C biochar was not tested in this study, Mg-treated oak 650°C (i.e., pre-PO_4^{3-} sorption) demonstrated good NH_4^+ sorption ability from batch sorption tests using synthetic wastewater (**Table 6.5**). For both in-situ and post-treatment magnesium modification processes, coexisting ions were not found to have an adverse effect on phosphate sorption: from a synthetic solution containing 450 mg NH_4^+ L^{-1} and 67 mg PO_4^{3-} L^{-1}, oak chips pyrolysed following Mg treatment (in-situ modification) recovered 66% and 72% phosphate at pH 7 and 8.5 respectively. This is expected, given that pH ranges >7 are typically used for struvite precipitation. Similarly, high phosphate removal efficiencies were maintained by in-situ modified greenhouse waste and oak biomass feedstocks in synthetic wastewater (**Table 6.5**). Other studies (Yao 2013; Zhang et al. 2009) similarly found that PO_4^{3-} sorption was not greatly affected by coexisting ions.

Over time, it is possible that Mg-treated chars may react with atmospheric CO_2 however; soil incubation tests with oak 650°C-Mg revealed that this char behaved differently from other chars in that negative CO_2 evolution occurred, suggestive of CO_2 sorption (Annex Fig. A4(a)). Inorganic nitrogen retention did not appear to be adversely affected however (Annex Fig. A4(b,c)). The dynamics of CO_2 interactions with Mg-treated char and the impact of such reactions on nutrient sorption and treated char storage therefore require further investigation.

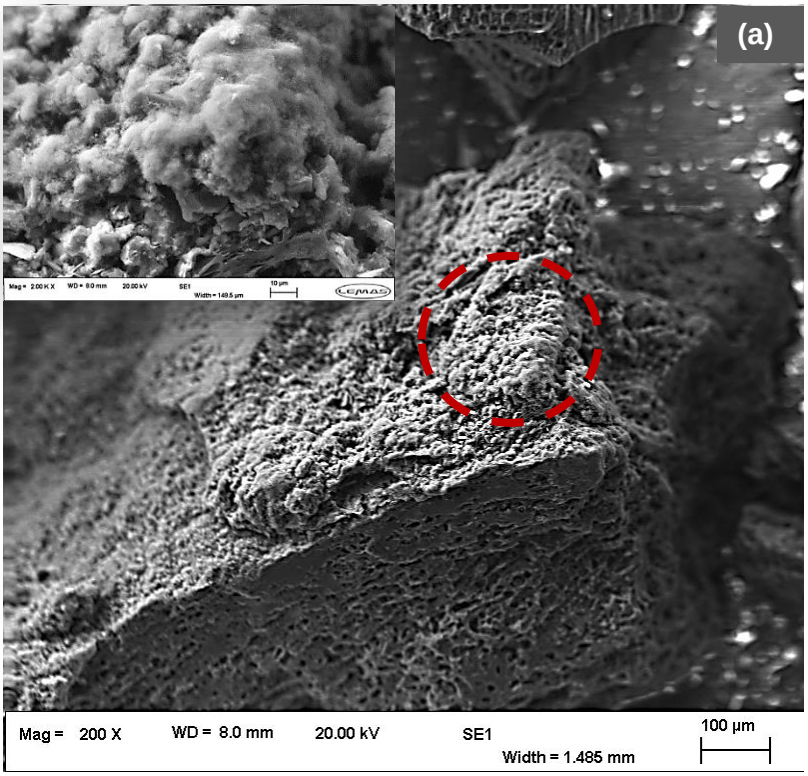

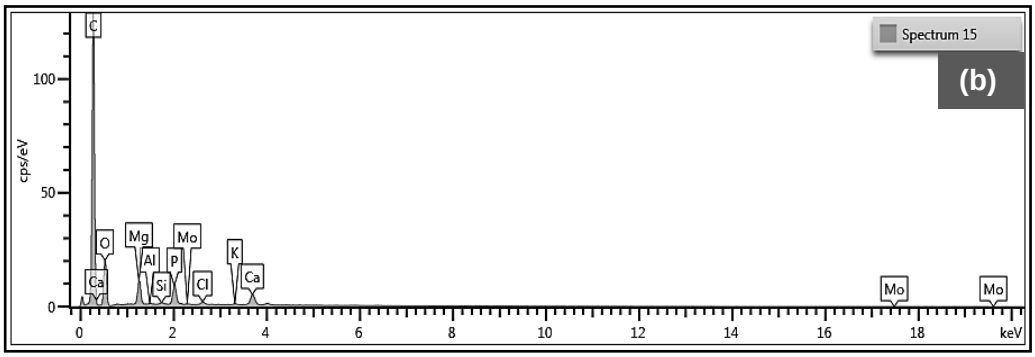

Spectrum 15

Element	Wt.%	Wt% Sigma
C	74.14	0.23
O	20.90	0.23
Mg	1.72	0.03
Al	0.05	0.01
Si	0.09	0.01
P	1.38	0.03
Cl	0.21	0.02
K	0.10	0.02
Ca	1.27	0.03
Mo	0.14	0.04
Total:	100.00	

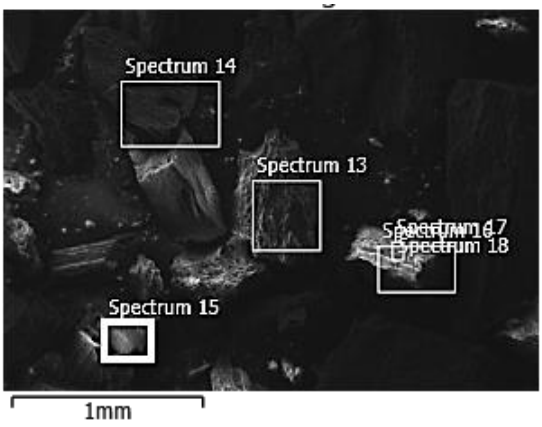

Figure 6.12 (a) SEM image of Mg-treated oak 650°C biochar following phosphate sorption; (b) EDS imaging confirming presence of Mg and P species on oak 650°C biochar

Table 6.5 Phosphate removal efficiencies of some adsorbents

	Present study			
	PO_4^{3-} sorption (C_o = 67 mg PO_4^{3-} L^{-1})		[a]PO_4^{3-} sorption (synthetic wastewater)	
Adsorbent	%	mg g^{-1}	%	mg g^{-1}
Oak 450 °C biochar	1.5	1.0 ± 2.2	7.2	14.8 ± 0.6
Oak 650 °C biochar	1	0.7 ± 0.1	6.1	4.1 ± 0.7
GHW 400 °C biochar	0	-2.2 ± 0.2	0	-4.9
Oak-Mg 600 °C biochar (in-situ)	95.9	64.6 ± 0.2	>95[b]	>64
GH-Mg 600 °C biochar (in-situ)	96.5	65.1 ± 1.3	>95[b]	>64

	Previous studies	
	% Phosphate sorption (C_o = 61 mg L^{-1})	Reference
La oak sawdust biochar (500 ºC)	~33	Wang et al. (2015a)
Fe (II) sugarcane bagasse fibre	97[c]	Carvalho et al. (2011)
MgO sugarcane bagasse biochar	>35	Zhang et al. (2012)
MgO sugar beet tailing biochar	>65	Zhang et al. (2012)
Digested sugar beet tailing biochar	>70	Yao (2013)
Fe-Mn binary oxide	>95	Zhang et al. (2009)
Fe (II) activated carbon	~63 – 96[c]	Wang et al. (2012)

[a]Synthetic wastewater concentrations (mg L^{-1}): SO_4^{2-}: 27.5 ± 0.5; NO_2^-: 46.4 ± 0.5; PO_4^{3-}: 67.4 ± 4.2; NO_3^-: 889.1 ± 7.3; Mg^{2+}: 28.6 ± 5.3; Ca^{2+}: 150.2 ± 0.6; Na^+: 318.7 ± 14.3; K^+: 513.5 ± 6.0; NH_4^+: 561.0 ± 5.4; [b]no PO_4^{3-} detected in final solution after 24 h so total PO_4^{3-} sorption assumed although Mg^{2+} present in synthetic wastewater may have contributed to PO_4^{3-} removal; [c]Initial PO_4^{3-} concentrations of 11-46 mg L^{-1}. Oak and GH biomass treated with Mg.

6.4.2 Iron treatment

Both ferric nitrate and chloride treatments performed on oak biochars resulted in only modest increases to phosphate removal efficiency despite the fact that up to 33 mg g^{-1} iron was present in the biochars treated with ferric nitrate. Yao (2013) found that surface modification of biochars with iron nitrate decreased their phosphate sorption capacity from pure phosphate solutions (pH 7) by about 51%. Conversely, Krishnan and Haridas (2008) and Nguyen et al. (2013) found that adsorbent treatment with iron nitrate and chloride salts increased phosphate sorption from

pure phosphate solutions (pH 3). Three hypotheses may be drawn from these studies: Fe-treated adsorbents may perform best in phosphate solutions with low pH; in other words, phosphate solution pH is more important than the nature of Fe salt used for adsorbent modification. This is understandable given that anion exchange capacity is pH-dependent (Biswas et al. 2007; Zhang et al. 2009). While Wang et al. (2011) demonstrated that adsorbent treatment with Fe^{2+} salt increased phosphate sorption capacity to a greater extent than with Fe^{3+} salt, maximum phosphate sorption was achieved at the lowest pH conditions for both Fe^{2+} and Fe^{3+} treated adsorbents. Secondly, Fe treatment process influences adsorbent phosphate sorption. Nguyen et al. (2014) recommended the base treatment (saponification) or oxidation of adsorbent materials prior to metal loading as evidence suggests that such cationization processes increase the effectiveness of metal deposition onto adsorbents, thus enhancing their phosphate removal efficiency. In one study however (Carvalho et al. 2011), although adsorbent etherification prior to Fe^{2+}-treatment increased adsorbent phosphate sorption, a comparable result was obtained by non-etherified Fe^{2+}-treated adsorbent, with 97% and 93% removal efficiencies respectively. Finally, it is reasonable for biomass or biochar composition to influence the effectiveness of Fe treatment. From the few studies highlighted earlier however, differences between high efficiency Fe-treated phosphate adsorbents (coir pith, sugarcane bagasse, orange waste, activated carbon) and low efficiency Fe-treated adsorbents (anaerobically digested sugar beet tailing biochar, oak biochar) were not readily discernible. Yao (2013) however suggested that ferric hydroxide precipitates might have coated biochar MgO (periclase), the latter likely being responsible for phosphate sorption.

Overall, these findings suggest that surface activation of biochars with or without a pre-treatment step is sufficient for increasing adsorbent phosphate removal efficiency. In this study, as further pyrolysis yielded only marginal increases to phosphate sorption, this additional heat treatment step was considered uneconomical. Furthermore, based on earlier highlighted studies, pH appeared to influence Fe-loaded adsorbent phosphate removal efficiency to a larger extent than adsorbent composition or treatment route. In other words, an additional pyrolysis step following biochar treatment in Fe solutions may not be necessary.

6.4.3 KOH treatment

SA-KOH treatment increased the phosphate sorption capacity of GH 400°C, and previous studies (Samadi 2006; Sarkhot et al. 2013) have suggested ligand

exchange between OH^- and PO_4^{3-}. Further studies are required however, as FTIR did not reveal a substantial increase in hydroxyl groups present in GHW 400 and most other chars in this study. Furthermore, preliminary phosphate sorption tests on SA-KOH treated oak biochars showed some increase in their removal efficiencies, but were comparable to CA-KOH treated oak biochars. Low phosphate sorption following similar CA-KOH treatment was also observed elsewhere (Park et al. 2015).

6.4.4 H_2O_2 treatment

H_2O_2-treated OAK 450 and GHW 400 did not increase phosphate sorption possibly due to a reduction in magnesium and other inorganic elements as earlier suggested, but further analysis is required to confirm this. This lack of increase following acid treatment has also been observed elsewhere (Park et al. 2015), attributed to the formation of greater negative functional groups on biochar surfaces after acid treatment (Wang et al. 2015b).

6.4.5 Char phosphate adsorption kinetics

Phosphate adsorption kinetics of some surface and chemically treated biochars as shown in **Table 6.6**. q_e values obtained from adsorption kinetics experiments were generally lower than batch adsorption q_e values possibly due to some sample loss while taking aliquots periodically. Experimental q_e values were fitted to the pseudo-first order, pseudo-second order and intra-particle diffusion models with parameters determined from models' plots. Both pseudo-first order and intra-particle diffusion models gave very poor fits for most biochars compared to the linearized pseudo-second order model. R^2 values in the lattermost were higher and there was better agreement between experimental and calculated q_e values although some K_2 values were negative possibly due to some phosphate release during the sorption tests. The pseudo-second order model has also been found to be a better fit for describing char dye sorption (Mahmoud et al. 2012). Intercept values were high in the intra-particle diffusion model and the regression plot not passing through the origin suggested that intra-particle diffusion was not a rate-controlling step (Cheung et al. 2007).

Table 6.6 Adsorption kinetics model parameters

Char	Pseudo-second order				Pseudo-First order R^2	Intra-particle Diffusion R^2
	$q_{e\ exp}$ (mg g^{-1})	$q_{e\ cal}$ (mg g^{-1})	k_2 (min g mg^{-1})	R^2		
OAK 450-KOH	17.2	16.1	-0.0008	0.994	0.486	0.037
OAK 650-KOH	25.9	21.2	0.0198	0.984	0.212	0.228
GH 400-KOH	21.5	21.2	0.0198	0.984	0.151	0.026
OAK 450-$Fe(NO_3)_3$	-15.0	-14.4	-0.0028	0.833	0.000	0.137
OAK 650-$Fe(NO_3)_3$	19.4	17.8	-0.0003	0.974	0.788	0.006
GH 400-$Fe(NO_3)_3$	16.1	14.5	-0.0013	0.854	0.330	0.332
OAK 450-$MgCl_2$	16.9	15.6	-0.0004	0.974	0.863	0.059
OAK 650-$MgCl_2$	101.8	108.7	0.0001	0.991	0.342	0.856
OAK 450-$FeCl_3$	16.6	16.0	-0.0009	0.991	0.475	0.293
OAK 650-$FeCl_3$	25.0	23.4	-0.0004	0.990	0.950	0.065

$q_{e\ exp}$ and $q_{e\ cal}$ refer to amount of PO_4^{3-} adsorbed by chars obtained from experimental data and from plots respectively. In Pseudo-second order model, parameters obtained from plot of t/q_t versus t. The pseudo-first order model generally had higher R^2 values than the first order model but in some cases was substantially higher, e.g., GH 400-KOH = 0.672; OAK 650-Mg = 0.912; OAK 450-$FeCl_3$ = 0.607.

6.5 Conclusions

The potential for increasing char ammonia, ammonium, and phosphate sorption capacities following chemical activation of biochars (post-treatment) and biomass (in-situ treatment) with metal salts, KOH and acids was investigated. Of the chemical treatments performed in this study, phosphoric acid showed the greatest potential for increasing ammonia and ammonium sorption capacities in both low and high temperature biochars. For phosphate recovery, while most chemical activation methods resulted in marginal increases, biochars and biomass feedstocks treated with magnesium salts increased phosphate sorption capacity the most. Compared to their untreated biochars, Mg-treatment of oak and greenhouse waste biomass feedstocks resulted in an increase in phosphate sorption capacity from 3.6% to 70.3% and from 2.1% to 66.4%, respectively. With further process optimization, chemical treatment of oak biochars could serve as templates for similar chemical treatments with waste-derived chars. These findings demonstrate that char surface functionality is more influential than surface area in terms of ammonia, ammonium, and phosphate recovery, thus modification processes aimed at increasing surface functionality are suitable methods for upgrading char sorption capacities for such nutrients.

CHAPTER 7

Conclusions, Recommendations and Future Work

This thesis set out to address three main research questions: Can hydrochars and biochars produced from herbaceous and treated municipal waste be used for nutrient recovery? Which char properties may serve as predictors of char nutrient (nitrogen and phosphorus) sorption capacity from wastewater? How do hydrochars and biochars influence inorganic nitrogen and carbon dioxide evolution in a relatively high pH soil, and are these effects comparable to widely used char stability measurement tools? It is anticipated that this study will contribute to growing hydrochar and biochar research, in terms of addressing wastewater quality issues and challenges associated with char commercial competitiveness. To address these research questions, an evaluation of key char physicochemical properties was performed, followed by modification of some of these properties using well-known carbon modification methods at mild activation conditions. Hydrochars and biochars produced at 250–650°C were derived from predominantly herbaceous waste and treated municipal waste feedstocks, namely pepper waste from a greenhouse; air-dried presscake from the anaerobic digestion of municipal organic waste; the cellulose-rich fraction of steam-autoclaved municipal waste; greenwaste, and pig manure. These were compared with relatively low-contaminant, bark-free holm oak wood hydrochars and biochars produced by a traditional pyrolysis kiln reactor and an auger reactor. A small set of 600–750°C gasification chars derived from greenhouse waste were also evaluated to gain better understanding of the relationships between feedstock properties and processing conditions on char properties.

Based on a comparison of key char physicochemical properties, pyrolysis reactor type appeared to influence mainly char surface physical properties likely due to re-deposition of condensable gases onto char pores within the auger screw conveyor pyrolysis reactor. Other char properties were comparable across all reactor types however: as expected, processing temperature accounted for most of the differencesin char functional groups; the degradation of lignocellulose structures were mostly similar in all feedstocks, while char inorganic contents were mostly feedstock-dependent. Short-term laboratory incubation tests designed to quantify

the carbon dioxide emissions and inorganic nitrogen (NH_4-N and NO_3-N) mineralisation of a pH 8 Mediterranean soil amended with hydrochars and biochars derived from oak, greenhouse waste and presscake were in agreement with elemental analysis and recalcitrance data, in that the chars tested had comparable effects on carbon dioxide and inorganic nitrogen mineralisation in soil although hydrochars, notably greenhouse waste hydrochar, generated higher amounts of ammonium and carbon dioxide compared to the 400°C biochars tested, showing higher mineralization rates in the former. These findings suggest that various pyrolysis reactors can be expected to yield chars with fairly similar chemical properties although the removal of condensable volatiles during pyrolysis may enhance char surface areas.

The relationships between char physicochemical properties and char behaviour in nutrient-rich environments as well as a high pH soil were explored as a means of predicting char suitability for nutrient recovery. Key physicochemical properties evaluated included surface area, CEC, ash and mineral content. From evaluations of char ammonium/ammonia and phosphate sorption capacities from pure solutions in batch sorption tests, it was found that ammonium and phosphate nutrient sorption was mostly independent of char surface areas and more a function of acidic oxygen functional groups and specific minerals (magnesium and calcium), respectively. This was demonstrated in the case of oak hydrochars, whose acidic nature favoured the sorption of ammonia compared to oak biochars. This implied that for chars deficient in such species, the incorporation of acidic oxygenated species and mineral matter via chemical treatment could enhance their ammonium/ammonia and phosphate sorption capacities. Conversely, greenhouse waste hydrochars were also acidic in nature behaved differently in the presence of ammonia gas possibly due to its higher nitrogen content. Overall however, there were similarities between all char sorption capacities, as ammonium and phosphate removal capacities ranged from 105.8–146.4 mg g^{-1} and 0–30 mg g^{-1}, equivalent to about 15% and 7%, respectively of which only a fraction was 0.01 M KCl-extractable.

As nutrient recovery from wastewater using untreated chars were generally low, various chemical treatments were evaluated to enhance char potential for nitrogen and phosphorus recovery based on frequently used char chemical modification methods. Furthermore, the effects of treatment route (i.e., biomass pre-treatment versus biochar post-treatment on char ammonium/ammonia and phosphate sorption were evaluated. Findings showed that char surface functionality was more influential

than surface area for both ammonium, ammonia, and phosphate recovery, and modification processes aimed at improving the former enhanced char ammonia and ammonium sorption to some extent. For instance, while untreated biochars adsorbed 0-4.4% $phosphate^-$, the treatment of oak and greenhouse waste increased phosphate adsorption from 3.6% to 70.3% in oak biochars, and from 2.1% to 66.4% in greenhouse waste biochars.

A number of studies on modifying chars for environmental management involve additional pyrolysis/calcination steps but as shown in this study, this is not always required. For instance, compared to surface activation of chars with iron nitrate, further pyrolysis of oak 450°C and oak 650°C treated with $FeCl_3$ did not increase both ammonium and phosphate sorption capacity sufficiently to justify increase in cost and energy. Similarly, simple surface activation processes with KOH which did not involve further high heat treatment yielded substantial improvements in char performance in a previous study. In this study, similar KOH surface activation of oak and greenhouse waste hydrochar resulted in increases to ammonia sorption particularly in the latter char. These findings suggest that other treatment parameters such as activating agent dosage or contact time are factors to consider for optimization before resorting to (high) temperature treatment, from a cost and energy perspective. Furthermore, based on this study, surface area does not influence char ammonia / ammonium and phosphate as much as char functional groups. In fact, it was expected that the high surface area of chars such as oak 650°C would respond better to chemical treatment in the sense that more sites would be available for the various species introduced during chemical treatment, yet this was not the case.

Potential applications for nitrogen-loaded chars may involve cascading-use systems, wherein hydrochars and modified biochars can be used to minimize ammonia emissions from animal housing and effluents. Likewise, phosphate-loaded chars could be applied directly to soil or incorporated in composts to minimise nitrogen losses during composting. However, the feasibility of using treated and untreated hydrochars and biochars as litter, animal bedding material, or soil / compost enhancers requires in depth investigation as to the effects of chemically treated adsorbents on livestock health and soil microbial activity. The ammonia batch set-up used in this study may be regarded as a useful tool for screening potential ammonia adsorbents, and benefits could also arise from comparison of adsorbent performance in dynamic test conditions, or in batch set-ups where humidity and other factors are better controlled. Overall, findings from this study suggest that it is

possible to enhance waste-derived char capacity for ammonia/ammonium and phosphate sorption by treatment of biochars or biochar precursors (raw feedstock) with inorganic chemicals, albeit with more process optimization.

Limitations of this study and recommendations for future work

1. The small-scale composting study would have benefitted from further analysis of the chars recovered from the composted mixtures to determine the organic and inorganic nitrogen species present in the chars, as this may have explained some of the differences between batch ammonia sorption tests and composting tests. Co-composting and soil incubation trials with more treated chars using the same soil/organic materials would have provided further comprehensive understanding of the impact of char treatment. Furthermore, plant growth trials preferably over long (> 1 year) timeframes including analyses of the effect of treated chars on nutrient retention and on soil microbial communities to provide more information on the potential benefits and shortcomings of treated chars for large-scale application.
2. Optimization of the chemical treatments which showed the greatest potential for nitrogen recovery was not possible due to time constraints. Furthermore, the full range of chemical treatments was limited to oak samples due to its relatively low contaminant concentrations. Realistically, oak is not sustainable and its low contaminant level does not provide a comprehensive outlook of the impact of chemical treatment on char nutrient sorption. Furthermore, the enhancement of waste-based feedstocks/chars is more sustainable from a waste management perspective.
3. Char ammonium and phosphate sorption capacities were evaluated at pH 7 as this is a typical range found in wastewater, and to ensure that findings from the study would be comparable with previous studies in the literature. Further tests recommended therefore include:
    (i) Ammonium and phosphate sorption tests at more pH ranges, particularly as previous studies have shown that for phosphate sorption, lower pH ranges of about 3 are most suitable for Fe-loaded adsorbents while higher pH ranges >8 are optimal for struvite recovery.
    (ii) Sorption kinetics tests with more frequent sampling intervals, particularly at the onset of adsorption tests as some studies

show that ammonium and phosphate sorption may occur rapidly within the first 30 min.

(iii) Ammonium and phosphate sorption tests over a wider range of concentrations to provide more accurate information on potential sorption model fits.

4. Repeat desorption cycles to determine ammonium and phosphate release rates would be useful to investigate as this would give a clearer idea of the potential agronomical benefits of such treated chars, since the number of times chars can be used for nitrogen and phosphorus recovery has impact on char economic viability, which ultimately facilitates sound decision-making on the economic viability and sustainability of the various treated chars. Further research is also required to better understand why adsorbed nutrient release was minimal for most biochars, as this determines biochars' potential for reuse or for soil amendment.
5. Experimental design: (i) while some studies have shown that experimental batch and column nutrient sorption systems are comparable, this study would have benefitted from a comparison of both setups particularly for best-performing chars using real wastewater; (ii) ammonia sorption tests using ammonia gas of known concentration would have validated the method used in this study, which involved the generation of ammonia from reagent reactions which, although carefully prepared, could still be vulnerable to operator errors. Furthermore, ammonia sorption setups which account for changes in humidity would provide more information on char sorption performance at different moisture conditions.
6. Results from chemical treatment of oak biochars could serve as templates for similar chemical treatments with waste-derived biochars. For instance, results from sorption tests with chemically treated chars shows that surface activation with KOH and with some acids is suitable for enhancing low temperature (250–450°C) char ammonia sorption capacity, while acid treatment may be more suitable for chars produced at higher temperatures. This is presumably due to the introduction of hydroxyl and other acidic species. Blending low and high temperature chars with waste matter rich in hydroxyl and mineral matter such as magnesium would be more sustainable for nitrogen and phosphorus recovery.

References

Abu El-Rub, Z., Bramer, E.A., Brem, G., 2008. Experimental comparison of biomass chars with other catalysts for tar reduction. Fuel 87, 2243–2252. doi:10.1016/j.fuel.2008.01.004

Ahmad, M., Rajapaksha, A.U., Lim, J.E., Zhang, M., Bolan, N., Mohan, D., Vithanage, M., Lee, S.S., Ok, Y.S., 2014a. Biochar as a sorbent for contaminant management in soil and water: A review. Chemosphere 99, 19–33. doi:10.1016/j.chemosphere.2013.10.071

Ahmad, M.A., Ahmad Puad, N.A., Bello, O.S., 2014b. Kinetic, equilibrium and thermodynamic studies of synthetic dye removal using pomegranate peel activated carbon prepared by microwave-induced KOH activation. Water Resour. Ind. 6, 18–35. doi:10.1016/j.wri.2014.06.002

Ahmed, M.J., 2016. Application of agricultural based activated carbons by microwave and conventional activations for basic dye adsorption: Review. J. Environ. Chem. Eng. 4, 89–99. doi:10.1016/j.jece.2015.10.027

Ahn, S.Y., Eom, S.Y., Rhie, Y.H., Sung, Y.M., Moon, C.E., Choi, G.M., Kim, D.J., 2013. Utilization of wood biomass char in a direct carbon fuel cell (DCFC) system. Appl. Energy 105, 207–216. doi:10.1016/j.apenergy.2013.01.023

Akagi, J., Zsolnay, A., Bastida, F., 2007. Quantity and spectroscopic properties of soil dissolved organic matter (DOM) as a function of soil sample treatments: air-drying and pre-incubation. Chemosphere 69, 1040–6. doi:10.1016/j.chemosphere.2007.04.036

Amonette, J., and Joseph, S., (2009). Characteristics of biochar: Microchemical properties. In: Lehmann, J. and Joseph, S., eds. Biochar for environmental management science and technology. London: Earthscan. pp.43-46, p. 48.

An, T., Nguyen, H., Ngo, H.H., Guo, W., Nguyen, T.V., 2012. Phosphorous Removal from Aqueous Solutions by Agricultural By-products: A Critical Review. J. Water Sustain. 3, 193–207.

Angın, D., Altintig, E., Köse, T.E., 2013. Influence of process parameters on the surface and chemical properties of activated carbon obtained from biochar by chemical activation. Bioresour. Technol. 148, 542–549. doi:10.1016/j.biortech.2013.08.164

Anyikude, K.U., 2016. “Analysis of pollutants in biochars and hydrochars produced by pyrolysis and hydrothermal carbonization of waste biomass”. PhD thesis, University of Leeds, Leeds, United Kingdom.

Apperley, D. C., Robin, H. K., & Hodgkinson, P. (2012). Chapter 3 – Spin-1/2 nuclei: A practical guide. In: Solid-State NMR: Basic Principles and Practice. New York, USA: Momentum Press LLC.

Arriagada, R., García, R., Reyes, P., 1994. Steam and carbon dioxide activation ofEucalyptus globulus charcoal. J. Chem. Technol. Biotechnol. 60, 427–433. doi:10.1002/jctb.280600414

Atkinson, C.J., Fitzgerald, J.D., Hipps, N.A., 2010. Potential mechanisms for achieving agricultural benefits from biochar application to temperate soils: a review. Plant Soil 337, 1–18. doi:10.1007/s11104-010-0464-5

Agency for Toxic Substances & Disease Registry (ATSDR), 2012. Public Health Statement: Styrene [online]. Available from: http://www.atsdr.cdc.gov/phs/phs.asp?id=419&tid=74

Ayoob, S., Gupta, A.K., 2008. Insights into isotherm making in the sorptive removal of fluoride from drinking water. J. Hazard. Mater. 152, 976–985. doi:10.1016/j.jhazmat.2007.07.072

Azargohar, R., Dalai, A.K., 2008. Steam and KOH activation of biochar: Experimental and modeling studies. Microporous Mesoporous Mater. 110, 413–421. doi:10.1016/j.micromeso.2007.06.047

Azargohar, R., 2009. Production of activated carbon and its catalytic application for oxidation of hydrogen sulphide. PhD thesis, University of Saskatchewan, Canada [online]. Available from: https://ecommons.usask.ca/bitstream/handle/10388/etd-04132009-133940/PhDThesis.pdf

Bagreev, A., Bandosz, T.J., Locke, D.C., 2001. Pore structure and surface chemistry of adsorbents obtained by pyrolysis of sewage sludge-derived fertilizer. Carbon N. Y. 39, 1971–1979. doi:10.1016/S0008-6223(01)00026-4

Bahng, M.-K., Mukarakate, C., Robichaud, D.J., Nimlos, M.R., 2009. Current technologies for analysis of biomass thermochemical processing: A review. Anal. Chim. Acta 651, 117–138. doi:10.1016/j.aca.2009.08.016

Bakhmutov, V. I. 2011. Solid-State NMR in Materials Science: Principles and applications. Boca Raton, London, New York: CRC Press. p74, p76.

Bargmann, I., Rillig, M.C., Kruse, A., Greef, J.-M., Kücke, M., 2014. Effects of hydrochar application on the dynamics of soluble nitrogen in soils and on plant availability. J. Plant Nutr. Soil Sci. 177, 48–58. doi:10.1002/jpln.201300069

Battistoni, P., Carniani, E., Fratesi, V., Balboni, P., Tornabuoni, P., 2006. Chemical−Physical Pretreatment of Phosphogypsum Leachate. Ind. Eng. Chem. Res. 45, 3237–3242. doi:10.1021/ie051252h

Beaty, R.D., Kerber, J.D., 1993. Concepts, Instrumentation and Techniques in Atomic Absorption Spectrophotometry, 2nd Edition [online]. Available from: http://www.ufjf.br/baccan/files/2011/05/AAS-Perkin.pdf

Belfer, S., Fainchtain, R., Purinson, Y., Kedem, O., 2000. Surface characterization by FTIR-ATR spectroscopy of polyethersulfone membranes-unmodified, modified and protein fouled. J. Memb. Sci. 172, 113–124. doi:10.1016/S0376-7388(00)00316-1

Benavente, V., Calabuig, E., Fullana, A., 2015. Upgrading of moist agro-industrial wastes by hydrothermal carbonization. J. Anal. Appl. Pyrolysis 113, 89–98. doi:10.1016/j.jaap.2014.11.004

Bernal, M.P., Sánchez-Monedero, M.A., Paredes, C., Roig, A., 1998. Carbon mineralization from organic wastes at different composting stages during their incubation with soil. Agric. Ecosyst. Environ. 69, 175–189. doi:10.1016/S0167-8809(98)00106-6

Biederman, L.A., Harpole, W.S., 2013. Biochar and its effects on plant productivity and nutrient cycling: a meta-analysis. GCB Bioenergy 5, 202–214. doi:10.1111/gcbb.12037

Bimer, J., Sałbut, P.D., Berłożecki, S., Boudou, J.-P., Broniek, E., Siemieniewska, T., 1998. Modified active carbons from precursors enriched with nitrogen functions: sulfur removal capabilities. Fuel 77, 519–525. doi:10.1016/S0016-2361(97)00250-0

Bishop, R., Denton, W., 1946. Production of pyrrole. Patent [online]. Available from: https://www.google.com/patents/US2478452

Biswas, B.K., Inoue, K., Ghimire, K.N., Ohta, S., Harada, H., Ohto, K., Kawakita, H., 2007. The adsorption of phosphate from an aquatic environment using metal-loaded orange waste. J. Colloid Interface Sci. 312, 214–23. doi:10.1016/j.jcis.2007.03.072

Björkman, E., & Strömberg, B. (1997). Release of chlorine from biomass at pyrolysis and gasification conditions1. Energy & Fuels, 0624(5), 1026–1032. http://doi.org/10.1021/ef970031o

Boehm, H.P., 1994. Some aspects of the surface chemistry of carbon blacks and other carbons. Carbon N. Y. 32, 759–769. doi:10.1016/0008-6223(94)90031-0

Bolan, N.S., Wong, L., Adriano, D.C., 2004. Nutrient removal from farm effluents. Bioresour. Technol. 94, 251–260. doi:10.1016/j.biortech.2004.01.012

Borchard, N., Wolf, A., Laabs, V., Aeckersberg, R., Scherer, H.W., Moeller, A., Amelung, W., 2012. Physical activation of biochar and its meaning for soil fertility and nutrient leaching - a greenhouse experiment. Soil Use Manag. 28, 177–184. doi:10.1111/j.1475-2743.2012.00407.x

Brennan, J.K., Bandosz, T.J., Thomson, K.T., Gubbins, K.E., 2001. Water in porous carbons. Colloids Surfaces A Physicochem. Eng. Asp. 187, 539–568.

Brewer, C.E., Schmidt-Rohr, K., Satrio, J.A., Brown, R.C., 2009. Characterization of biochar from fast pyrolysis and gasification systems. Environ. Prog. Sustain. Energy 28, 386–396. doi:10.1002/ep.10378

Brewer, C.E., 2012. Biochar characterization and engineering. Graduate Theses and Dissertations. Paper 12284, Iowa State University [online]. Available from: http://lib.dr.iastate.edu/cgi/viewcontent.cgi?article=3291&context=etd

Brunauer, S., Deming, L.S., Deming, W.E., Teller, E., 1940. On a Theory of the van der Waals Adsorption of Gases. J. Am. Chem. Soc. 62, 1723–1732. doi:10.1021/ja01864a025

Budarin, V., Luque, R., Macquarrie, D.J., Clark, J.H., 2007. Towards a Bio-Based Industry: Benign Catalytic Esterifications of Succinic Acid in the Presence of Water. Chem. - A Eur. J. 13, 6914–6919. doi:10.1002/chem.200700037

Burg, P., Fydrych, P., Cagniant, D., Nanse, G., Bimer, J., Jankowska, A., 2002. The characterization of nitrogen-enriched activated carbons by IR, XPS and LSER methods. Carbon N. Y. 40, 1521–1531. doi:10.1016/S0008-6223(02)00004-0

Burnham, A.K., Zhou, X., Broadbelt, L.J., 2015. Critical Review of the Global Chemical Kinetics of Cellulose Thermal Decomposition. Energy & Fuels 29, 2906–2918. doi:10.1021/acs.energyfuels.5b00350

Busch, D., Glaser, B., 2015. Stability of co-composted hydrochar and biochar under field conditions in a temperate soil. Soil Use Manag. 31, 251–258. doi:10.1111/sum.12180

Cai, T., Park, S.Y., Li, Y., 2013. Nutrient recovery from wastewater streams by microalgae: Status and prospects. Renew. Sustain. Energy Rev. 19, 360–369. doi:10.1016/j.rser.2012.11.030

Cam, L.M., Hung, T. Van, Thu, N.T., Khu, L. Van, Phu, N.H., n.d. Activated carbon (AC) containing transition metal oxides (MeO x) in phenol adsorption and catalytic oxidation of adsorbed phenol by hydrogen peroxide.

Canals-Batlle, C., Ros, A., Lillo-Ródenas, M.A., Fuente, E., Montes-Morán, M.A., Martin, M.J., Linares-Solano, A., 2008. Carbonaceous adsorbents for NH3 removal at room temperature. Carbon N. Y. 46, 176–178. doi:10.1016/j.carbon.2007.10.017

Cao, X., Ro, K.S., Libra, J.A., Kammann, C.I., Lima, I., Berge, N., Li, L., Li, Y., Chen, N., Yang, J., Deng, B., Mao, J., 2013. Effects of biomass types and carbonization conditions on the chemical characteristics of hydrochars. J. Agric. Food Chem. 61, 9401–11. doi:10.1021/jf402345k

Cao, X., Harris, W., 2010. Properties of dairy-manure-derived biochar pertinent to its potential use in remediation. Bioresour. Technol. 101, 5222–5228. doi:10.1016/j.biortech.2010.02.052

Carvalho, W.S., Martins, D.F., Gomes, F.R., Leite, I.R., Gustavo da Silva, L., Ruggiero, R., Richter, E.M., 2011. Phosphate adsorption on chemically modified sugarcane bagasse fibres. Biomass and Bioenergy 35, 3913–3919. doi:10.1016/j.biombioe.2011.06.014

Cetin, E., Moghtaderi, B., Gupta, R., Wall, T.F., 2004. Influence of pyrolysis conditions on the structure and gasification reactivity of biomass chars.

Chen, B., Chen, Z., Lv, S., 2011. A novel magnetic biochar efficiently sorbs organic pollutants and phosphate. Bioresour. Technol. 102, 716–23. doi:10.1016/j.biortech.2010.08.067

Chen, B., Chen, Z., Lv, S., 2011. A novel magnetic biochar efficiently sorbs organic pollutants and phosphate. Bioresour. Technol. 102, 716–23. doi:10.1016/j.biortech.2010.08.067

Chen, T., Deng, S., Wang, B., Huang, J., Wang, Y., Yu, G.,2015. CO_2 adsorption on crab shell derived activated carbons: contribution of micropores and nitrogen-containing groups. RSC Adv. 5, 48323–48330. doi:10.1039/C5RA04937G

Chen, Y.-X., Huang, X.-D., Han, Z.-Y., Huang, X., Hu, B., Shi, D.-Z., Wu, W.-X., 2010. Effects of bamboo charcoal and bamboo vinegar on nitrogen conservation and heavy metals immobility during pig manure composting, Chemosphere. doi:10.1016/j.chemosphere.2009.12.029

Cheung, W.H., Szeto, Y.S., McKay, G., 2007. Intraparticle diffusion processes during acid dye adsorption onto chitosan. Bioresour. Technol. 98, 2897–904. doi:10.1016/j.biortech.2006.09.045

Chou, L., Tsai, R., Chang, J., Lee, M., 2006. Regenerable adsorbent for removing ammonia evolved from anaerobic reaction of animal urine. J. Environ. Sci. 18, 1176–1181. doi:10.1016/S1001-0742(06)60058-2

Chun, Y., Sheng, G., Chiou, C.T., Xing, B., 2004. Compositions and Sorptive Properties of Crop Residue-Derived Chars. Environ. Sci. Technol. 38, 4649–4655. doi:10.1021/es035034w

Chung, J.W., Foppen, J.W., Gerner, G., Krebs, R., Lens, P.N.L., 2015. Removal of rotavirus and adenovirus from artificial ground water using hydrochar derived from sewage sludge. J. Appl. Microbiol. 119, 876–84. doi:10.1111/jam.12863

Clough, T., Condron, L., Kammann, C., Müller, C., 2013. A Review of Biochar and Soil Nitrogen Dynamics. Agronomy 3, 275–293. doi:10.3390/agronomy3020275

Coates, J., 2000. Interpretation of infrared spectra, a practical approach, In: Meyers, R.A. (Ed). Encyclopedia of Analytical Chemistry. Chichester: John Wiley & Sons Ltd, Chichester. pp. 10815–10837

Corre, Y., Seredych, M., Bandosz, T.J., 2013. Analysis of the chemical and physical factors affecting reactive adsorption of ammonia on graphene/nanoporous carbon composites. Carbon N. Y. 55, 176–184. doi:10.1016/j.carbon.2012.12.024

Creamer, R.E., Schulte, R.P.O., Stone, D., Gal, A., Krogh, P.H., Lo Papa, G., Murray, P.J., Pérès, G., Foerster, B., Rutgers, M., Sousa, J.P., Winding, A., 2014. Measuring basal soil respiration across Europe: Do incubation temperature and incubation period matter? Ecol. Indic. 36, 409–418. doi:10.1016/j.ecolind.2013.08.015

Crombie, K., Mašek, O., 2014. Investigating the potential for a self-sustaining slow pyrolysis system under varying operating conditions. Bioresour. Technol. 162, 148–156. doi:10.1016/j.biortech.2014.03.134

Cross, A., Sohi, S.P., 2013. A method for screening the relative long-term stability of biochar. GCB Bioenergy 5, 215–220. doi:10.1111/gcbb.12035

Cuetos, M.J., Morán, A., Otero, M., Gómez, X., 2009. Anaerobic co-digestion of poultry blood with OFMSW: FTIR and TG-DTG study of process stabilization. Environ. Technol. 30, 571–82. doi:10.1080/09593330902835730

Cuetos, M.J., Gómez, X., Otero, M., Morán, A., 2010. Anaerobic digestion of solid slaughterhouse waste: study of biological stabilization by Fourier Transform infrared spectroscopy and thermogravimetry combined with mass spectrometry. Biodegradation 21, 543–56. doi:10.1007/s10532-009-9322-7

Daifullah, A.A.., Girgis, B.., Gad, H.M., 2004. A study of the factors affecting the removal of humic acid by activated carbon prepared from biomass material. Colloids Surfaces A Physicochem. Eng. Asp. 235, 1–10. doi:10.1016/j.colsurfa.2003.12.020

Danso-Boateng, E., Shama, G., Wheatley, A.D., Martin, S.J., Holdich, R.G., 2015. Hydrothermal carbonisation of sewage sludge: effect of process conditions on product characteristics and methane production. Bioresour. Technol. 177, 318–27. doi:10.1016/j.biortech.2014.11.096

Deenik, J.L., Diarra, A., Uehara, G., Campbell, S., Sumiyoshi, Y., Antal, M.J., 2011. Charcoal Ash and Volatile Matter Effects on Soil Properties and Plant Growth in an Acid Ultisol. Soil Sci. 176, 336–345. doi:10.1097/SS.0b013e31821fbfea

Deenik, J.L., McClellan, T., Uehara, G., Antal, M.J.J., Campbell, S., 2010. Charcoal Volatile Matter Content Influences Plant Growth and Soil Nitrogen Transformations. Soil Sci. Soc. Am. J. 1259-1270. doi:10.2136/sssaj2009.0115

Dehkhoda, A.M., Ellis, N., Gyenge, E., 2016. Effect of activated biochar porous structure on the capacitive deionization of NaCl and ZnCl2 solutions. Microporous Mesoporous Mater. 224, 217–228. doi:10.1016/j.micromeso.2015.11.041

Dempster, D.N., Gleeson, D.B., Solaiman, Z.M., Jones, D.L., Murphy, D. V., 2012. Decreased soil microbial biomass and nitrogen mineralisation with Eucalyptus biochar addition to a coarse textured soil. Plant Soil 354, 311–324. doi:10.1007/s11104-011-1067-5

Dias, B.O., Silva, C.A., Higashikawa, F.S., Roig, A., Sánchez-Monedero, M.A., 2010. Use of biochar as bulking agent for the composting of poultry manure: effect on organic matter degradation and humification. Bioresour. Technol. 101, 1239–46. doi:10.1016/j.biortech.2009.09.024

Dias, J.M., Alvim-Ferraz, M.C.M., Almeida, M.F., Rivera-Utrilla, J., Sánchez-Polo, M., 2007. Waste materials for activated carbon preparation and its use in aqueous-phase treatment: a review. J. Environ. Manage. 85, 833–46. doi:10.1016/j.jenvman.2007.07.031

Diebold, J.P., 1994. A unified, global model for the pyrolysis of cellulose. Biomass and Bioenergy 7, 75–85. doi:10.1016/0961-9534(94)00039-V

Do, D., 1998, Adsorption analysis: Equilibria and kinetics, Series on Chemical Engineering Volume 2, London: Imperial College Press, p.2, pp.5-6, pp.11-13.

Donohue, M.D., Aranovich, G.L., 1999. A new classification of isotherms for Gibbs adsorption of gases on solids. Fluid Phase Equilib. 158, 557–563. doi:10.1016/S0378-3812(99)00074-6

Doonan, C.J., Tranchemontagne, D.J., Glover, T.G., Hunt, J.R., Yaghi, O.M., 2010. Exceptional ammonia uptake by a covalent organic framework. Nat. Chem. 2, 235–8. doi:10.1038/nchem.548

Dorward, C., Sitali, S., Ross, A.B. (*in prep*., 2016). Evaluation of the ammonia uptake capacities of various biomass and hydrochars (Working title).

Downie, A., Crosky, A., and Munroe, P. (2009). Physical properties of biochar. In: Lehmann, J. and Joseph, S., eds. Biochar for environmental management science and technology. London: Earthscan. p. 16, pp.24-25.

Duku, M.H., Gu, S., Hagan, E. Ben, 2011. Biochar production potential in Ghana—A review. Renew. Sustain. Energy Rev. 15, 3539–3551. doi:10.1016/j.rser.2011.05.010

Eberhardt, T.L., Min, S.-H., Han, J.S., 2006. Phosphate removal by refined aspen wood fiber treated with carboxymethyl cellulose and ferrous chloride. Bioresour. Technol. 97, 2371–6. doi:10.1016/j.biortech.2005.10.040

Ehrburger, P., Addoun, A., Addoun, F., Donnet, J.-B., 1986. Carbonization of coals in the presence of alkaline hydroxides and carbonates: Formation of activated carbons. Fuel 65, 1447–1449. doi:10.1016/0016-2361(86)90121-3

EPA, 1999. Understanding variation in partition coefficient, k_d, values Volume I: The K_d model, methods of measurement, and application of chemical reaction codes [online]. Available from: https://www.epa.gov/sites/production/files/2015-05/documents/402-r-04-002c.pdf

Epstein, E., 1997. The Science of composting. Basel, Switzerland: Technomic Publishing Company, pp.101-103.

EBC, 2012. 'European Biochar Certificate - Guidelines for a Sustainable Production of Biochar.' European Biochar Foundation (EBC), Arbaz, Switzerland. [online]. Available from: http://www.europeanbiochar.org/en/download. Version 6.2E of 04th February 2016, DOI: Guidelines European Biochar Certificate for a sustainable production of biochar 2 10.13140/RG.2.1.4658.7043

Ekpo, U., Ross, A.B., Camargo-Valero, M.A., Williams, P.T., 2016. A comparison of product yields and inorganic content in process streams following thermal hydrolysis and hydrothermal processing of microalgae, manure and digestate. Bioresour. Technol. 200, 951–960. doi:10.1016/j.biortech.2015.11.018

Fang, B., Lee, X., Zhang, J., Li, Y., Zhang, L., Cheng, J., Wang, B., Cheng, H., 2016. Impacts of straw biochar additions on agricultural soil quality and greenhouse gas fluxes in karst area, Southwest China. Soil Sci. Plant Nutr. 1–8. doi:10.1080/00380768.2016.1202734

Fang, J., Gao, B., Chen, J., Zimmerman, A.R., 2015. Hydrochars derived from plant biomass under various conditions: Characterization and potential applications and impacts. Chem. Eng. J. 267, 253–259. doi:10.1016/j.cej.2015.01.026

Fernando, W.A.R.N., Xia, K., Rice, C.W., 2005. Sorption and Desorption of Ammonium from Liquid Swine Waste in Soils. Soil Sci. Soc. Am. J. 69, 1057. doi:10.2136/sssaj2004.0268

Fidel, R.B., Laird, D.A., Thompson, M.L., Lawrinenko, M., 2017. Characterization and quantification of biochar alkalinity. Chemosphere 167, 367–373. doi:10.1016/j.chemosphere.2016.09.151

Foo, K.Y., Hameed, B.H., 2010. Insights into the modeling of adsorption isotherm systems. Chem. Eng. J. 156, 2–10. doi:10.1016/j.cej.2009.09.013

Fritz, J.S., Gjerde, D.T., 2000. Ion chromatography, Third Edition, Weinheim, Germany: Wiley-VCH Verlag GmbH & Co, KGaA. pp. 1-4.

Fryda, L., Visser, R., 2015. Biochar for Soil Improvement: Evaluation of Biochar from Gasification and Slow Pyrolysis. Agriculture 5, 1076–1115. doi:10.3390/agriculture5041076

Gai, X., Wang, H., Liu, J., Zhai, L., Liu, S., Ren, T., Liu, H., 2014. Effects of feedstock and pyrolysis temperature on biochar adsorption of ammonium and nitrate. PLoS One 9, e113888. doi:10.1371/journal.pone.0113888

Galinato, S.P., Yoder, J.K., Granatstein, D., 2011. The economic value of biochar in crop production and carbon sequestration. Energy Policy 39, 6344–6350. doi:10.1016/j.enpol.2011.07.035

Ganesh, K., Jambeck, J.R., 2013. Treatment of landfill leachate using microbial fuel cells: Alternative anodes and semi-continuous operation, Bioresource Technology. doi:10.1016/j.biortech.2013.04.013

Gaskin, J.W., Speir, A., Morris, L.M., Ogden, L., Harris, K., Lee, D., Das, K.C., 2007. Potential for pyrolysis char to affect soil moisture and nutrient status of a loamy sand soil. Conference proceedings. [Online]. Accessed 21 June 2015. Available from: https://smartech.gatech.edu/bitstream/handle/1853/48168/Gaskin_5.7.4.pdf?sequence=1&isAllowed=y

Gaskin, J.W., Steiner, C., Harris, K., Das, K.C., Bibens, B., 2008. Effect of low-temperature pyrolysis conditions on biochar for agricultural use. Trans. ASABE 51, 2061–2069.

Gaur, V., Sharma, A., Verma, N., 2008. Removal of SO2 by Activated Carbon Fibre Impregnated with Transition Metals. Can. J. Chem. Eng. 85, 188–198. doi:10.1002/cjce.5450850207

Ghosh, U., Luthy, R.G., Cornelissen, G., Werner, D., Menzie, C.A., 2011. In-situ sorbent amendments: a new direction in contaminated sediment management. Environ. Sci. Technol. 45, 1163–8. doi:10.1021/es102694h

Giles, C.H., Smith, D., Huitson, A., 1974. A general treatment and classification of the solute adsorption isotherm. I. Theoretical. J. Colloid Interface Sci. 47, 755–765. doi:10.1016/0021-9797(74)90252-5

Glaser, B., Birk, J.J., 2012. State of the scientific knowledge on properties and genesis of Anthropogenic Dark Earths in Central Amazonia (terra preta de Índio). Geochim. Cosmochim. Acta 82, 39–51. doi:10.1016/j.gca.2010.11.029

Glaser, B., Lehmann, J., Zech, W., 2002. Ameliorating physical and chemical properties of highly weathered soils in the tropics with charcoal - a review. Biol. Fertil. Soils 35, 219–230. doi:10.1007/s00374-002-0466-4

Gokce, C.E., Guneysu, S., Aydin, S., Arayici, S., 2009. Comparison of Activated Carbon and Pyrolyzed Biomass for Removal of Humic Acid From Aqueous Solution. Open Environ. Pollut. Toxicol. J. 1.

Gomez-Serrano, V., Acedoramos, M., Lopezpeinado, A., Valenzuelacalahorro, C., 1994. Oxidation of activated carbon by hydrogen peroxide. Study of surface functional groups by FT-i.r. Fuel 73, 387–395. doi:10.1016/0016-2361(94)90092-2

Granatstein, D., Kruger, C., Educator, B., Collins, H., Garcia-Perez, M., Yoder, J., n.d. Use of Biochar from the Pyrolysis of Waste Organic Material as a Soil Amendment Sustainable Agriculture Specialist Use of Biochar from the Pyrolysis of Waste Organic Material as a Soil Amendment.

Gronwald, M., Don, A., Tiemeyer, B., Helfrich, M., 2015. Effects of fresh and aged chars from pyrolysis and hydrothermal carbonization on nutrient sorption in agricultural soils 1, 475–489. doi:10.5194/soil-1-475-2015

Gronwald, M., Vos, C., Helfrich, M., Don, A., 2016. Stability of pyrochar and hydrochar in agricultural soil - a new field incubation method. Geoderma 284, 85–92. doi:10.1016/j.geoderma.2016.08.019

Grzmil, B., Wronkowski, J., 2006. Removal of phosphates and fluorides from industrial wastewater. Desalination 189, 261–268. doi:10.1016/j.desal.2005.07.008

Gu, Z., Wang, X., 2013. Carbon materials from high ash bio-char: A Nanostructure Similar to Activated Graphene. Am. Trans. Eng. Appl. Sci. 2, 15-34.

Guerrero, M., Ruiz, M.P., Alzueta, M.U., Bilbao, R., Millera, A., 2005. Pyrolysis of eucalyptus at different heating rates: studies of char characterization and oxidative reactivity. J. Anal. Appl. Pyrolysis 74, 307–314. doi:10.1016/j.jaap.2004.12.008

Guo, X., Wang, S., Wang, K., Liu, Q., Luo, Z., 2010. Influence of extractives on mechanism of biomass pyrolysis. J. Fuel Chem. Technol. 38, 42–46. doi:10.1016/S1872-5813(10)60019-9

Gwenzi, W., Chaukura, N., Mukome, F.N.D., Machado, S., Nyamasoka, B., 2015. Biochar production and applications in sub-Saharan Africa: Opportunities, constraints, risks and uncertainties. J. Environ. Manage. 150, 250–261. doi:10.1016/j.jenvman.2014.11.027

Haider, G., Steffens, D., Müller, C., Kammann, C.I., 2016. Standard Extraction Methods May Underestimate Nitrate Stocks Captured by Field-Aged Biochar. J. Environ. Qual. 45, 1196–204. doi:10.2134/jeq2015.10.0529

Hale, S.E., Alling, V., Martinsen, V., Mulder, J., Breedveld, G.D., Cornelissen, G., 2013. The sorption and desorption of phosphate-P, ammonium-N and nitrate-N in cacao shell and corn cob biochars. Chemosphere 91, 1612–9. doi:10.1016/j.chemosphere.2012.12.057

Hao, W., Björkman, E., Lilliestråle, M., Hedin, N., 2014. Activated Carbons for Water Treatment Prepared by Phosphoric Acid Activation of Hydrothermally Treated Beer Waste. Ind. Eng. Chem. Res. 53, 15389–15397. doi:10.1021/ie5004569

Harada, Y., Inoko, A., 1975. Cation-exchange properties of soil organic matter, 1: Effects of conditions for the measurement on cation-exchange capacity values of humic acid preparations. Soil Sci. Plant Nutr. 21, 361-369, DOI: 10.1080/00380768.1975.10432651

Harry, I.D., Saha, B., Cumming, I.W., 2006. Effect of electrochemical oxidation of activated carbon fiber on competitive and noncompetitive sorption of trace toxic metal ions from aqueous solution. J. Colloid Interface Sci. 304, 9–20. doi:10.1016/j.jcis.2006.08.012

Harvey, O.R., Herbert, B.E., Kuo, L., Louchouarn, P., 2012a. Generalized Two-Dimensional Perturbation Correlation Infrared Spectroscopy Reveals Mechanisms for the Development of Surface Charge and Recalcitrance in Plant-Derived Biochars. Environ. Sci. Technol. 46, 10641-10650. dx.doi.org/10.1021/es302971d |

Harvey, O.R., Kuo, L.J., Zimmerman, A.R., Louchouarn, P., Amonette, J.E., Herbert, B.E., 2012b. An Index-Based Approach to Assessing Recalcitrance and Soil Carbon Sequestration Potential of Engineered Black Carbons (Biochars). Environ. Sci. Technol. 46, 1415–1421. doi:10.1021/es2040398

Heilmann, S.M., Jader, L.R., Harned, L.A., Sadowsky, M.J., Schendel, F.J., Lefebvre, P.A., von Keitz, M.G., Valentas, K.J., 2011. Hydrothermal carbonization of microalgae II. Fatty acid, char, and algal nutrient products. Appl. Energy 88, 3286–3290. doi:10.1016/j.apenergy.2010.12.041

Higasio, Y.S., Shoji, T., 2001. Heterocyclic compounds such as pyrroles, pyridines, pyrollidins, piperdines, indoles, imidazol and pyrazins. Appl. Catal. A Gen. 221, 197–207. doi:10.1016/S0926-860X(01)00815-8

Ho, Y.S., Mckay, G., 1998. Kinetic Models for the Sorption of Dye from Aqueous Solution by Wood. Process Saf. Environ. Prot. 76, 183–191. doi:10.1205/095758298529326

Ho, Y.-S., 2004. Selection of optimum sorption isotherm. Carbon N. Y. 42, 2115–2116. doi:10.1016/j.carbon.2004.03.019

Hoekman, S.K., Broch, A., Robbins, C., 2011. Hydrothermal Carbonization (HTC) of Lignocellulosic Biomass. doi:10.1021/ef101745n

Houba, V.J.G., Novozamsky, I., Huybregts, A.W.M., van der Lee, J.J., 1986. Comparison of soil extractions by 0.01M $CaCl_2$, by EUF and by some conventional extraction procedures. Plant Soil 96, 433–437. doi:10.1007/BF02375149

Houben, D., Evrard, L., Sonnet, P., 2013. Mobility, bioavailability and pH-dependent leaching of cadmium, zinc and lead in a contaminated soil amended with biochar. Chemosphere 92, 1450–1457. doi:10.1016/j.chemosphere.2013.03.055

Höxter, S.T., Ramke, H.-G., Blöhse, D., Lehmann, H.-J., Fettig, J., n.d. Hydrothermal Carbonization of Organic Waste Sardinia 2009: Twelfth International Waste Management and Landfill Symposium.

Hsu, J.-H., Lo, S.-L., 1999. Chemical and spectroscopic analysis of organic matter transformations during composting of pig manure. Environ. Pollut. 104, 189–196. doi:10.1016/S0269-7491(98)00193-6

Huff, M.D., Lee, J.W., 2016. Biochar-surface oxygenation with hydrogen peroxide. J. Environ. Manage. 165, 17–21. doi:10.1016/j.jenvman.2015.08.046

Hunt, J., Duponte, M., Sato, D., Kawabata, A., 2010. The basics of biochar : A natural soil amendment. soil and crop management [online]. Available from: http://www.ctahr.hawaii.edu/oc/freepubs/pdf/SCM-30.pdf

IEA Bioenergy, 2007. Biomass Pyrolysis. [online]. Available from: http://www.ieabioenergy.com/wp-content/uploads/2013/10/Task-34-Booklet.pdf

International Biochar Initiative (IBI) 2015. Standardized product definition and product testing guidelines for biochar that is used in soil (aka IBI Biochar Standards) [online]. Available from: http://www.biochar-international.org/sites/default/files/IBI_Biochar_Standards_V2.1_Final.pdf

Inyang, M., Dickenson, E., 2015. The potential role of biochar in the removal of organic and microbial contaminants from potable and reuse water: A review. Chemosphere 134, 232–240. doi:10.1016/j.chemosphere.2015.03.072

Ioannidou, O., Zabaniotou, A., 2007. Agricultural residues as precursors for activated carbon production—A review. Renew. Sustain. Energy Rev. 11, 1966–2005. doi:10.1016/j.rser.2006.03.013

Ippolito, J.A., Spokas, K.A., Novak, J.M., Lentz, R.D., Cantrell, K.B., n.d. Biochar elemental composition and factors infl uencing nutrient retention.

Ishiwatari, R., 1969. Fractionation and characterization of humic acid from a lake sediment. Geochem. J. 2, 175–184. doi:10.2343/geochemj.2.175

Islam, M.A., Benhouria, A., Asif, M., Hameed, B.H., 2015. Methylene blue adsorption on factory-rejected tea activated carbon prepared by conjunction of hydrothermal carbonization and sodium hydroxide activation processes. J. Taiwan Inst. Chem. Eng. 52, 57–64. doi:10.1016/j.jtice.2015.02.010

Ismadji, S., Tong, D.S., Soetaredjo, F.E., Ayucitra, A., Yu, W.H., Zhou, C.H., 2016. Bentonite hydrochar composite for removal of ammonium from Koi fish tank. Appl. Clay Sci. 119, 146–154. doi:10.1016/j.clay.2015.08.022

International Union of Pure and Applied Chemistry (IUPAC), 2014. Compendium of Chemical Terminology Gold Book [online]. Accessed 15 July 2015. Available from: http://goldbook.iupac.org/PDF/goldbook.pdf

Jahirul, M., Rasul, M., Chowdhury, A., Ashwath, N., 2012. Biofuels Production through Biomass Pyrolysis —A Technological Review. Energies 5, 4952–5001. doi:10.3390/en5124952

Jandl, R., Sollins, P., 1997. Water-extractable soil carbon in relation to the belowground carbon cycle. Biol. Fertil. Soils 25, 196–201. doi:10.1007/s003740050303

Jassal, R.S., Johnson, M.S., Molodovskaya, M., Black, T.A., Jollymore, A., Sveinson, K., 2015. Nitrogen enrichment potential of biochar in relation to pyrolysis temperature and feedstock quality. J. Environ. Manage. 152, 140–4. doi:10.1016/j.jenvman.2015.01.021

Jeffery, S., Bezemer, T.M., Cornelissen, G., Kuyper, T.W., Lehmann, J., Mommer, L., Sohi, S.P., van de Voorde, T.F.J., Wardle, D.A., van Groenigen, J.W., 2013. The way forward in biochar research: targeting trade-offs between the potential wins. GCB Bioenergy 7, 1–13. doi:10.1111/gcbb.12132

Jenkins, B.., Baxter, L.., Miles, T.., Miles, T.., 1998. Combustion properties of biomass. Fuel Process. Technol. 54, 17–46. doi:10.1016/S0378-3820(97)00059-3

Jindo, K., Suto, K., Matsumoto, K., García, C., Sonoki, T., Sanchez-Monedero, M.A., 2012a. Chemical and biochemical characterisation of biochar-blended composts prepared from poultry manure. Bioresour. Technol. 110, 396–404. doi:10.1016/j.biortech.2012.01.120

Jindo, K., Sánchez-Monedero, M.A., Hernández, T., García, C., Furukawa, T., Matsumoto, K., Sonoki, T., Bastida, F., 2012b. Biochar influences the microbial community structure during manure composting with agricultural wastes. Sci. Total Environ. 416, 476–481. doi:10.1016/j.scitotenv.2011.12.009

Jindo, K., Sonoki, T., Matsumoto, K., Canellas, L., Roig, A., Sanchez-Monedero, M.A., 2016. Influence of biochar addition on the humic substances of composting manures. Waste Manag. 49, 545–552. doi:10.1016/j.wasman.2016.01.007

Jospeh, S., C. Peacocke, J. Lehmann and P. Munroe, 2009. Developing a biochar classification and test methods.In: Lehmann, J. and Joseph, S., eds. Biochar for environmental management science and technology. London: Earthscan. pp. 107-108.

Jung, K.-W., Hwang, M.-J., Jeong, T.U., Ahn, K.-H., 2015. A novel approach for preparation of modified-biochar derived from marine macroalgae: Dual purpose electro-modification for improvement of surface area and metal impregnation, Bioresource Technology. doi:10.1016/j.biortech.2015.05.052

Jurewicz, K., Babeł, K., Ziółkowski, A., Wachowska, H., 2004. Capacitance behaviour of the ammoxidised coal. J. Phys. Chem. Solids 65, 269–273. doi:10.1016/j.jpcs.2003.10.023

Kalderis, D., Kotti, M.S., Méndez, A., Gascó, G., 2014. Characterization of hydrochars produced by hydrothermal carbonization of rice husk. Solid Earth 5, 477–483. doi:10.5194/se-5-477-2014

Kambo, H.S., Dutta, A., 2015. A comparative review of biochar and hydrochar in terms of production, physico-chemical properties and applications. Renew. Sustain. Energy Rev. 45, 359–378. doi:10.1016/j.rser.2015.01.050

Kammann, C.I., Schmidt, H.-P., Messerschmidt, N., Linsel, S., Steffens, D., Müller, C., Koyro, H.-W., Conte, P., Joseph, S., Stephen, J., 2015. Plant growth improvement mediated by nitrate capture in co-composted biochar. Sci. Rep. 5, 11080. doi:10.1038/srep11080

Kastner, J.R., Miller, J., Das, K.C., 2009. Pyrolysis conditions and ozone oxidation effects on ammonia adsorption in biomass generated chars. J. Hazard. Mater. 164, 1420–1427. doi:10.1016/j.jhazmat.2008.09.051

Kastner, J.R., Miller, J., Geller, D.P., Locklin, J., Keith, L.H., Johnson, T., 2012. Catalytic esterification of fatty acids using solid acid catalysts generated from biochar and activated carbon. Catal. Today 190, 122–132. doi:10.1016/j.cattod.2012.02.006

Keeney, D. R., Bremner, J.M., 1969. Determination of soil cation exchange capacity by a simple semimicro technique : Soil Science. Soil Sci. 107, 334–336.

Keiluweit, M., Nico, P.S., Johnson, M.G., Kleber, M., 2010. Dynamic molecular structure of plant biomass-derived black carbon (biochar). Environ. Sci. Technol. 44, 1247–53. doi:10.1021/es9031419

Kelleher, B.., Leahy, J.., Henihan, A.., O'Dwyer, T.., Sutton, D., Leahy, M.., 2002. Advances in poultry litter disposal technology – a review. Bioresour. Technol. 83, 27–36. doi:10.1016/S0960-8524(01)00133-X

Keown, D.M., Favas, G., Hayashi, J., Li, C.-Z., 2005. Volatilisation of alkali and alkaline earth metallic species during the pyrolysis of biomass: differences between sugar cane bagasse and cane trash. Bioresour. Technol. 96, 1570–1577. doi:10.1016/j.biortech.2004.12.014

Khan, N., Clark, I., Sánchez-Monedero, M.A., Shea, S., Meier, S., Bolan, N., 2014. Maturity indices in co-composting of chicken manure and sawdust with biochar. Bioresour. Technol. 168, 245–251. doi:10.1016/j.biortech.2014.02.123

Kirchmann, H., Witter, E., 1992. Composition of fresh, aerobic and anaerobic farm animal dungs. Bioresour. Technol. 40, 137–142. doi:10.1016/0960-8524(92)90199-8

Kisiki, N., H., Hale, S.E., Cornelissen, G., Bachmann, R.T., 2015. Designing and Performance Evaluation of Biochar Production in a Top-Lit Updraft Upscaled Gasifier. J. Sustain. Bioenergy Syst. 5, 41–55. doi:10.4236/jsbs.2015.52004

Kithome, M., Paul, J.W., Bomke, A.A., 1999. Reducing Nitrogen Losses during Simulated Composting of Poultry Manure using Adsorbents or Chemical Amendments. J. Environ. Qual. 28, 194. doi:10.2134/jeq1999.00472425002800010023x

Kizito, S., Wu, S., Kipkemoi Kirui, W., Lei, M., Lu, Q., Bah, H., Dong, R., 2015. Evaluation of slow pyrolyzed wood and rice husks biochar for adsorption of ammonium nitrogen from piggery manure anaerobic digestate slurry. Sci. Total Environ. 505, 102–12. doi:10.1016/j.scitotenv.2014.09.096

Kleen, M., Gellerstedt, G., 1995. Influence of inorganic species on the formation of polysaccharide and lignin degradation products in the analytical pyrolysis of pulps. J. Anal. Appl. Pyrol. 35, 15-41. doi:10.1016/0165-2370(95)00893-J

Klobes, P., Meyer, K., Munro, R.G., 2006. Porosity and Specific Surface Area Measurements for Solid Materials. [online]. Available from: http://ws680.nist.gov/publication/get_pdf.cfm?pub_id=854263

Kney, a D., Zhao, D., 2004. A pilot study on phosphate and nitrate removal from secondary wastewater effluent using a selective ion exchange process. Environ. Technol. 25, 533–42. doi:10.1080/09593330.2004.9619344

Knežević, D., Van Swaaij, W., Kersten, S., 2010. Hydrothermal Conversion of biomass. II. Conversion of wood, pyrolysis oil, and glucose in hot compressed water. doi:10.1021/ie900964u

Knicker, H., 2007. How does fire affect the nature and stability of soil organic nitrogen and carbon? A review. Biogeochemistry 85, 91–118. doi:10.1007/s10533-007-9104-4

Krishnan, K.A., Haridas, A., 2008. Removal of phosphate from aqueous solutions and sewage using natural and surface modified coir pith. J. Hazard. Mater. 152, 527–35. doi:10.1016/j.jhazmat.2007.07.015

Kuhlbusch, T.A.J., 1995. Method for Determining Black Carbon in Residues of Vegetation Fires. Environ. Sci. Technol. 29, 2695–2702. doi:10.1021/es00010a034

Kumar, K.V., Sivanesan, S., 2006a. Isotherm parameters for basic dyes onto activated carbon: Comparison of linear and non-linear method. J. Hazard. Mater. 129, 147-150. doi:10.1016/j.jhazmat.2005.08.022

Vasanth Kumar, K., Sivanesan, S., 2006b. Equilibrium data, isotherm parameters and process design for partial and complete isotherm of methylene blue onto activated carbon. J. Hazard. Mater. 134, 237–244. doi:10.1016/j.jhazmat.2005.11.002

Prasad, R., Srivastava, S.N., 2009. Sorption of distillery spent wash onto fly ash: Kinetics and mass transfer studies. Chem. Eng. J. 146, 90–97. doi:10.1016/j.cej.2008.05.021

Laird, D.A., Fleming, P., Davis, D.D., Horton, R., Wang, B., Karlen, D.L., 2010a. Impact of biochar amendments on the quality of a typical Midwestern agricultural soil. Geoderma 158, 443–449. doi:10.1016/j.geoderma.2010.05.013

Laird, D.A., Fleming, P., Wang, B., Horton, R., Karlen, D., 2010b. Biochar impact on nutrient leaching from a Midwestern agricultural soil. Geoderma 158, 436–442. doi:10.1016/j.geoderma.2010.05.012

Latham, K.G., Jambu, G., Joseph, S.D., Donne, S.W., 2014. Nitrogen Doping of Hydrochars Produced Hydrothermal Treatment of Sucrose in H_2O, H_2SO_4 , and NaOH. ACS Sustain. Chem. Eng. 2, 755–764. doi:10.1021/sc4004339

Lawrinenko, M., Laird, D.A. Anion exchange capacity of biochar. Green Chem. 17, 4628–4636. doi:10.1039/C5GC00828J

Lazányi, J., Loch, J., 2006. Evaluation of 0.01 M CaCl 2 Extractable Nitrogen Forms in a Long-term Experiment. Agrokémia és Talajt. 55, 135–144. doi:10.1556/Agrokem.55.2006.1.15

Le Leuch, L.M., Bandosz, T.J., 2007. The role of water and surface acidity on the reactive adsorption of ammonia on modified activated carbons. Carbon N. Y. 45, 568–578. doi:10.1016/j.carbon.2006.10.016

Lehmann, J., 2007. Bio-energy in the black. Front. Ecol. Environ. 5, 381–387. doi:10.1890/1540-9295(2007)5[381:BITB]2.0.CO;2

Lehmann, J., Gaunt, J., Rondon, M., 2006. Mitigation and Adaptation Strategies for Global Change 11: 403–427 bio-char sequestration in terrestrial ecosystems – a review. doi:10.1007/s11027-005-9006-5

Lehmann, J., C. Czimczik, D. Laird, and S. Sohi, 2009. Stability of biochar in the soil. In: Lehmann, J. and Joseph, S., eds. Biochar for environmental management science and technology. London: Earthscan. p.241.

Liang, B., Lehmann, J., Solomon, D., Kinyangi, J., Grossman, J., O'Neill, B., Skjemstad, J.O., Thies, J., Luizão, F.J., Petersen, J., Neves, E.G., 2006. Black Carbon Increases Cation Exchange Capacity in Soils. Soil Sci. Soc. Am. J. 70, 1719. doi:10.2136/sssaj2005.0383

Liang, X., Zeng, M., Qi, C., 2010. One-step synthesis of carbon functionalized with sulfonic acid groups using hydrothermal carbonization. Carbon N. Y. 48, 1844–1848. doi:10.1016/j.carbon.2010.01.030

Libra, J.A., Ro, K.S., Kammann, C., Funke, A., Berge, N.D., Neubauer, Y., Titirici, M.-M., Fühner, C., Bens, O., Kern, J., Emmerich, K.-H., 2014. Hydrothermal carbonization of biomass residuals: a comparative review of the chemistry, processes and applications of wet and dry pyrolysis. Biofuels. doi: 10.4155/BFS.10.81

Lillo-Ródenas, M.., Cazorla-Amorós, D., Linares-Solano, A., 2003. Understanding chemical reactions between carbons and NaOH and KOH: An insight into the chemical activation mechanism. Carbon N. Y. 41, 267–275. doi:10.1016/S0008-6223(02)00279-8

Lim, W.C., Srinivasakannan, C., Balasubramanian, N., 2010. Activation of palm shells by phosphoric acid impregnation for high yielding activated carbon. J. Anal. Appl. Pyrolysis 88, 181–186. doi:10.1016/j.jaap.2010.04.004

Limousin, G., Gaudet, J.-P., Charlet, L., Szenknect, S., Barthès, V., Krimissa, M., 2007. Sorption isotherms: A review on physical bases, modeling and measurement. Appl. Geochemistry 22, 249–275. doi:10.1016/j.apgeochem.2006.09.010

Lin, Y.-C., Cho, J., Tompsett, G.A., Westmoreland, P.R., Huber, G.W., 2009. Kinetics and Mechanism of Cellulose Pyrolysis. J. Phys. Chem. C 113, 20097–20107. doi:10.1021/jp906702p

Lin, Y., Munroe, P., Joseph, S., Henderson, R., Ziolkowski, A., 2012. Water extractable organic carbon in untreated and chemical treated biochars. Chemosphere 87, 151–7. doi:10.1016/j.chemosphere.2011.12.007

Lin, Y., Munroe, P., Joseph, S., Ziolkowski, A., van Zwieten, L., Kimber, S., Rust, J., 2013. Chemical and structural analysis of enhanced biochars: thermally treated mixtures of biochar, chicken litter, clay and minerals. Chemosphere 91, 35–40. doi:10.1016/j.chemosphere.2012.11.063

Liu, J.C., 2009. Recovery of phosphate and ammonium as struvite from semiconductor wastewater. Sep. Purif. Technol. 64, 368–373. doi:10.1016/j.seppur.2008.10.040

Liu, Y., He, Z., Uchimiya, M., 2015. Comparison of Biochar Formation from Various Agricultural By-Products Using FTIR Spectroscopy. Mod. Appl. Sci. 9, 246. doi:10.5539/mas.v9n4p246

Long, X., Cheng, H., Xin, Z., Xiao, W., Li, W., Yuan, W., 2008. Adsorption of ammonia on activated carbon from aqueous solutions. Environ. Prog. 27, 225–233. doi:10.1002/ep.10252

López-Cano, I., Roig, A., Cayuela, M.L., Alburquerque, J.A., Sánchez-Monedero, M.A., 2016. Biochar improves N cycling during composting of olive mill wastes and sheep manure. Waste Manag. 49, 553–559. doi:10.1016/j.wasman.2015.12.031

Lopez-Ramon, M.V., Stoeckli, F., Moreno-Castilla, C., Carrasco-Marin, F., 1999. On the characterization of acidic and basic surface sites on carbons by various techniques. Carbon N. Y. 37, 1215–1221. doi:10.1016/S0008-6223(98)00317-0

Lu, X., Pellechia, P.J., Flora, J.R. V, Berge, N.D., 2013. Influence of reaction time and temperature on product formation and characteristics associated with the hydrothermal carbonization of cellulose. Bioresour. Technol. 138, 180–90. doi:10.1016/j.biortech.2013.03.163

Lynam, J.G., Coronella, C.J., Yan, W., Reza, M.T., Vasquez, V.R., 2011. Acetic acid and lithium chloride effects on hydrothermal carbonization of lignocellulosic biomass. Bioresour. Technol. 102, 6192–9. doi:10.1016/j.biortech.2011.02.035

Mahmoud, D.K., Salleh, M.A.M., Karim, W.A.W.A., Idris, A., Abidin, Z.Z., 2012. Batch adsorption of basic dye using acid treated kenaf fibre char: Equilibrium, kinetic and thermodynamic studies. Chem. Eng. J. 181-182, 449–457. doi:10.1016/j.cej.2011.11.116

Malek, A., Farooq, S., 1996. Comparison of isotherm models for hydrocarbon adsorption on activated carbon. AIChE J. 42, 3191–3201. doi:10.1002/aic.690421120

Malghani, S., Jüschke, E., Baumert, J., Thuille, A., Antonietti, M., Trumbore, S., Gleixner, G., 2015. Carbon sequestration potential of hydrothermal carbonization char (hydrochar) in two contrasting soils; results of a 1-year field study. Biol. Fertil. Soils 51, 123–134. doi:10.1007/s00374-014-0980-1

Malińska, K., Zabochnicka-Świątek, M., Dach, J., 2014. Effects of biochar amendment on ammonia emission during composting of sewage sludge. Ecol. Eng. 71, 474–478. doi:10.1016/j.ecoleng.2014.07.012

Mallampati, R., Valiyaveettil, S., 2013. Apple peels--a versatile biomass for water purification? ACS Appl. Mater. Interfaces 5, 4443–9. doi:10.1021/am400901e

Mane, V.S., Mall, I.D., Srivastava, V.C., 2007. Use of bagasse fly ash as an adsorbent for the removal of brilliant green dye from aqueous solution. Dye. Pigment. 73, 269–278. doi:10.1016/j.dyepig.2005.12.006

Mani, S., Kastner, J.R., Juneja, A., 2013. Catalytic decomposition of toluene using a biomass derived catalyst. Fuel Process. Technol. 114, 118–125. doi:10.1016/j.fuproc.2013.03.015

MIT, 2008, Clausius Clapeyron Equation (Thermodynamics and kinetics), Spring 2008. (Massachusetts Institute of Technology: MIT OpenCouseWare), http://ocw.mit.edu/courses/chemistry/5-60-thermodynamics-kinetics-spring-2008/lecture-notes/5_60_lecture19.pdf (Accessed 2016-12-01). License: Creative Commons BY-NC-SA

Maurya, N.S., Mittal, A.K., 2006. Applicability of Equilibrium Isotherm Models for the Biosorptive Uptakes in Comparison to Activated Carbon-Based Adsorption. J. Environ. Eng. 132, 1589–1599. doi:10.1061/(ASCE)0733-9372(2006)132:12(1589)

McCormack, S.A., Ostle, N., Bardgett, R.D., Hopkins, D.W., Vanbergen, A.J., 2013. Biochar in bioenergy cropping systems: Impacts on soil faunal communities and linked ecosystem processes. GCB Bioenergy 5, 81–95. doi:10.1111/gcbb.12046

McCreary, J.J., Snoeyink, V.L., 1980. Characterization and activated carbon adsorption of several humic substances. Water Res. 14, 151–160. doi:10.1016/0043-1354(80)90231-6

McGinnes, E.A.J., Harlow, C.A., Beall, F.C., 1976. Use of scanning electron microscopy and image processing in wood charcoal studies. Proc. Scanning Electron Microsc. Symp.

Méndez, A., Terradillos, M., Gascó, G., 2013. Physicochemical and agronomic properties of biochar from sewage sludge pyrolysed at different temperatures. J. Anal. Appl. Pyrolysis 102, 124–130. doi:10.1016/j.jaap.2013.03.006

Merlic. 1997. IR Absorption Table [online]. Available from: http://webspectra.chem.ucla.edu/irtable.html

Mészáros, E., Jakab, E., Várhegyi, G., Bourke, J., Manley-Harris, M., Nunoura, T., Antal, M.J., 2007. Do All Carbonized Charcoals Have the Same Chemical Structure? 1. Implications of Thermogravimetry−Mass Spectrometry Measurements. Ind. Eng. Chem. Res. 46, 5943–5953. doi:10.1021/ie0615842

Miles, T.R., Miles, T.R., Baxter, L.L., Bryers, R.W., Jenkins, B.M., Oden, L.L., 1996. Boiler deposits from firing biomass fuels. Biomass and Bioenergy 10, 125–138. doi:10.1016/0961-9534(95)00067-4

Min, S.H., Han, J.S., Shin, E.W., Park, J.K., 2004. Improvement of cadmium ion removal by base treatment of juniper fiber. Water Res. 38, 1289–95. doi:10.1016/j.watres.2003.11.016

Mohan, D., Kumar, A., Pittman, C.U., 2016. Sustainable Biochar - A Tool for Climate Change Mitigation, Soil Management and Water and Wastewater Treatment, in: Geostatistical and Geospatial Approaches for the Characterization of Natural Resources in the Environment. Springer International Publishing, Cham, pp. 949–952. doi:10.1007/978-3-319-18663-4_146

Mohan, D., Sarswat, A., Ok, Y.S., Pittman, C.U., 2014. Organic and inorganic contaminants removal from water with biochar, a renewable, low cost and sustainable adsorbent – A critical review. Bioresour. Technol. 160, 191–202. doi:10.1016/j.biortech.2014.01.120

Molinuevo, B., García, M.C., Karakashev, D., Angelidaki, I., 2009. Anammox for ammonia removal from pig manure effluents: Effect of organic matter content on process performance. Bioresour. Technol. 100, 2171–2175. doi:10.1016/j.biortech.2008.10.038

Mondal, S., Aikat, K., Halder, G., 2016. Biosorptive uptake of ibuprofen by chemically modified Parthenium hysterophorus derived biochar: Equilibrium, kinetics, thermodynamics and modeling. Ecol. Eng. 92, 158–172. doi:10.1016/j.ecoleng.2016.03.022

Mondini, C., Sinicco, T., Cayuela, M.L., Sanchez-Monedero, M.A., 2010. A simple automated system for measuring soil respiration by gas chromatography. Talanta 81, 849–55. doi:10.1016/j.talanta.2010.01.026

Moradi, O., 2011. Chapter 8: Thermodynamics of Interfaces. *In*: Moreno-Pirajan, J.C. (Ed). Thermodynamics - interaction studies - solids, liquids and gases. InTech. doi:10.5772/20083

Morales, V.L., Pérez-Reche, F.J., Hapca, S.M., Hanley, K.L., Lehmann, J., Zhang, W., 2015. Reverse engineering of biochar. Bioresour. Technol. 183, 163–174. doi:10.1016/j.biortech.2015.02.043

Moreno-Castilla, C., Lopez-Ramon, M. V, Carrasco-Marın, F., 2000. Changes in surface chemistry of activated carbons by wet oxidation. Carbon 38, 1995-2001. doi:10.1016/S0008-6223(00)00048-8

Moreno-Castilla, C., Ferro-Garcia, M.A., Joly, J.P., Bautista-Toledo, I., Carrasco-Marin, F., Rivera-Utrilla, J., 1995. Activated Carbon Surface Modifications by Nitric Acid, Hydrogen Peroxide, and Ammonium Peroxydisulfate Treatments. Langmuir 11, 4386–4392. doi:10.1021/la00011a035

Morse, G., Brett, S., Guy, J., Lester, J., 1998. Review: Phosphorus removal and recovery technologies. Sci. Total Environ. 212, 69–81. doi:10.1016/S0048-9697(97)00332-X

Mukherjee, S., 2003. Demineralization and Desulfurization of High-Sulfur Assam Coal with Alkali Treatment. Energy & Fuels 17, 559–564. doi:10.1021/ef0201836

Mukherjee, A., Zimmerman, A.R., Harris, W., 2011. Surface chemistry variations among a series of laboratory-produced biochars. Geoderma 163, 247–255. doi:10.1016/j.geoderma.2011.04.021

Mukherjee, A., Zimmerman, A.R., 2013. Organic carbon and nutrient release from a range of laboratory-produced biochars and biochar–soil mixtures. Geoderma 193-194, 122–130. doi:10.1016/j.geoderma.2012.10.002

Myśliwiec, D., Chylińska, M., Szymańska-Chargot, M., Chibowski, S., Zdunek, A., Revision of adsorption models of xyloglucan on microcrystalline cellulose. Cellulose 23, 2819-2829. DOI 10.1007/s10570-016-0995-x

Nahm, K.H., 2003. Evaluation of the nitrogen content in poultry manure. Worlds. Poult. Sci. J. 59, 77–88. doi:10.1079/WPS20030004

Nakajima, K., Okamura, M., Kondo, J.N., Domen, K., Tatsumi, T., Hayashi, S., Hara, M., 2009. Amorphous Carbon Bearing Sulfonic Acid Groups in Mesoporous Silica as a Selective Catalyst. Chem. Mater. 21, 186–193. doi:10.1021/cm801441c

Namasivayam, C., Ranganathan, K., 1994. Recycling of "waste" F_E(III)/C_R(III) hydroxide for the removal of nickel from wastewater: Adsorption and equilibrium studies. Waste Manag. 14, 709–716. doi:10.1016/0956-053X(94)90058-2

Ng, C., Losso, J.N., Marshall, W.E., Rao, R.M., 2002. Freundlich adsorption isotherms of agricultural by-product-based powdered activated carbons in a geosmin–water system. Bioresour. Technol. 85, 131–135. doi:10.1016/S0960-8524(02)00093-7

Nguyen, T.A.H., Ngo, H.H., Guo, W.S., Zhang, J., Liang, S., Tung, K.L., 2013. Feasibility of iron loaded "okara" for biosorption of phosphorous in aqueous solutions. Bioresour. Technol. 150, 42–9. doi:10.1016/j.biortech.2013.09.133

Nguyen, T.A.H., Ngo, H.H., Guo, W.S., Zhang, J., Liang, S., Lee, D.J., Nguyen, P.D., Bui, X.T., 2014. Modification of agricultural waste/by-products for enhanced phosphate removal and recovery: potential and obstacles. Bioresour. Technol. 169, 750–62. doi:10.1016/j.biortech.2014.07.047

Nguyen, M.L., Tanner, C.C., 1998. Ammonium removal from wastewaters using natural New Zealand zeolites Ammonium removal from wastewaters using natural New Zealand zeolites. New Zeal. J. Agric. Res. 413, 427–446. doi:10.1080/00288233.1998.9513328

Novak, J.M., Lima, I., Xing, B., Gaskin, J.W., Steiner, C., Das, K.C., Ahmedna, M., Rehrah, D., Watts[1], D.W., Busscher[1], W.J., Schomberg, H., 2009. Characterization of designer biochar produced at different temperatures and their effects on a loamy sand. Ann. Environ. Sci. 3, 195–206.

Nuopponen, M., Vuorinen, T., Jämsä, S., Viitaniemi, P., 2005. Thermal Modifications in Softwood Studied by FT-IR and UV Resonance Raman Spectroscopies. J. Wood Chem. Technol. 24, 13–26. doi:10.1081/WCT-120035941

Oleszczuk, P., Hale, S.E., Lehmann, J., Cornelissen, G., 2012. Activated carbon and biochar amendments decrease pore-water concentrations of polycyclic aromatic hydrocarbons (PAHs) in sewage sludge. Bioresour. Technol. 111, 84–91. doi:10.1016/j.biortech.2012.02.030

Oya, A., Iu, W.G., 2002. Deodorization performance of charcoal particles loaded with orthophosphoric acid against ammonia and trimethylamine. Carbon N. Y. 40, 1391–1399. doi:10.1016/S0008-6223(01)00273-1

Papanicolaou, E.P., Overstreet, R., 1969. The determination of cation exchange capacity over a wide range of pH using various index cations. Zeitschrift für Pflanzenernährung und Bodenkd. 123, 205–212. doi:10.1002/jpln.19691230305

Pardo, J.M., Quintero, F.J., 2002. Plants and sodium ions: keeping company with the enemy. Genome Biol. 3, 1017.1–1017.4.

Park, J.H., Ok, Y.S., Kim, S.H., Cho, J.S., Heo, J.S., Delaune, R.D., Seo, D.C., 2015. Evaluation of phosphorus adsorption capacity of sesame straw biochar on aqueous solution: influence of

activation methods and pyrolysis temperatures. Environ. Geochem. Health 37, 969–83. doi:10.1007/s10653-015-9709-9

Park, S.-J., Jin, S.-Y., 2005. Effect of ozone treatment on ammonia removal of activated carbons, Journal of Colloid and Interface Science. doi:10.1016/j.jcis.2005.01.043

Parshetti, G.K., Chowdhury, S., Balasubramanian, R., 2014. Hydrothermal conversion of urban food waste to chars for removal of textile dyes from contaminated waters. Bioresour. Technol. 161, 310–9. doi:10.1016/j.biortech.2014.03.087

Parshetti, G.K., Kent Hoekman, S., Balasubramanian, R., 2013. Chemical, structural and combustion characteristics of carbonaceous products obtained by hydrothermal carbonization of palm empty fruit bunches. Bioresour. Technol. 135, 683–689. doi:10.1016/j.biortech.2012.09.042

Patwardhan, P.R., Satrio, J.A., Brown, R.C., Shanks, B.H., 2010. Influence of inorganic salts on the primary pyrolysis products of cellulose. Bioresour. Technol. 101, 4646-4655. doi:10.1016/j.biortech.2010.01.112

Pérez, J., Munõz-Dorado, A.J., De La, T., Ae, R., Martıez, J., 2002. Biodegradation and biological treatments of cellulose, hemicellulose and lignin: an overview. doi:10.1007/s10123-002-0062-3

Pereira, M.F.R., Soares, S.F., Órfão, J.J., Figueiredo, J.L., 2003. Adsorption of dyes on activated carbons: influence of surface chemical groups. Carbon N. Y. 41, 811–821. doi:10.1016/S0008-6223(02)00406-2

Pérez, J., Muñoz-Dorado, J., de la Rubia, T., Martínez, J., 2002. Biodegradation and biological treatments of cellulose, hemicellulose and lignin: an overview. Int. Microbiol. 5, 53–63. doi:10.1007/s10123-002-0062-3

PerkinElmer, 1996. Analytical Methods for Atomic Absorption Spectroscopy [online]. Available from: http://www.lasalle.edu/~prushan/Intrumental%20Analysis_files/AA-Perkin%20Elmer%20guide%20to%20all!.pdf

Petit, C., Bandosz, T.J., 2009. Role of surface heterogeneity in the removal of ammonia from air on micro/mesoporous activated carbons modified with molybdenum and tungtsen oxides. Microporous Mesoporous Mater. 118, 61–67. doi:10.1016/j.micromeso.2008.08.016

Petit, C., Kante, K., Bandosz, T.J., 2010. The role of sulfur-containing groups in ammonia retention on activated carbons. Carbon N. Y. 48, 654–667. doi:10.1016/j.carbon.2009.10.007

Petrov, N., Budinova, T., Khavesov, I., 1992. Adsorption of the ions of zinc, cadmium, copper, and lead on oxidized anthracite. Carbon N. Y. 30, 135–139. doi:10.1016/0008-6223(92)90072-5

Pietrzak, R., Jurewicz, K., Nowicki, P., Babeł, K., Wachowska, H., 2007. Microporous activated carbons from ammoxidised anthracite and their capacitance behaviours. Fuel 86, 1086–1092. doi:10.1016/j.fuel.2006.10.006

Pietrzak, R., 2009. XPS study and physico-chemical properties of nitrogen-enriched microporous activated carbon from high volatile bituminous coal. Fuel 88, 1871–1877. doi:10.1016/j.fuel.2009.04.017

Poerschmann, J., Weiner, B., Koehler, R., Kopinke, F.-D., 2015. Organic breakdown products resulting from hydrothermal carbonization of brewer's spent grain. Chemosphere 131, 71–7. doi:10.1016/j.chemosphere.2015.02.057

Pognani, M., Barrena, R., Font, X., Scaglia, B., Adani, F., Sánchez, A., 2010. Monitoring the organic matter properties in a combined anaerobic/aerobic full-scale municipal source-separated waste treatment plant, Bioresource Technology. doi:10.1016/j.biortech.2010.03.110

Pollard, S.J.T., Fowler, G.D., Sollars, C.J., Perry, R., 1992. Low-cost adsorbents for waste and wastewater treatment: a review. Sci. Total Environ. 116, 31–52. doi:10.1016/0048-9697(92)90363-W

Pradhan, B.K., Sandle, N.K., 1999. Effect of different oxidizing agent treatments on the surface properties of activated carbons. Carbon N. Y. 37, 1323–1332. doi:10.1016/S0008-6223(98)00328-5

Prommer, J., Wanek, W., Hofhansl, F., Trojan, D., Offre, P., Urich, T., Schleper, C., Sassmann, S., Kitzler, B., Soja, G., Hood-Nowotny, R.C., 2014. Biochar Decelerates Soil Organic Nitrogen Cycling but Stimulates Soil Nitrification in a Temperate Arable Field Trial. PLoS One 9, e86388. doi:10.1371/journal.pone.0086388

Provenzano, M.R., Malerba, A.D., Pezzolla, D., Gigliotti, G., 2014. Chemical and spectroscopic characterization of organic matter during the anaerobic digestion and successive composting of pig slurry. Waste Manag. 34, 653–660. doi:10.1016/j.wasman.2013.12.001

Puri, B.R., Bansal, R.., 1964. Studies in surface chemistry of carbon blacks Part II. Surface acidity in relation to chemisorbed oxygen. Carbon N. Y. 1, 457–464. doi:10.1016/0008-6223(64)90007-7

Qayyum, M.F., Steffens, D., Reisenauer, H.P., Schubert, S., 2012. Kinetics of Carbon Mineralization of Biochars Compared with Wheat Straw in Three Soils. J. Environ. Qual. 41, 1210. doi:10.2134/jeq2011.0058

Rajapaksha, A.U., Chen, S.S., Tsang, D.C.W., Zhang, M., Vithanage, M., Mandal, S., Gao, B., Bolan, N.S., Ok, Y.S., 2016. Engineered/designer biochar for contaminant removal/immobilization from soil and water: Potential and implication of biochar modification. Chemosphere 148, 276–291. doi:10.1016/j.chemosphere.2016.01.043

Rashid, M.A., King, L.H., 1969. Molecular weight distribution measurements on humic and fulvic acid fractions from marine clays on the Scotian Shelf. Geochim. Cosmochim. Acta 33, 147–151. doi:10.1016/0016-7037(69)90099-4

Reusch, 2013. Infrared Spectroscopy [www Document]. URL https://www2.chemistry.msu.edu/faculty/reusch/virttxtjml/Spectrpy/InfraRed/infrared.htm

Reza, M.T., Andert, J., Wirth, B., Busch, D., Pielert, J., Lynam, J.G., Mumme, J., 2014. Hydrothermal Carbonization of Biomass for Energy and Crop Production. Appl. Bioenergy 1. doi:10.2478/apbi-2014-0001

Reza, M.T., Lynam, J.G., Uddin, M.H., Coronella, C.J., 2013. Hydrothermal carbonization: Fate of inorganics. Biomass and Bioenergy 49, 86–94. doi:10.1016/j.biombioe.2012.12.004

Rhoades, J.D., 1982. Cation Exchange Capacity. *In*: Page, A.L. (Ed.), Methods of soil analysis. Part 2: Chemical and microbiological properties (2nd ed.) Agronomy. pp.149-152.

Rillig, M.C., Wagner, M., Salem, M., Antunes, P.M., George, C., Ramke, H.-G., Titirici, M.-M., Antonietti, M., 2010. Material derived from hydrothermal carbonization: Effects on plant growth and arbuscular mycorrhiza. Appl. Soil Ecol. 45, 238–242. doi:10.1016/j.apsoil.2010.04.011

Rittmann, B.E., Mayer, B., Westerhoff, P., Edwards, M., 2011. Capturing the lost phosphorus. Chemosphere 84, 846–853. doi:10.1016/j.chemosphere.2011.02.001

Ritz, C.W., Tasistro, A.S., Kissel, D.E., Fairchild, B.D., 2011. Evaluation of surface-applied char on the reduction of ammonia volatilization from broiler litter. J. Appl. Poult. Res. 20, 240–245. doi:10.3382/japr.2010-00327

Roberts, K.G., Gloy, B.A., Joseph, S., Scott, N.R., Lehmann, J., 2010. Life Cycle Assessment of Biochar Systems: Estimating the Energetic, Economic, and Climate Change Potential. Environ. Sci. Technol. 44, 827–833. doi:10.1021/es902266r

Robinson, J.W., 1960. Atomic Absorption Spectroscopy. Anal. Chem. 32, 17A–29A. doi:10.1021/ac60164a712

Rodriguez-Reinoso, F., 1998. Plenary Lecture- The role of carbon materials in heterogeneous catalysis. Carbon 36, 159–175.

Rodrigues, C.C., de Moraes, D., da Nóbrega, S.W., Barboza, M.G., 2007. Ammonia adsorption in a fixed bed of activated carbon. Bioresour. Technol. 98, 886–91. doi:10.1016/j.biortech.2006.03.024

Ross, D.S., Ketterings, Q., 2009. Recommended methods for determining soil cation exchange capacity [online]. Available from: http://em1.stanford.edu/ICPData/ICP-OES/GCLI/sci/CHAP9-95.pdf

Rout, G.R., Das, P., 2009. Effect of Metal Toxicity on Plant Growth and Metabolism: I. Zinc, in: Sustainable Agriculture. Springer Netherlands, Dordrecht, pp. 873–884. doi:10.1007/978-90-481-2666-8_53

Rutherford, D.W., Wershaw, R.L., Reeves, III, J.B., 2007. Development of Acid Functional Groups and Lactones During the Thermal Degradation of Wood and Wood Components. Scientific Investigations Report. [online]. Available from: http://pubs.usgs.gov/sir/2007/5013/pdf/SIR07-5013.pdf

Saddawi, A., Jones, J.M., Williams, A., Le Coeur, C., 2012. Commodity Fuels from Biomass through Pretreatment and Torrefaction: Effects of Mineral Content on Torrefied Fuel Characteristics and Quality. Energy & Fuels 120119162934000. doi:10.1021/ef2016649

Saiz-Jimenez, C., 1994. Analytical Pyrolysis of Humic Substances; Pitfalls, Limitations, and Possible Solutions. Envlron. Scl. Technol. 28, 1773-1780. doi: 10.1021/es00060a005

Sakadevan, K., Bavor, H.J., 1998. Phosphate adsorption characteristics of soils, slags and zeolite to be used as substrates in constructed wetland systems. Water Res. 32, 393–399. doi:10.1016/S0043-1354(97)00271-6

Saleh, M., A. Mahmoud, and M. Rashad, (2012), Peanut biochar as a stable adsorbent for removing NH_4-N from wastewater: A preliminary study, Advances in Environmental Biology, 6(7), 2170-2176.

Salehi, A., 2012. Chemical interactions between fatty acids and wood components during oxidation processes.
PhD thesis. Kungliga Tekniska Högskolan, Stockholm [online]. Available from: http://www.diva-portal.org/smash/get/diva2:556760/FULLTEXT01.pdf

Samadi, A., 2010. Phosphorus sorption characteristics in relation to soil properties in some calcareous soils of western azarbaijan province. J. Agric. Sci. Technol. 8, 251–264.

Sánchez-García, M., Sánchez-Monedero, M.A., Roig, A., López-Cano, I., Moreno, B., Benitez, E., Cayuela, M.L., 2016. Compost vs biochar amendment: a two-year field study evaluating soil C build-up and N dynamics in an organically managed olive crop. Plant Soil 1–14. doi:10.1007/s11104-016-2794-4

Sánchez-Monedero, M.A., Roig, A., Martínez-Pardo, C., Cegarra, J., Paredes, C., 1996. A microanalysis method for determining total organic carbon in extracts of humic substances. Relationships between total organic carbon and oxidable carbon. Bioresour. Technol. 57, 291–295. doi:10.1016/S0960-8524(96)00078-8

Sánchez-Monedero, M.A., Cegarra, J., García, D., Roig, A., 2002. Chemical and structural evolution of humic acids during organic waste composting. Biodegradation 13, 361–371. doi:10.1023/A:1022888231982

Sánchez–Monedero, M.., Roig, A., Cegarra, J., Bernal, M., 1999. Relationships between water-soluble carbohydrate and phenol fractions and the humification indices of different organic wastes during composting. Bioresour. Technol. 70, 193–201. doi:10.1016/S0960-8524(99)00018-8

Sarkhot, D. V, Ghezzehei, T.A., Berhe, A.A., 2013. Effectiveness of biochar for sorption of ammonium and phosphate from dairy effluent. J. Environ. Qual. 42, 1545–54. doi:10.2134/jeq2012.0482

Sarkhot, D. V, Berhe, A.A., Ghezzehei, T.A. 2012. Impact of biochar enriched with dairy manure effluent on carbon and nitrogen dynamics. J. Environ. Qual. 41, 1107–14. doi:10.2134/jeq2011.0123

Sasaki, M., Fang, Z., Fukushima, Y., Adschiri, T., Arai, K., 2000. Dissolution and Hydrolysis of Cellulose in Subcritical and Supercritical Water. Ind. Eng. Chem. Res. 39, 2883–2890. doi:10.1021/ie990690j

Scheller, H.V., Ulvskov, P., 2010. Hemicelluloses. Annual Review of Plant Biology. doi:10.1146/annurev-arplant-042809-112315

Schimmelpfennig, S., Glaser, B., 2012. One step forward toward characterization: some important material properties to distinguish biochars. J. Environ. Qual. 41, 1001–13. doi:10.2134/jeq2011.0146

Schlegel, M.L., Charlet, L., Manceau, A.,1999. Sorption of Metal Ions on Clay Minerals. J. Colloid Interface Sci. 220, 392–405. doi:10.1006/jcis.1999.6538

Schmidt, H.P., 2011. Ways of Making Terra Preta: Biochar Activation [online]. Available from: http://seachar.org/wp-content/uploads/2011/04/biochar-activation.pdf

Schmidt , H.P., 2012. Treating liquid manure with biochar [online]. Ithaka Journal 1/2012: 273–276 www.ithaka-journal.net

Schneider, P., 1995. Adsorption isotherms of microporous-mesoporous solids revisited. Appl. Catal. A Gen. 129, 157–165. doi:10.1016/0926-860X(95)00110-7

Schulz, H., Glaser, B., 2012. Effects of biochar compared to organic and inorganic fertilizers on soil quality and plant growth in a greenhouse experiment. J. Plant Nutr. Soil Sci. 175, 410–422. doi:10.1002/jpln.201100143

Sevilla, M., Fuertes, A.B., 2009. The production of carbon materials by hydrothermal carbonization of cellulose. Carbon N. Y. 47, 2281–2289. doi:10.1016/j.carbon.2009.04.026

Shafizadeh, F., 1982. Introduction to pyrolysis of biomass. J. Anal. Appl. Pyrolysis 3, 283–305. doi:10.1016/0165-2370(82)80017-X

Shen, D., Xiao, R., Gu, S., Zhang, H., 2013. The Overview of Thermal Decomposition of Cellulose in Lignocellulosic Biomass, in: Cellulose - Biomass Conversion. InTech. doi:10.5772/51883

Shen, D., Xiao, R., Gu, S., Zhang, H., 2013. The Overview of Thermal Decomposition of Cellulose in Lignocellulosic Biomass, in: Cellulose - Biomass Conversion. InTech. doi:10.5772/51883

Sigma Aldrich, n.d. Ion exchange resins: Classification and properties [online]. Available from: https://www.sigmaaldrich.com/content/dam/sigma-aldrich/docs/Aldrich/Instructions/ion_exchange_resins.pdf

Sikora, F.J., Moore, K.P., Crouse, K.K., Hardy, D.H., Heckendorn, S., Huluka, G., Kissel, D.E., Joines, D.K., Miller, R., Mylavarapu, R., Oldham, J.L., Mitchell, C.C., Provin, T., Savoy, H.J., Sonon, L., Wang, J.J., Warncke, D.D., Zhang, H., 2014. Soil Test Methods From the Southeastern United States.

Silber, A., Levkovitch, I., Graber, E.R., 2010. pH-dependent mineral release and surface properties of cornstraw biochar: agronomic implications. Environ. Sci. Technol. 44, 9318–23. doi:10.1021/es101283d

Silvério, F.O., Barbosa, L.C.A., Piló-Veloso, D., 2008. A pirólise como técnica analítica. Quim. Nova 31, 1543–1552. doi:10.1590/S0100-40422008000600045

Sing, K.S.W., Everett, D.H., Haul, R.A.W., Moscou, L., Pierotti, R.A., Rouquerol, J., Siemieniewska, T., Sing, K.S.W., Everett, D.H., Haul, R.A.W., Moscou, L., Pierotti, R.A., Rouquerol, J., Siemieniewska, T., 2008. Reporting Physisorption Data for Gas/Solid Systems, in: Handbook of Heterogeneous Catalysis. Wiley-VCH Verlag GmbH & Co. KGaA, Weinheim, Germany. doi:10.1002/9783527610044.hetcat0065

Singh, B.P., Cowie, 2014. Long-term influence of biochar on native organic carbon mineralisation in a low-carbon clayey soil. Sci. Rep. 4, 56. doi:10.1038/srep03687

Singh, J., Kalamdhad, A.S., 2012. Reduction of heavy metals during composting- A review. Int. J. Environ. Prot 2, 36-43.

Skinner, M.F., Zabowski, D., Harrison, R., Lowe, A., Xue, D., 2001. Measuring the cation exchange capacity of forest soils. commun. soil sci. plant anal 32, 1751–1764.

Smith, B., 2006. Fundamentals of Fourier transform infrared spectroscopy. Vasa 40, 464. doi:10.1002/1521-3773(20010316)40:6<9823::AID-ANIE9823>3.3.CO;2-C

Smith, A.M., Singh, S., Ross, A.B., 2016. Fate of inorganic material during hydrothermal carbonisation of biomass: Influence of feedstock on combustion behaviour of hydrochar. Fuel 169, 135–145. doi:10.1016/j.fuel.2015.12.006

Sohi, S., Lopez-Capel, E., Krull, E., Bol, R., 2009. Biochar, climate change and soil: A review to guide future research [online]. Available from: http://www.feasta.org/wp-content/uploads/2009/03/csiro-biochar-climate-change-and-soil-report-feb-20091.pdf

Song, W., Guo, M., 2012. Quality variations of poultry litter biochar generated at different pyrolysis temperatures. J. Anal. Appl. Pyrolysis 94, 138–145. doi:10.1016/j.jaap.2011.11.018

Song, Y.-H., Qiu, G.-L., Yuan, P., Cui, X.-Y., Peng, J.-F., Zeng, P., Duan, L., Xiang, L.-C., Qian, F., 2011. Nutrients removal and recovery from anaerobically digested swine wastewater by struvite crystallization without chemical additions. J. Hazard. Mater. 190, 140–9. doi:10.1016/j.jhazmat.2011.03.015

Sparkes, J., Stoutjesdijk, P., 2011. Biochar: implications for agricultural productivity Ownership of intellectual property rights. Department of Agriculture, Fisheries and Forestry [online]. Available from: daff.gov.au/abares/publications

Sparks, D.L., Page, A.L., Helmke, P.A., Loeppert, R.H., Sumner, M.E., Miller, W.P., 1996. Cation Exchange Capacity and Exchange Coefficients, in: Methods of Soil Analysis Part 3—Chemical Methods. Soil Science Society of America, American Society of Agronomy, pp. 1201–1229. doi:10.2136/sssabookser5.3.c40

Spokas, K.A., Novak, J.M., Masiello, C.A., Johnson, M.G., Colosky, E.C., Ippolito, J.A., Trigo, C., 2014. Physical Disintegration of Biochar: An Overlooked Process. Environ. Sci. Technol. Lett. 1, 326–332. doi:10.1021/ez500199t

Spokas, K.A., 2010. Review of the stability of biochar in soils: predictability of O:C molar ratios. Carbon Manag. 1, 289–303. doi:10.4155/cmt.10.32

Spokas, K.A., Cantrell, K.B., Rey, J., Novak, M., Archer, D.W., Ippolito, J.A., Collins, H.P., Boateng, A.A., Lima, I.M., Lamb, M.C., Mcaloon, A.J., Lentz, R.D., Nichols, K.A., 2012. Biochar: A Synthesis of Its Agronomic Impact beyond Carbon Sequestration. doi:10.2134/jeq2011.0069

Spokas, K.A., Novak, J.M., Venterea, R.T., 2011. Biochar's role as an alternative N-fertilizer: ammonia capture. Plant Soil 350, 35–42. doi:10.1007/s11104-011-0930-8

Sricharoenchaikul, V., Pechyen, C., Aht-ong, D., Atong, D., 2008. Preparation and Characterization of Activated Carbon from the Pyrolysis of Physic Nut (Jatropha curcas L.) Waste. Energy & Fuels 22, 31–37. doi:10.1021/ef700285u

Starck, J., Burg, P., Muller, S., Bimer, J., Furdin, G., Fioux, P., Vix_Guterl, C., Begin, D., Faure, P., Azambre, B., 2006. The influence of demineralisation and ammoxidation on the adsorption properties of an activated carbon prepared from a Polish lignite. Carbon N. Y. 44, 2549–2557. doi:10.1016/j.carbon.2006.05.052

Steiner, C., Das, K.C., Melear, N., Lakly, D., 2010. Reducing Nitrogen Loss during Poultry Litter Composting Using Biochar. J. Environ. Qual. 39, 1236. doi:10.2134/jeq2009.0337

Stemann, J., Putschew, A., Ziegler, F., 2013. Hydrothermal carbonization: Process water characterization and effects of water recirculation. Bioresour. Technol. 143, 139–146. doi:10.1016/j.biortech.2013.05.098

Su, Y., Cui, H., Li, Q., Gao, S., Shang, J.K., 2013. Strong adsorption of phosphate by amorphous zirconium oxide nanoparticles. Water Res. 47, 5018–5026. doi:10.1016/j.watres.2013.05.044

Subedi, R., Kammann, C., Pelissetti, S., Taupe, N., Bertora, C., Monaco, S., Grignani, C., 2015. Does soil amended with biochar and hydrochar reduce ammonia emissions following the application of pig slurry? Eur. J. Soil Sci. 66, 1044–1053. doi:10.1111/ejss.12302

Suliman, W., 2015. Toward an understanding of the role of biochar as an agro-environmental tool: Potential for control, water release, bacterial retention, and greenhouse gas emissions.

Sun, K., Ro, K., Guo, M., Novak, J., Mashayekhi, H., Xing, B., 2011. Sorption of bisphenol A, 17α-ethinyl estradiol and phenanthrene on thermally and hydrothermally produced biochars. Bioresour. Technol. 102, 5757–5763. doi:10.1016/j.biortech.2011.03.038

Suwelack, K.U., Wüst, D., Fleischmann, P., Kruse, A., 2016. Prediction of gaseous, liquid and solid mass yields from hydrothermal carbonization of biogas digestate by severity parameter. Biomass Convers. Biorefinery 6, 151–160. doi:10.1007/s13399-015-0172-8

Taghizadeh-Toosi, A., Clough, T.J., Sherlock, R.R., Condron, L.M., 2012a. Biochar adsorbed ammonia is bioavailable. Plant Soil 350, 57–69. doi:10.1007/s11104-011-0870-3

Taghizadeh-Toosi, A., Clough, T.J., Sherlock, R.R., Condron, L.M., 2012b. A wood based low-temperature biochar captures NH3-N generated from ruminant urine-N, retaining its bioavailability. Plant Soil 353, 73–84. doi:10.1007/s11104-011-1010-9

Tan, X., Liu, Y., Zeng, G., Wang, X., Hu, X., Gu, Y., Yang, Z., 2015. Application of biochar for the removal of pollutants from aqueous solutions. Chemosphere 125, 70–85. doi:10.1016/j.chemosphere.2014.12.058

Thorn, K.A., Mikita, M.A., 1992. Ammonia fixation by humic substances: a nitrogen-15 and carbon-13 NMR study. Sci. Total Environ. 113, 67–87. doi:10.1016/0048-9697(92)90017-M

Tian, J., Miller, V., Chiu, P.C., Maresca, J.A., Guo, M., Imhoff, P.T., 2016. Nutrient release and ammonium sorption by poultry litter and wood biochars in stormwater treatment. Sci. Total Environ. 553, 596–606. doi:10.1016/j.scitotenv.2016.02.129

Titirici, M.M., Antonietti, 2010. Chemistry and materials options of sustainable carbon materials made by hydrothermal carbonization. Chem. Soc. Rev. 39, 103–116. doi:10.1039/B819318P

Toda, M., Takagaki, A., Okamura, M., Kondo, J.N., Hayashi, S., Domen, K., Hara, M., 2005. Green chemistry: biodiesel made with sugar catalyst. Nature 438, 178. doi:10.1038/438178a

Tryon, E.H., 1948. Effect of Charcoal on Certain Physical, Chemical, and Biological Properties of Forest Soils. Ecol. Monogr. 18, 81–115. doi:10.2307/1948629

Tseng, H.-H., Wey, M.-Y., 2004. Study of SO 2 adsorption and thermal regeneration over activated carbon-supported copper oxide catalysts. doi:10.1016/j.carbon.2004.05.004

Urabe, Y., Ishikura, T., Kaneko, K., 2008. Development of porosity in carbons from yeast grains by activation with alkali metal carbonates. J. Colloid Interface Sci. 319, 381–3. doi:10.1016/j.jcis.2007.10.057

Uzoma, K.C., Inoue, M., Andry, H., Fujimaki, H., Zahoor, A., Nishihara, E., 2011. Effect of cow manure biochar on maize productivity under sandy soil condition. Soil Use Manag. 27, 205–212. doi:10.1111/j.1475-2743.2011.00340.x

Vandecasteele, B., Sinicco, T., D'Hose, T., Vanden Nest, T., Mondini, C., 2016. Biochar amendment before or after composting affects compost quality and N losses, but not P plant uptake. J. Environ. Manage. 168, 200–209. doi:10.1016/j.jenvman.2015.11.045

Vasanth Kumar, K., Sivanesan, S., 2007. Sorption isotherm for safranin onto rice husk: Comparison of linear and non-linear methods. Dye. Pigment. 72, 130–133. doi:10.1016/j.dyepig.2005.07.020

Viswanathan, B., Indra Neel, P., Varadarajan, T.K., 2009. Methods of activation and specific applications of carbon materials [online]. Available from: https://nccr.iitm.ac.in/e%20book-Carbon%20Materials%20final.pdf

Wang, B., Lehmann, J., Hanley, K., Hestrin, R., Enders, A., 2015a. Adsorption and desorption of ammonium by maple wood biochar as a function of oxidation and pH. Chemosphere 138, 120–126. doi:10.1016/j.chemosphere.2015.05.062

Wang, Z., Guo, H., Shen, F., Yang, G., Zhang, Y., Zeng, Y., Wang, L., Xiao, H., Deng, S., 2015b. Biochar produced from oak sawdust by Lanthanum (La)-involved pyrolysis for adsorption of ammonium (NH_4^+), nitrate (NO_3^-), and phosphate (PO_4^{3-}). Chemosphere 119, 646–653. doi:10.1016/j.chemosphere.2014.07.084

Wang, Z., Nie, E., Li, J., Yang, M., Zhao, Y., Luo, X., Zheng, Z., 2011. Equilibrium and kinetics of adsorption of phosphate onto iron-doped activated carbon. Environ. Sci. Pollut. Res. Int. 19, 2908–17. doi:10.1007/s11356-012-0799-y

Warner, S.A., 1977. Cation exchange properties of forest litter as influenced by vegetation type and decomposition. MSc thesis, Oregon State University, USA. [online]. Available from: http://hdl.handle.net/1957/43660

White, J.E., Catallo, W.J., Legendre, B.L., 2011. Biomass pyrolysis kinetics: A comparative critical review with relevant agricultural residue case studies. J. Anal. Appl. Pyrolysis 91, 1–33. doi:10.1016/j.jaap.2011.01.004

Whitman, T., Lehmann, J., 2009. Biochar - One way forward for soil carbon in offset mechanisms in Africa? Environ. Sci. Policy. doi:10.1016/j.envsci.2009.07.013

Wiedner, K., Fischer, D., Walther, S., Criscuoli, I., Favilli, F., Nelle, O., Glaser, B., 2015. Acceleration of Biochar Surface Oxidation during Composting? Agric. Food Chem. doi:10.1021/acs.jafc.5b00846

Wiedner, K., Naisse, C., Rumpel, C., Pozzi, A., Wieczorek, P., Glaser, B., 2013a. Chemical modification of biomass residues during hydrothermal carbonization – What makes the difference, temperature or feedstock? Org. Geochem. 54, 91–100. doi:10.1016/j.orggeochem.2012.10.006

Wiedner, K., Rumpel, C., Steiner, C., Pozzi, A., Maas, R., Glaser, B., 2013b. Chemical evaluation of chars produced by thermochemical conversion (gasification, pyrolysis and hydrothermal

carbonization) of agro-industrial biomass on a commercial scale. Biomass and Bioenergy 59, 264–278. doi:10.1016/j.biombioe.2013.08.026

Williams, P.T., Reed, A.R., 2004. High grade activated carbon matting derived from the chemical activation and pyrolysis of natural fibre textile waste. J. Anal. Appl. Pyrolysis 71, 971–986. doi:10.1016/j.jaap.2003.12.007

Wilson, M.A., Philip, R.P., Gillam, A.H., Gilbert, T.D., Tate, K.R., 1983. Comparison of the structures of humic substances from aquatic and terrestrial sources by pyrolysis gas chromatography-mass spectrometry. Geochimico el Cosmochimica Acta. 47, 497-502.

Wong, J.W.C., Wang, X., Selvam, A., 2017. Improving compost quality by controlling nitrogen loss during composting. In: Current developments in biotechnology and bioengineering: Solid waste management. Ends: Wong, J.W.C., Ashok, R.D., Ashok, P., 2017. Elsevier B.V. pp. 69-70.

Woolf, D., Amonette, J.E., Street-Perrott, F.A., Lehmann, J., Joseph, S., 2010. Sustainable biochar to mitigate global climate change. Nat. Commun. 1, 1–9. doi:10.1038/ncomms1053

Wooten, J.B., Seeman, J.I., Hajaligol, M.R., 2004. Observation and Characterization of Cellulose Pyrolysis Intermediates by ^{13} C CPMAS NMR. A New Mechanistic Model. Energy & Fuels 18, 1–15. doi:10.1021/ef0300601

Wu, H., Zhao, Y., Long, Y., Zhu, Y., Wang, H., Lu, W., 2011. Evaluation of the biological stability of waste during landfill stabilization by thermogravimetric analysis and Fourier transform infrared spectroscopy. Bioresour. Technol. 102, 9403–8. doi:10.1016/j.biortech.2011.07.029

Wu, W., Yang, M., Feng, Q., McGrouther, K., Wang, H., Lu, H., Chen, Y., 2012. Chemical characterization of rice straw-derived biochar for soil amendment. Biomass and Bioenergy 47, 268–276. doi:10.1016/j.biombioe.2012.09.034

Xiao, X., Chen, Z., Chen, B., 2016. H/C atomic ratio as a smart linkage between pyrolytic temperatures, aromatic clusters and sorption properties of biochars derived from diverse precursory materials. Sci. Rep. 6, 22644. doi:10.1038/srep22644

Xie, T., Reddy, K.R., Wang, C., Yargicoglu, E., Spokas, K., 2015. Characteristics and Applications of Biochar for Environmental Remediation: A Review. Crit. Rev. Environ. Sci. Technol. 45, 939–969. doi:10.1080/10643389.2014.924180

Xu, G., Wei, L.L., Sun, J.N., Shao, H.B., Chang, S.X., 2013. What is more important for enhancing nutrient bioavailability with biochar application into a sandy soil: Direct or indirect mechanism? Ecol. Eng. 52, 119–124. doi:10.1016/j.ecoleng.2012.12.091

Xu, G., Sun, J., Shao, H., Chang, S.X., 2014. Biochar had effects on phosphorus sorption and desorption in three soils with differing acidity. Ecol. Eng. 62, 54–60. doi:10.1016/j.ecoleng.2013.10.027

Xue, Y., Gao, B., Yao, Y., Inyang, M., Zhang, M., Zimmerman, A.R., Ro, K.S., 2012. Hydrogen peroxide modification enhances the ability of biochar (hydrochar) produced from hydrothermal carbonization of peanut hull to remove aqueous heavy metals: Batch and column tests. Chem. Eng. J. 200-202, 673–680. doi:10.1016/j.cej.2012.06.116

Xue, Y., Hou, H., Zhu, S., 2009. Characteristics and mechanisms of phosphate adsorption onto basic oxygen furnace slag. J. Hazard. Mater. 162, 973–80. doi:10.1016/j.jhazmat.2008.05.131

Yakout, S.M., 2015. Monitoring the Changes of Chemical Properties of Rice Straw–Derived Biochars Modified by Different Oxidizing Agents and Their Adsorptive Performance for Organics. Bioremediat. J. 19, 171–182. doi:10.1080/10889868.2015.1029115

Yamato, M., Okimori, Y., Wibowo, I.F., Anshori, S., Ogawa, M., 2006. Effects of the application of charred bark of Acacia mangium on the yield of maize, cowpea and peanut, and soil chemical

properties in South Sumatra, Indonesia. Soil Sci. Plant Nutr. 52, 489–495. doi:10.1111/j.1747-0765.2006.00065.x

Yan, W., Hoekman, S.K., Broch, A., Coronella, C.J., 2014. Effect of hydrothermal carbonization reaction parameters on the properties of hydrochar and pellets. Environ. Prog. Sustain. Energy 33, 676–680. doi:10.1002/ep.11974

Yang, G.X., Jiang, H., 2014. Amino modification of biochar for enhanced adsorption of copper ions from synthetic wastewater. Water Res. 48, 396–405. doi:10.1016/j.watres.2013.09.050

Yang, H., Yan R., Chen, H., Le, D.H., Zheng, C., 2007. Characteristics of hemicellulose, cellulose and lignin pyrolysis. Fuel. 86, 1781-1788. doi: 10.1016/j.fuel.2006.12.013

Yao, Y., 2013. Sorption of phosphate and other contaminants on biochar and its environmental implications. PhD thesis, University of Florida, USA. [online]. Available from: http://ufdcimages.uflib.ufl.edu/UF/E0/04/54/09/00001/YAO_Y.pdf

Yao, Y., Gao, B., Chen, J., Yang, L., 2013. Engineered biochar reclaiming phosphate from aqueous solutions: mechanisms and potential application as a slow-release fertilizer. Environ. Sci. Technol. 47, 8700–8. doi:10.1021/es4012977

Yao, Y., Gao, B., Inyang, M., Zimmerman, A.R., Cao, X., Pullammanappallil, P., Yang, L., 2011. Biochar derived from anaerobically digested sugar beet tailings: characterization and phosphate removal potential. Bioresour. Technol. 102, 6273–8. doi:10.1016/j.biortech.2011.03.006

Ye, J., Cong, X., Zhang, P., Hoffmann, E., Zeng, G., Liu, Y., Fang, W., Wu, Y., Zhang, H., 2015. Interaction between phosphate and acid-activated neutralized red mud during adsorption process. Appl. Surf. Sci. 356, 128–134. doi:10.1016/j.apsusc.2015.08.053

Ye, Z.-L., Chen, S.H., Wang, S.M., Lin, L.F., Yan, Y.J., Zhang, Z.J., Chen, J.S., 2010. Phosphorus recovery from synthetic swine wastewater by chemical precipitation using response surface methodology. J. Hazard. Mater. 176, 1083–8. doi:10.1016/j.jhazmat.2009.10.129

Yin, X., Han, H., Gunji, I., Endou, A., Cheettu Ammal, S.S., Kubo, M., Miyamoto, A., 1999. NH_3 Adsorption on the Brönsted and Lewis Acid Sites of V 2 O 5 (010): A Periodic Density Functional Study. J. Phys. Chem. B 103, 4701–4706. doi:10.1021/jp990363p

Yuan, J.-H., Xu, R.-K., Zhang, H., 2011. The forms of alkalis in the biochar produced from crop residues at different temperatures. Bioresour. Technol. 102, 3488–97. doi:10.1016/j.biortech.2010.11.018

Zeng, Z., Zhang, S., Li, T., Zhao, F., He, Z., Zhao, H., Yang, X., Wang, H., Zhao, J., Rafiq, M.T., 2013. Sorption of ammonium and phosphate from aqueous solution by biochar derived from phytoremediation plants. J. Zhejiang Univ. Sci. B 14, 1152–61. doi:10.1631/jzus.B1300102

Zhang, C., Fu, Z., Liu, Y.C., Dai, B., Zou, Y., Gong, X., Wang, Y., Deng, X., Wu, H., Xu, Q., Steven, K.R., Yin, D., 2012. Ionic liquid-functionalized biochar sulfonic acid as a biomimetic catalyst for hydrolysis of cellulose and bamboo under microwave irradiation. Green Chem. 14, 1928. doi:10.1039/c2gc35071h

Zhang, D., Yan, M., Niu, Y., Liu, X., van Zwieten, L., Chen, D., Bian, R., Cheng, K., Li, L., Joseph, S., Zheng, J., Zhang, X., Zheng, J., Crowley, D., Filley, T.R., Pan, G., 2016. Is current biochar research addressing global soil constraints for sustainable agriculture? Agric. Ecosyst. Environ. 226, 25–32. doi:10.1016/j.agee.2016.04.010

Zhang, G., Liu, H., Liu, R., Qu, J., 2009. Removal of phosphate from water by a Fe-Mn binary oxide adsorbent. J. Colloid Interface Sci. 335, 168–74. doi:10.1016/j.jcis.2009.03.019

Zhang, J., Wang, Q., 2015. Sustainable mechanisms of biochar derived from brewers' spent grain and sewage sludge for ammonia-nitrogen capture. J. Clean. Prod. 112, 3927–3934. doi:10.1016/j.jclepro.2015.07.096

Zhang, M., Gao, B., Yao, Y., Xue, Y., Inyang, M., 2012. Synthesis of porous MgO-biochar nanocomposites for removal of phosphate and nitrate from aqueous solutions. Chem. Eng. J. 210, 26–32. doi:10.1016/j.cej.2012.08.052

Zhang, S., Asadullah, M., Dong, L., Tay, H.L., Li, C.Z., 2013. An advanced biomass gasification technology with integrated catalytic hot gas cleaning. Part II: Tar reforming using char as a catalyst or as a catalyst support. Fuel 112, 646–653. doi:10.1016/j.fuel.2013.03.015

Zhao, L., Cao, X., Mašek, O., Zimmerman, A., 2013a. Heterogeneity of biochar properties as a function of feedstock sources and production temperatures. J. Hazard. Mater. 256-257, 1–9. doi:10.1016/j.jhazmat.2013.04.015

Zhao, L., Cao, X., Wang, Q., Yang, F., Xu, S., 2013b. Mineral Constituents Profile of Biochar Derived from Diversified Waste Biomasses: Implications for Agricultural Applications. J. Environ. Qual. 42, 545. doi:10.2134/jeq2012.0232

Zheng, H., Wang, Z., Zhao, J., Herbert, S., Xing, B., 2013. Sorption of antibiotic sulfamethoxazole varies with biochars produced at different temperatures. Environ. Pollut. 181, 60–7. doi:10.1016/j.envpol.2013.05.056

Zheng, W., Sharma, B.K., Rajagopalan, N., 2010. Using biochar as a soil amendment for sustainable agriculture [online]. Available from: https://www.ideals.illinois.edu/bitstream/handle/2142/25503/Using%20Biochar%20as%20a%20Soil%20Amendment%20for%20Sustainable%20Agriculture-final%20report%20from%20Zheng.pdf?sequence=2

Annex A: Char physico-chemical properties as a function of processing conditions and feedstock properties

Table A1. Biochar and hydrochar properties and possible influencing factors

Property	Property	Property	Property
Carbon structure	Condensed, predominantly aromatic C.	Amorphous, mostly aliphatic C lignin-type molecules.	Cao and Harris (2010); Sun et al. (2011); Wiedner et al. (2013a).
Elemental content	C content tends to increase with pyrolysis temperature while oxygen content decreases with pyrolysis temperature, thus surface hydrophilicity decreases with temperature as well.With temperature, O/C ratios tend to decrease with pyrolysis temperature while N content varies.	C content tends to increase with temperature and residence time while O content decreases. O/C ratio therefore decreases with temperature. Temperature appears to have a slightly more pronounced effect on elemental content compared to residence time however. N content varies.	Benavente et al. (2015); Cao and Harris (2010); Chun et al. (2004); Danso-Boateng et al. (2015); Fang et al. (2015); Gronwald et al. (2015); Hoekman et al. (2011); Kalderis et al. (2014); Parshetti et al. (2014); Tian et al. (2016); Wiedner et al. (2013a); Xie et al. (2014); Zhao et al. (2013b).
Mineral content	P, Ca, Mg tend to increase with pyrolysis temperature	Varies with feedstock and temperature: *Decrease:* [d,g]Relative to original biomass, Na, Ca, Mg, Al, S, P, Si, Fe, K and Mn decreased with increasing temperature up to a certain point, [e]some decrease in K, Ca, Fe while most other minerals were unaffected. *No effect:* [c]Temperature did not appear to influence Ca, Mg, Al although minerals leached into aqueous phase; [e]no effect on Mg, Zn, Al, Li, B. *Increase*: with temperature, [d]P increased but no definite trend for Ca, Mg, K though an increase observed in some cases; [f]Zn and [e]Na increased.	[a]Cao and Harris (2010); [b]Danso-Boateng et al. (2015); [c]Fang et al. (2015); [d]Gronwald et al. (2015); [e]Parshetti et al. (2014); [f]Kalderis et al. (2014); [g]Reza et al. (2013).
Surface area (BET, N_2)	Tend to be higher than hydrochar surface areas although exceptions exist: [h]2.1–6.7 m^2 g^{-1} (higher in poultry litter than wheat straw biochar); positive correlation found between surface area and ash content; [a]ranged from 2.7–13.2 m^2 g^{-1}.	Temperature, time and feedstock dependent; increases with temperature but to a certain point:[h]4.0–8.8 m^2 g^{-1} (higher in poultry litter than sewage solid hydrochar), and positive correlation found between surface area and ash content. Surface areas were highest at 200 °C in studies[c,d,e,f] but a general decrease > 300 °C[c]. A six-fold decrease (6.1 to 1.0 m^2 g^{-1}) as temperature increased from 250 °C to 350 °C[e]. [f]Increase in surface area with time.	[a]Cao and Harris (2010); [c]Fang et al. (2015); [d]Gronwald et al. (2015); [e]Parshetti et al. (2014); [f]Kalderis et al. (2014); [h]Sun et al. (2011)
Ash content	Tends to increase with temperature due to concentration of mineral matter relative to other species.	Varies with temperature and feedstock: *Decrease*: [l,n]generally decreased with temperature but also dependent on feedstock: relative to raw biomass, ash content decreased in olive mill waste and lignocelluloses but increased in organic wastes -artichoke, orange juice waste, sewage sludge. *Increase*: [b,d,f, j] with temperature and residence time; [j,n]ash increased with temperature but lower compared to raw feedstock between 180-210 ºC compared to 230 ºC in all hydrochars.	[i]Benavente et al. (2015); [a]Cao and Harris (2010); [b]Danso-Boateng et al. (2015); [d]Gronwald et al. (2015); [f]Kalderis et al. (2014); [n]Smith et al. (2016) [j]Wiedner et al. (2013a)

Table A1. Biochar and hydrochar properties and possible influencing factors

Property	Property	Property	Property
Volatile matter (VM)	Decreases with increasing temperature; woody biomass may have higher VM than agric.residues.	Tends to decrease with process temperature.	Kalderis et al. (2014); Xie et al. (2014)
pH	Biochars mostly alkaline and are temperature- and feedstock-dependent[a,k,m]: [a]pH of raw feedstock was alkaline but became acidic after 200 °C pyrolysis. Beyond 200 °C, pH rose and peaked at about 350 °C suggesting formation of acidic species due to cellulose and hemicellulose degradation at 200 °C, but other studies[k] report cellulose degradation at higher temperature (400 ºC).	Hydrochars are mostly acidic and effect of processing temperature varies: *No effect*: [j]pH did not change between 180-230 ºC and was comparable between biochar types studied. *Decrease*: [f]temperature and time dependent but former had a more pronounced effect.	[a]Cao and Harris (2010); [k]Gaskin et al. (2008); [f]Kalderis et al. (2014); [j]Wiedner et al. (2013a); [l]Xie et al. (2014); [m]Zhao et al. (2013a)
PAH, PCB, PCDD	3-,4- and 5-ring PAH but generally low total PAH content in pyrolysis and gasification chars.	Likely temperature and feedstock dependent: Single total PAH content increase with temperature; all hydrochars in the study had low levels of 6-ring PAH as temperature increased, but variations in the increase in levels of 2-, 4- and 5-rings were observed for hydrochars from different feedstocks. PCDD contents low in the hydrochars likely due to the low temperature (<250–300 ºC) involved. At 300 ºC, presence of chlorine and organic C led to PCDD formation.	Wiedner et al. (2013a; 2013b)
Yield	Generally dependent on feedstock properties e.g., high lignin results in higher char yields; decreases with temperature.	Decrease with process temperature and residence time.	Ahmad et al. (2014a); Danso-Boateng et al. (2015); Hoekman et al. (2011); Sohi et al. (2009); Wiedner et al. (2013a)
Char HHV (MJ kg^{-1})	Likely increase with temperature due to increase in 5-HMF.	Increase with temperature and residence time.	Danso-Boateng et al. (2015);; Kalderis et al. (2014); Stemman et al. (2013).

Key processing conditions:
Benavente et al. (2015): Fresh olive mill, artichoke and orange juice waste, 200 g wet-weight, 200–225 °C, 2–24 h.
Cao and Harris (2010): Dairy manure biochars, 100–500 °C 4h, 25 °C min^{-1}.
Chun et al. (2004): Wheat residue biochars 300–700 °C, 6 h followed by acid washing to demineralise chars.
Danso-Boateng et al. (2015): Sewage sludge hydrochar 160–200 °C, 1-4 h.
Eibisch et al. (2015): Corn digestate, miscanthus, woodchips of poplar and willow: biochars: 750 °C, 45 min; hydrochars: 200 °C and 250 °C, 6h.
Fang et al. (2015): Bagasse, hickory and peanut hull hydrochars, 13–18 wt.% ratio, 200–300 °C, 6 h rinsed with tap and deionised water for 1 h 10 min to remove water-soluble volatile matter.
Gronwald et al. (2015): Maize digestate, miscanthus and woodchip hydrochars, 200 °C and 250 °C, 10 wt.%, 6 h.
Hoekman et al. (2011): Pine and fir (Tahoe Mix) hydrochar, 216–295 °C, 5–60 min.
Kalderis et al. (2014): Rice husk; washed with water and dried. 1:5 biomass/water ratio, pre-heated to 85 °C prior to HTC at 200 and 300 °C for 2 –16 h, filtered, washed with acetone followed by water and air-dried for 24 h.
Parshetti et al. (2014): Foodwaste; 250 °C and 350 °C, 25 wt.% ratio, 20 min followed by rapid quenching, hydrochars rinsed with deionised water.
Reza et al. (2013): Corn stover, miscanthus, rice hull, switch grass hydrochars produced at 200, 230 and 260 °C, 5 min. 1:5 biomass/water ratio, reactor purged with nitrogen, Reactor vessel rapidly cooled to room temperature with ice-water bath. Chars filtered and oven dried.
Smith et al. (2016). Willow, miscanthus, oak, greenhouse waste, presscake from AD, sewage sludge, food waste, municipal solid waste, microalgae, macro algae; 250 °C, 1 h, 10 wt.% unrinsed.
Sun et al. (2011): Poultry litter and swine solid hydrochars 250 °C, 20 h followed by acetone washing to remove tarry matter; poultry litter and wheat straw biochar 400 °C, 2–7 h followed by acid washing to remove minerals.
Wiedner et al. (2013a): Poplar wood, olive residue and wheat straw hydrochar 180–230 ºC, about 30 wt.%, 8 h; Zhao et al. (2013b): 500 °C, 4 h.

Annex B: Adsorption models

Table A2 Classical equilibrium and kinetic adsorption models

S/N	Model	Expression	Plot	Definition of key terms and their implications	References
A. Typical equilibrium sorption models					
1	Langmuir for concave isotherms	(A2.1) $Q = Q_{max}\frac{LC}{1+LC}$ or $q_e = \frac{Q_o b C_e}{1+bC_e}$ Linearised: (A2.2) $\frac{C_e}{q_e} = \frac{1}{bQ_o} + \frac{C_e}{Q_o}$ or $\frac{C_e}{q_e} = \frac{1}{k_a q_m} + \frac{C_e}{q_m}$ (A2.3) $\frac{1}{q_e} = \left(\frac{1}{k_a q_m}\right)\frac{1}{C_e} + \frac{1}{q_m}$ (A2.4) $q_e = q_m - \left(\frac{1}{k_a}\right)\frac{q_e}{C_e}$ (A2.5) $\frac{q_e}{C_e} = k_a q_m - k_a q_e$ (A2.6) $Q_i = Q_{max,\,i}\frac{L_1 C_i}{1+\sum_{j=1}^{q} L_j C_j}$	 $\frac{C_e}{q_e}$ vs C_e $\frac{1}{q_e}$ vs $\frac{1}{C_e}$ q_e vs $\frac{q_e}{C_e}$ $\frac{q_e}{C_e}$ vs q_e n.a	2 degrees of freedom; Q_{max} is saturated monolayer adsorption (mg g^{-1}); b is the ratio of adsorption and desorption rate constants, and is related to the binding energy of adsorption, higher values suggest that desorption will be more challenging; at very low concentrations, $Q_{max}L$ becomes K_D (distribution coefficient) so that $q_e = K_D C_e$ thus obeying Henry's Law. C_e is equilibrium concentration (mg L^{-1}); q_e is amount of adsorbed solute in adsorbent at equilibrium (mg g^{-1}); Q_o is maximum monolayer coverage capacity (mg g^{-1}). Linear versions of Equations (4.6) and (4.7) are more popular because their error distribution is better (Kumar and Sivanesan, 2007). Here, Q_{max} is unaffected by competing species while L_j (affinity constant) is.	Ayoob and Gupta (2008); Foo and Hameed (2010); Limousin et al. (2007); Maurya and Mittal (2006); Kumar and Sivanesan (2007); Prasad and Srivastava (2009); Sun et al. (2015); Wang et al. (2012)
2	Freundlich for concave (L and H) isotherms	(A2.7) $q_e = {}_{K_F}C_e^{\frac{1}{n}}$ (A2.8) Linearised: $\log q_e = \log K_F + \frac{1}{n}\log C_e$	Log q_e vs log C_e	2 degrees of freedom; n is adsorption intensity or surface heterogeneity: high n is said to be indicative of sample heterogeneity; 1/n is slope, and $0 < 1/n < 1$	Ayoob and Gupta (2008);Foo and Hameed, (2010); Limousin et al. (2007); Lin et al. (2009); Maurya and Mittal (2006); Wang et al. (2012)

S/N	Model	Expression	Plot	Definition of key terms and their implications	References
		(A2.9) Modified Freundlich: $Q = F_i C_i \left(\sum_{j=1}^{m} a_{i,j} C_{i,j}\right)^{n_i - 1}$		*i, j* refer to competing species.	
3	Langmuir-Freundlich	(A2.10) $Q_e = \frac{K_{LF}\, q_{max}\, C_e^n}{1 + K_{LF}\, C_e^n}$		K_{LF} is the Langmuir-Freundlich affinity parameter ($L^n\ mg^{-n}$); n is the Freundlich linearity constant (dimensionless); q_{max} is maximum adsorbent adsorption capacity (mg g^{-1}); C_e is the equilibrium concentration (mg L^{-1}).	Ye et al. (2015)
4	Linear with intercept for C curve	(A2.11) $Q = K_d C + m$	n.a	2 degrees of freedom; Applicable at high concentrations	Limousin et al. (2007); Maurya and Mittal (2006)
5	Sips	(A2.12) $q_e = \frac{K_s C_e^{\beta} S}{1 + a_s C_e^{\beta} S}$ (A2.13) Linearised: $\beta_s \ln(C_e) = -\ln\frac{K_s}{q_e} + \ln(a_s)$	$\ln\frac{K_s}{q_e}$ vs $\ln(C_e)$	3 degrees of freedom; K_s is Sips isotherm model constant (L g^{-1}); a_s is Sips isotherm model constant (L mg^{-1}). β_s is the Sips isotherm model exponent.	Foo and Hameed (2010); Maurya and Mittal (2006)
6	Redlich-Peterson	(A2.14) $q_e = \frac{kgC_e}{1 + a_R C_e^g}$ (A2.15) Linearised: $\ln\left(K_R \frac{C_e}{q_e} - 1\right) = g\ln(C_e) + \ln(a_R)$	$\ln\left(K_R \frac{C_e}{q_e} - 1\right)$ vs $\ln(C_e)$	3 degrees of freedom; g is Redlich-Peterson isotherm exponent; a_R is Redlich-Peterson isotherm constant (mg^{-1}); K_R is Redlich-Peterson isotherm constant (L mg^{-1}).	Foo and Hameed (2010); Kumar and Sivanesan (2007); Mane et al. (2007); Maurya and Mittal (2006)
7	Dubinin-Radushkevich	(A2.16) $q_e = q_m \exp(-B\varepsilon^2)$		2 degrees of freedom	Maurya and Mittal (2006)
B. Typical kinetic sorption models					
1	First order	(A2.17) $\frac{dQ}{dt} = \frac{\theta}{\rho} K_1 C - K_{-1} Q$	n.a	Θ is volumetric water content; ρ is bulk density.	Limousin et al. (2007) Namasivayam and Ranganathan (1994)

S/N	Model	Expression	Plot	Definition of key terms and their implications	References
		(A2.18): $\log\left(q_e - q\right) = \log q_e - \frac{k_1}{2.303} t$			
2	Pseudo-first-order	(A2.19) $\frac{dq_t}{dt} = k_f(q_e - q_t)$ (A2.20) Linearised: $\ln(q_e - q_t) = \ln q_e - k_1 t$	$\ln(q_e - q_t)$ vs t	q_t is amount of adsorbed solute in adsorbent at equilibrium (mg g^{-1}); k_f is the pseudo-first-order rate constant (min^{-1}).	Ahmad et al. (2014b); Mane et al. (2007)
3	(Ho's) Pseudo-second-order	(A2.21) $\frac{dq_t}{dt} = k_s(q_e - q_t)^2$ (A2.22) $\frac{t}{q_t} = \frac{1}{k_2 q_e^2} + \frac{1}{q_e} t$	$\frac{t}{q_e}$ vs t	K_s is the pseudo-second-order rate constant (g mg^{-1} min^{-1})	Ahmad et al. (2014b); Mane et al. (2007); Prasad and Srivastava (2009)
4	Elovich	(A2.23) $\frac{dq_t}{dt} = \alpha \exp(-\beta q_t)$ (A2.24) Linearised: $q_t = \frac{1}{\beta}\ln\alpha\beta + \frac{1}{\beta}\ln t$	q_t vs ln t	α is initial sorption rate (mg g^{-1} min^{-1}); β is sorption constant (g mg^{-1})	Ahmad et al. (2014b); Prasad and Srivastava (2009)
5	External diffusion model	(A2.25) $\ln\frac{C_t}{C_o} = -k_f \frac{a}{V} t$	$\ln\frac{C_t}{C_o}$ vs t	a is total interfacial particle area (cm^2); V is total solution volume (L); k_f is external mass transfer coefficient	Prasad and Srivastava (2009)

n.a denotes unavailable data.

Annex C: Ammonium and phosphate linear regression plots

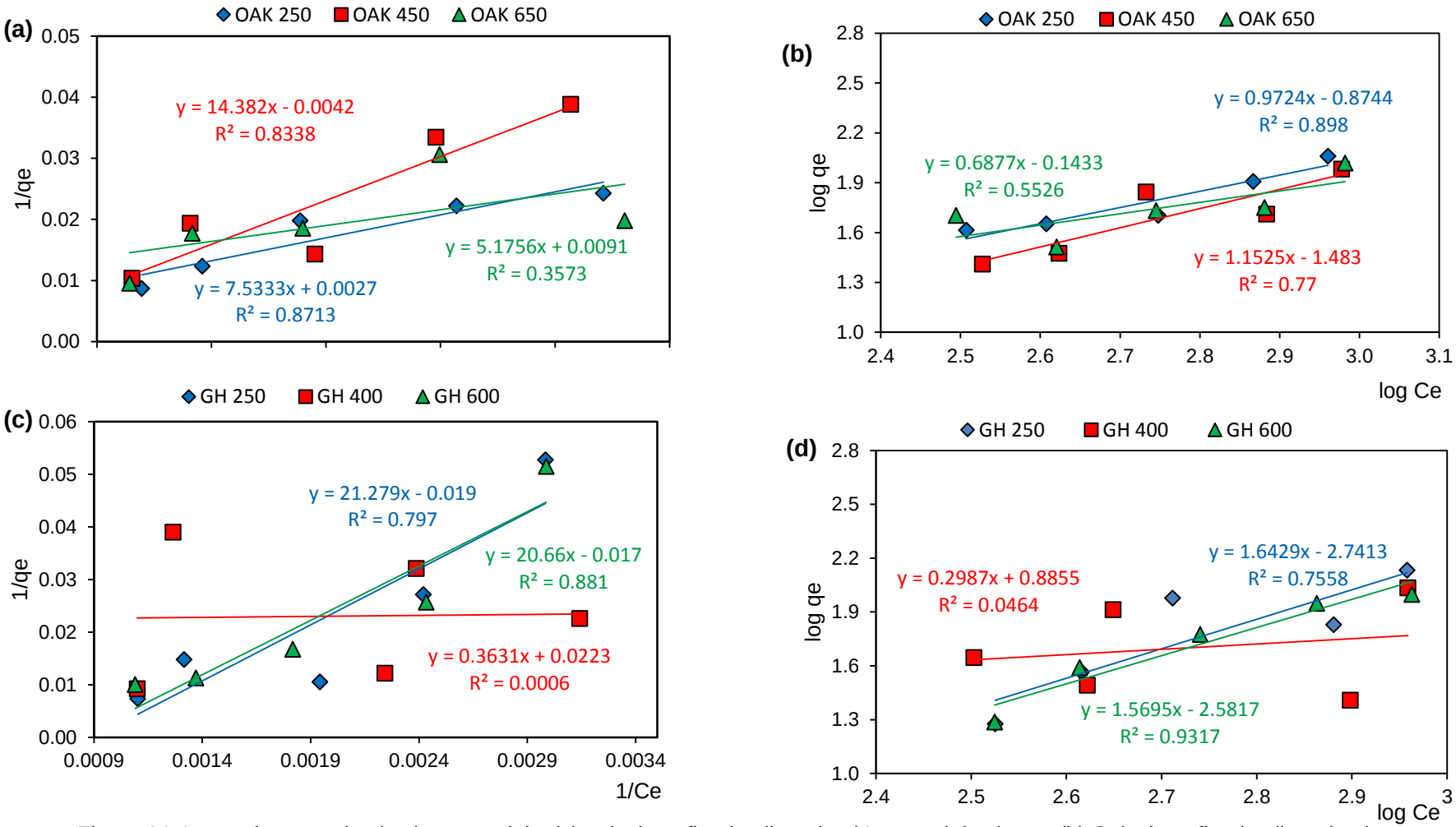

Figure A1 Ammonium sorption isotherm models: (a) oak chars fitted to linearised Langmuir isotherm; (b) Oak chars fitted to linearised Freundlich isotherms; (c) Greenhouse waste chars fitted to linearized Langmuir isotherms; (d) Greenhouse waste chars fitted to linearized Freundlich isotherms. Initial NH_4^+ concentrations ≈ 360, 450, 600, 800 and 1000 mg L^{-1}.

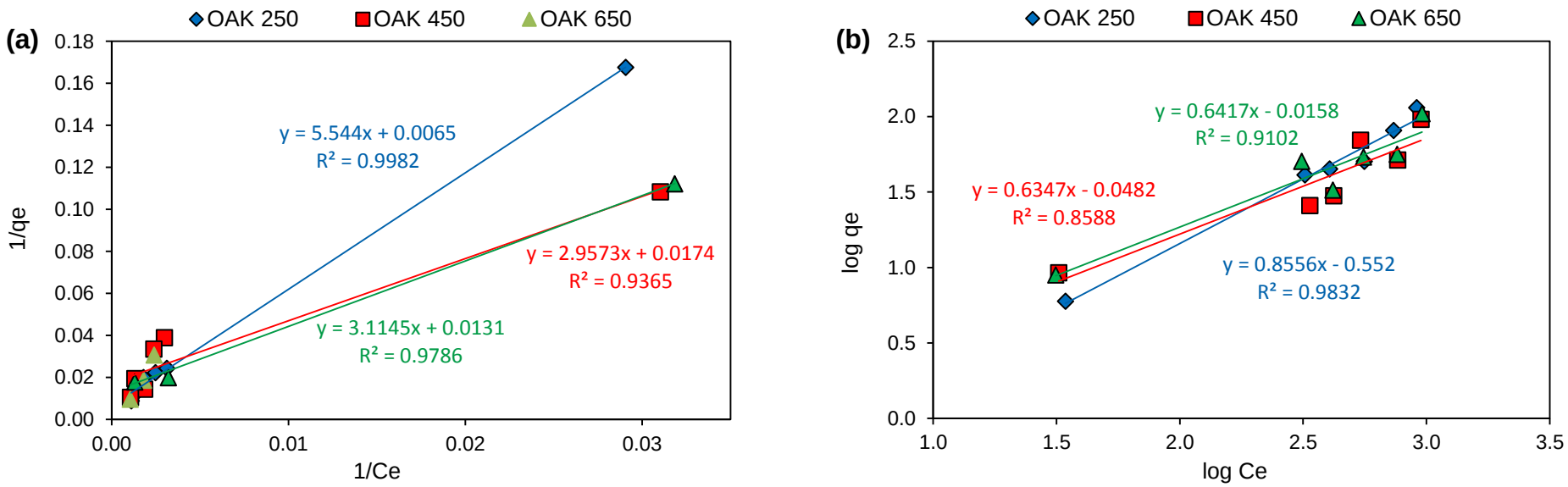

Figure A2 Ammonium sorption isotherm models for oak chars fitted to (a) linearised Langmuir; (b) linearised Freundlich isotherm models. Initial NH_4^+ concentrations ≈ 40, 360, 450, 600, 800 and 1000 mg L^{-1}.

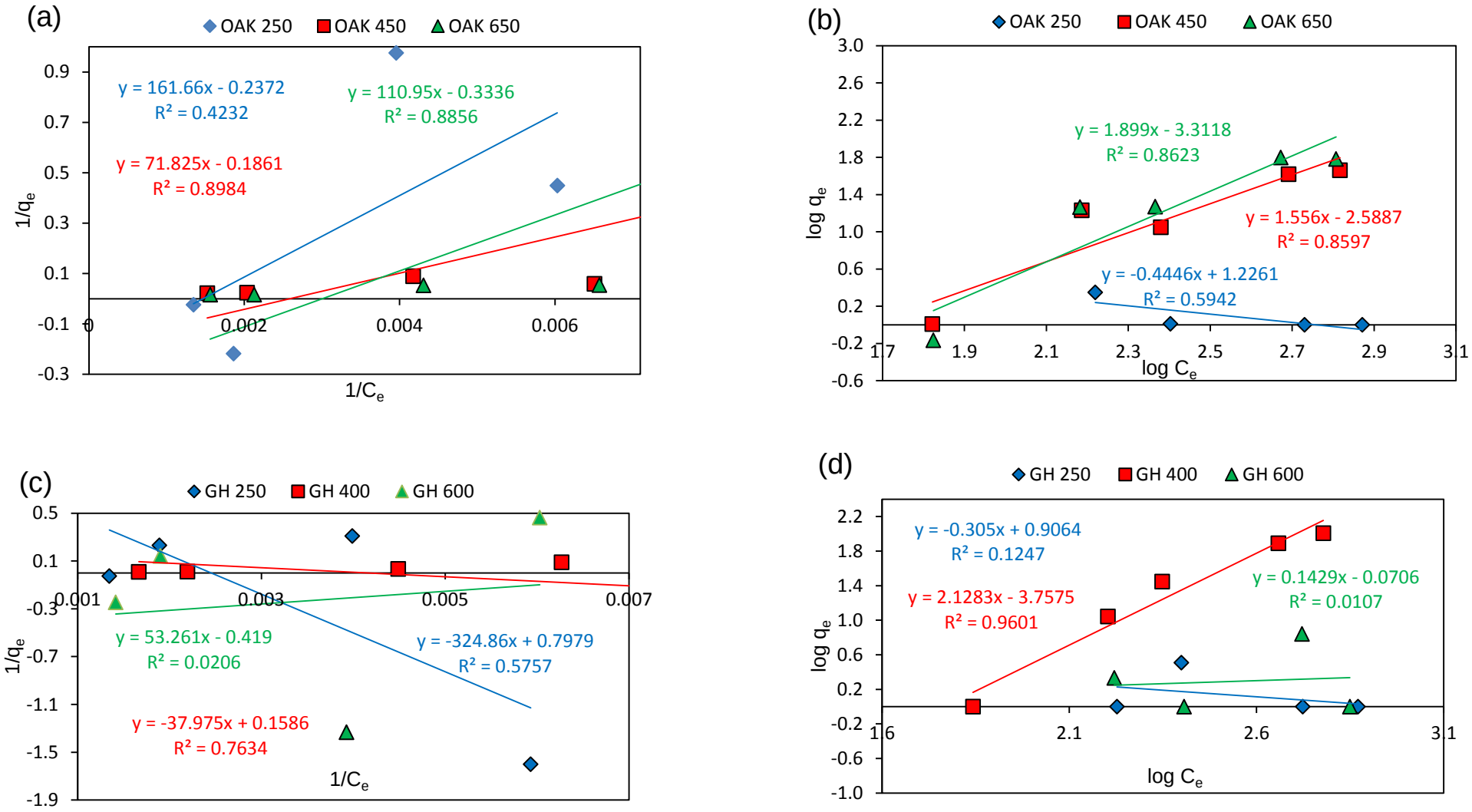

Figure A3 Phosphate sorption isotherm models: (a) oak chars fitted to linearized Langmuir isotherm; (b) Oak chars fitted to linearized Freundlich isotherms; (c) Greenhouse waste chars fitted to linearized Langmuir isotherms; (d) Greenhouse waste chars fitted to linearized Freundlich isotherms. Initial PO_4^{3-} concentrations 61–700 mg L^{-1} for Oak 450, 650 and GH 400 and between 170–700 mg L^{-1} for remaining chars.

Annex D: CEC Calculations

Equation of reaction: $NH_4^+ : H_2BO_3^- + HCl \rightarrow NH_4Cl + H_3BO_3$

CEC Method 2

$$NH_4^+ : H_2BO_3^- + H^+Cl^- \rightarrow NH_4Cl + H_3BO_3$$

C = ?
n = ?
v = 20 mL = 0.02 L

C = 0.01 M
n = ?
v = titre volume (L)

$$\frac{0.01\ \cancel{mol}\ HCl \mid 1\ Eq\ HCl}{L \mid 1\ \cancel{mol}} = 0.01\ Eq\ L^{-1}$$

If titre value = 9.8 mL = 0.0098 L

Then $n_{HCl} = CV = 0.01 \frac{Eq}{L} \times 0.0098\ L = 0.00098\ Eq\ HCl$

Since stoichiometric equation shows that 1 mol of NH_4^+ reacts with 1 mol of H^+,

0.00098 Eq of NH_4^+ will react with 0.000098 Eq of H^+

$$\text{Thus } C_{NH4} = \frac{0.000098\ Eq}{0.020\ L} = 0.0049 \frac{Eq}{L}\ NH_4^+$$

$$\frac{0.0049\ Eq \mid 0.025\ \cancel{L}}{\cancel{L} \mid 2.5\ g} = 0.000049 \frac{Eq}{g} = 0.049 \frac{mEq}{g}$$

$$CEC: 0.049 \frac{m\ Eq}{g} \times 100 = \underline{4.9\ mEq\ /100\ g}$$

This CEC calculation is based on Eq. (3.9): $CEC\ (mEq\ /100\ g) = \frac{(V_1 - V_2) \times N}{V_a} \times \frac{V_L}{w} \times 100$

There were differences in titrant concentration and volume of sample leachate used in CEC Methods 2 and 3; in Method 2, 20 mL aliquots of the final leachates were distilled and titrated against 0.01 M HCl while the entire 200 mL of the final leachate was distilled and titrated against 0.1 M HCl in Method 3. To account for these differences, slight variations to the CEC calculations were made.

CEC Method 3

Eq. (3.10) as outlined in **Section 3.4.5.3** is as follows:

$$\text{CEC (meq/100 g)} = \frac{(V_1 - V_2)\ \text{L} \times \text{N} \frac{\text{Eq}}{\text{L}} \times 100 \times 1000}{\text{Mass of sample g}}$$

where V_1 and V_2 = titre values for sample and blank resp. (L); N = normality of HCl based on stoichiometric equation = 0.1 Eq L^{-1}. Thus, given a sample titre of 64.3 mL,

$$\text{CEC} = \frac{(0.0643 - 0.0005)\ \cancel{\text{L}} \times 0.1 \frac{\text{Eq}}{\cancel{\text{L}}} \times 100 \times 1000}{10\ \text{g}} = \underline{63.8\ \text{mEq /100 g}}$$

Theoretical NH_4^+ uptake based on CEC ($cmol_c\ kg^{-1}$ or mEq/100 g)

Theoretical (maximum) NH_4^+ uptake capacity (mg g^{-1}) calculated from CEC ($cmol_c\ kg^{-1}$):

$1 \times 10^{-2}\ \cancel{mol_c}$	$1\ \cancel{mol}\ NH_4^+$	$18\ \cancel{g}\ NH_4^+$	$1\ \cancel{kg}$	$1000\ mg$
$\cancel{kg}$	$1\ \cancel{mol_c}\ NH_4^+$	$1\ \cancel{mol}\ NH_4^+$	$1000\ \cancel{g}$	$1\ g$

Thus 1 $cmol_c\ kg^{-1}$ = 0.18 mg NH_4^+ per g, so that char having a CEC of 88.3 $cmol_c\ kg^{-1}$ should be able to retain 88.3 × 0.18 = 15.89 mg NH_4^+ per gram of char.

Alternatively, 1 $cmol_c\ kg^{-1}$ = 0.14 mg NH_4^+-N as frequently used in the literature, which is equivalent to 12.36 mg NH_4^+ per gram of char.

Table A3. Titre values obtained from CEC-2 (displacement after washing method)

Sample	Titre 1 (mL)	Titre 2 (mL)	Titre 3 (mL)
ECN Cellmat 400 °C, 60min	9.8	9.9	-
ECN Cellmat 600 °C, 30min	30.5	18.7	15.1
ECN Cellmat 600 °C, 60min, 1% O_2	26.3	22.7	-
ECN Cellmat 600 °C, 60min	13.3	8.9	-
ECN Presscake 400 °C, 60min	9.8	13.4	-
ECN Presscake 600 °C, 30min	19.3	22.2	-
ECN Presscake 600 °C, 60min, 1% O_2	29.0	24.3	-
ECN Presscake 600 °C, 60min	4.7	6.0	-
ECN Presscake 700 °C, 60min	10.0	7.0	-
ECN Greenhouse waste 400 °C, 60min	67.3	75.4	73.0
ECN Greenhouse waste 600 °C, 60min, 0% O_2	46.8	-	-
ECN Oak 400 °C, 60min	32.3	54.6	-
ECN Oak 600 °C, 60min	34.6	46.0	-
Proininso Oak 450 °C	23.3	20.9	-
Proininso Oak 650 °C	14.4	15.2	-
Proininso 650 °C in vermi compost	28.9	23.9	-
ECN Greenwaste 400 °C, 60min	31.8	11.0	-
ECN Greenwaste 600 °C, 60min, 0% O_2	14.2	12.0	10.3

Dashed lines indicate unavailable data.

Table A4. Titre values obtained from CEC-3 (direct displacement method)

Sample	Titre (mL)
ECN Presscake 600 °C, 30 mins, 0% O_2	64.3
ECN Cellmat 400 °C, 60 mins, 0% O_2	29.7
ECN Oak 400 °C, 60 mins, 0% O_2	99.0
ECN Presscake 600 °C, 60 mins, 0% O_2	35.1
ECN Press cake 400 °C, 60 mins, 0% O_2	31.7
ECN Presscake 700 °C, 60 mins, 0% O_2	47.6
Proinsino Oak 650 °C	74.0
ECN Cellmat 600 °C, 60mins, 1% O_2	122.7
ECN Cellmat 600 °C, 30 mins, 0% O_2	45.9

Annex E: Composting calculations

Equation of reaction during titration of NH_4^+ analyte with H_2SO_4:

N mole balance: $a\underset{4}{\overset{+}{NH}} : \underset{2}{H}\underset{3}{\overset{-}{BO}} + bH_2SO_4 \rightarrow c(NH_4)_2SO_4 + dH_3BO_3$ $\quad \boldsymbol{a} = 2\boldsymbol{c}$

H mole balance: $6\boldsymbol{a} + 2\boldsymbol{b} = 8\boldsymbol{c} + 3\boldsymbol{d}$

BO_3^- mole balance: $\boldsymbol{a} = \boldsymbol{d}$

SO_4^{2-} mole balance: $\boldsymbol{b}$ =

Balanced equation: $2\underset{4}{\overset{+}{NH}} : \underset{2}{H}\underset{3}{\overset{-}{BO}} + H_2SO_4 \rightarrow (NH_4)_2SO_4 + 2H_3BO_3$

C = ?	C = 0.04 M
n = ?	n = ?
v = 50 mL	v = Titre value (mL)

If sample titre = 10 mL, then $n_{H2SO4} = 0.04 \frac{mol}{L} \times 0.010\ L = 0.0004\ mol$

As 2 mol NH_4^+ reacts with 1 mol H^+, 2 × 0.0004 mol NH_4^+ will react with 0.0004 mol H^+

so that $C_{NH4} = \frac{n}{v} = \frac{0.0008}{0.050} = 0.016\ mol\ L^{-1} = 288\ mg\ NH_4^+\ L^{-1} \times \frac{17}{18} = \underline{272\ mg\ NH_3\ L^{-1}}$

Alternatively, since 1 mg NH_4-N per L = 1 mg NH_3-N per L,

$$C_{NH_3\text{-}N} = 0.016 \frac{\cancel{mol}}{L} \times 14 \frac{g}{\cancel{mol}} \times 1000 \frac{mg}{\cancel{g}} = 224\ mg\ NH_3\text{-}N\ L^{-1}$$

To confirm:

1 M H_2SO_4 = 2 Eq H_2SO_4 L^{-1} so that 0.04 M = 0.08 Eq L^{-1}

$$NH_3\text{-}N\ (mg\ L^{-1}) = \frac{(0.010 - 0)L}{0.050\ L} \times \frac{0.08\ Eq_{H+}}{L} \times \frac{14\ g}{1\ Eq_{NH3\text{-}N}} \times \frac{1000\ mg}{1\ g} = 224\ mg\ NH_3\text{-}N\ L^{-1}$$

CO_2 and inorganic N dynamics:

The performance of OAK 650-$MgCl_2$ was evaluated in soil incubation trials as shown in **Fig. A4**.

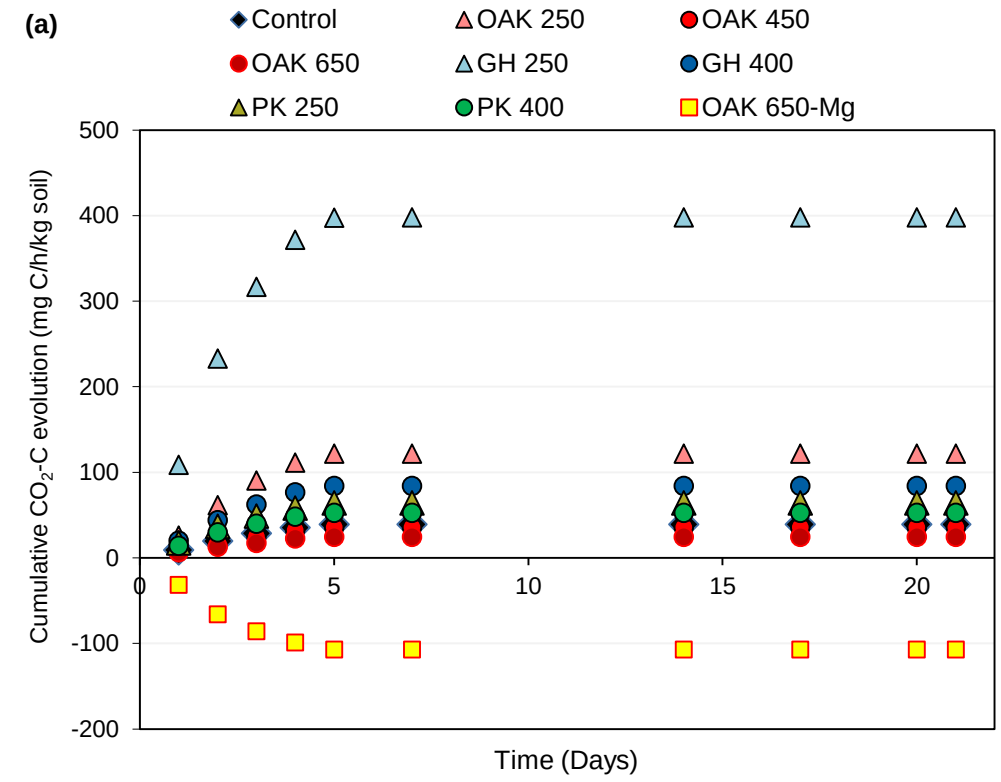

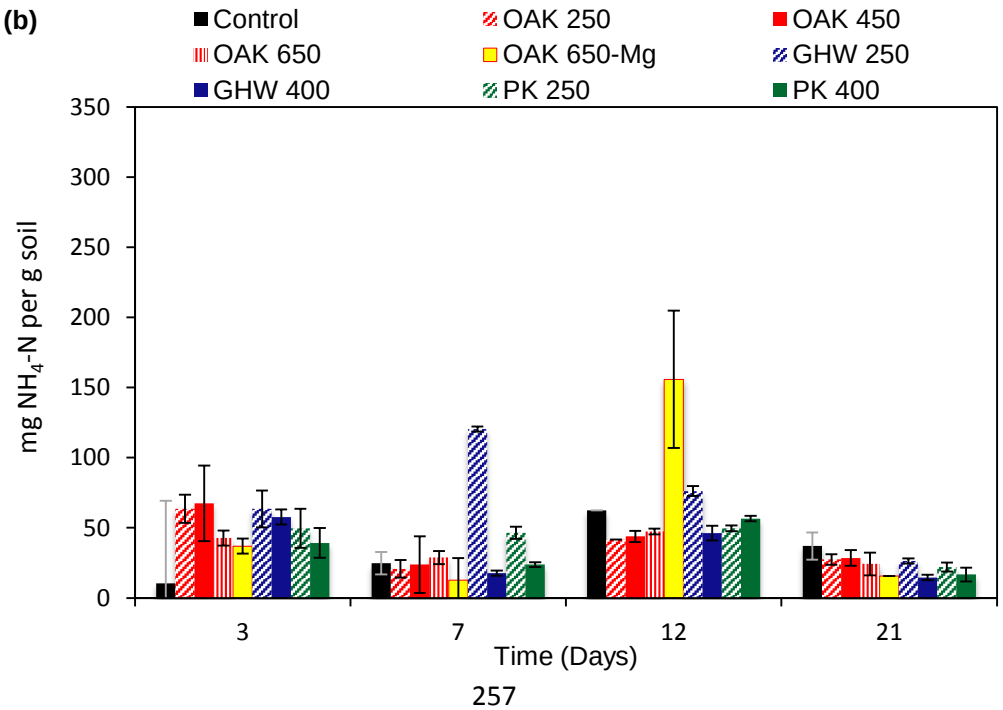

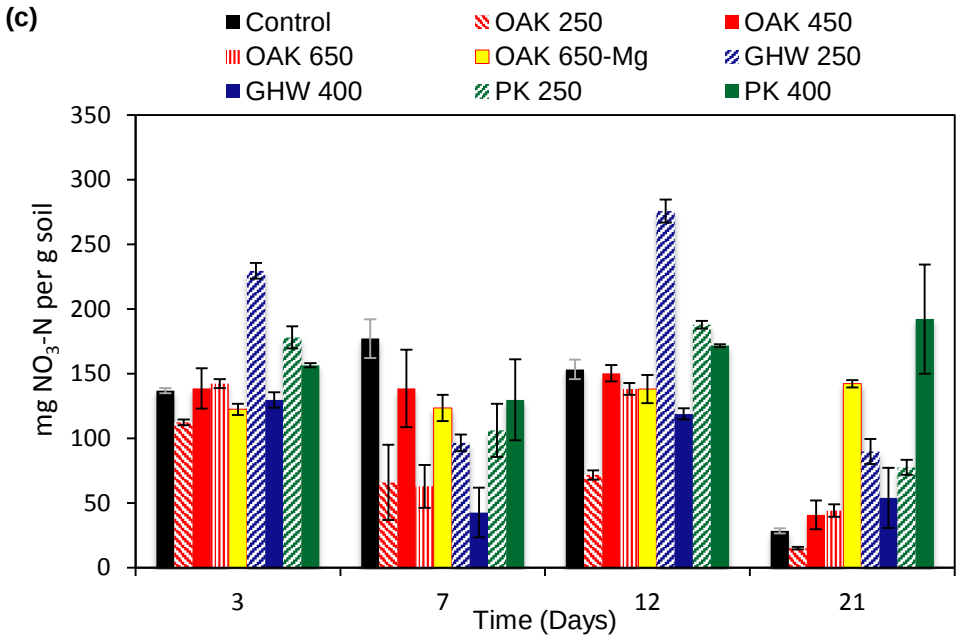

Figure A4 (a) Comparison of cumulative CO_2 evolution during soil incubation tests with various untreated chars and Mg-treated Oak 650 °C; (b) peak NH_4^+-N by 12 days of incubation with OAK 650-Mg while NO_3^--N contents similar for all treatments.

Annex F: NH_3 / NH_4^+ Additional Information

Table A5 Char nitrogen content before and after NH_3 batch sorption test

Char	[a]mg NH_3 generated	Initial N content (mg g^{-1})	N content after sorption (mg g^{-1})
Untreated chars			
[b]OAK (a.r.)	43	1.4±0.2	12.5±0.4
OAK 250 °C	43	4.3±0.2	19.7±1.6
OAK 250 °C	450	4.3±0.2	27.8±0.1
OAK 250 °C	1000	4.3±0.2	36.3±0.1
OAK 250 °C	1500	4.3±0.2	40.8±3.1
OAK 450 °C	43	5.3±0.9	7.7±1.1
OAK 650 °C	43	5.5±1.0	6.1±0.1
[b]GH (a.r.)	43	11.3±1.6	11.7±1.8
GH 250 °C	43	28.3±0.8	23.2±0.6
GH 400 °C	43	11.3±1.7	12.4±0.4
GH 600 °C	43	9.4±0.5	7.5±3.1

Table A5 Char nitrogen content before and after NH_3 batch sorption test

Char	[a]mg NH_3 generated	Initial N content (mg g^{-1})	N content after sorption (mg g^{-1})
Acid-treated chars			
OAK 250-H_3PO_4	43	3.4±0.3	17.99±0.02
OAK 450-H_3PO_4	43	4.3±0.7	11.5±0.3
OAK 650-H_3PO_4	43	5.2±0.6	8.4±1.9
OAK 250-H_2SO_4	43	3.9±0.3	16.7±0.5
OAK 450-H_2SO_4	43	5.4±0.8	12.2±0.7
OAK 650-H_2SO_4	43	5.9±0.1	7[c]
GH 400-H_2SO_4	43	12.9±1.6	20[c]
OAK 250-H_2O_2	43	3.3±0.3	23.7±1.4
OAK 450-H_2O_2	43	4.6±0.8	12.9±1.0
OAK 650-H_2O_2	43	4.9±0.5	4.8±0.8
KOH-treated chars			
OAK 250-KOH	43	3.7±0.6	24.2±0.7
OAK 450-KOH	43	6.3±1.0	11.0±0.3
OAK 650-KOH	43	7.0±0.3	7.8±0.6
GH 250-KOH	43	23.0±1.1	37[c]
GH 400-KOH	43	16.1±1.6	31.71±0.01
Mg-treated chars			
OAK 450-Mg 400 °C	43	11.8±5.0	10.9±0.4
OAK 650-Mg 600 °C	43	7.5±3.9	10.1±0.6
[d]OAK (a.r.)-Mg 600 °C	43	3.3±0.4	6[c]
[d]GH (a.r.)-Mg 600 °C	43	8.7±0.3	10[c]
Solvent-extracted hydrochars			
OAK 250-C_7H_8	43	4.2±0.3	20.5±0.3
GH 250-C_7H_8	43	17.7±0.9	26.1±3.9
OAK 250-NaOH	43	7.5±0.8	12.4±0.6
GH 250-NaOH	43	15.6±2.3	22.1±0.5

[a]Based on mg NH_3 generated according to Equation (3.26); N contents reported as average of duplicate analysis ± standard deviation; [b]unprocessed oak and greenhouse waste biomass respectively; [c]single analysis only; [d]unprocessed oak and greenhouse waste biomass pre-treated with Mg and pyrolysed at 600 °C.

Annex G: Safety Data Sheet of commercial compost

As outlined in Section 3.12.1, composting experiments were performed using a 60% commercial-brand multipurpose compost (≤ 4.75 mm) and 40% shredded savoy cabbage (≤ 9.50 mm) mixture. Information on the commercial-brand compost is provided in Table A6.

Table A6 Key properties of commercial-brand multipurpose compost

1	**Product company and identification**	
	Product name:	Peat-free growing media
	Company:	Bord na Mona Horticulture Limited.
	Address:	Bord na Mona, Main Street, Newbridge, County Kildare, Ireland.
2	**Composition / Ingredient information**	
	Composted and stabilised coniferous tree bark fines plus added nutrients	100%
3	**Physical and chemical characteristics**	
	Appearance:	Brown soil-like bark material with an earthy smell.
	Properties:	Composted coniferous bark fines. Insoluble in water, but will retain up to 70% green weight moisture. Bulk density 300–500 g L^{-1}.
4	**Stability and reactivity**	
	Stability:	Stable under normal ambient conditions.
	Conditions to avoid:	Extreme temperatures, sources of ignition.
		None specifically
	Materials to avoid:	Produces smoke if ignited.
	Hazardous decomposition products:	
5	**Recommended use**	
	Non-hazardous.For use in general gardening and horticultural applications.	

Created: 10 January 2008. Full details available online: http://www.diy.com/departments/verve-multipurpose-compost-peat-free-12l/236990_BQ.prd